MCEER / ATC 49-1

ATC/MCEER Joint Venture
A Partnership of:
Applied Technology Council and
Multidisciplinary Center for Earthquake Engineering Research

ATC

MCEER
MULTIDISCIPLINARY CENTER FOR EARTHQUAKE ENGINEERING RESEARCH
A National Center of Excellence in Advanced Technology Applications

Liquefaction Study Report

Recommended LRFD guidelines for the seismic design of highway bridges

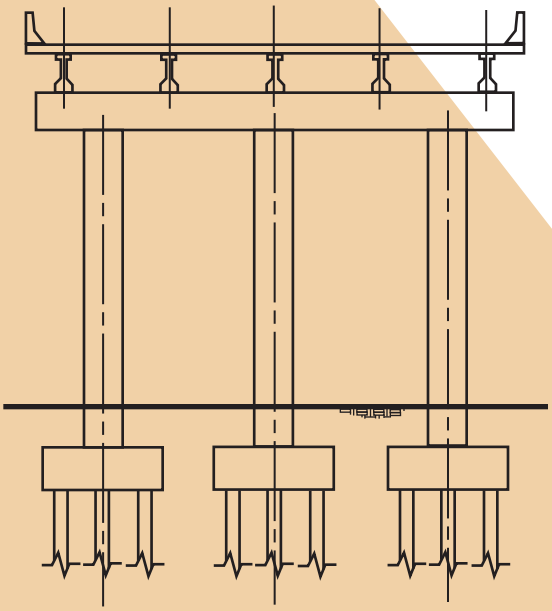

Applied Technology Council

The Applied Technology Council (ATC) is a nonprofit, tax-exempt corporation established in 1971 through the efforts of the Structural Engineers Association of California. ATC's mission is to develop state-of-the-art, user-friendly engineering resources and applications for use in mitigating the effects of natural and other hazards on the built environment. ATC also identifies and encourages needed research and develops consensus opinions on structural engineering issues in a non-proprietary format. ATC thereby fulfills a unique role in funded information transfer.

ATC is guided by a Board of Directors consisting of representatives appointed by the American Society of Civil Engineers, the National Council of Structural Engineers Associations, the Structural Engineers Association of California, the Western Council of Structural Engineers Associations, and four at-large representatives concerned with the practice of structural engineering. Each director serves a three-year term.

Project management and administration are carried out by a full-time Executive Director and support staff. Project work is conducted by a wide range of highly qualified consulting professionals, thus incorporating the experience of many individuals from academia, research, and professional practice who would not be available from any single organization. Funding for ATC projects is obtained from government agencies and from the private sector in the form of tax-deductible contributions.

Multidisciplinary Center for Earthquake Engineering Research

The Multidisciplinary Center for Earthquake Engineering Research (MCEER) is a national center of excellence in advanced technology applications that is dedicated to the reduction of earthquake losses nationwide. Headquartered at the University at Buffalo, State University of New York, the Center was originally established by the National Science Foundation (NSF) in 1986, as the National Center for Earthquake Engineering Research (NCEER).

Comprising a consortium of researchers from numerous disciplines and institutions throughout the United States, the Center's mission is to reduce earthquake losses through research and the application of advanced technologies that improve engineering, pre-earthquake planning and post-earthquake recovery strategies. Toward this end, the Center coordinates a nationwide program of multidisciplinary team research, education and outreach activities.

Funded principally by NSF, the State of New York and the Federal Highway Administration (FHWA), the Center derives additional support from the Federal Emergency Management Agency (FEMA), other state governments, academic institutions, foreign governments and private industry.

ATC/MCEER Joint Venture

The ATC/MCEER Joint Venture, a partnership of the Applied Technology Council (ATC) and the Multidisciplinary Center for Earthquake Engineering Research (MCEER), was established to conduct the NCHRP 12-49 project, Development of Comprehensive Specifications for the Seismic Design of Bridges, which was funded by the Transportation Research Board of the National Research Council.

ATC/MCEER Joint Venture Management Committee
Christopher Rojahn (ATC representative), Chair and Authorized Representative
Michel Bruneau (MCEER representative)
Ian Buckle (MCEER representative)
Ian Friedland (ATC representative)

Notice

This report was prepared by the Applied Technology Council (ATC) and the Multidisciplinary Center for Earthquake Engineering Research (MCEER) through a contract from the Federal Highway Administration and other sponsors. Neither ATC, MCEER, their associates, sponsors, nor any person acting on their behalf:

a. makes any warranty, express or implied, with respect to the use of any information, apparatus, method, or process disclosed in this report or that such use may not infringe upon privately owned rights; or

b. assumes any liabilities of whatsoever kind with respect to the use of, or the damage resulting from the use of, any information, apparatus, method, or process disclosed in this report.

Any opinions, findings, and conclusions or recommendations expressed in this publication are those of the author(s) and do not necessarily reflect the views of ATC, MCEER, Federal Highway Administration or other sponsors. The material presented in this publication should not be used or relied upon for any specific application without competent examination and verification of its accuracy, suitability, and applicability by qualified professionals.

MCEER Report Number: MCEER-03-SP08

MCEER/ATC-49-1

Liquefaction Study Report

Recommended LRFD Guidelines for the Seismic Design of Highway Bridges

Prepared under

NCHRP Project 12-49, FY '98
"Comprehensive Specification for the Seismic Design of Bridges"
National Cooperative Highway Research Program

Prepared by

ATC/MCEER JOINT VENTURE

A partnership of the
Applied Technology Council
(www.ATCouncil.org)
and the
Multidisciplinary Center for Earthquake Engineering Research
(http://mceer.buffalo.edu)

NCHRP 12-49 PROJECT PARTICIPANTS

Project Team

Ian Friedland, Principal Investigator
Ronald Mayes, Technical Director
Donald Anderson
Michel Bruneau
Gregory Fenves
John Kulicki
John Mander
Lee Marsh
Geoffrey Martin
Andrzej Nowak
Richard Nutt
Maurice Power
Andrei Reinhorn

Project Engineering Panel

Ian Buckle, Co-Chair
Christopher Rojahn, Co-Chair
Serafim Arzoumanidis
Mark Capron
Ignatius Po Lam
Paul Liles
Brian Maroney
Joseph Nicoletti
Charles Roeder
Frieder Seible
Theodore Zoli

2003

TABLE OF CONTENTS

* The appendices are provided on the enclosed CD-ROM.

LIST OF FIGURES

LIST OF TABLES

1 INTRODUCTION

1.1 Purpose and Scope

In support of the NCHRP 12-49 effort to develop the next generation of seismic design provisions for new bridges, a study of the effects of liquefaction and the associated hazards, lateral spreading and flow, was undertaken. This report presents the results of that study.

The motivation for the study was the recommended change in the design return period for ground motions for a rare or "Maximum Considered Earthquake" (MCE) used in the recommended revisions. The recommended provisions are based on using ground motions for the MCE that correspond to a probability of exceedence of three percent in 75 years (2,475-year return period) for most of the United States. In areas near highly active faults, ground motions are bounded deterministically to values that are lower than ground motions for a 2,475-year return period. In contrast, the design ground motion hazard in the current AASHTO Division 1-A has a probability of exceedence of 10 percent in 50 years (approximately 15 percent PE in 75 years or 475-year return period). With the increase in return period comes an increase in the potential for liquefaction and liquefaction-induced ground movements. These ground movements could damage bridge structures. Concerns that liquefaction hazards under the recommended provisions may prove to be too costly to accommodate in construction led to this study.

The project team believed that, along with increases in the likelihood of liquefaction, there also exists some conservatism in current design practices. If such conservatism exists, then the use of state-of-the-art design procedures could lead to designs that perform satisfactorily in larger earthquakes, and may not be much more expensive than those being currently built.

The purpose of the study was to investigate liquefaction hazard implications for the design of bridges from the perspective of real sites and real structures. The study scope was limited to two sites in relatively high seismicity locations, one in the western U.S. in Washington State and one in the central U.S. in Missouri. The Washington site is located near the Cascadia subduction zone, and the Missouri site is located near the New Madrid seismic zone. Actual site profile data and actual bridge configurations were used for the study. The site data were idealized by providing limited simplification, although the overall engineering character of the sites was preserved.

The investigation of the two sites and their respective bridges focused on the resulting response and design differences between the recommended ground shaking level (2,475-year earthquake) and that corresponding to the current AASHTO Division I-A provisions (475-year earthquake). Additionally, the recommended provisions require that a 100-year return period service-level earthquake be considered, and this earthquake was thus considered in this study. In fact, it may occasionally control the vibration design of bridges on some sites.

The scope of the study for each of the two sites and bridges includes:

1. Simplified, conventional liquefaction analyses;
2. Development of both 475-year and 2,475-year acceleration time-histories;
3. Nonlinear assessment of the site response to these accelerations, including the time history of pore water increases;
4. Assessment of stability of abutment end slopes;
5. Estimations of lateral spreading and/or flow conditions at the sites;
6. Design of structural systems to withstand the predicted response and flow conditions;
7. Evaluation of geotechnical mitigation of liquefaction-related ground displacement; and
8. Evaluation of cost impacts of the structural and geotechnical mitigation strategies.

The results for the 475-year and 2,475-year events were compared against one another to assess the implications of using the larger event for design. Additionally, the conduct of the study helped synthesize an overall approach for handling liquefaction-induced movements in the recommended design provisions.

1.2 Organization of the Report

Chapter 2 provides a detailed discussion of procedures to evaluate liquefaction potential and lateral spread effects. Also discussed are ground mitigation design approaches and procedures to evaluate the beneficial effects of pile pinning in restraining lateral spread.

Chapter 3 covers the results for a Western U.S. site and Chapter 4 covers a Central U.S. site. The contents of Chapters 3 and 4 each follow the same outline. The site selection is first described, followed by a description of the bridge used for the site. Earthquake hazard levels are then discussed, including response spectra and acceleration time histories generated for each site. Next, the assessment of the effects of liquefaction are covered, including simplified analyses, nonlinear response analysis of the soil column, estimates of lateral spreading using traditional Newmark charts, and site-specific Newmark analyses. The structures are then designed for earthquake-induced vibration for both no liquefaction and liquefied site conditions. Using the vibration-designed structure, the implications of predicted lateral spread/flow conditions are then assessed, in essence using a pushover type approach. If the structural system does not produce acceptable performance for these conditions, then structural and/or geotechnical mitigation alternatives are developed and evaluated.

Chapter 5 provides a summary of the results of the analysis, design, and assessment for the two sites. The chapter also provides an overview of recommended procedures that have been developed to accommodate design for liquefaction, lateral spread, and flow effects.

Appendices are provided that contain detailed information for each site and each structure's analysis and design.

2. LIQUEFACTION HAZARD ASSESSMENT AND MITIGATION METHODS

2.1 General

The design of bridge structures for liquefaction effects generally has two components. The first is that the bridge must perform adequately with liquefaction-induced soil changes alone. This means that the mechanical properties of soil layers that may liquefy are changed to reflect values that occur during liquefaction (i.e., properties such as stiffness are reduced). Design for these cases is, in reality, a design for structural vibration effects, and code-based procedures can be used. The second component of the design is the consideration of liquefaction-induced ground movements. These can take several forms:

1. Flow slides representing large translational or rotational embankment failures mobilized by existing static stresses (i.e., the site static factor of safety against slope failure drops below unity (1.0) due to low residual strengths of liquefied soil layers)
2. Limited cyclic or permanent lateral spreads, of the order of feet or more, triggered and sustained by the earthquake ground shaking.
3. Post-liquefaction ground settlement.

Each of these hazards and their potential must be addressed, along with mitigation options.

These three displacement mechanisms place deformation demands on the bridge, which can result in structural damage or bridge collapse from:

1. Lateral deformation of abutments and piers arising from liquefaction-induced flow failures or lateral spreads, leading to substructure pile damage and potential span collapse.
2. Liquefaction-induced differential ground lurch at adjacent pier supports causing potential span collapse.
3. Post-liquefaction differential settlement of bridge-pile supports (pile down drag).
4. Loss of foundation stiffness and capacity leading to structural damage.

The potential interaction or combination of these effects must be addressed in the design. For most bridge projects, the recommended methodology is to consider the two effects independently; i.e., de-coupled. The reasoning behind this was that it is not likely that the peak vibration response and the peak spreading or flow effect will occur simultaneously. For many earthquakes, the peak vibration response occurs somewhat in advance of the maximum ground movement loading. For very large earthquakes where liquefaction may occur before peak ground accelerations, the peak vibration response is likely to be significantly attenuated and, hence, inertial loading reduced from peak design values. In addition, peak displacement demands arising from lateral spread are likely to generate maximum pile moments at depths well below peak moments arising from inertial loading. Furthermore, the de-coupling of response allows the flexibility to use separate and different performance criteria for design to accommodate the two phenomena.

Current practice and site response analysis methods for assessing the liquefaction hazards are summarized in the remainder of this section. This summary includes a discussion of methods to assess liquefaction potential through the use of simplified and site response analysis methods; estimate the effects of liquefaction, including displacements; and mitigate the hazard through use of both ground improvement and structural pinning procedures.

2.2 Liquefaction Hazard Assessment – Current Practice

Current methods for assessing the hazards associated with liquefaction typically involve a several-step process. The potential for liquefaction is first established. This is followed by an assessment of the effects of liquefaction, if it is predicted, on the foundation system and approach fill. If the potential consequences are significant, then typically either the structure is designed to withstand the effects of liquefaction or some type of ground improvement method is implemented to mitigate the potential effects. These mitigation methods, whether they involve structural changes or ground improvement, can involve significant costs, and therefore, methods used to assess the liquefaction potential must take full advantage of current predictive methods.

2.2.1 Simplified Methods for Evaluating Liquefaction Potential

For most design projects, simplified methods are used to assess the potential for liquefaction. These methods involve correlations between in situ determination of soil denseness, such as measured by the Standard Penetration Test (SPT) or the Cone Penetrometer Test (CPT), and the liquefaction strength of the soil, referred to as the cyclic resistance ratio (CRR). In this report they are referred to as the SPT and CPT simplified methods.

The SPT simplified method was introduced several decades ago by Seed and Idriss (1971). A version of this method dating from the late 1970s is included in the commentary of the current AASHTO Standard Specification. As more information has been collected on the performance of liquefiable soils over the past two decades, the SPT simplified method has been modified somewhat to better account for both the stresses developing in the soil during an earthquake and the ability of soils to resist these stresses with the development of liquefaction. More recently, CPT simplified methods were developed along the same lines as the SPT simplified method.

Appendix D to Part II: Commentary and Appendices of *Recommended LRFD Guidelines for the Seismic Design of Highway Bridges* (ATC/MCEER 2003) includes a summary of the recommended procedures and associated charts for conducting simplified SPT and CPT-based analyses. These recommendations are based on conclusions reached during a consensus workshop held in early 1996 (Youd and Idriss, 1997). Already researchers are suggesting modifications to the procedures based on their observations and studies of the liquefaction phenomena; however, until these methods have been critiqued and accepted by the profession at large, the proceedings from the 1996 workshop are considered to be the baseline method.

As noted in the commentary to the AASHTO Standard Specifications, there is an alternative to the evaluation of liquefaction potential. This involves analytical site-specific response methods and is discussed in the following section.

2.2.2 Effects of Liquefaction

While the procedures for evaluating the potential for liquefaction are relatively well-established, procedures for assessing the effects of liquefaction are less well-defined. It is generally recognized that liquefied soil loses strength. Until not too long ago, it was assumed that the liquefied soil had essentially no strength (i.e., it was a liquid with a low viscosity) and analyses were conducted with the liquefied zone as a zero-strength layer. Now, it is recognized that the liquefied soil has a strength that can range from less than a 100 pounds per square foot (psf) to greater than 500 psf. Relationships between SPT blow counts and residual strength (e.g., Seed and Harder, 1990) are currently used to estimate this residual strength. Alternate relationships between SPT blow counts or CPT end resistance values and the undrained critical strength ratio for the liquefied soil have also been proposed (e.g., Olson and Stark, 2002; Stark and Olson, 1995). All of these methods for determining residual strength involve uncertainty, and therefore, decisions must be made regarding the use of upper, lower, or mean values.

The effects of liquefaction are evaluated by replacing the strength of the soil in the liquefied layer with the residual strength, determined using one of the methods identified above. For example, the "p-y curves" in the liquefied zone are modified for the lower strength to determine the effects of liquefaction on the lateral response of the pile. Similar procedures can be used to evaluate changes in the factor of safety (FOS) for bearing capacity of a spread footing, the stability of a retaining structure, or the loss in capacity of a pile. Normally, the same limit-equilibrium methods of analysis used for gravity loading are used for these liquefaction assessments. These limit-equilibrium analyses may or may not include the changes in loading from the inertial response of the structure.

The stability of an approach fill overlying a liquefied zone is evaluated by conducting pseudo-static stability analyses or by conducting deformation analyses, as summarized below:

1. **Pseudo-Static Approach**: A pseudo-static seismic coefficient is applied to the embankment to represent the inertial forces within the soil. This seismic coefficient is assumed to be one-half to two-thirds of the peak ground acceleration to define an average cyclic loading condition. When determining this coefficient, it is also generally recognized that liquefaction affects the level of inertial forces; however, for conservatism, the seismic coefficient is assumed to be the same as that which occurs without liquefaction. The factor of safety (FOS) for instability is determined using a conventional slope stability computer program such as PCSTABL, but with a residual strength assigned to the layers that have liquefied. If factors of safety are less than 1.1 to 1.2, the condition is considered unacceptable, as is normally the case for gravity loading conditions.
2. **Deformation Approach** A second approach is to predict the deformations that develop during liquefaction based on limit equilibrium analyses, but with an applied acceleration time history. It is generally assumed that deformations will be essentially zero if the static FOS is

greater than 1.0. As the FOS drops further below 1.0, progressively greater earthquake-induced displacements occur, although no simple correlation between FOS and deformation exists.

Two alternatives are normally considered if unacceptable factors of safety or excessive deformations are obtained for the approach fill analysis:

a. modify the slope of the approach fill until an acceptable factor of safety or deformation is obtained, or
b. improve the ground so that liquefaction does not occur in the area that will affect the stability of the approach fill.

Both procedures can involve significant additional costs, either by requiring longer bridges or by the cost of the ground improvement.

2.2.3 Predicting Lateral Spread Displacements

There are several methods for making displacement assessments. These include simplified displacement charts and equations, numerical integration of the earthquake record in a "Newmark Time History Analysis," and two-dimensional nonlinear, effective stress modeling of the slope as described by Qiu (1998) and by use of a computer program such as FLAC (Itasca, 1998). Only the simplified charts and the integration of earthquake records are covered in this discussion. Use of FLAC requires special expertise, and will not be used for most bridge design projects.

2.2.3.1 Simplified Charts and Equations

The simplified methods include charts such as those developed by Franklin and Chang (1977) and shown in earlier editions of the AASHTO Standard Specifications. Other similar methods have been suggested by Hynes and Franklin (1984), Wong and Whitman (1982), and Martin and Qiu (1994). These methods involve correlations between the seismic coefficient that results in a FOS of 1 in the embankment, referred to as the yield acceleration (k_y), and the embankment displacement. Acceleration records from a variety of databases were used to develop the displacement charts. With this prediction of displacement, it is possible to determine more explicitly the consequences of liquefaction.

A number of other simplified methods are available for predicting displacements, as discussed by Kramer (1996). Several of these methods are based on correlations between a number of source parameters and site conditions. These methods provide a good means of performing preliminary displacement screening studies but typically lack the precision needed for bridge assessments. Other methods, such as the Makdisi and Seed (1978) method, are thought to be more suited to estimating displacements of earth dams, as they implicitly include amplification effects of the dam.

The simplified chart approach, such as represented in the Franklin and Chang, Hynes and Franklin, and Wong and Whitman methods, is not new to earthquake studies. It was suggested in the 1960s by Newmark (1965). This procedure is routinely applied during the design of earth dams. A version of this method was suggested in ATC 6 (1981), and was later incorporated within the commentary to the AASHTO Standard Specifications. These methods are limited by the databases used in the development of the relationship between yield acceleration and displacement. These databases were generally limited to earthquake magnitudes less than 7.5.

2.2.3.2 Integration of Earthquake Records

The second simplified method of estimating displacements involves direct integration of site-specific earthquake records. This procedure has also been used to estimate displacement of approach fills for bridges on special projects. Because of the previous difficulties in finding suitable earthquake records, its use on transportation projects was limited. However, use of the Newmark method for predicting the displacement of earth dams has been common place for over three decades.

In this approach, displacements are determined from an earthquake record by double integrating the portion of the earthquake record above the yield acceleration. The double integration can be carried out by hand or by using simple computer programs. In this approach, the change in residual strength, as liquefaction progressively develops, can be accounted for by determining yield accelerations as a function of time, and using different yield accelerations in different portions of the earthquake records.

The key phase of the Newmark analysis is the selection of the earthquake record. The current approach generally involves conducting a one-dimensional ground response analyses with a computer program such as SHAKE (Idriss and Sun, 1992) to determine the acceleration record at the bottom of the sliding mass. Procedures for selecting the earthquake record for a SHAKE analysis are given in Appendix C of Part II: Commentary and Appendices of *Recommended LRFD Guidelines for the Seismic Design of Highway Bridges* (ATC/MCEER 2003). If firm-ground conditions exist below the liquefied layer, it is possible to select records directly from the catalogue of earthquake records. In this case, a search must be made to find records obtained on comparable ground conditions.

If soft layers or liquefiable layers exist below the sliding zone, determination of the earthquake record for use in a Newmark analysis becomes more difficult. For these situations, it is generally necessary to use a non-linear, effective stress method of analysis, such as that applied in this study. These non-linear methods account for the softening of the soil during cycles of loading. They have been in use since the late 1970s but until recently have been used only within academia or by specialists in the consulting business. With the rapid evolution of the computer software industry and the ease of using desktop computers, these non-linear methods may likely become routine in the next five years.

2.3 Liquefaction Hazard Assessment – Site Response Analyses

The simplified empirical liquefaction hazard assessment method described above is widely used in current practice, and is recognized as a reasonably reliable method for evaluating the likely occurrence or non occurrence of liquefaction at a site. However, there are several limitations to the approach:

1. It does not provide information on the time at which liquefaction is triggered in an earthquake.
2. It cannot provide guidance on how complex stratigraphy reflecting variable factors of safety (<1) against liquefaction, influence site response and triggering of liquefaction in the strata.
3. It cannot indicate how the effects of redistribution of excess pore water pressure induced by earthquake loading, can influence liquefaction response.

In this study, in addition to the use of the simplified method, the use of the one-dimensional, nonlinear dynamic effective stress response analysis program DESRA as modified at the University of Southern California (DESRA-MUSC), was adopted for the study. The use of this approach overcomes the above limitations, and allows for an improved understanding of the mechanics of liquefaction at a site and the associated "seat" of post liquefaction ground deformations.

A publication describing the background to the DESRA-MUSC program and its practical application, is included in this report as Appendix A. A more detailed description of the program is documented in Qiu, 1998.

As for the widely used SHAKE program, the DESRA-MUSC program uses G/G_{max} versus shearing strain amplitude (γ) curves to characterize nonlinear site behavior. However, as the program operates in the time domain, the above curves are transformed into a nonlinear backbone curve (τ versus γ), which is asymptotic to an assumed large strain strength. This curve defines the hysteretic damping response under earthquake loading. The constitutive model used to generate the time history of earthquake-induced pore water pressures is based on parameters defined by field liquefaction strength curves which are keyed to the same SPT data used for the simplified procedure, and to assumed one-dimensional elastic rebound curves. The latter curves, when combined with assumed permeability coefficients, allow for redistribution of pore water pressure in response cycles. The nonlinear backbone curve is degraded as a function of pore pressure increases, until the maximum post-liquefaction strength is reached.

As for the SHAKE program, earthquake response analyses require input acceleration time histories at a transmitting boundary defined at an appropriate depth. For the studies presented in this report, this depth is defined by dense soils reflecting a soil type "C" (shear wave velocities > 1200 ft/sec) as defined in the recommended LRFD provisions (and the NEHRP and UBC seismic design guidelines). These time histories, along with the site characteristics needed for DESRA-MUSC parameter calculations, are developed in Chapters 3 and 4 of this report.

2.3.1 Lateral Spread Evaluations using Analysis Results

The use of the site response analysis results for the determination of lateral spread displacements follows a similar concept to that described in Section 2.2.3.2 but with several refinements. These refinements are discussed with reference to Figure 2.1, which shows an idealized bridge embankment fill sited on underlying liquefiable strata.

The DESRA-MUSC one-dimensional site response analyses provide time histories of pore water pressure increases for each liquefiable layer. Although it can be demonstrated that the embankment static shear stresses on these layers will reduce the rate of pore water pressure build up from one-dimensional analyses for shaking in the longitudinal direction, this would not be the case for wide embankments for shaking in the transverse direction. In any event, it is a conservative design assumption to use the one-dimensional pore water pressure increases to predict the onset of liquefaction, and the depth of the layer in which this first occurs.

It is a reasonable assumption that the base of the first layer to liquefy will become the "seat" of lateral spread deformations and will "base isolate" higher layers which may subsequently liquefy from significant lateral deformations. In the case of the simplified liquefaction analysis previously described, the layer with the lowest factor of safety will most likely establish the "seat" of lateral spreads. Consequently, the pseudo-static stability analysis search for the critical failure geometry and the minimum yield acceleration (assuming the factor of safety against a flow failure is greater than one) should focus on this layer, where residual strengths for the liquefied layer are assumed in stability analyses.

The DESRA-MUSC analyses provide a time history of acceleration for the layer immediately underlying the liquefied layer. This time history then becomes the acceleration input for estimating lateral displacements using the Newmark analysis approach, where the strength of the layer which liquefies is degraded to reach the residual strength at the time liquefaction is triggered.

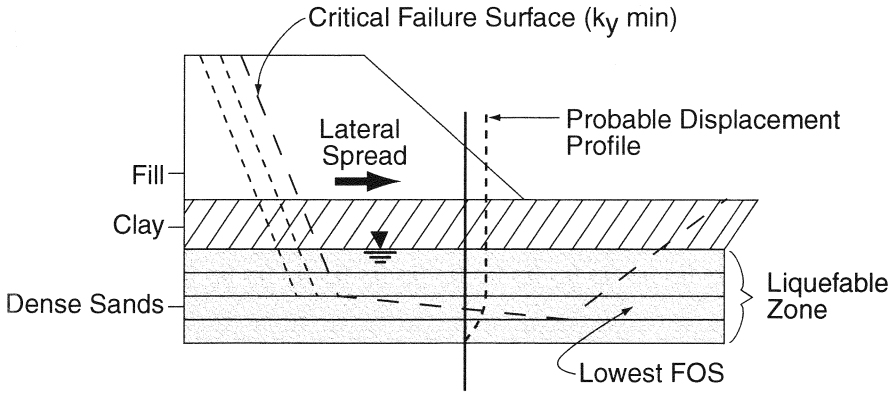

Figure 2.1 Lateral Spread Illustrated for an Idealized Bridge Embankment

It is recognized that the Newmark method assumes that the sliding mass is in effect a rigid block sliding on the plane of failure, whereas the actual problem involves a non-rigid sliding mass with deformation occurring over a layer of finite thickness as shown in Figure 2.1. However, two-dimensional response analyses incorporating failure surfaces of finite thickness, indicate the displacements predicted by the Newmark approach show similar patterns of behavior and are approximately equal to or somewhat less (by up to about 100 percent less) than more refined two-dimensional analysis results. Given all the assumptions involved in deformation analyses and the uncertainties associated with the soil properties and ground motions, the Newmark analyses may be considered the best practical approach at the present time, for design purposes.

2.4 Mitigation of Liquefaction Effects

Where highway bridge site liquefaction problems are identified that are of concern in relation to the potential earthquake-induced bridge damage modes described above, mitigation methods need to be addressed. Apart from relocating the bridge to another less vulnerable site, two basic options are normally considered.

1. Foundation/bridge structural design to accommodate the predicted liquefaction and related ground deformation demands. This requires soil-foundation structure interaction analyses to determine if the deformation and load capacity of the existing foundation/bridge system is adequate to accommodate the ground deformation demands without collapse or can meet prescribed performance criteria. If not, mitigation methods focused on strengthening the structural foundation system can be evaluated, and costs compared to the ground modification mitigation option described below. A discussion of evaluation methods used for this approach is given in Section 2.5.
2. The use of site remediation techniques, where stabilizing measures or ground modification and improvement approaches are undertaken to prevent liquefaction and/or minimize ground displacement demands. Such methods include:

    - In situ ground densification of liquefiable soils in zones surrounding bridge piers, and in zones at or underneath the toe of approach fills, to reduce ground deformations to tolerable levels.
    - The use of deep soil mixing using cement, to form stabilizing zones similar to those developed using ground densification techniques.
    - Other types of ground improvement such as dewatering, installation of gravel drains, or permeation grouting.

A more detailed summary of two ground improvement methods for liquefaction remediation is provided in Section 2.4.1. Overviews of the state of practice are documented in an ASCE (1997) publication, and by Andrus and Chung (1995). A comprehensive report on ground remediation measures for liquefaction at existing bridge sites has been authored by Cooke and Mitchell (1999).

2.4.1 Mitigation Using Site Improvement

To prevent liquefaction and reduce lateral ground deformation to acceptable levels in terms of the governing structural performance criteria, site remediation approaches such as ground densification in selected liquefiable soil zones are commonly deployed. Two of the more common procedures for accomplishing this remediation are described below:

- **Vibro-Replacement**: The most widely used densification method is the vibro-replacement technique. This method involves the repeated insertion and withdrawal of a large vibrating probe in the soil, to the desired depth of densification, as shown in Figure 2.2. As vibration-induced liquefaction occurs, crushed stone backfill is placed around the vibrator leading to the development of a stone column approximately 3 feet in diameter. The stone column provides for an increased effectiveness of vibration transmission, and facilitates drainage of excess pore water pressures as densification occurs. The procedure is repeated at grid spacing of 7 to 12 feet. Relative densities of the order of 80 percent, can be accomplished by the method which has been shown to be effective in past earthquakes (Mitchell et. al., 1995). The method has been shown to be effective if sands to be densified contain less than 15-20 percent fines, although the use of wick drains placed at the midpoints of stone column grid points to aid drainage, can potentially lead to densification of sandy silts (Luehring et. al., 1998). Details on design information and equipment applications can be found in many publications such as Baez (1995) Baez and Martin (1995), Hayden and Baez (1994), and Martin (1998).

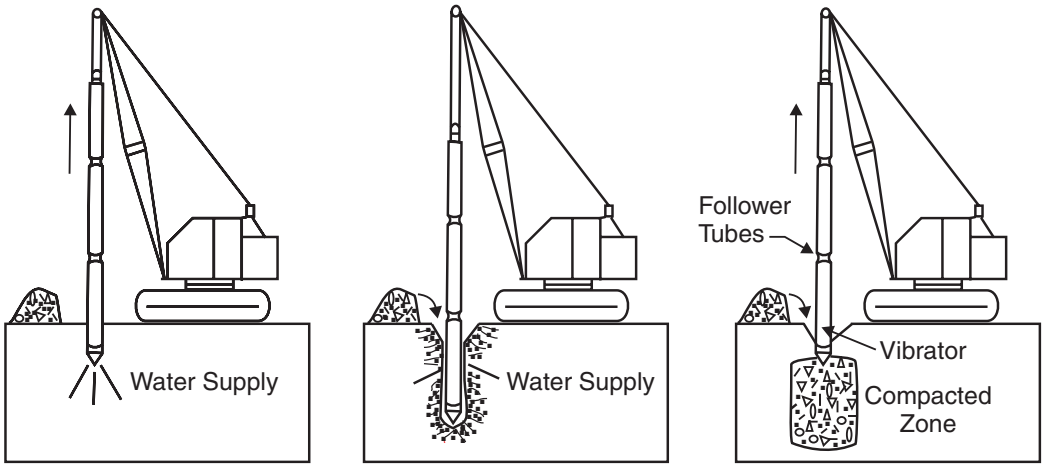

Figure 2.2 Vibro-Replacement Site Mitigation Technique

A representative application of vibro-replacement is shown in Figure 2.3, where a densified stone column buttress has been constructed at the toe of an embankment. The effect of the buttress is to increase values of soil resistance in the liquefied zone. This in turn reduces lateral spread displacements. A Newmark approach can then be used to determine the buttress width that leads to acceptable displacement performance of abutment or bridge pier piles in the failure zone. An example of this approach is described by Egan et al. (1992). A further application is shown in Figure 2.4, where a densified soil zone has been placed

around a pile-supported bridge pier. The placement of such a zone (normally with a radius of 1.5 to 2 times the thickness of the liquefiable layer) would be used to eliminate post liquefaction down drag on the piles, and the potential effects of cyclic ground lurch (progressive unidirectional movement of soil due to high ground accelerations).

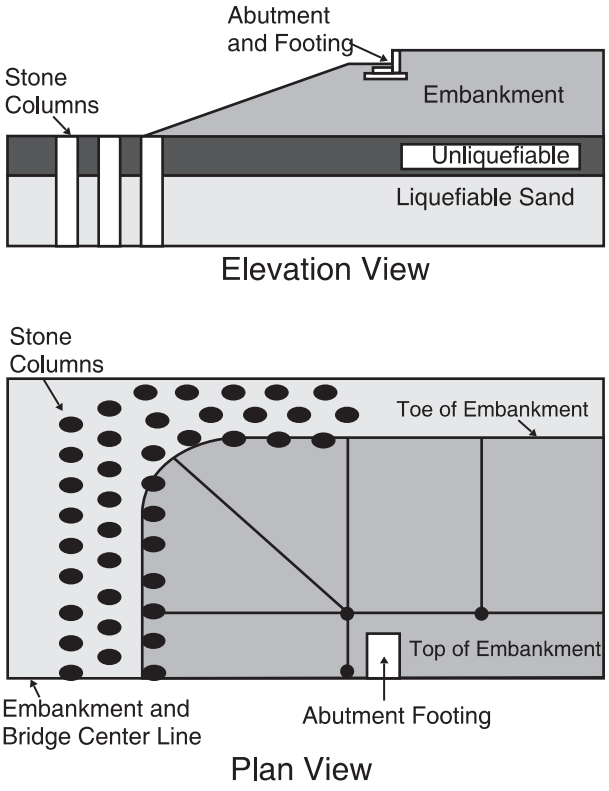

Figure 2.3 Representative Application of Stone Columns

- **Compaction Grouting:** This method of ground remediation is shown schematically in Figure 2.5. The method involves pumping a stiff mix of soil, cement, and water into the ground under high pressure to compress or densify the soil. For sites where vibratory techniques may be impractical, compaction grouting can be used. Typically, a very stiff (1 to 2 inch slump) soil-cement-water mixture is injected into the soil, forming grout bulbs which displace and potentially densify the surrounding ground, without penetrating the soil pores. A grid or network of grout columns formed by bottom up grouting, results in improved liquefaction resistance over a required areal extent, similar to the use of a network of stone columns described above. An overview of this approach is documented by Boulanger and Hayden (1995). A theoretical study of the mechanics of ground improvement in sands (Mace, 1999) has shown that increased liquefaction resistance arises primarily from increased lateral stresses as opposed to densification. Consequently, liquefaction strength increases are best measured using CPT correlations as described by Salgado et. al. (1997). In this respect, some uncertainties still remain as to the permanence of lateral stress increases.

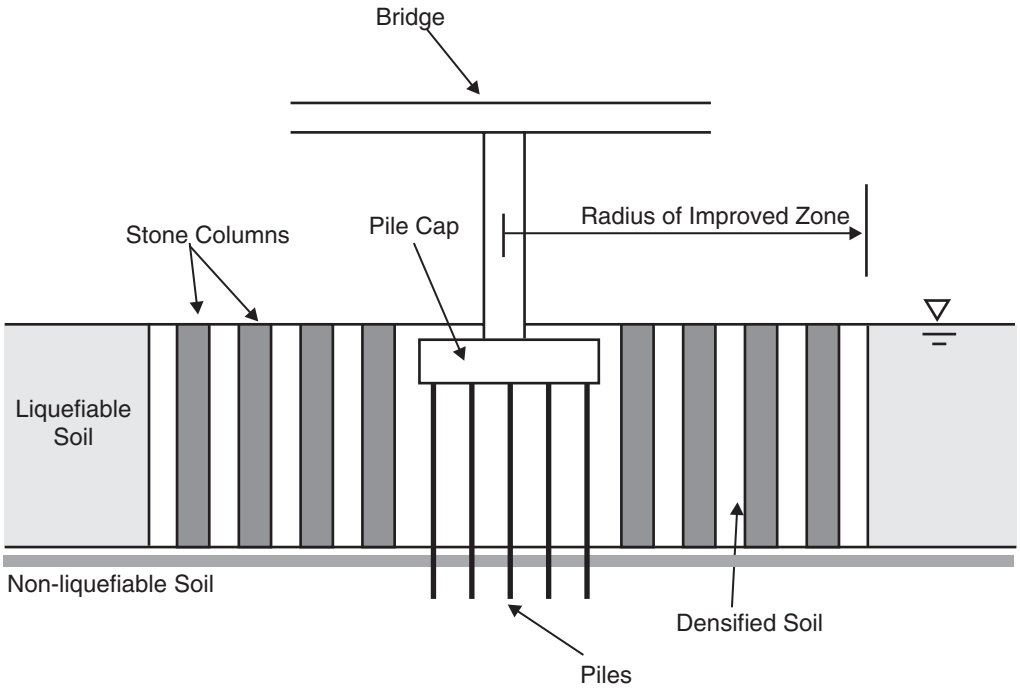

Figure 2.4 Stone Columns Used to Densify the Soil Adjacent to a Pile-Supported Bridge Pier

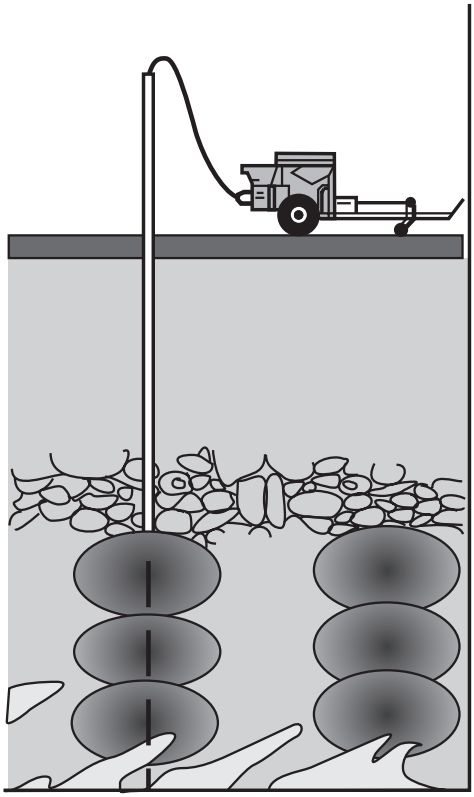

Figure 2.5 Compaction Grouting Site Mitigation Technique

The higher strength of the improved ground can be used to revise estimates of lateral spread displacement discussed in Section 2.2.3. This involves determining the yield acceleration for slope movement through the improved ground, and then using the simplified charts, equations, or integrated earthquake records to revise the displacement procedure. By making different assumptions on the width and strength of the improved ground, it is possible to optimize the cost of the improvement while limiting deformations to levels that can be tolerated by the structure.

2.4.2 Structural Approach to Mitigation

Given results defining the magnitude of liquefaction-induced lateral deformations and the geometry of the most likely failure surfaces based on stability analyses, an assessment can be made to determine if the shear and moment capacities of pile foundations are sufficient to prevent collapse of the bridge structure under the imposed displacement demands on the foundation system. It is assumed in these analyses that the effects of ground displacement can be decoupled from the effects of structural inertial loading. In most cases, this is a reasonable solution as peak vibration response is likely to occur in advance of maximum ground displacements, and displacement induced maximum moments and shear will generally occur at deeper depths than maximum moments and shear from structural inertial loading.

The magnitudes of moments and shear induced in pile foundations by ground displacements may be computed using soil-pile interaction programs such as LPILE (Wang and Reese, 1998), where the assumed displacement field is applied to interface springs or p-y curves. Examples of such analyses are given by Jakura and Abghari (1994), O'Rourke et al. (1994), Soydemir et al., (1997), and Ishihara and Cubrinovski (1998). In the liquefied zone, the soil is normally treated as a soft cohesive soil when calculating lateral spring characteristics (or p-y curves) where the maximum soil cohesion is assumed equal to the residual strength of liquefied soil. In some cases, large ground deformations may slide past the foundation system, exerting full passive pressures in the process. However, foundations may remain intact without failure, as in the case history reported by Berrill et al. (1997).

A refinement of the above approach is to consider the reinforcing or pinning effects the piles or pile group have on the lateral stability, by representing the pile shear forces at the location of the failure plane as an equivalent shear strength in the calculation of yield accelerations used in the Newmark analyses. This becomes an iterative approach as shear forces are a function of displacements, which in turn are reduced as shear forces increase. Because the foundation, as designed for the non-spreading load cases, will typically possess some lateral resistance capable of reducing the magnitude of spreading, this capacity should be utilized. If the lateral displacements are too great for the structure to adequately accommodate, then geotechnical improvements will be necessary, unless the performance objective under spreading loads is to accept a severely damaged bridge that likely will need to be replaced. Therefore, the most cost effective approach is to account for the beneficial restraint action of the existing (as-designed for non-spreading effects) foundation.

The impact of a lateral spread on a pile foundation depends on a number of geotechnical factors such as the thickness of a crustal layer overlying the liquefied zone, the thickness of the liquefied layer, and the magnitude of lateral displacement. Pinning action becomes less effective as the thickness of liquefied soil increases.

In the event that the pile foundations cannot accommodate the displacement demands, one option is to install additional foundation piles using a pile cap overlay (if feasible) to increase the pinning action, hence, reducing displacement demands. Another option is to use pinch piles driven through the liquefiable layer and failure surface, to provide additional pinning action. The former option is particularly relevant if additional piles are required because of retrofit needs to accommodate high overturning moments or to minimize down drag effects. Where additional piles are required as a remediation measure, the costs of the piles should be compared with the costs of the ground remediation option described previously, and the optimal solution adopted.

Other structural systems such as battered piles and/or tie-back systems may be considered. These systems must be evaluated using realistic force levels that may develop. These were not considered for the cases outlined in this report. However, such systems have been used to help resist the effects of spreading loads.

2.5 Simplified Approach for Structural Analysis and Design

The foundation of the structure was designed to accommodate the non-seismic load conditions and the vibration cases of seismic loading. Then, this foundation system was assessed for its capability to resist the lateral spreading-induced ground movements. As mentioned previously, it is believed to be appropriate to design for vibration and lateral spreading in a decoupled manner. This stems from the typical occurrence that peak accelerations of the structure happen before full liquefaction develops, and therefore, before significant soil movement begins.

2.5.1 Vibration Design

Vibration design refers to the normal design using response spectra or seismic coefficients as structural loading for which the structure is proportioned or assessed. This phase is considered separately from the effects of liquefaction-induced ground movements. For the purposes of the vibration design, the only effects of liquefaction included are the reduced soil resistances adjacent to the foundation and the potential alteration of the input seismic spectra due to softening and energy dissipation in the soil.

In this study, the same preliminary configurations of the bridges are used as starting points for the designs for 475- and 2,475-year earthquakes. The designs are assessed for adequacy for both the existing and the recommended specifications. The configurations selected are based on designs that meet the requirements of the Division I-A provisions; thus any changes required are those necessary to meet the recommended specifications. These are outlined for the respective bridges in Chapters 3 and 4.

For both sites and both designs, the modal analysis method is used to determine the design forces for the structures. In the case of the recommended specification, SDAP E is used for both the Western and Central U.S. designs. This method requires the use of a nonlinear static or pushover analysis to assess the adequacy of the design. As such, this method is the most liberal of those included in the recommended specifications. For the purposes of this study, the pushover assessments have been applied in approximate fashion to keep the analysis relatively simple and straightforward.

Both bridges have been designed such that the passive resistance offered by the approach fill in the longitudinal direction is relied upon. Furthermore, the maximum value of passive resistance allowed by the recommended LRFD specifications has been used; thus, the designs are categorized as 'Permissible with Owner Approval.' As with the SDAP, this reflects the most liberal category.

2.5.2 Lateral Spreading Design

The designs for lateral spreading and/or flow conditions were done using best estimates of appropriate engineering practices, because direct design procedures are not currently included in the AASHTO I-A provisions. Although many agencies are currently requiring some type of design for spreading effects in their criteria, the criteria and methodologies typically vary widely. Certainly the understanding of the phenomenon has developed in the past decade or so, and procedures and software are available for use. For example, LPILE and similar programs can provide useful information for the design of foundations to resist the effects of lateral soil movements.

2.5.2.1 Design Approach

The design approach used in this study and recommended for the new AASHTO LRFD provisions involves four basic elements:

1. Stability analysis;
2. Newmark sliding block analysis;
3. Assessments of the passive force that can ultimately develop ahead of a pile or foundation as soil movement occurs; and
4. Assessment of the likely plastic mechanisms that may develop in the foundations and substructure.

The rationale behind this approach is to determine the likely magnitude of lateral soil movement and assess the structure's ability to both accommodate this movement and/or potentially limit the movement. The approach is based on use of a deep foundation system, such as piles or drilled shafts. Spread footing types of foundations typically will not be used when soil conditions lead to the possibility of lateral spreading.

The concept of considering a plastic mechanism in the foundation under the action of spreading forces is tantamount to accepting substantial damage in the foundation. This is a departure from seismic design for structural inertial loading alone, and the departure is felt reasonable because it

is unlikely that the formation of a mechanism in the foundation will lead to structure collapse. The reasoning behind this is that spreading is essentially a displacement-controlled process. Thus the estimated soil displacements represent a limit on the structure displacement, excluding the phenomena of buckling of the piles or shafts below grade and the continued displacement that could be produced by large P-Δ effects. Buckling should be checked, and methods that include the soil residual resistance should be used. Meyersohn, et. al. (1992) provides a method for checking buckling as an example. The effects of P-Δ amplification are discussed later in this section.

The fact that inelastic deformations may occur below grade and that these may be difficult to detect and inspect, should be considered. However, typically the presence of large ground movements induced by earthquake motions is discernible. Thus, it should be possible to postulate whether inelastic deformations have occurred from the post-earthquake inspection information. Additionally, inclinometer tubes could be installed in selected elements of deep foundations to allow quantitative assessment of pile/shaft movement following an earthquake. Also, post-earthquake investigation using downhole video cameras can be used to assess damage.

A flowchart of the methodology for consideration of spreading is given in Figure 2.6. Key components of the methodology are numbered in the flowchart, and this chart along with the following commentary provide a 'roadmap' to the procedure used in this study for the lateral spreading resistance design. The primary feature of the recommended methodology is the use of inelastic action in the piles to accommodate the movement of soil and foundations. If the resulting movements are unacceptable, then mitigation must be implemented.

- Step 1. The soil layers that are likely to liquefy are identified.

- Step 2. A stability analysis is executed to determine the likelihood of soil movements, and to determine the extent of such movements. This would include the depths of soil likely to move and the plan extent of the likely soil failure block. Assessment of the impacts to a bridge structure can then be made by considering the proximity of the failure block to the foundation system.

- Step 3. The maximum displacement of the soil is estimated. This may be accomplished using the simplifed Newmark charts, Newmark time history analysis, or more advanced techniques.

- Step 4. An assessment is made whether soil flows around the foundation or movement of the foundation will occur. The assessment requires a comparison between the estimated passive soil forces that can be exerted on the foundation system and the ultimate structural resistance that can be developed by the structure itself. This assessment requires estimating the forces that can develop if soil is to actually flow around the foundation system and comparing them with the likely resistance the structure will provide. In cases where a crust of non-liquefied material may exist at or near the ground surface, the full structural resistance is likely to be less than the flow-induced passive forces, and in such cases the foundation is likely to move with the soil. In many cases, it

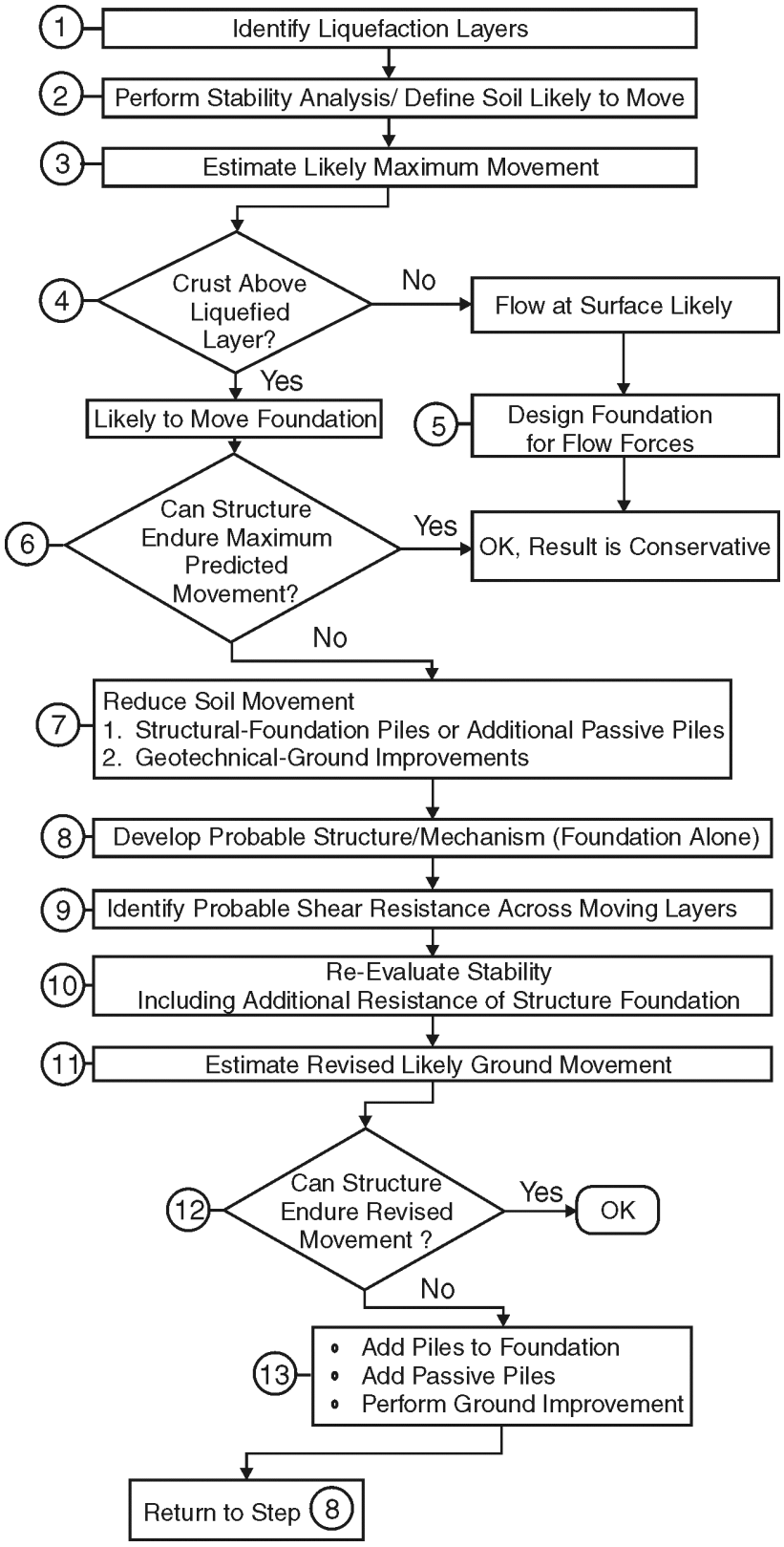

Figure 2.6 Flowchart of Design to Resist Lateral Spreading Forces

may be immediately obvious which condition, soil flow or foundation movement, is more likely. Qualitative illustrations of the two scenarios are given in Figures 2.7 and 2.8.

- Step 5. If flow of soil around the structure is indicated, the foundation is designed to withstand the passive pressures created by the soil flowing around the structure. The induced forces are effectively the largest forces that the structure will experience, and for this reason it is conservative to design a structure for such forces.

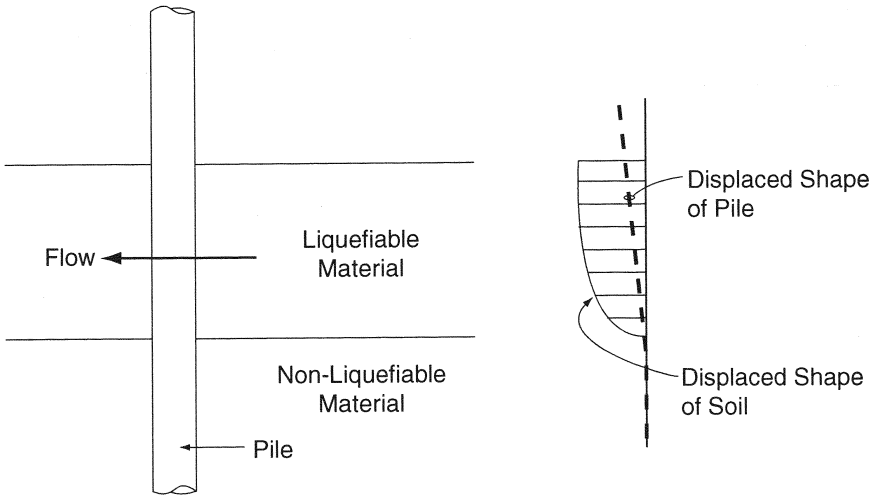

Figure 2.7 Soil Flow Around Piles

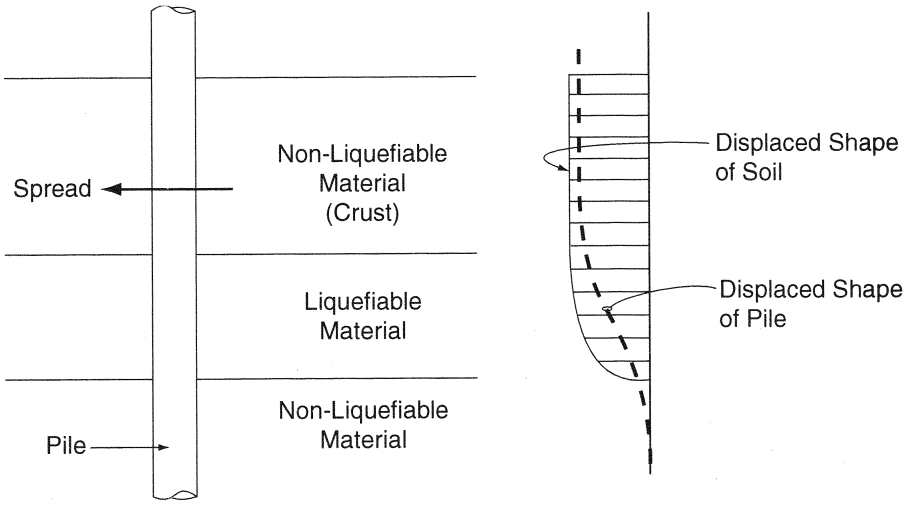

Figure 2.8 Spreading that Displaces Foundation with Soil

- Step 6. If on the other hand, the assessment indicates that movement of the foundation is likely, then the structure must be evaluated for adequacy at the maximum expected displacement. The implication of this assessment is that for relatively large ground movements, soil displacements are likely to induce similar magnitude movements of the foundation. In this context, "large" is taken relative to the structural yield resistance. The resulting induced movements of the foundations may produce substantial plasticity in the foundations, and may induce relatively large reactions in the superstructure.

  The recommended acceptance criteria is the same as for SDAP E, the pushover method. Plastic hinge rotation limits of 0.05 radians are used for an upper level event, and the allowance of plasticity in the foundation is believed to be reasonable, even though plasticity may be below grade, because such damage in the foundation is not likely to pose a collapse hazard.

- Step 7. If such deformations are not acceptable, there are realistically only two ways to restrict the foundation and substructure forces to acceptable values. The first method is to design the foundations to resist the forces that would accompany passive flow of the soil around the foundations. The other method would be to limit the ground movement by providing either ground and/or structural remediation. It is the structural option that provides the most rational first path, and this makes use of the "pinning" or dowel action that pile or shaft foundations contribute as they cross the potential failure plane of the moving soil mass.

- Step 8. The determination of the plastic mechanism that is likely to occur in the presence of spreading should be done in a reasonable manner. Due to the range of inherent uncertainties, great precision in the determination may not produce more accuracy. Thus simple estimates of the mechanism and its corresponding lateral resistance capability is often adequate. For instance, one method is to use the upper bound method of plasticity and postulate potential mechanisms, then using judgment assess the mechanism that is likely to control. The acceptance criteria are basically the structural deformation criteria for SDAP E, which uses the pushover method. In fact, the piles are the elements that limit the acceptable displacements of the system.

  The lateral shear that produces the plastic mechanism can be adjusted downward to account for the driving effect of the P-Δ effect. Because the lateral soil force that produces a plastic mechanism in the foundation/substructure system is required, the reduction in shear required to produce a mechanism due to P-Δ should be considered. Figures 2.9 and 2.10 illustrate a first-order correction for P-Δ effects for a stub abutment and for an intermediate pier with piles and pile cap. Figure 2.11 illustrates a similar correction for an integral abutment supported on piles where the superstructure is capable of providing resistance to the top of the piles.

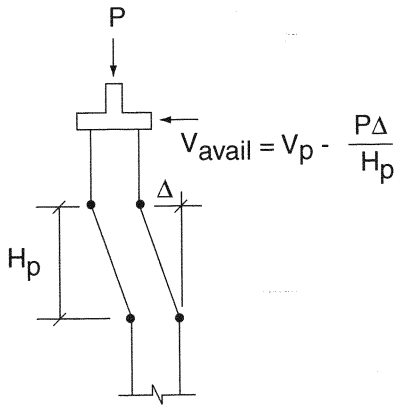

Figure 2.9 Plastic Mechanism of a Stub Abutment with Two Rows of Piles and Sliding Bearing Beneath the Superstructure

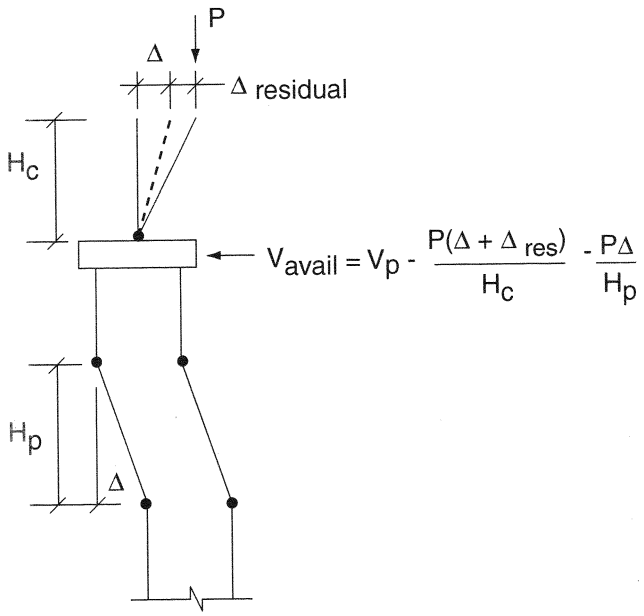

Figure 2.10 Plastic Mechanism for a Pier with Piles and an Integral or Pinned Connection to the Superstructure

A more precise method of determining the plastic mechanism would be to use an approach that ensures compatibility of deformations between the soil and piles (e.g., similar to LPILE) and which accounts for plastic deformations in the piles themselves. This second requirement could be satisfied by using software that is capable of performing pushover analysis, then using p-y curves from a program such as LPILE (Reese et al., 1998) to produce boundary support elements that ensure compatibility.

- Step 9. The system then must be assessed for a prescribed displacement field to represent the likely soil spreading deformation. From this analysis, an estimate of the likely shear resistance the foundation will provide is estimated and this shear can then be incorporated back into the stability analysis.

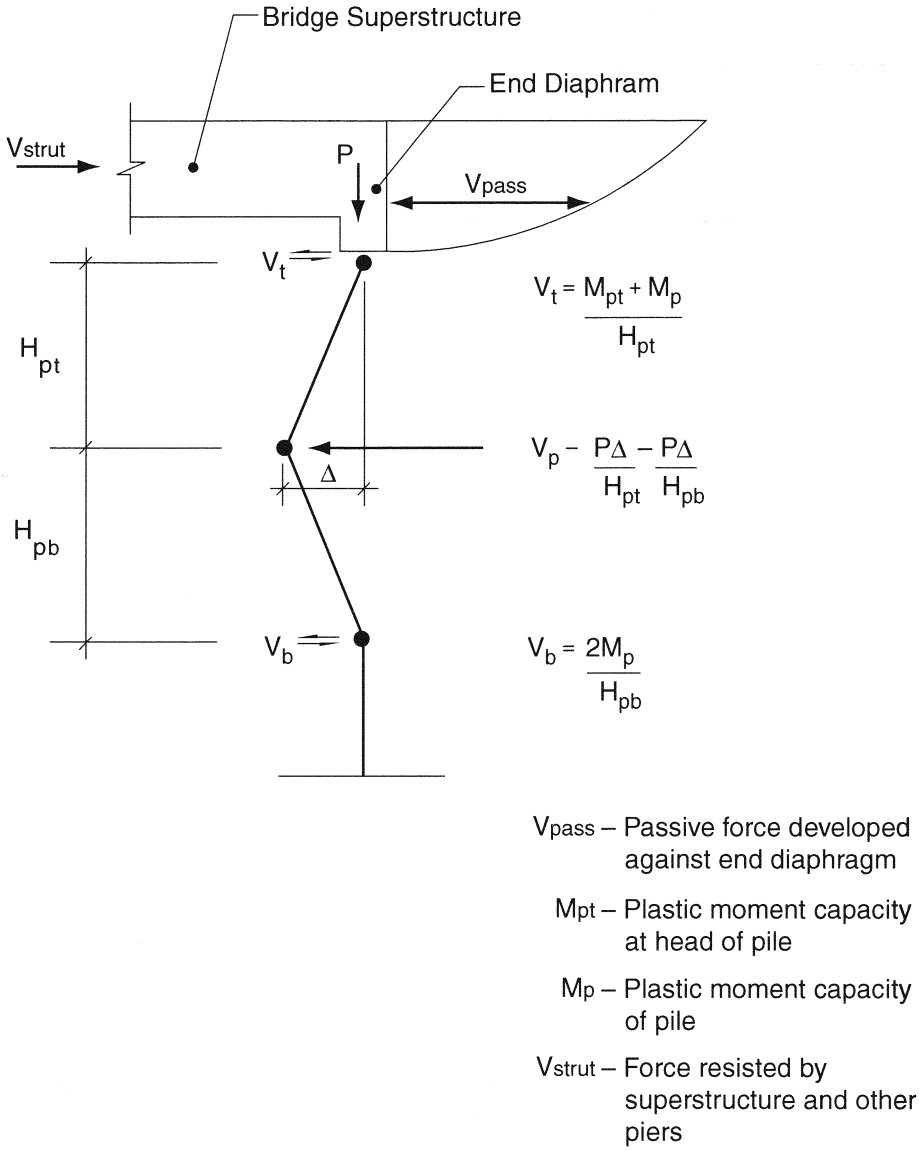

Figure 2.11 Plastic Mechanism for an Integral Abutment Supported on Piles

- Step 10. If substantial resistance is provided, then its effect on limiting the instability driven movement of the soil block should be introduced into the analysis. This step is typically not included in current assessments of potential foundation movements, although inclusion of such resistance may often improve the structure's expected performance.

- Steps 11 and 12. The overall displacement is re-calculated with the revised resistance levels considered. Once a realistic displacement is calculated, then the foundation and structural system can be assessed for this movement. It is at this point that more permissive displacements than for substructure design can be relied upon. This implies

that plastic rotations, and potentially large ones, may be allowed to occur in the foundation under such conditions.

- Step 13. If the structure's behavior is acceptable, then the design is complete; if not, then the engineer must assess whether to try to produce adequacy either through additional piles or shafts, and these may not need to connect to the foundation (passive piles). Alternately, ground improvement approaches may be considered, for instance, stone columns. The selection of structural or geotechnical remediation methods is based on the relative economy of the system being used.

The process is repeated by returning to Step 8 and modifying the available resistance until the slope is stabilized.

3. WESTERN UNITED STATES SITE

3.1 General

The Western U.S. site was selected in the Puget Sound area of Washington for several reasons:

1. The western portion of Washington has many seismic features similar to the coastal areas of Alaska and Oregon. All three states have a potential for earthquakes with a magnitude of 8.0 or more. The primary seismic source for the three states is a subduction zone event, which is somewhat different than the more commonly studied crustal mechanisms of California. It was therefore reasoned that results from the Washington evaluation would also be meaningful to Oregon and Alaska.
2. As a result of the recommended changes from a 475-year to a 2,475-year design basis, acceleration levels will increase by a factor of two or more (i.e., from 0.3g to 0.6g in the Puget Sound area), similar to the other two states. For all three states, the increase in acceleration level occurs in a highly populated area, and therefore the economic consequences of the change could be significant.
3. The geology of Washington is not unlike that which occurs in Alaska and Oregon. All three have soils that result from rapid erosion of soils deposited by recent volcanic activity. All three sites also often have very hard soils located below the recent materials, typically occurring within 100 feet of the ground surface.
4. The Washington State Department of Transportation (WSDOT) initially expressed greatest concern about the implications of the recommended changes and their effects on liquefaction potential. When contacted regarding the study, they indicated considerable interest in assisting with this evaluation and offered to work with members of the project team in selecting a suitable site and bridge configuration. Since two members of the project team are located in Washington, logistics of meeting with the WSDOT staff were simplified.

During the course of the study, members of the project team met with WSDOT staff several times to discuss alternatives to obtain data and to seek WSDOT's views and advice on assumptions made for conducting the study. These meetings were very helpful to the project team in identifying the owner's perspective in approaching the liquefaction assessment.

3.2 Site Selection and Characterization

Because the purpose of the study was to investigate sites that are realistic, an actual site was chosen as the prototype for the Western U.S. site. The site is located within a large river basin in the Puget Sound area of Washington State, and it is situated near the mouth of the river in the estuary zone. The basin is an area that was overridden by glaciers during the last ice age and therefore has over consolidated material at depth. Additionally, the basin contains significant amounts of recently deposited loose material over the glacially consolidated materials.

3.2.1 General Geology for the Site

Due to the influence of the Cascadia Subduction Zone, a back arc of volcanoes exists all along the west slopes of the Cascade Mountains. In this case, Mt. Rainier lies to the east and up river of the site. Eruptions of this volcano in the recent geologic time have added significant depths of loose, unconsolidated material in the basin. This situation is not unusual in the Pacific Northwest, and consequently many of the river basins have significant extents of liquefiable soils, comprised of young deposits of silts and sands.

3.2.2 Site Information

Following meetings with WSDOT's bridge and geotechnical staff, a prototype site was selected. This site had undergone a recent detailed exploration by WSDOT. The available data from the site included multiple CPT soundings to over 150 feet depth, SPTs using a calibrated automatic hammer, and shear wave velocity measurements to depths of 100 feet. Seismic CPT procedures were used to determine the shear wave velocities. WSDOT also had conducted an extensive laboratory testing program, including grain-size analyses, water content determinations, and Atterberg limit tests. All exploration data, including CPT data in digital form, were provided to the project team.

After reviewing the information provided by WSDOT, soil conditions at one of the bridge piers were selected to represent the soil profile for the study. This location, which is referred to as Location H-13 after the borehole designation, was selected from the available information for two reasons: (1) a pair of explorations consisting of a CPT sounding (C-8) and an SPT soil boring (H-13) was available at this location and (2) the range of CPT and SPT data was such that some layers in the upper 75 feet were more liquefiable than others. Note that no effort was made to investigate other locations or to combine SPT and CPT data from other locations to define a composite site condition. For demonstration purposes, this was not thought to be needed. However, in an actual design study, all locations would normally have to be considered in the liquefaction assessment.

Soil profiles established by WSDOT during their original design work on this project are included in Appendix B. Boring log H-13 and CPT log C-8 are also included in this appendix.

3.2.3 Simplified Soil Model Used for Evaluation

At the prototype site, the material at depths less than 150 feet are generally alluvial deposits. At greater depths, some estuarine materials exist and below about 200 feet dense glacial materials are found. This then produces a site with the potential for deep liquefiable soils.

The actual soil profile at the site has many layers of material with broad variations of properties and densities. Figure 3.1 shows the SPT and CPT data that were selected to represent the prototype site. Of note are the low SPT blow counts at depth and the variations of the CPT data.

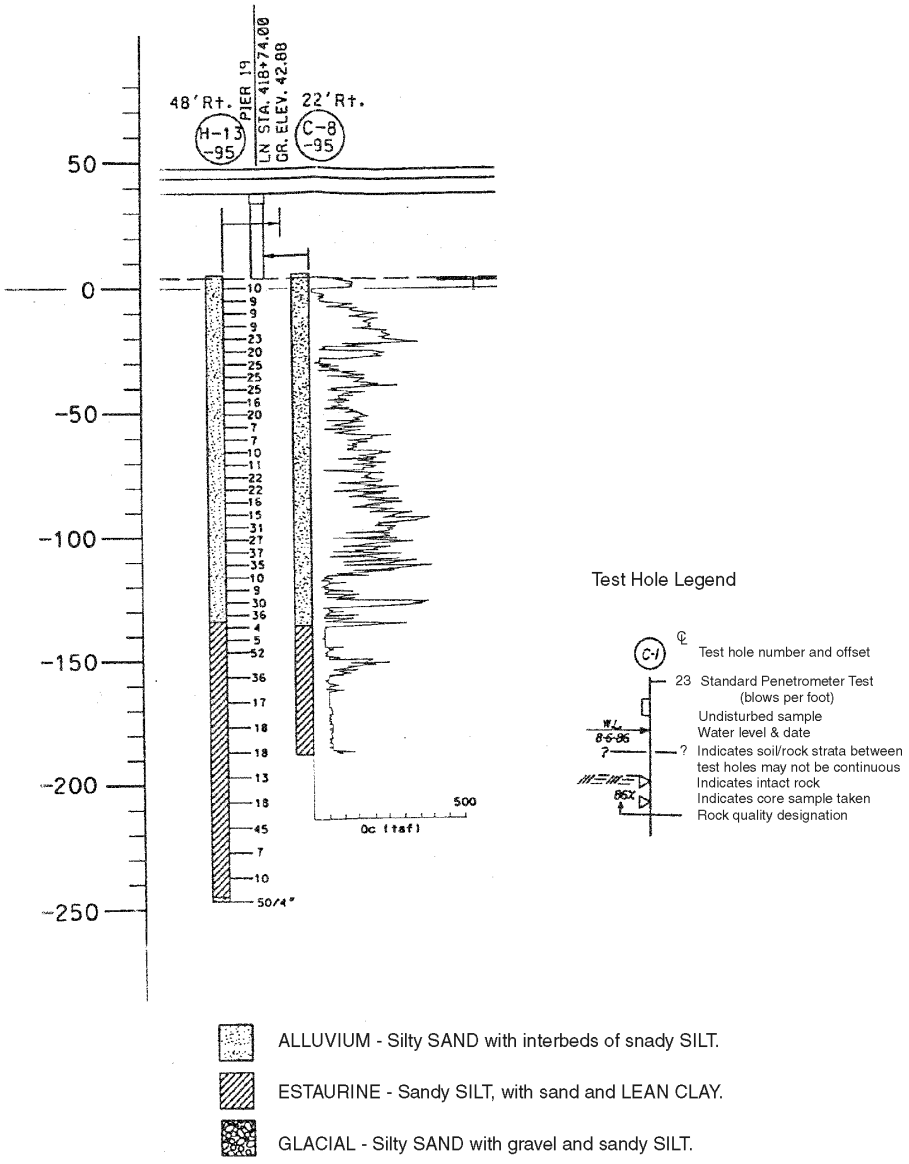

Figure 3.1 Typical Boring Data for Prototype of Western Washington Site

For the purposes of this study, the actual site profile was simplified such that fewer layers exist and the profile is the same across the entire site. The simplified profile retains features and layering that produce the significant responses of the actual site. The simplified soil profile is given in Figure 3.2. This figure also includes relevant properties of the soil layers that have been used for the seismic response assessments and bridge design. Shear wave velocity (V_s), undrained shearing strength (c_u), soil friction angle (φ), and residual soil strength (S_{ur}) were interpreted from the field and laboratory data provided by WSDOT for an actual site with similar geologic history. The cyclic resistance ratio (CRR) was obtained by conducting simplified liquefaction analyses using both the SPT and CPT methods to obtain CRR values. These CRR values are plotted in Figure 3.3. Average CRR values were determined for liquefiable materials, and represent clean sand values for a M7.5 event.

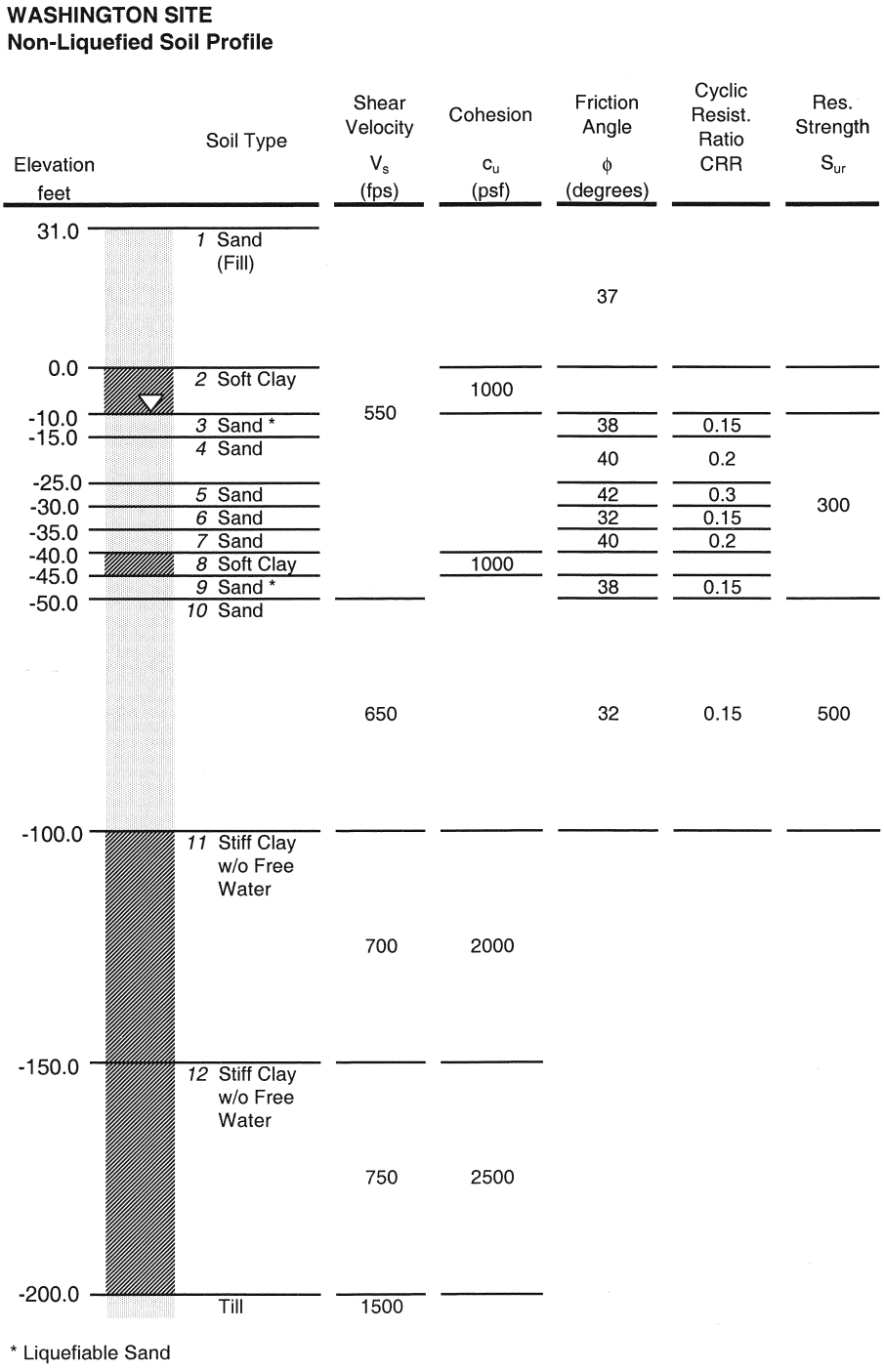

Figure 3.2 Simplified Soil Profile for the Western U.S. Site

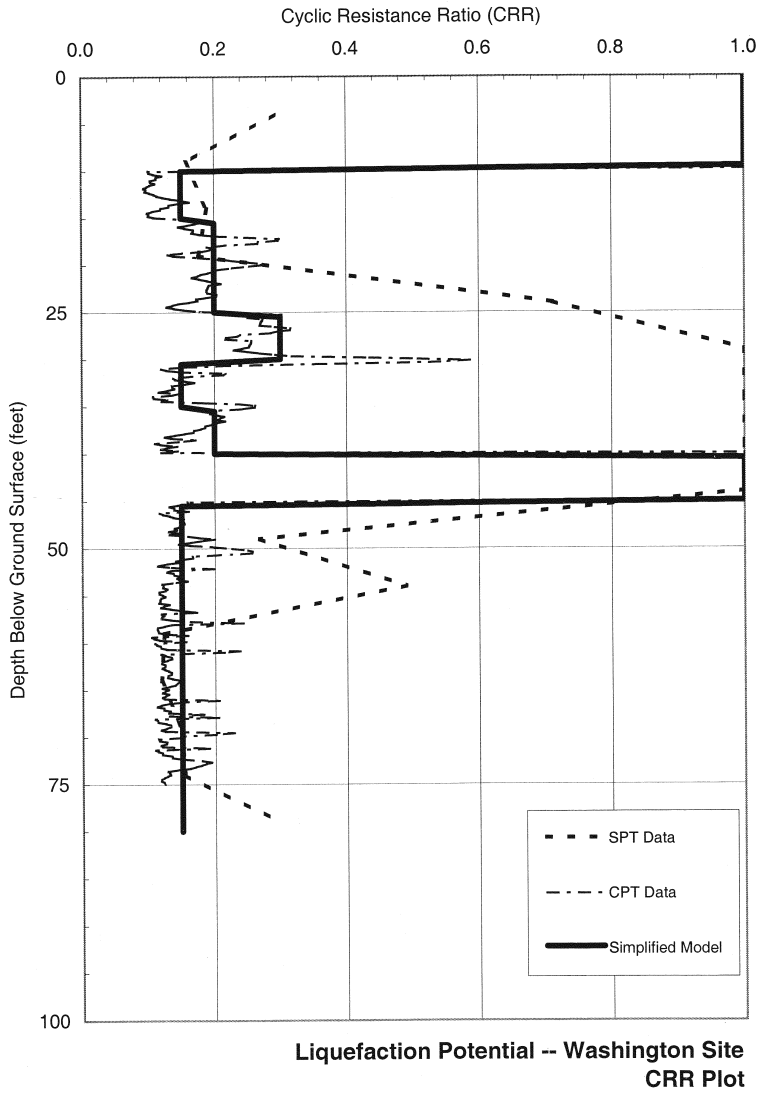

Figure 3.3 WSDOT Location H-13 CRR Plot

Figure 3.3 shows that relatively similar CRR values were obtained from the SPT and CPT methods except between 25 and 40 feet depth. In this depth interval, the CRR from the SPT was significantly higher, indicating material with much higher resistance to liquefaction. These higher values were consistent with higher SPT blow counts. In the same depth interval, the CPT did not detect significantly stronger materials. The two explorations are located 70 feet apart, probably indicating different soil conditions at the two locations. For this study, priority was given to the CPT results when establishing a simplified soil model. However, if this were for an actual design, more detailed studies would be conducted to determine which of the two methods provided the more reliable data in this depth range, or if it reflected actual differences in material conditions between the exploration locations.

The prototype site profile and the structure elevation are shown in Figure 3.4. The modified site is a smaller river crossing than the original since the total length of the bridge was substantially shortened for the study. Only enough length was used to illustrate the issues of soil movement and design. In this case, the total length of the bridge is 500 feet. The ground surface is shown in Figure 3.4 as the 0-foot elevation. As can be seen in the figure, approach fills are present at both ends of the bridge, and in this case, they are relatively tall at 30 feet each.

An approach fill comprised of a relatively clean sandy gravel was assumed at each abutment. The sandy gravel was assigned a friction angle of 37 degrees.

3.3 Bridge Type

The prototype bridge from which the study data were drawn is a river crossing with several superstructure and foundation types along the structure. The actual structure was simplified for the study. The 500-foot long structure is comprised of a 6-foot deep concrete box girder that is continuous between the two abutments. The intermediate piers are two-column bents supported on pile caps and 24-inch steel piles filled with reinforced concrete. The roadway is 40 feet wide. The two 4-foot diameter columns for each pier are approximately 23 feet apart, and due to the relatively large size of the pile caps, a single combined pile cap was used for both columns at each pier. Figure 3.5 shows the general arrangement of an intermediate pier.

The centermost pier in this example is located at the deepest point of the river channel, as shown in Figure 3.4. While this is somewhat unusual, in that a longer span might often be used to avoid such an arrangement, the river pier was used here for simplicity. The columns of this pier are also relatively slender, and they were deliberately left this way to allow any negative seismic effects of the slenderness, for instance P-Δ, to be assessed. In a final design, the size of these columns might likely be increased. In fact, non-seismic load combinations/conditions may require the columns to be enlarged.

The abutments are of the overhanging stub abutment type. Figure 3.6 shows the transverse and longitudinal elevations of the abutments used for the bridge. For this type of abutment, the backfill is placed directly against the end diaphragm of the superstructure. This has the seismic advantage of providing significant longitudinal resistance for all displacement levels, since the passive resistance of the backfill is mobilized as the superstructure moves. This type of abutment also eliminates the need for expansion joints at the ends of the structure, and for this reason, is limited to the shorter total length structures.

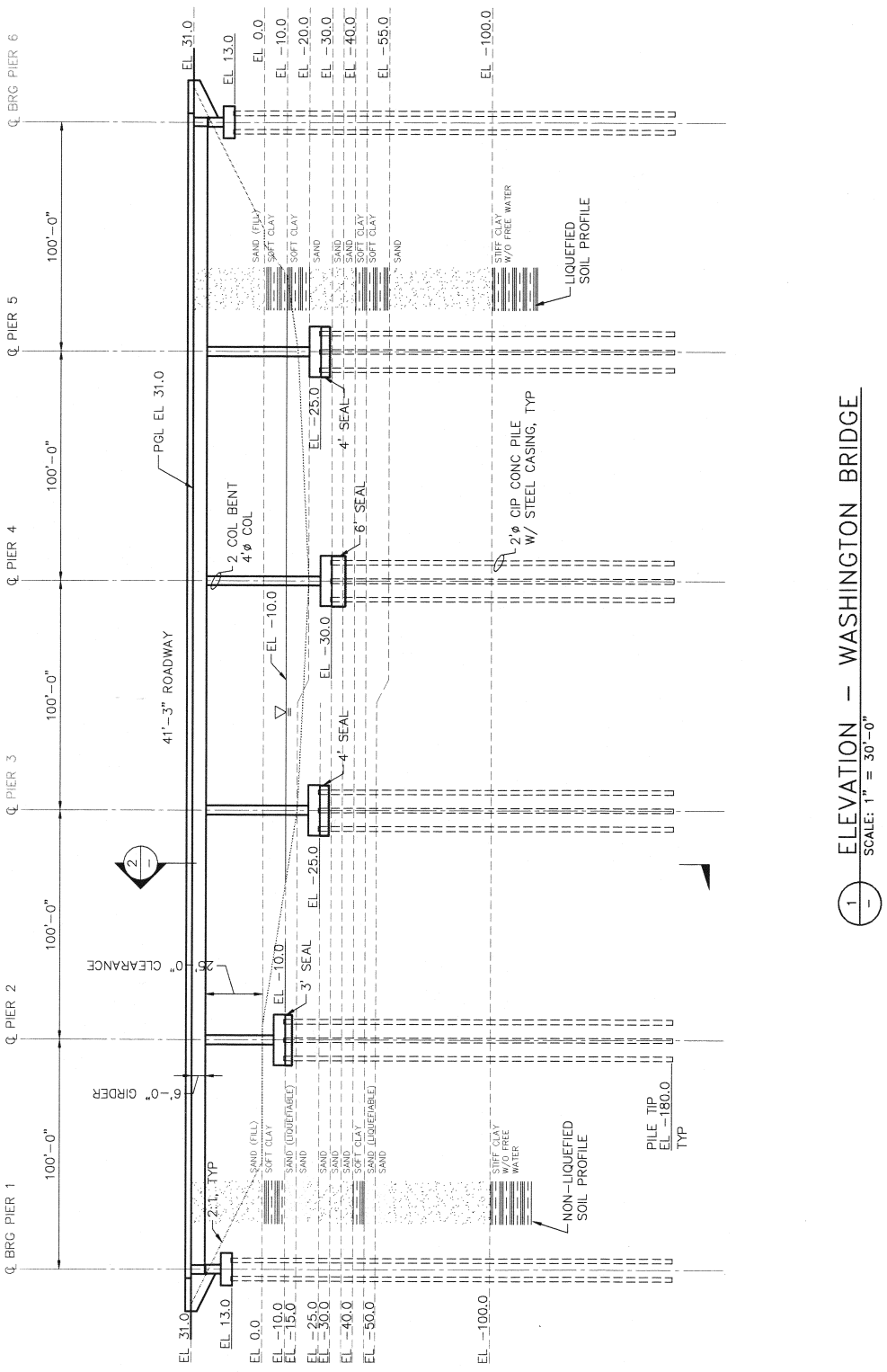

Figure 3.4 Site Profile and Structure Elevation

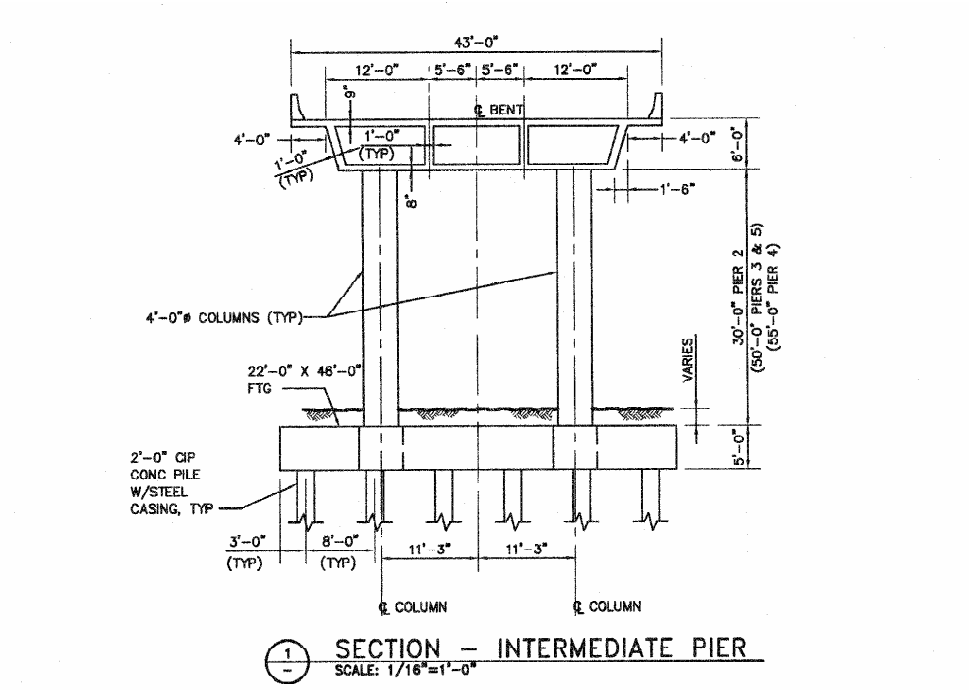

Figure 3.5 Elevation of an Intermediate Pier

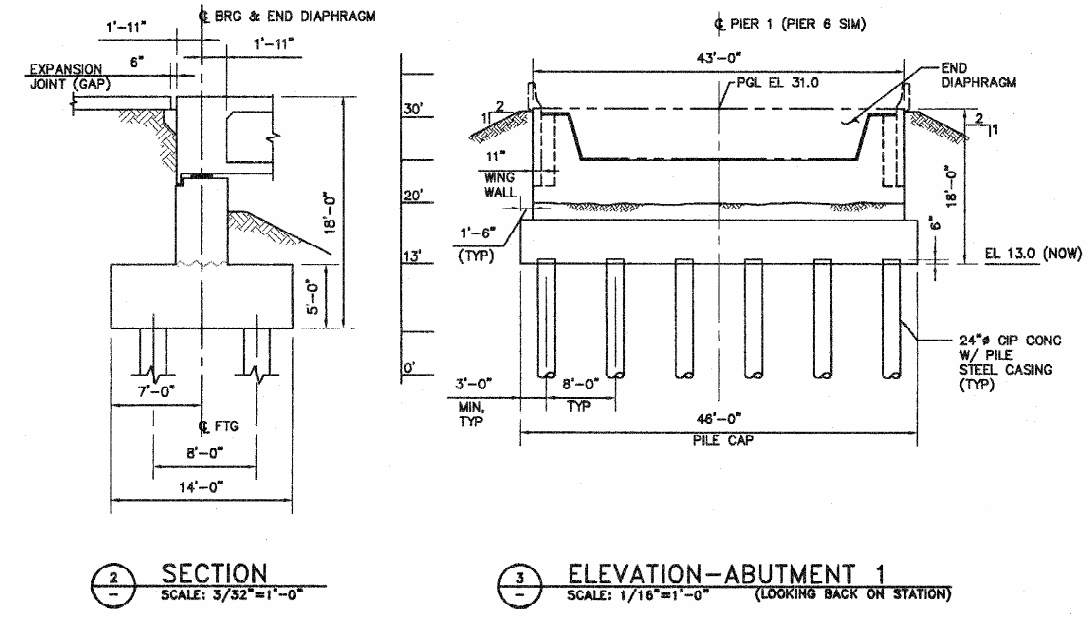

Figure 3.6 Elevations of the Abutment

The structure has also been simplified to have no horizontal curves, vertical curves, crowns, or superelevation. It has no grade from one end to the other, and it has no skew. All the piers and abutments are square to the profile grade line of the structure.

The foundations are comprised of 24-inch steel pipe piles that are driven 180 feet into the native material. This is similar to the piles used for the actual structure. The piles are filled with concrete over their entire length and this concrete contains a reinforcing cage over the entire height. At each pier, the piles are driven in three rows longitudinally and at the abutments, the piles are arranged in two rows. This provides overturning resistance to the abutment system. The lower portion of the abutment must resist the active soil pressures that develop, whereas the upper portion, which comprises the end diaphragm, has the lateral earth pressures delivered directly to the superstructure and not to the abutment. The abutments also support standard wingwalls to contain the backfill soil in the transverse direction.

3.4 Earthquake Hazard Levels

The site identified by WSDOT for this study is located on the Duwamish River, approximately four miles south of downtown Seattle. A preliminary review of the potential seismic loading at this site determined that the 2,475-year return period design motion would be dominated by a seismic event on the Seattle Fault, which occurs just north of the site. An event on this source mechanism would produce very high firm-ground accelerations at the site (e.g., in excess of 0.7g) and a unique response spectrum because of the proximity of the site to the fault. The Seattle Fault does not, however, contribute to the 500-year motions because of its assigned recurrence rate. In view of the somewhat unique loading caused by the Seattle Fault for the upper level return period, a decision was made to "move" the site to a location that would not be dominated by a single source mechanism. The benefit of this relocation was also that seismic source conditions would be more representative of western Washington, as well as Alaska and western Oregon. Olympia, Washington was selected as the new site; actual soil conditions were not modified from the simplified model described previously.

3.4.1 Design Response Spectra

The design response spectra for current AASHTO Specifications and recommended LRFD Specifications were constructed using the procedures and site factors described in the respective specifications. For current AASHTO Specifications, the hazard level of 10 percent probability of exceedance in 50 years was used. For the recommended LRFD Specifications, both the rare earthquake (termed Maximum Considered Earthquake or MCE) having a probability of exceedance of 3 percent in 75 years with deterministic bounds near highly active faults and the frequent earthquake (also termed the expected earthquake) having a probability of exceedance of 50 percent in 75 years were used as design earthquakes. The probability of exceedence of 3 percent in 75 years is equivalent to a return period of 2,475 years, similarly, the probability of exceedence of 10 percent in 50 years is equivalent to 475 years, and the probability of 50 percent in 75 years is approximately equivalent to 100 years.

Design response spectra based on current AASHTO Specifications were constructed using a (rock) peak ground acceleration (PGA) of 0.24g for the Olympia site. This peak ground acceleration value was determined from the AASHTO map contained in the current AASHTO Specifications. Design spectra for the MCE of the recommended LRFD Specifications were constructed using rock (site class B) spectral accelerations at 0.2-second period and 1.0-second period. These two spectral values were obtained from maps published by the U.S. Geological Survey (USGS) and contained in the recommended LRFD Specifications. This information is also available from the "Seismic Design Parameters" CD-ROM prepared by the USGS (Leyendecker et al., 2000). The procedures used to construct the design spectra for the frequent earthquake are similar to those of the MCE. However, because paper maps for the probability level of the frequent earthquake (50 percent probability of exceedance in 75 years) are not yet available, the needed spectral values at 0.2-second and 1-second periods were interpolated from the hazard curves published on the CD-ROM containing the USGS national probabilistic ground motion mapping results (Frankel and Leyendecker, 2000). The 0.2-second and 1.0-second spectral accelerations on rock for the MCE and the frequent earthquake of the recommended LRFD Specifications are summarized in Table 3.1.

Table 3.1 0.2-Second and 1.0-Second Spectral Acceleration on Rock (Site Class B) for the Rare Earthquake (MCE) and the Frequent Earthquake for the Olympia, Washington Site

	Response Spectral Accelerations on Rock (Site Class B)	
Earthquake	**0.2-Second Period**	**1.0-Second Period**
MCE	1.175	0.411
Frequent	0.261	0.081

Figure 3.7 presents the design response spectra for current AASHTO Specifications, on site class II, and for the MCE of the recommended LRFD Specifications, on site class C. These site classifications represent the assessed subsurface conditions defined at the base of the soil column, for which outcropping acceleration time histories were developed for the site response analyses to assess the liquefaction hazard at the site.

Figure 3.8 presents the design response spectra for current AASHTO Specifications, on soil profile type III, and for the MCE and the frequent earthquake of the recommended LRFD Specifications, on site class E. These site classifications represent the assessed soil profile below the ground surface where response spectra are defined for structural vibration design and peak ground accelerations are used for simplified liquefaction analyses. Note in Figure 3.7 and Figure 3.8 that the short-period branch of the AASHTO spectra are assumed to drop from the acceleration plateau at a period of 0.096 seconds to the peak ground acceleration at 0.02-second period, the same as for the MCE spectra. Also note that, because the long-period branch of the AASHTO spectra declines more slowly with period than those of the MCE (as $1/T^{2/3}$ in AASHTO compared to 1/T in the recommended LRFD Specifications), the AASHTO and MCE spectra come closer together as the period increases.

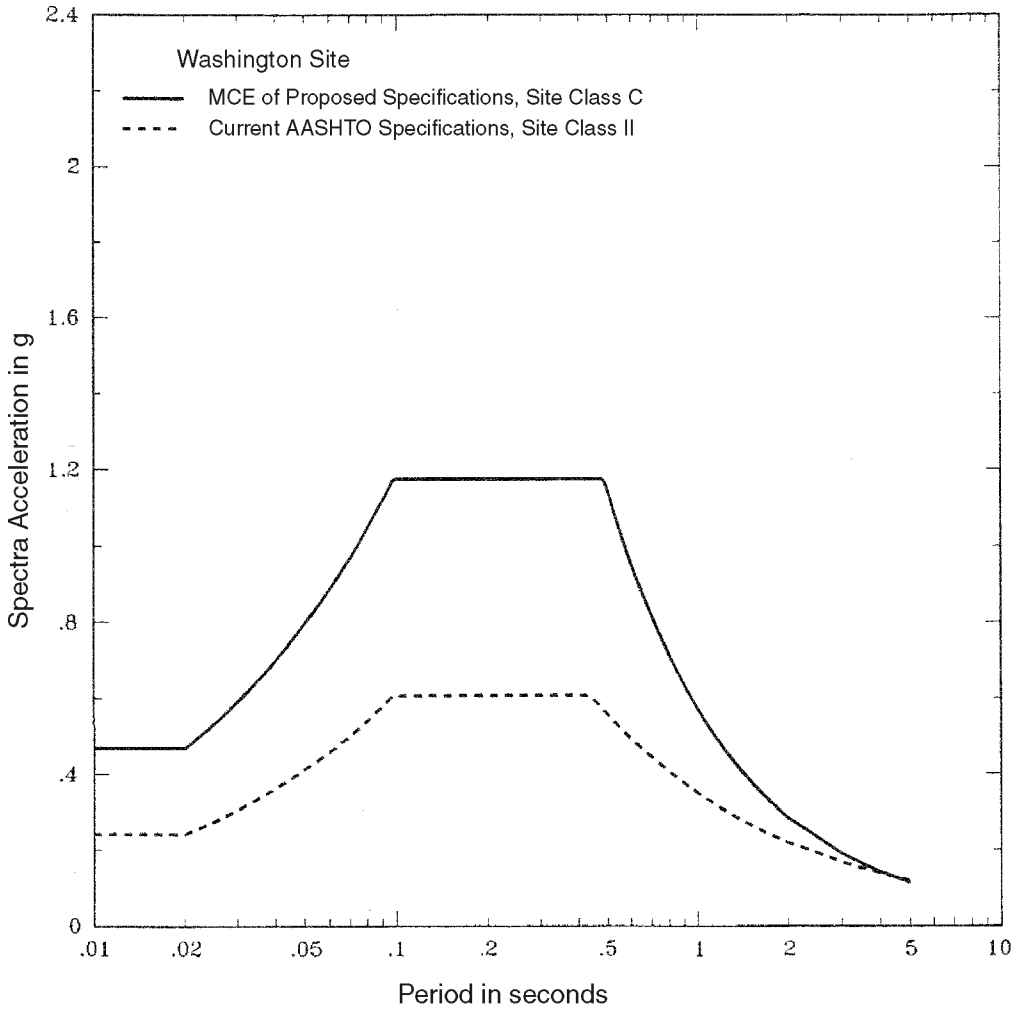

Figure 3.7 Design Response Spectra Based on Current AASHTO Specifications, Site Class II, and the MCE of Recommended LRFD Specifications, Site Class C, Washington Site

3.4.2 Acceleration Time Histories

3.4.2.1 Approach for Time History Development

Acceleration time histories consistent with current AASHTO Specifications and with MCE ground motions of the recommended LRFD Specifications were developed as firm soil outcropping motions for input to the one-dimensional, nonlinear site response analyses to assess the liquefaction hazard of the site. These time histories were developed in accordance with the requirements and guidelines of the recommended LRFD Specifications and the following steps:

1. Identify earthquake magnitudes and source-to-site distances that contribute most significantly to the ground motion hazard at the site;
2. Select recorded acceleration time histories representative of the conditions assessed in (1); and

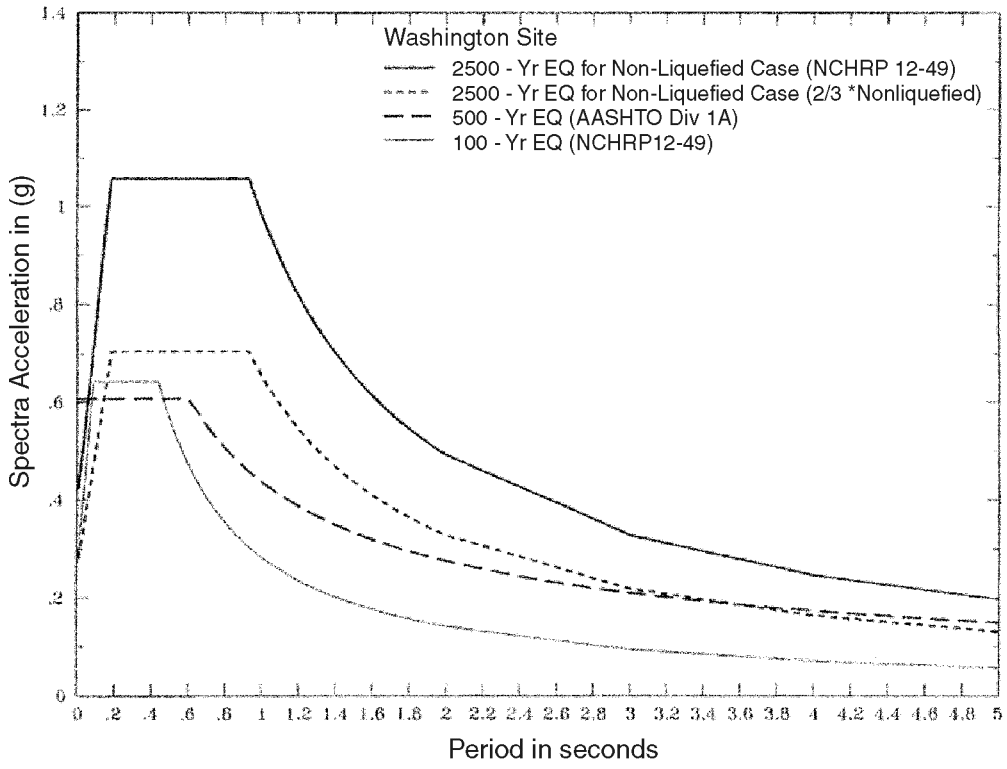

Figure 3.8 Design Response Spectra Based on Current AASHTO Specifications, Site Class III, and the MCE and the Frequent Earthquake of Recommended LRFD Specifications, Site Class E, Washington Site

3. Scale the time histories selected in (2) to the approximate level of the spectra shown in Figure 3.7 and then modify the time histories through a spectral matching process so that the spectra of the time histories approximately match the design response spectra in selected period ranges.

3.4.2.2 Deaggregation to Determine Magnitude and Distance Contributions to the Ground Motion Hazard

To accomplish Step 1 above, the contributions to the ground motion hazard at the Olympia site were deaggregated using the resources provided by the USGS Internet web site *(http://geohazards.cr.usgs.gov/eq/)*. Hazard deaggregation was obtained for the return periods of 475 years and 2,475 years, which correspond to the probabilities of exceedance for the current AASHTO Specifications and the MCE of the recommended LRFD Specifications, respectively. Deaggregation plots for the 475- and 2,475-year return periods are shown in Figure 3.9 and Figure 3.10 for response spectral accelerations at zero-period, respectively. Similar deaggregation plots for the 475-year and 2,475-year return periods for a 0.2-second period and 1.0-second period are given in Appendix C, Figure C.1 through Figure C.4.

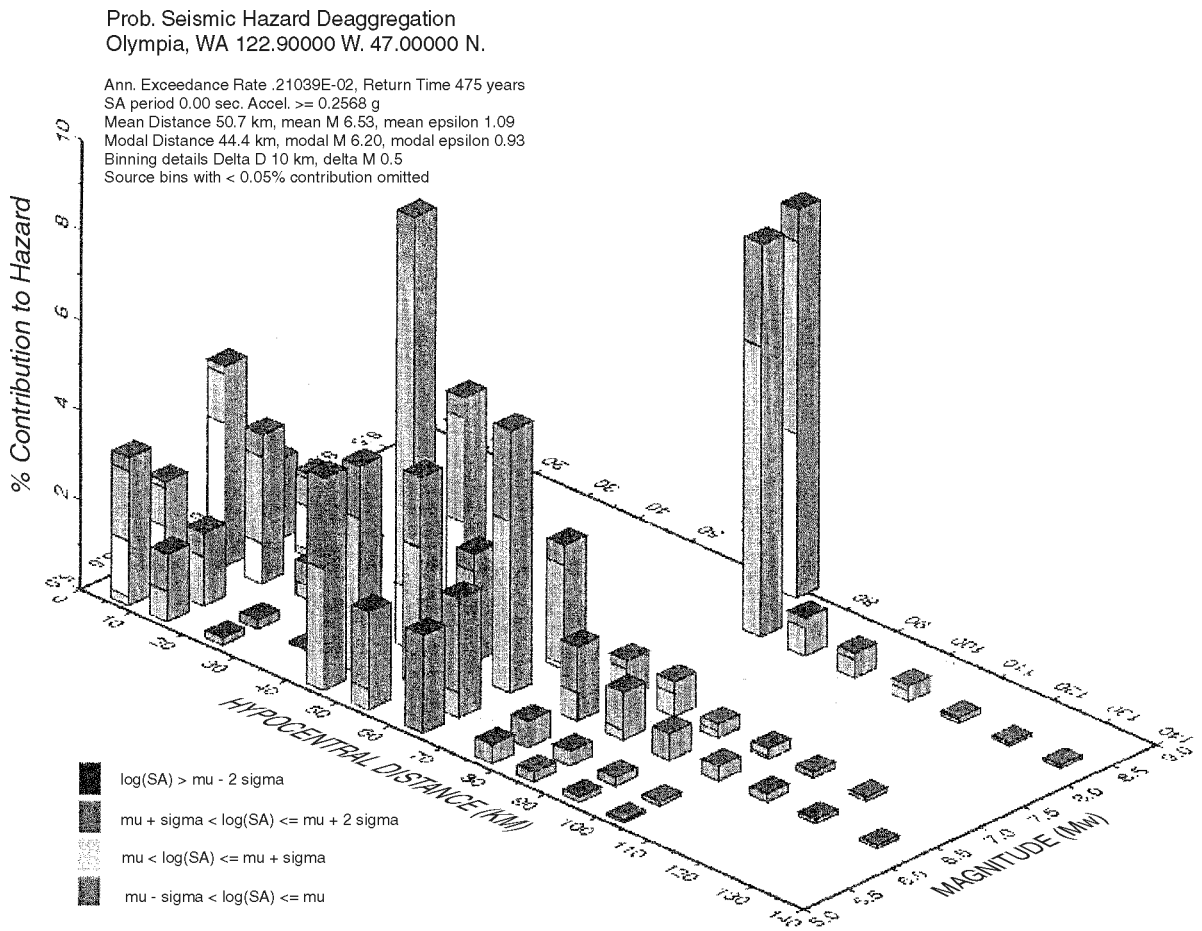

Figure 3.9 Hazard Deaggregation, 475-Year Return Period, Zero-Period Spectral Acceleration, Washington Site

In all of these deaggregation plots, the relative contribution to the ground motion hazard (defined as the percentage contribution to the annual frequency of exceedance, where the annual frequency of exceedance is the reciprocal of the return period) is portrayed by the relative height of the columns occupying different magnitude and distance ranges contributing to the hazard. Also indicated for each column is the distribution of contributions coming from different parts of the uncertainty band around the median predictions of the ground motion attenuation relationships used in the USGS probabilistic ground motion analyses.

Comparisons of Figure 3.9 and Figure C.1 with Figure C.2 and Figure 3.10 and Figure C.3 with Figure C.4 show that, for both a 475-year return period and a 2,475-year return period, the relative contributions of magnitudes and distances to the hazard are quite different for short-period and long-period ground motions. For both return periods, the long-period (1.0-second) contributions are dominated by magnitude 8 to 9 earthquakes occurring 70 to 80 km from the site (Figure C.2 and Figure C.4). These are megathrust earthquakes occurring on the Cascadia subduction zone interface between the Juan de Fuca plate and the North American plate. On the other hand, significant contributions to the probability of exceeding short-period ground motions (Figure 3.9, Figure C.1, Figure 3.10 and Figure C.3) come from three magnitude-distance ranges:

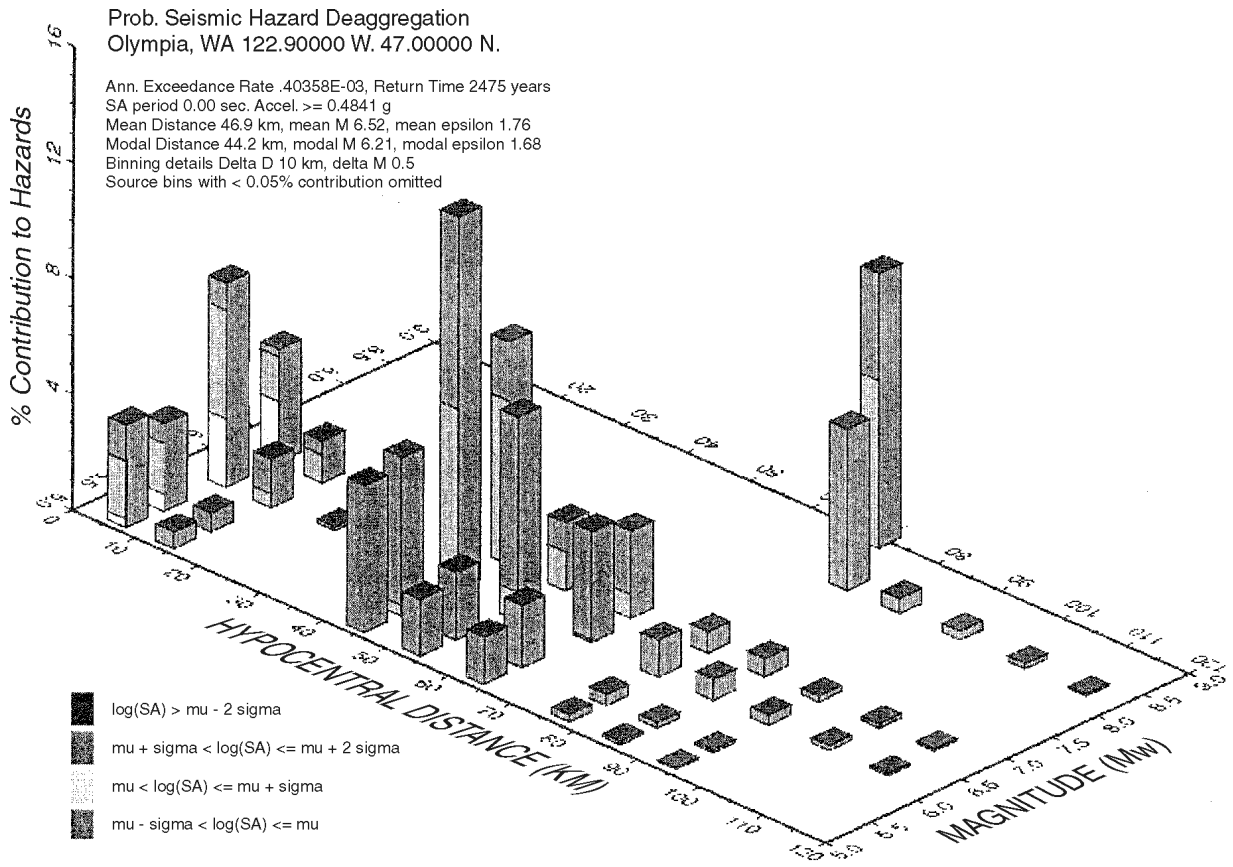

Figure 3.10 Hazard Deaggregation, 2,475-Year Return Period, Zero-Period Spectral Acceleration, Washington Site

(1) magnitude 8 to 9 earthquakes occurring at 70 to 80 km distance; (2) magnitude 5 to 7 earthquakes occurring at 40 to 70 km distance; and (3) magnitudes 5 to 6.5 earthquakes occurring at distances less than 20 km. These three magnitude-distance ranges are associated, respectively, with (1) large-magnitude subduction zone interface earthquakes mentioned above, (2) moderate magnitude earthquakes occurring within the subducting slab of the Juan de Fuca plate at depths beneath western Washington and in the shallow crust of the North American plate at relative large distances from the site, and (3) moderate magnitude earthquakes occurring in the shallow crust of the North American plate in the near vicinity of the site.

3.4.2.3 Selection of Recorded Time Histories

Three natural recordings were selected to represent the acceleration time histories from the three types of earthquakes summarized above. Table 3.2 summarizes the selected ground motion recordings and their earthquake sources. The three earthquake recordings are 1) a large megathrust subduction zone earthquake (1985 Chile earthquake), 2) a moderate magnitude

subduction zone intraslab earthquake (1949 western Washington earthquake); and 3) a moderate magnitude local shallow crustal earthquake (1986 North Palm Springs, California earthquake).

Table 3.2 Time Histories Selected to Represent the Design Earthquakes for the Washington Site

Earthquake Name	Station Name	Component	M_w	Distance (km)	PGA (g)
1985 Chile Earthquake	San Fernando	90	7.9	66.8	0.339
1949 Western Washington Earthquake	Olympia	86	7	75.9	0.274
1986 North Palm Springs Earthquake	Desert Hot Springs	90	6	8.0	0.406

3.4.2.4 Scaling and Spectral Matching of Selected Time Histories

Each of these recordings was first scaled to the approximate level of the design spectra representing the outcropping motions for the site response analysis for the current AASHTO Specifications and the MCE of the recommended LRFD Specifications (Figure 3.7). Then a time-domain spectrum-matching process (Lilhanand and Tseng, 1988; Abrahamson, 1992) was undertaken to adjust each time history to approximately match the design spectra (for current AASHTO and for the recommended MCE) over a selected period range. Representative results of the scaling process are presented in Figure 3.11 through Figure 3.15. Additional results are included in Appendix C.

Figure C.5 through Figure C.7 compare the response spectra of the three time histories before and after spectral matching with the design spectrum based on current AASHTO. Figure 3.11 compares the response spectra of the three time histories, after spectral matching, with the AASHTO spectrum. Similar comparisons to the MCE spectrum of the recommended LRFD Specification are shown in Figure C.8 through Figure C.10 and Figure 3.12. Because the megathrust event on the subduction zone interface dominates the contributions to the frequency of exceeding the long-period spectral accelerations, only the time history for this megathrust event was matched to the long-period declining branch of the spectrum. All three time histories were matched to the short-period part of the design spectra because each earthquake type contributed significantly to the frequency of exceeding the short-period part. Matching the interface event time history (the 1985 Chile earthquake recording) to the entire spectrum is somewhat conservative for the short-period part of the spectrum because the other two types of earthquakes also contribute significantly to the frequency of exceedance in the short period range. Although a lower short-period response spectrum could be justified for the interface event time history, such an adjustment was not made for this analysis because it would not affect the conclusions of the liquefaction hazard analysis at the Olympia site.

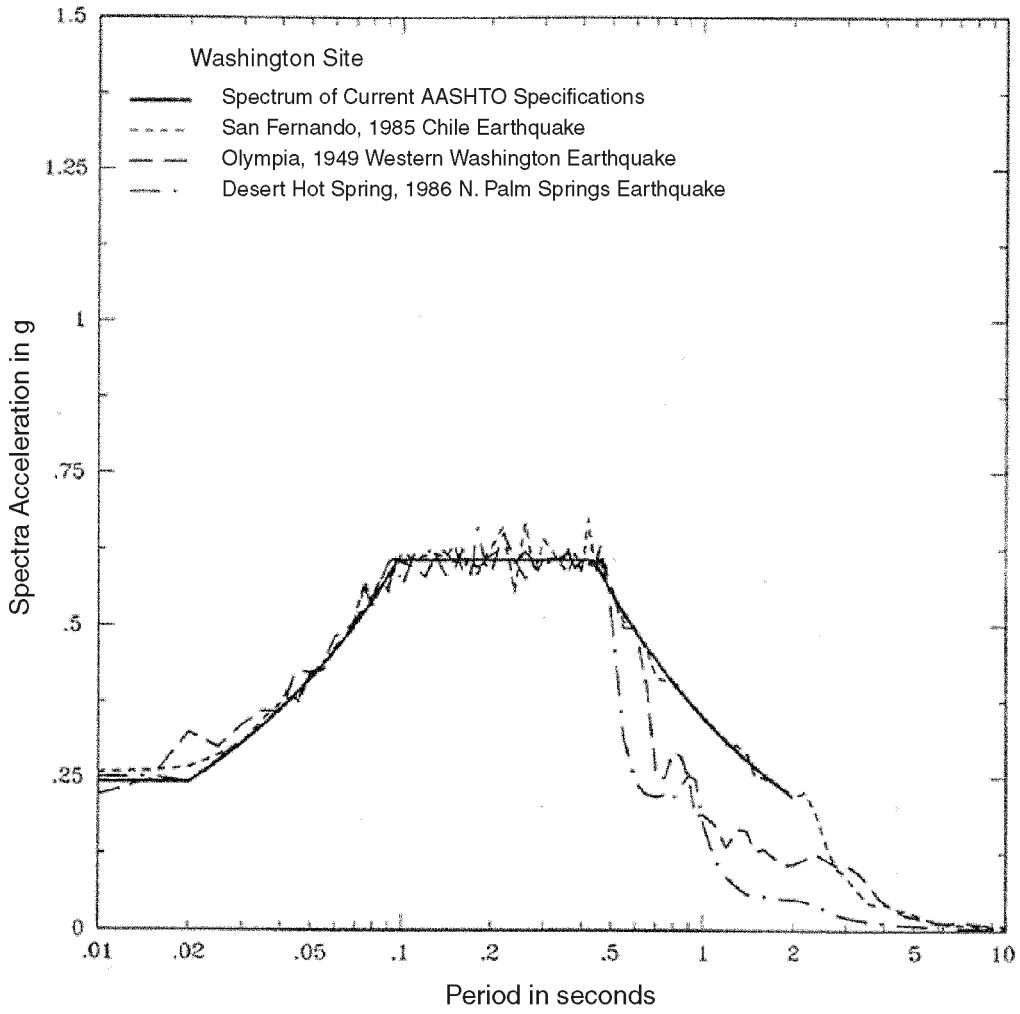

Figure 3.11 Comparison of Response Spectra of Spectrum-Matched Time Histories With Design Response Spectrum Based on Current AASHTO Specifications, Site Class II, Washington Site

Figure 3.13, Figure C.11 and Figure C.12 show the acceleration, velocity, and displacement time histories of the three selected recordings before scaling and spectral matching. Representative time histories after scaling and spectral matching to the design spectrum of current AASHTO Specifications are shown in Figure 3.14, Figure C.13 and Figure C.14. Similarly, the time histories after scaling and spectral matching to the design MCE spectrum of the recommended LRFD Specifications are shown in Figure 3.15, Figure C.15 and Figure C.16. Comparisons of Figure 3.13 with Figure 3.14 and Figure 3.15 illustrate that the spectral matching process did not greatly alter the pulse sequencing of the time histories.

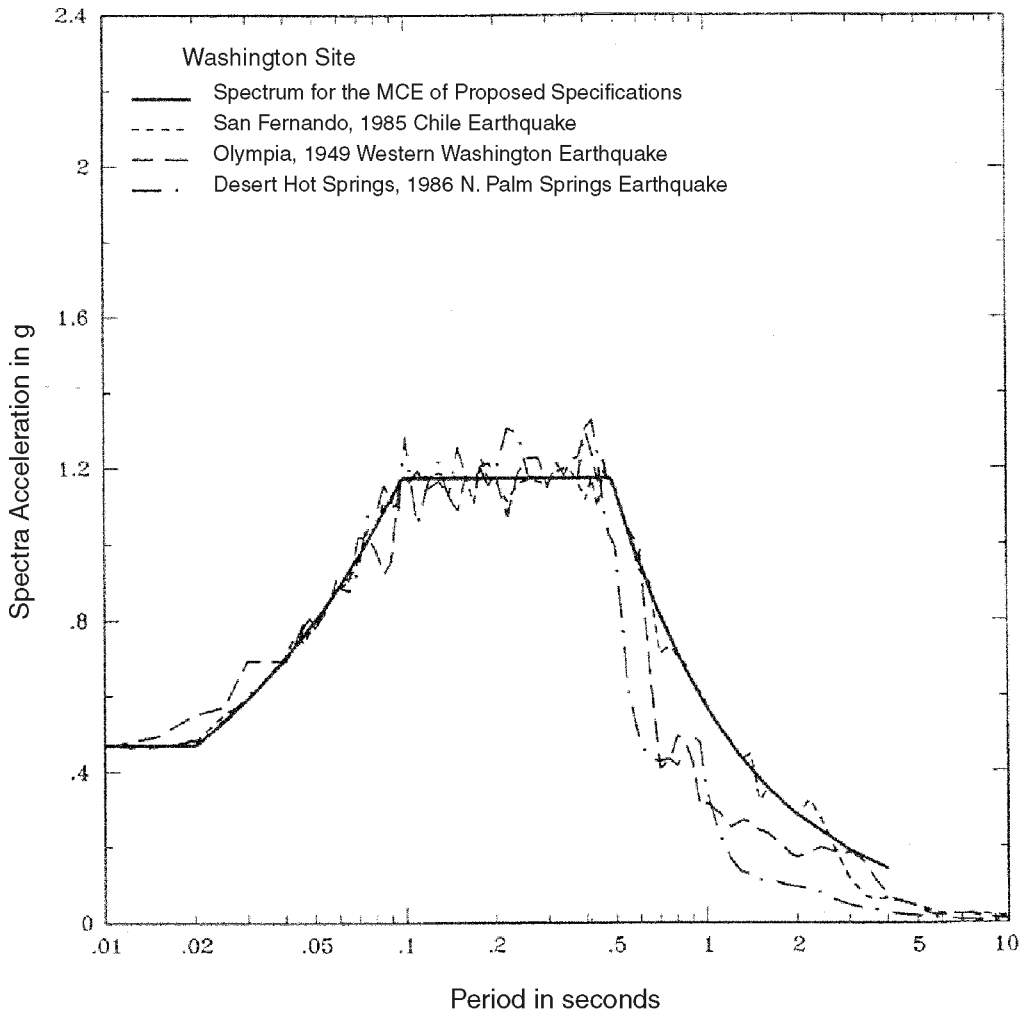

Figure 3.12 Comparison of Response Spectra of Spectrum-Matched Time Histories With MCE Design Response Spectrum of Recommended LRFD Specifications, Site Class C, Washington Site

3.5 Ground Response Studies

The ground response study for the Washington bridge site involved two phases. In the first, a series of liquefaction analyses were conducted using the SPT and CPT simplified methods. Results of these analyses were used to determine the depths at which liquefaction could occur during the 475-year and 2,475-year earthquakes. These results were also used as a basis for determining the residual strength of the soil. Concurrent with these analyses, a series of one-dimensional nonlinear, effective stress analyses was conducted to define more explicitly the mechanisms for pore water pressure increase within the soil profile and the changes in ground accelerations and deformations resulting from the development of liquefaction.

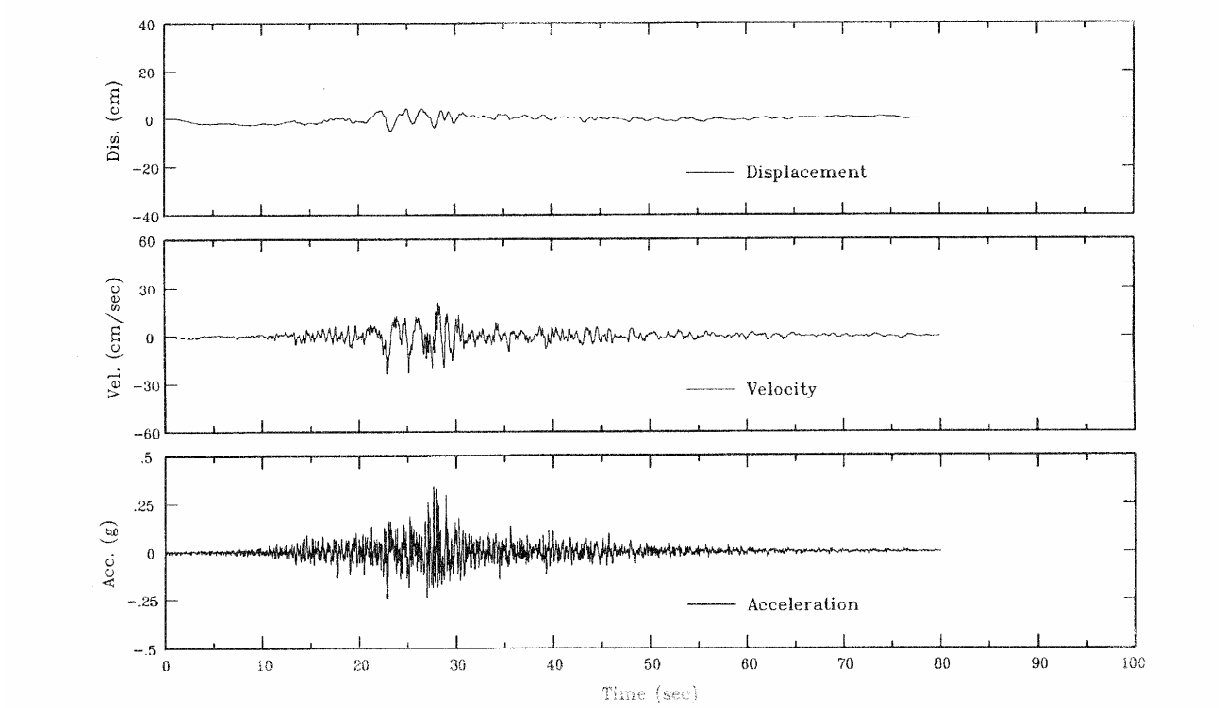

Figure 3.13 Acceleration, Velocity and Displacement Time Histories of 1985 Chile Earthquake Recording

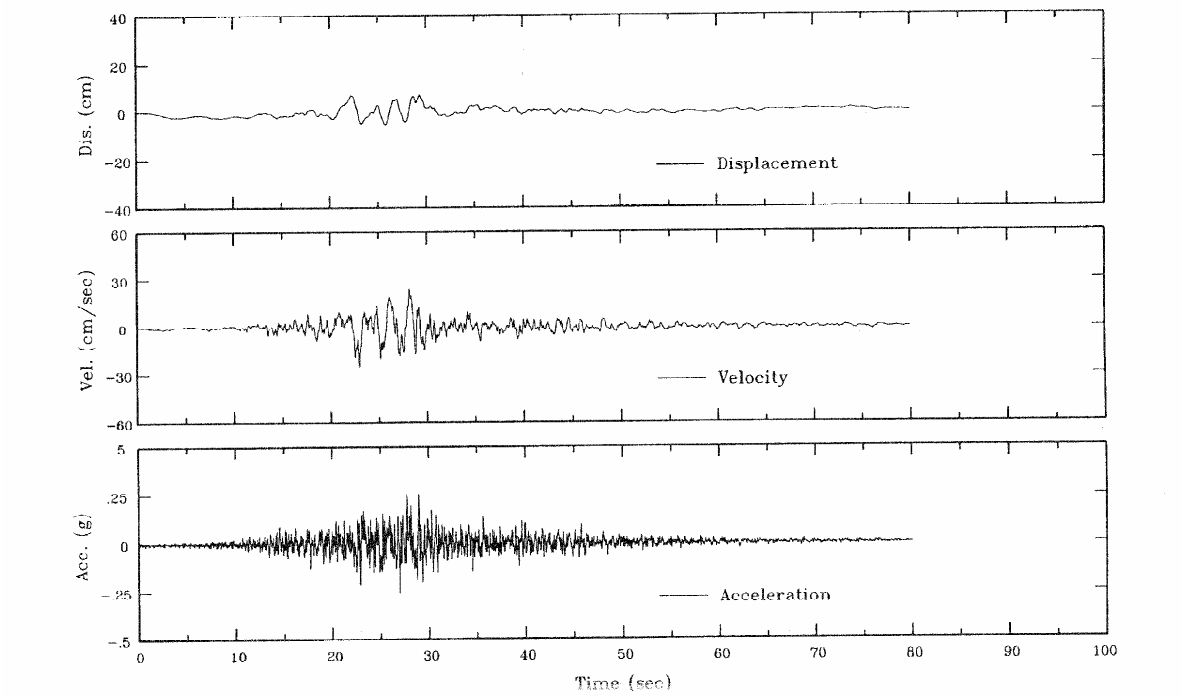

Figure 3.14 Acceleration, Velocity and Displacement Time Histories of 1985 Chile Earthquake Recording, after Scaling and Spectrum Matching the Recording to the Design Response Spectrum based on Current AASHTO Specifications, Site Class II, Washington Site

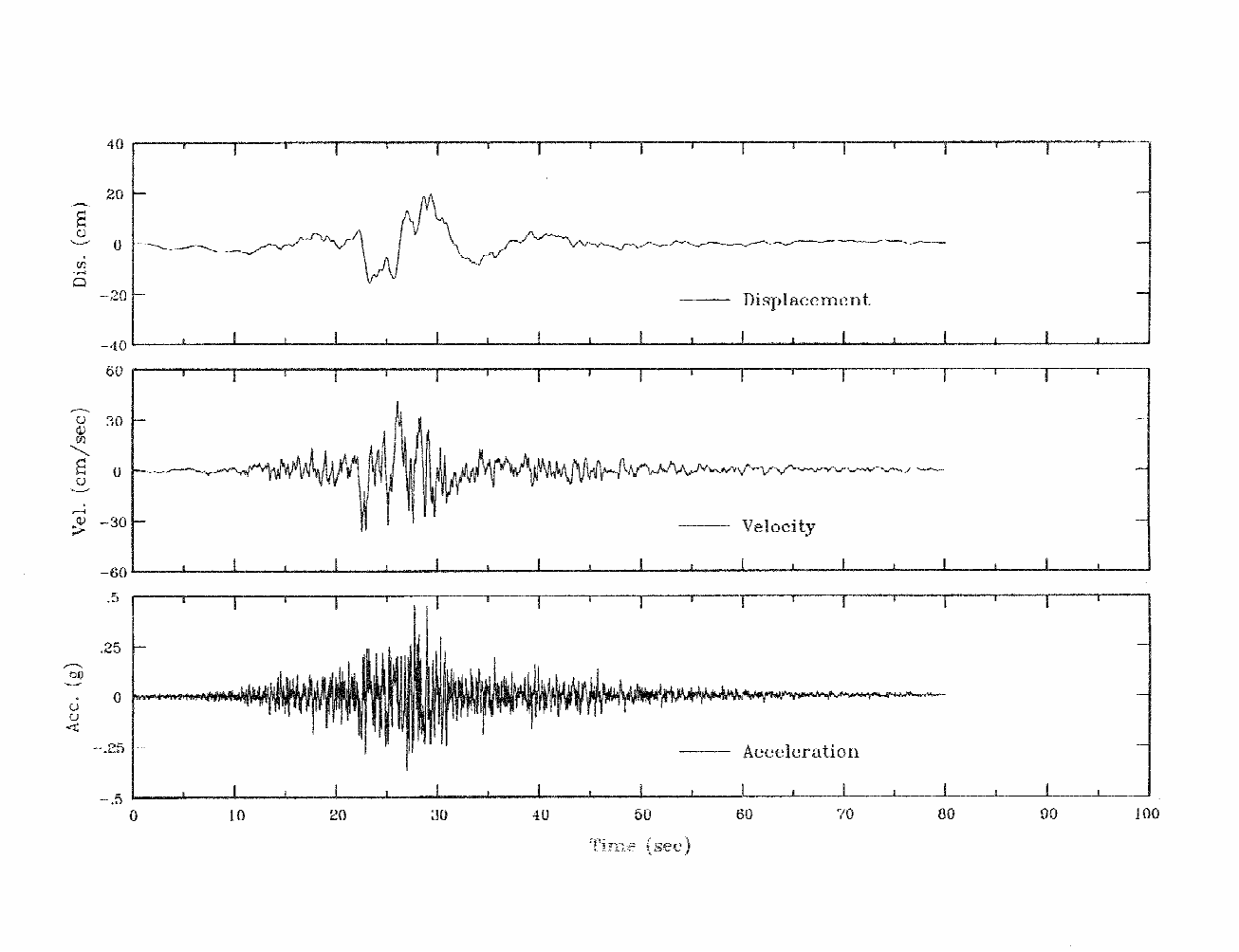

Figure 3.15 Acceleration, Velocity and Displacement Time Histories of 1985 Chile Earthquake Recording, after Scaling and Spectrum Matching the Recording to the MCE Design Response Spectrum based on the Recommended LRFD Specifications, Site Class C, Washington Site

3.5.1 Simplified Liquefaction Analyses

The first step of the procedure outlined in Section 2.5.2.1 is to determine whether liquefaction occurs.

Simplified liquefaction analyses were conducted using the procedures given in Youd and Idriss (1997). These are the same procedures as recommended in Appendix D of Part II: Commentary and Appendices of *Recommended LRFD Guidelines for the Seismic Design of Highway Bridges* (ATC/MCEER 2003). Two levels of peak ground acceleration (PGA) were used, one representing the acceleration from the current AASHTO LRFD with its 475-year return period and the other representing the recommended 2,475-year event. The PGA for the 475-year event was not adjusted for site effects, consistent with the approach recommended in the AASHTO

Standard Specifications[1]. Ground motions for the 2,475-year event were adjusted to Site Class E, as recommended in Section 3 of the recommended provisions. The resulting PGA values for each case are summarized below.

Input Parameter	475-Year Return Period	2,475-Year Return Period
Peak ground acceleration	0.24g	0.42g
Mean magnitude	6.5	6.5

The magnitude of the design earthquake was required for the SPT and CPT simplified analyses. As discussed previously, results of deaggregation studies from the USGS database for deaggregation suggest that the mean magnitude for the 475- and 2,475-year events is 6.5. However, common practice within the State of Washington has been to use a magnitude 7.5 event, as being representative of the likely size of a subduction zone event occurring directly below the Puget Sound area. In view of this common practice, a range of magnitudes was used during the liquefaction analyses.

For these analyses, ground water was assumed to occur 10 feet below the ground surface for the non-fill case. Evaluations were also performed using a simplified model to evaluate the effects of the fill. For the fill model, the soil profile with the associated soil properties was the same as the free-field case. However, an additional 30 feet of embankment was added to the soil profile. This change results in a lower imposed shearing stress (i.e., demand) because of the lower soil flexibility factor (R_d). No adjustments were made to the normalized CRR values for the greater overburden. As discussed in Youd and Idriss (1997), the recommended approach for a site where fill is added is to use the pre-fill CRR value, under the assumption that the overburden effects from the fill will not have an appreciable effect on the density of the material.

Factors of safety results from the liquefaction evaluations at the three magnitudes are shown in Figure 3.16 and Figure 3.17 for the 475-year and 2,475-year seismic events, respectively, for the case of no approach fill. These results indicate that liquefaction could occur at two depths within the soil profile for the 475-year ground motion, depending somewhat on the assumed earthquake magnitude. For the 2,475-year event, liquefaction is predicted to depths of 75 feet, regardless of the assumption on the earthquake magnitude[2].

[1] Common practice is to adjust the PGA for the site factors given in Table 3.5.1 of Division 1-A. While this adjustment may be intuitively correct, these site factors are not explicitly applied to the PGA. If the site coefficient were applied at the Washington site, the PGA would be increased by a factor of 1.5, reducing the difference in the ground motions between the 475- and 2,475-year events.

[2] The maximum depth of liquefaction was cut-off at 75 feet, consistent with WSDOT's normal practice. There is some controversy whether a maximum depth of liquefaction exists. Some have suggested that liquefaction does not occur beyond 55 feet. Unfortunately, quantitative evidence supporting liquefaction beyond 55 feet is difficult to find; however, cases of deep liquefaction were recorded in the 1964 Alaskan earthquake. For expediency, liquefaction in the simplified analysis was limited to 75 feet.

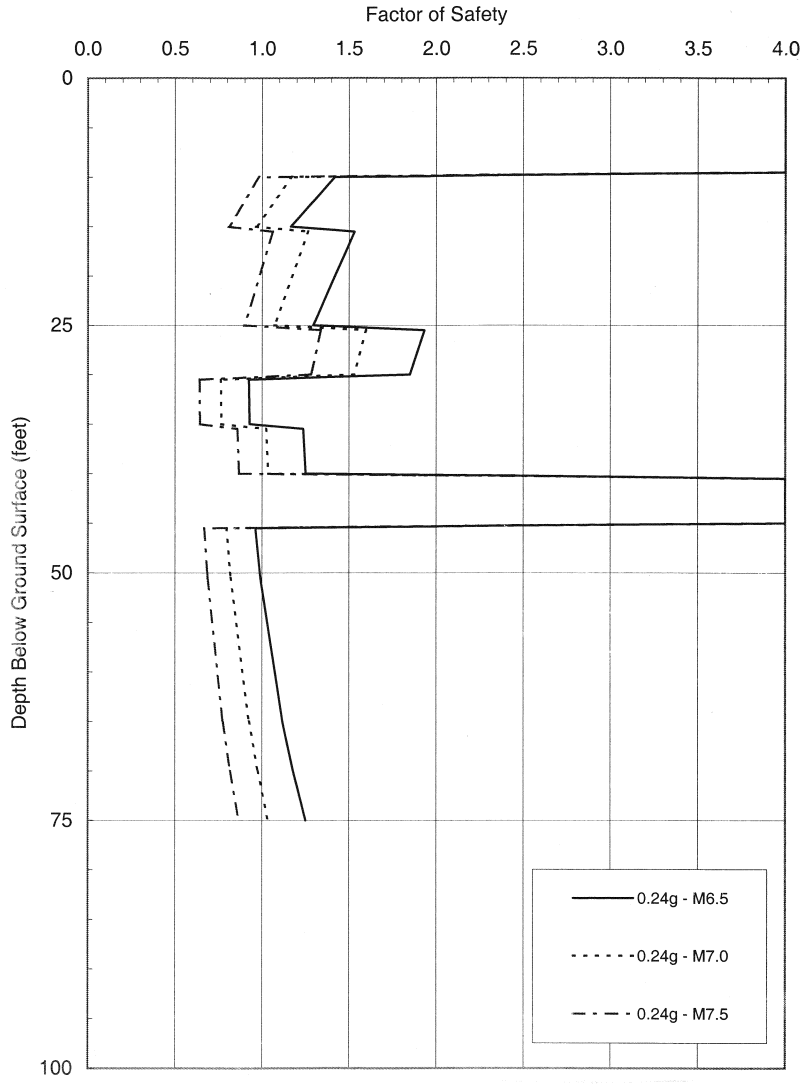

Figure 3.16 Liquefaction Potential – 475-Year Return Period

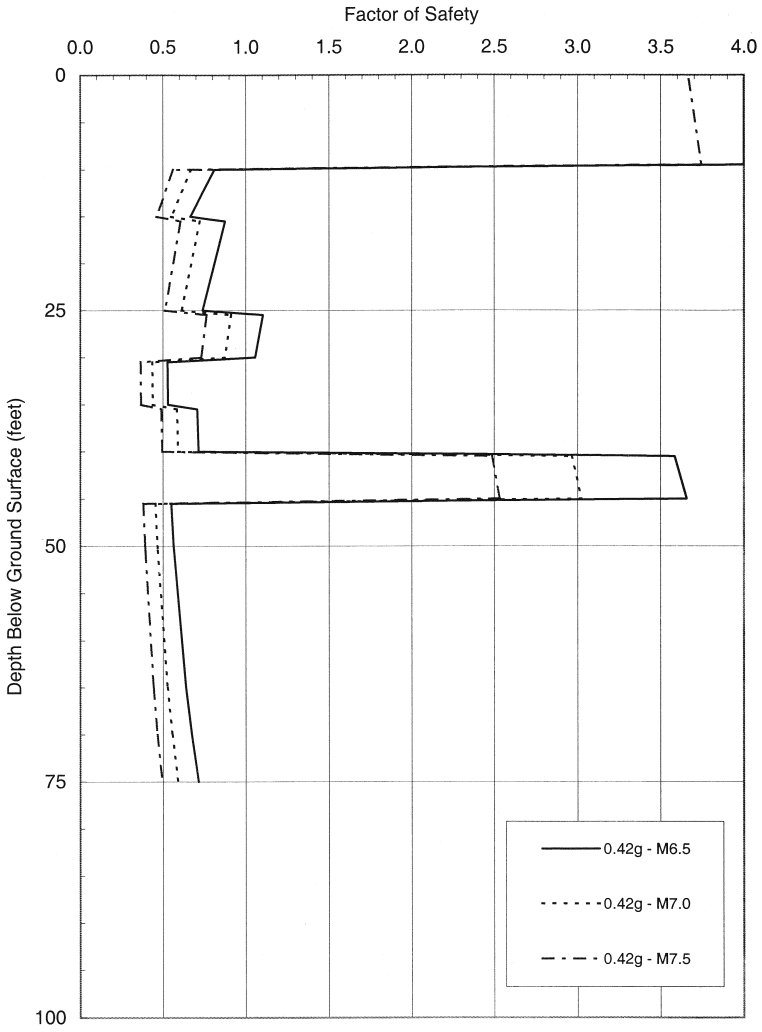

Figure 3.17 Liquefaction Potential – 2,475-Year Return Period

The results given in Figure 3.16 and Figure 3.17 are for the simplified soil model discussed in Section 2.2.3. Site-specific results of SPT and CPT liquefaction evaluations for soil boring H-13 and CPT sounding C-8 are given in Appendix B. The site-specific results are generally consistent with the simplified model, indicating that liquefaction is to be expected for the 475-year return period event at certain depths, depending on magnitude, and to a depth of 75 feet for the 2,475-year event. Factors of safety appear to be slightly lower in the liquefiable zones for the CPT results relative to the SPT results by 0.2 to 0.3. This trend has been noted previously (Baez and Martin, 1995) and is attributed to the conservatism built into the CPT strength curves. As noted previously, there is also a large discrepancy in the liquefaction potential between 25 and 40 feet between the SPT and CPT data. The reason for this difference was not determined, although it is likely the result of the 70 feet of separation between the two exploration locations.

Results of the liquefaction analyses with the approach fill are shown in Figure 3.18 and Figure 3.19. The fill case results in somewhat lower liquefaction potential (i.e., higher FOS) due to the lower imposed shearing stress. Figure 3.20 and Figure 3.21 show a direct comparison for the most likely magnitude.

3.5.2 DESRA-MUSC Ground Response Studies

A more detailed and refined approach to assess if liquefaction occurs and the resulting ground motion is to use a nonlinear dynamic effective stress approach as discussed in Section 2.3. For this assessment, one-dimensional nonlinear effective stress site response analyses were conducted using the program DESRA-MUSC (Qiu, 1998).

The idealized site profile and related soil properties adopted for the response analyses are shown in Figure 3.2. Response analyses were performed for the three earthquake input motions, assuming a transmitting boundary input level at a depth of 200 feet, corresponding to the till interface. Analyses were conducted for both the 475- and 2,475-year return period events and for site profiles with and without embankment fill. The DESRA-MUSC parameters utilized for analyses for the various soil strata (G/G_{max} curves, backbone curves and liquefaction strength curves) are documented in Appendix D together with the result of response analyses for all cases defined above. A representative set of results for the time history matching the site spectra, but based on the 1985 Chile earthquake, which has the highest energy levels of the three events used for analyses (representative of a M7.5 event), are described below.

3.5.2.1 Without Embankment Fill

The site response for the 475-year earthquake is summarized in four figures:

- Figure 3.22 Input and output acceleration time histories and response spectra
- Figure 3.23 Maximum shear strains induced as a function of depth
- Figure 3.24 Time histories of pore water pressure generation at various depths
- Figure 3.25 Shear stress-shear strain hysteretic loops at various depths

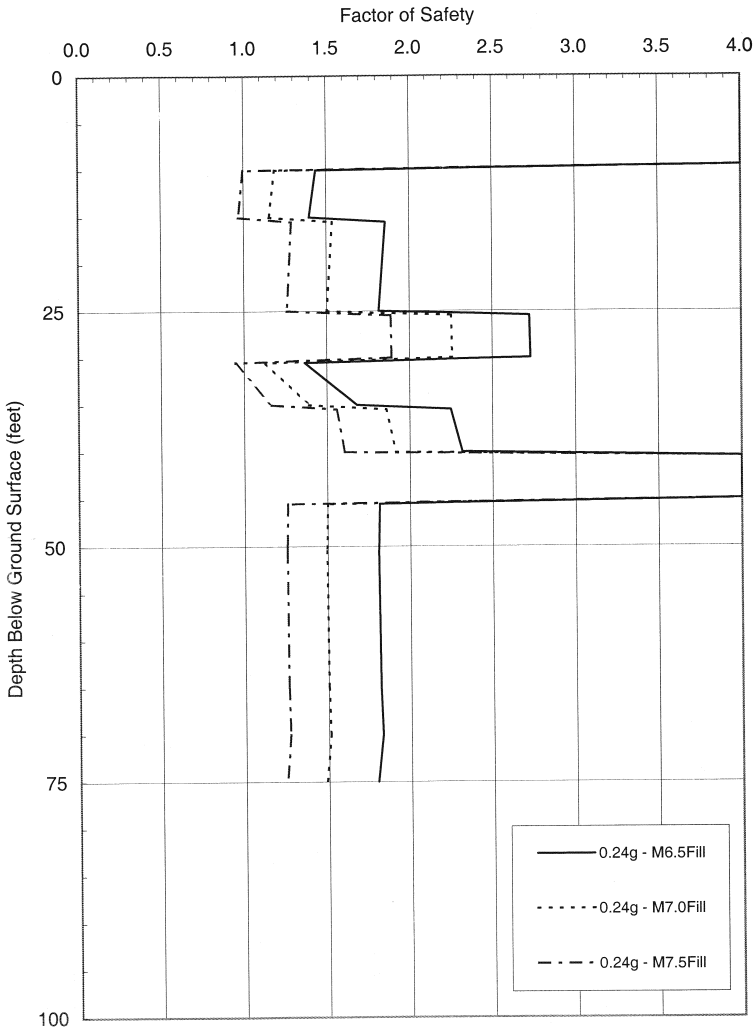

Figure 3.18 Liquefaction Potential – 475-Year Return Period with 30-Foot Fill

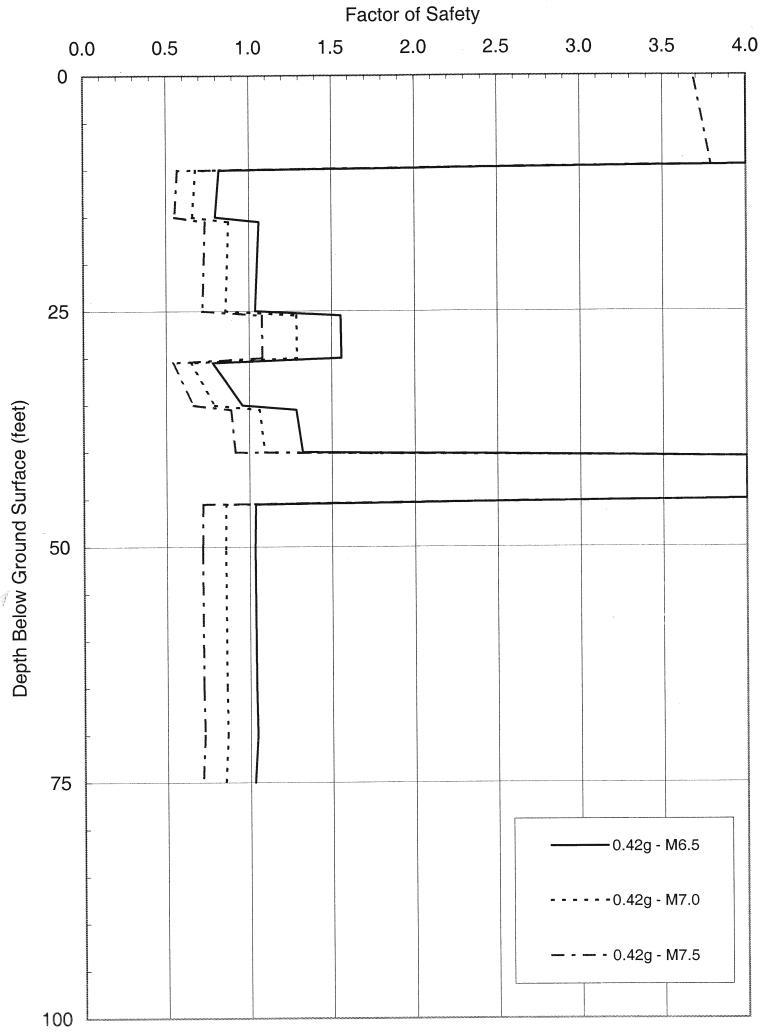

Figure 3.19 Liquefaction Potential – 2,475-Year Return Period with 30-Foot Fill

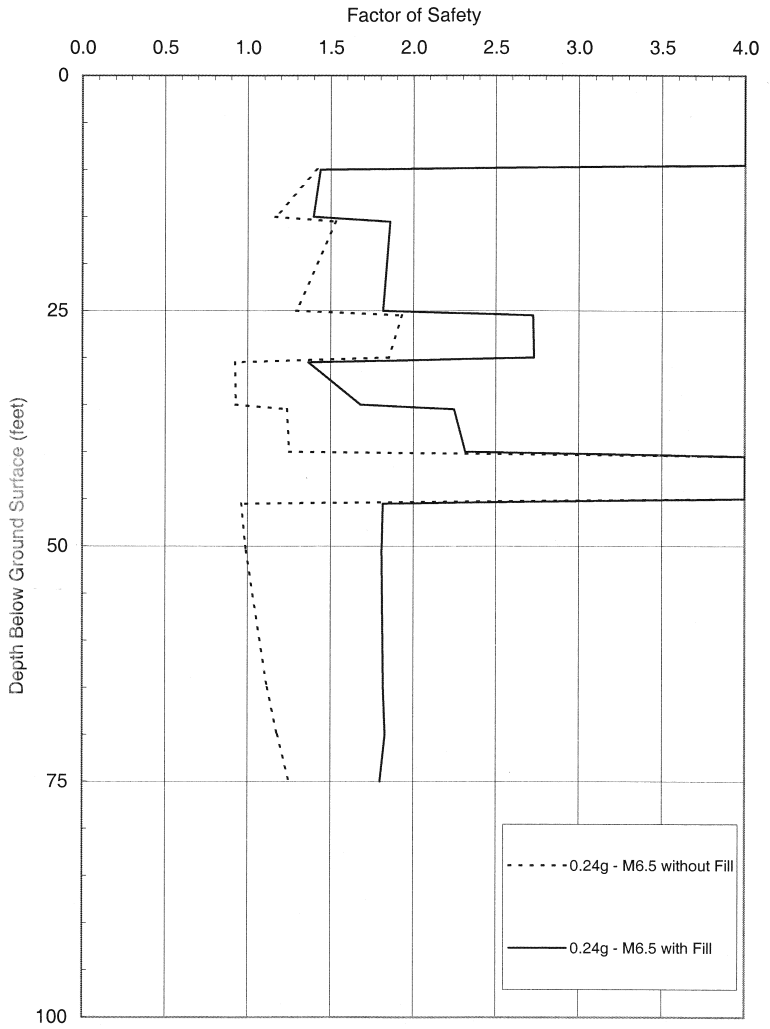

Figure 3.20 Liquefaction Potential – 475-Year Return Period without and with 30-Foot Fill

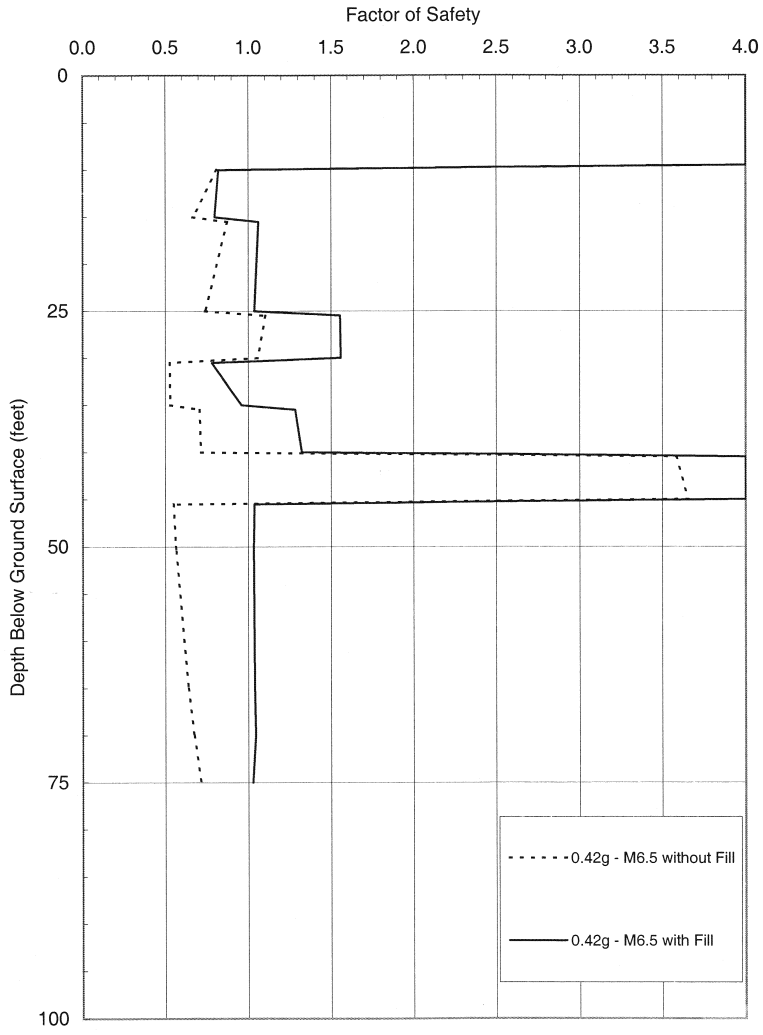

Figure 3.21 Liquefaction Potential – 2,475-Year Return Period without and with 30-Foot Fill

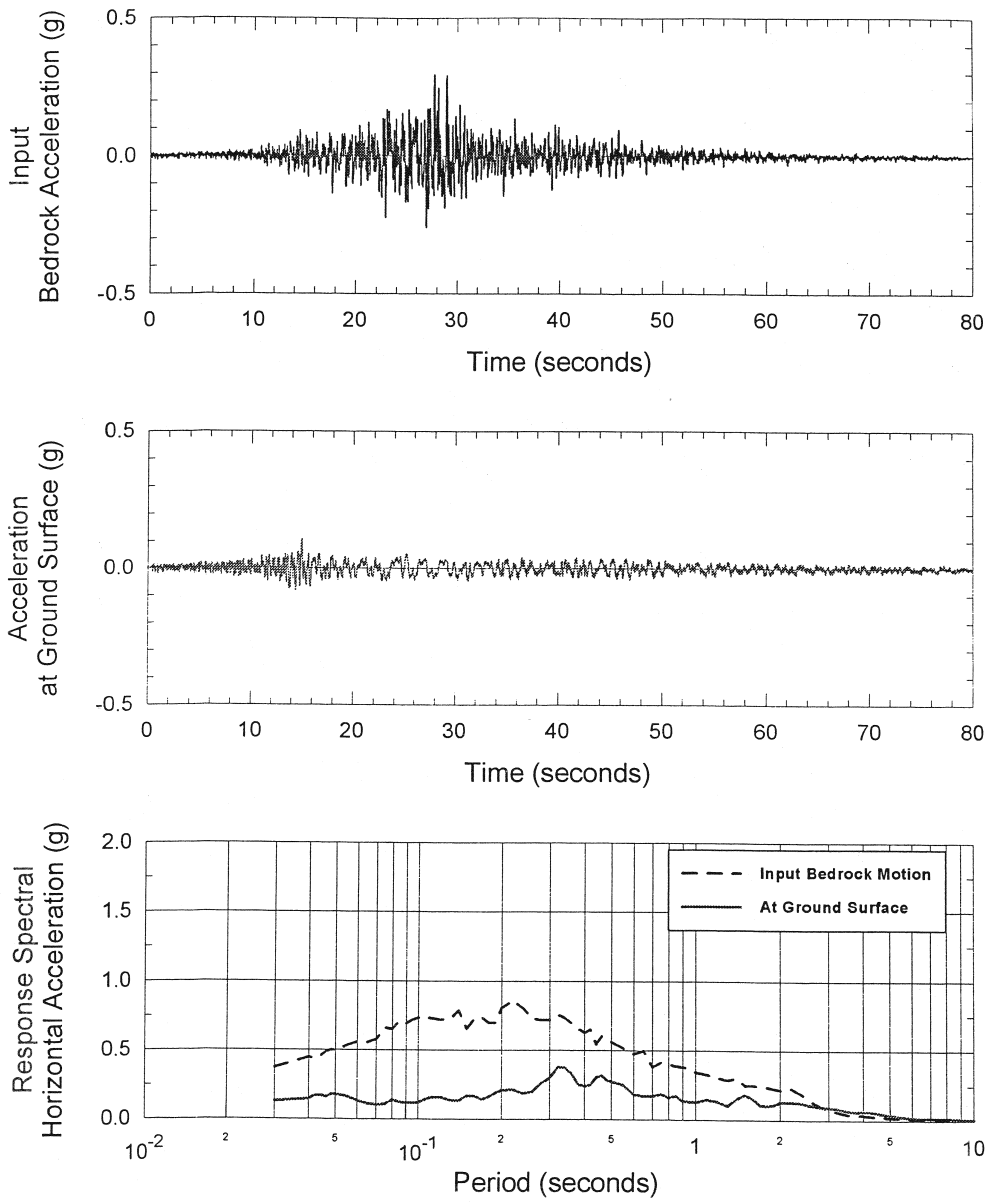

Figure 3.22 Input and Output Acceleration Time Histories and Response Spectra, 475-Year Earthquake without Fill, 1985 Chile Earthquake

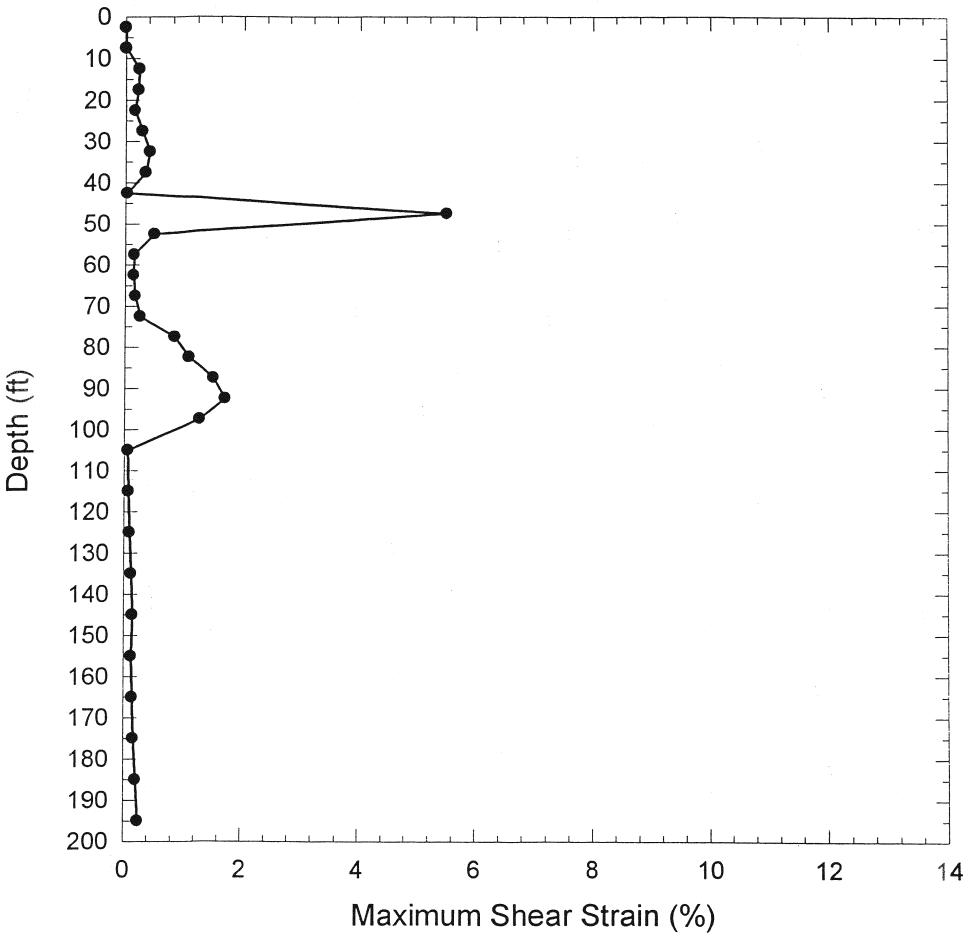

Figure 3.23 Maximum Shear Strains Induced as a Function of Depth, 475-Year Earthquake without Fill, 1985 Chile Earthquake

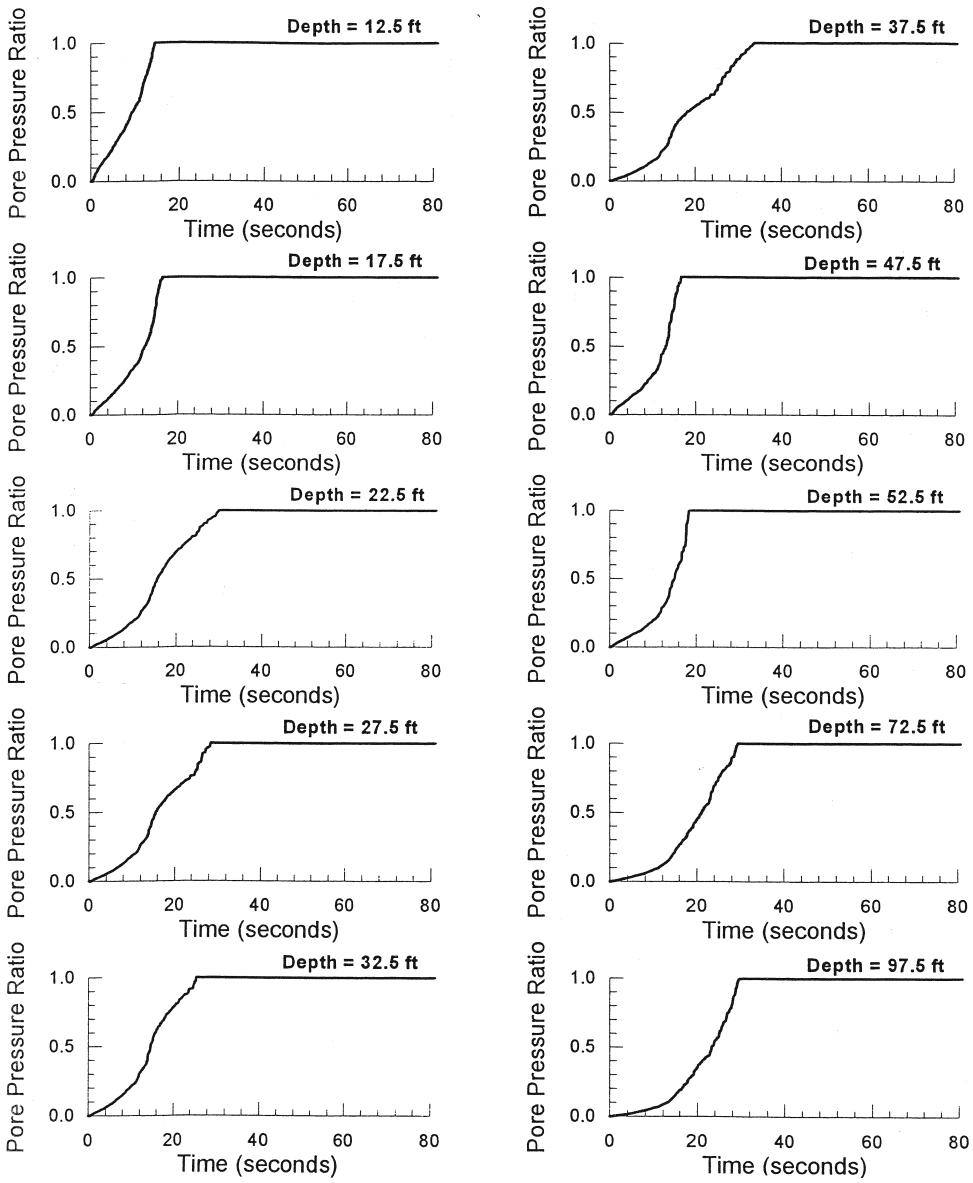

Figure 3.24 Time Histories of Pore Pressure Generation at Various Depths, 475-Year Earthquake without Fill, 1985 Chile Earthquake

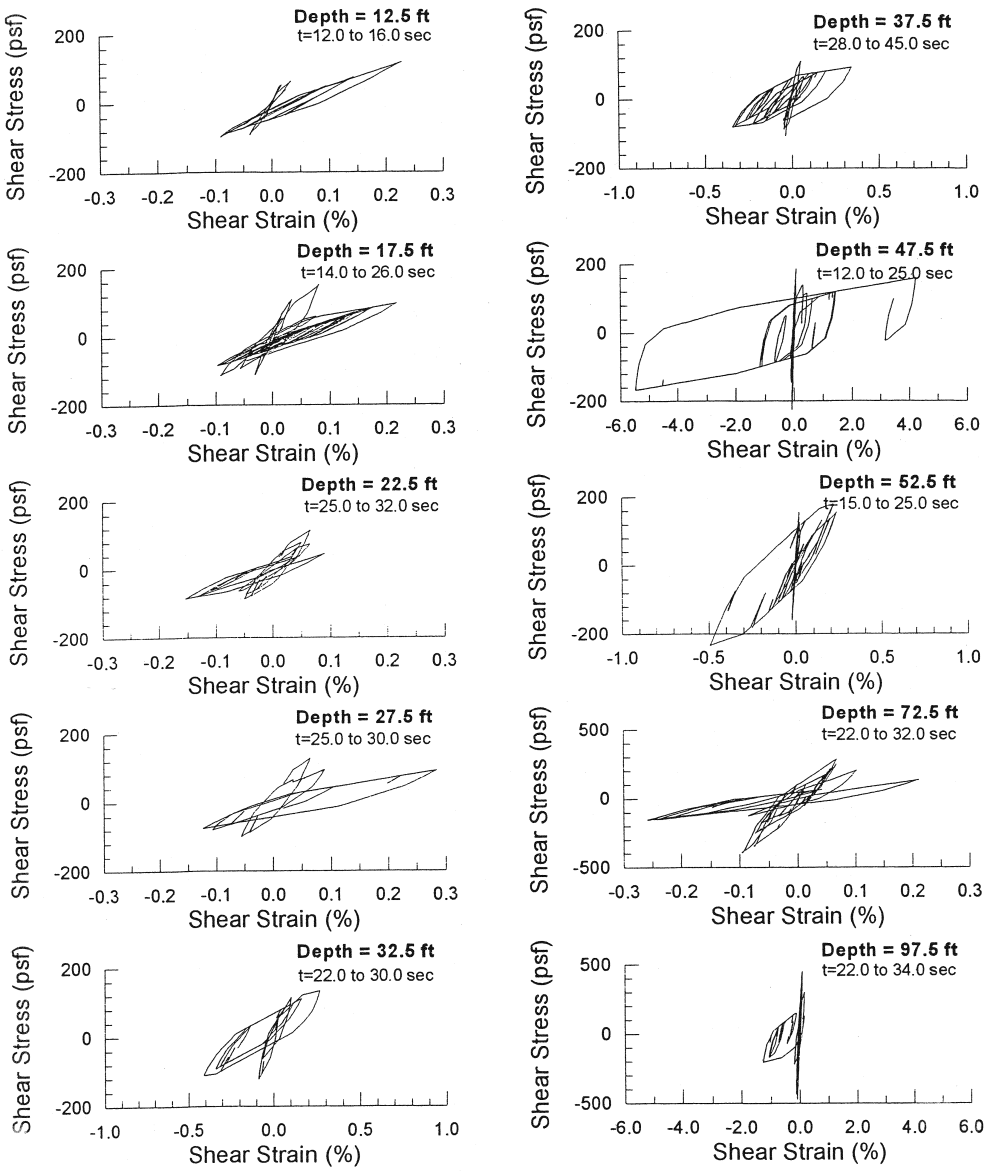

Figure 3.25 Shear Stress – Shear Strain Hysteretic Loops at Various Depths, 475-Year Earthquake without Fill, 1985 Chile Earthquake

Figure 3.26 through Figure 3.29 summarize similar data for the 2,475-year earthquake. The following are key observations from the data plots:

1. The pore water pressure time history response and output accelerations are very similar for the 475- and 2,475-year cases. The underlying reason for this is the fact that the higher input accelerations for the 2,475-year case are more strongly attenuated when transmitted through the clayey silts between 100 to 200 feet, such that input accelerations at the 100-foot level for both cases, are of the order of 0.25g.
2. All liquefiable soils between 10 and 100 feet eventually liquefied for both cases. However, liquefaction was first triggered in the 45- to 50-foot layer, which became the focal point for shear distortion and associated ground lurch (see Figure 3.23, Figure 3.27, Figure 3.25 and Figure 3.29). Maximum shear strains of about 6 and 10 percent for the 475- and 2,475-year events, respectively, over the 5-foot depth of this layer, would suggest maximum ground lurches of about 0.3 and 0.5 feet, respectively. Liquefaction also occurred at about the same time for the layer between 10 and 20 feet. Maximum shear strains in this and other layers were relatively small, but still sufficient to eventually generate liquefaction. The strong focal point for shear strains for the 45- to 50-foot layer suggests that this layer would also be the primary seat of lateral spread distortion.
3. Liquefaction at the 45- to 50-foot depth, which was triggered at about a time of 17 seconds, effectively generated a base isolation layer, subsequently suppressing the transmission of accelerations above that depth, and generating a much “softer” soil profile. This is graphically illustrated in Figure 3.22 and Figure 3.30, which show suppression of input accelerations and longer period response after about 17 seconds. Such behavior is representative of observations at sites, which liquefied during the Niigata and Kobe earthquakes.

Similar trends to those described above were seen for the time histories based on the Olympia and Desert Hot Springs earthquakes, as may be seen in Appendix D. However, for the Desert Hot Spring event, more representative of a M6.5 event, liquefaction did not occur at depths greater than 55 feet and only barely occurred at depths between 20 and 30 feet, for the 475-year event.

The above results are generally consistent with the factor of safety calculations using the simplified method. However, one notable difference is the observation that the sand layer between 25 and 30 feet (CRR = 0.3) tends to build up pore water pressure and liquefy in a similar manner to the layers above (CRR = 0.2) and below (CRR = 0.15) due to pore water pressure redistribution effects in DESRA-MUSC, whereas the simplified method which assumes no drainage during earthquake shaking, indicates factors of safety greater than one for 475-year events. The effects of redistribution also tend to suppress the rate of pore water pressure build up in the layer between 30 and 35 feet.

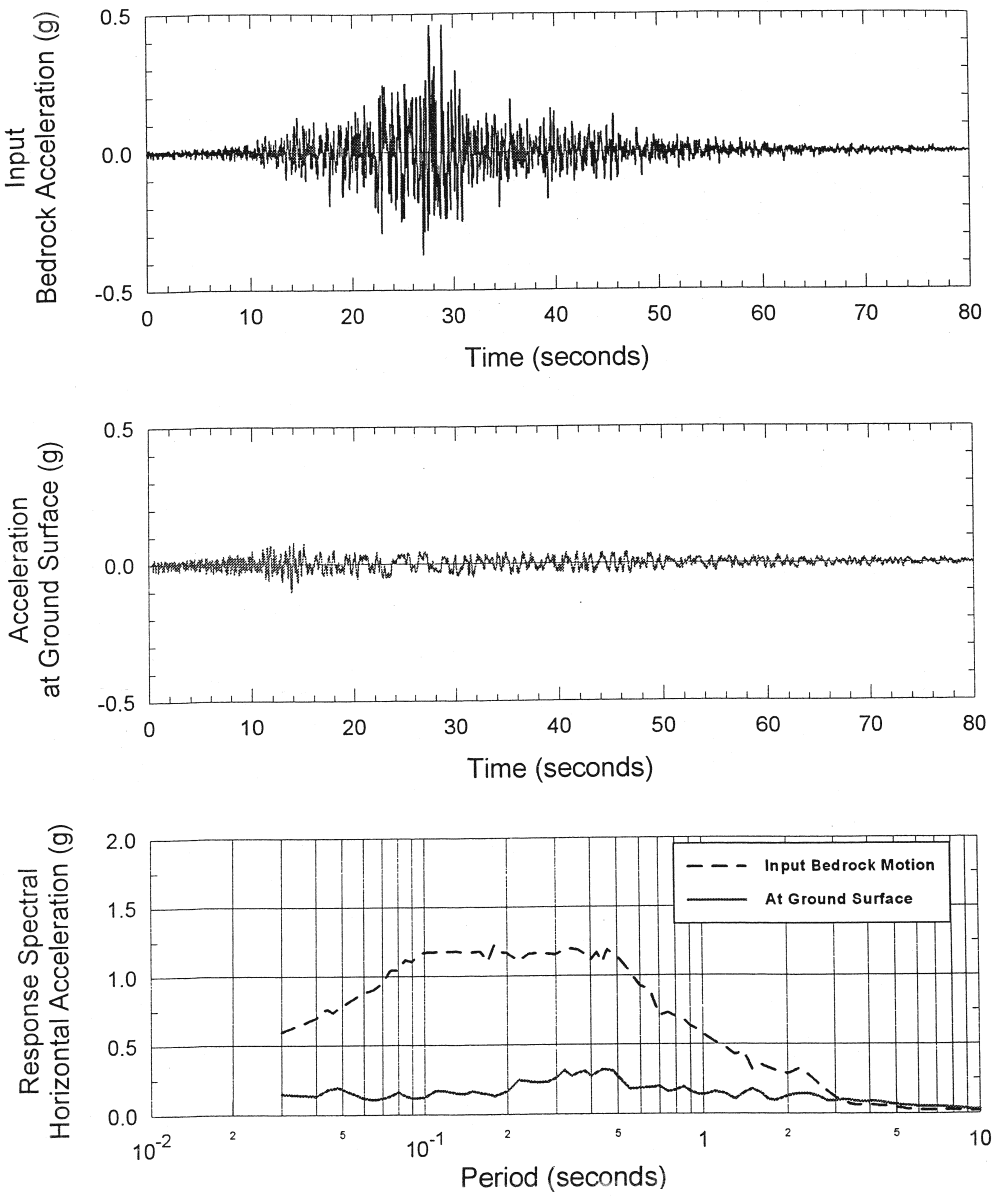

Figure 3.26 Input and Output Acceleration Time Histories and Response Spectra, 2,475-Year Earthquake without Fill, 1985 Chile Earthquake

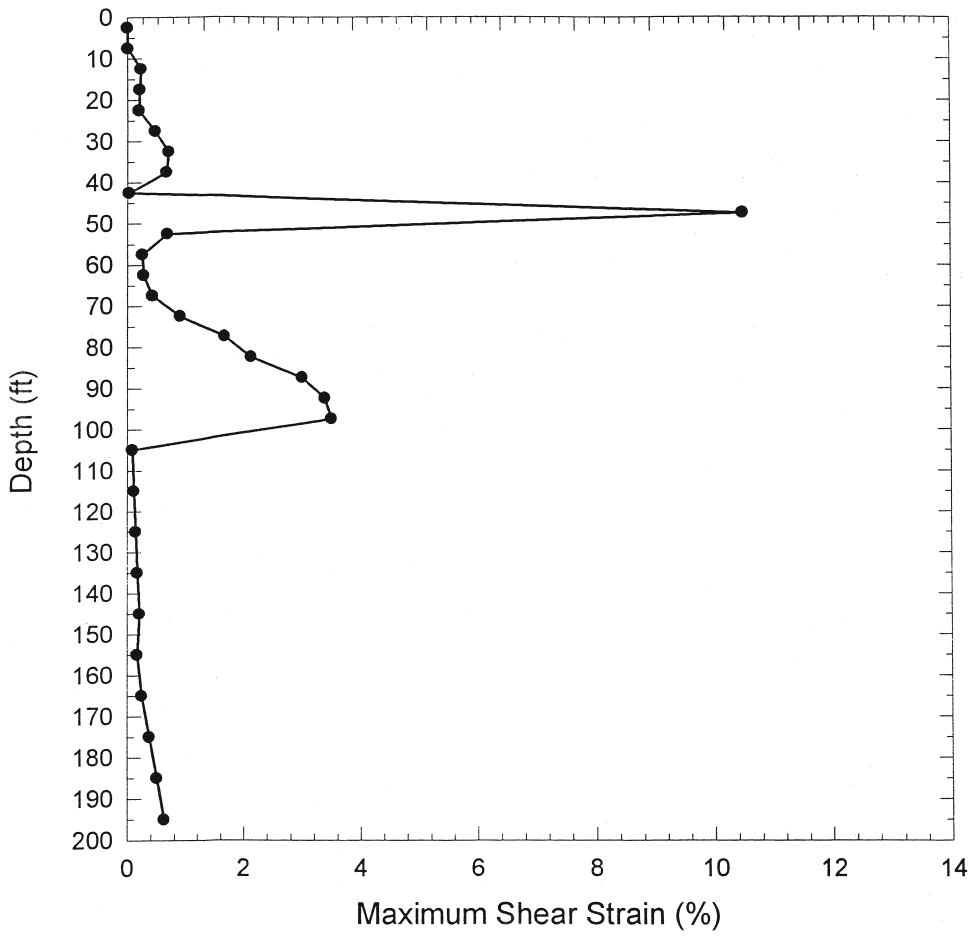

Figure 3.27 Maximum Shear Strains Induced as a Function of Depth, 2,475-Year Earthquake without Fill, 1985 Chile Earthquake

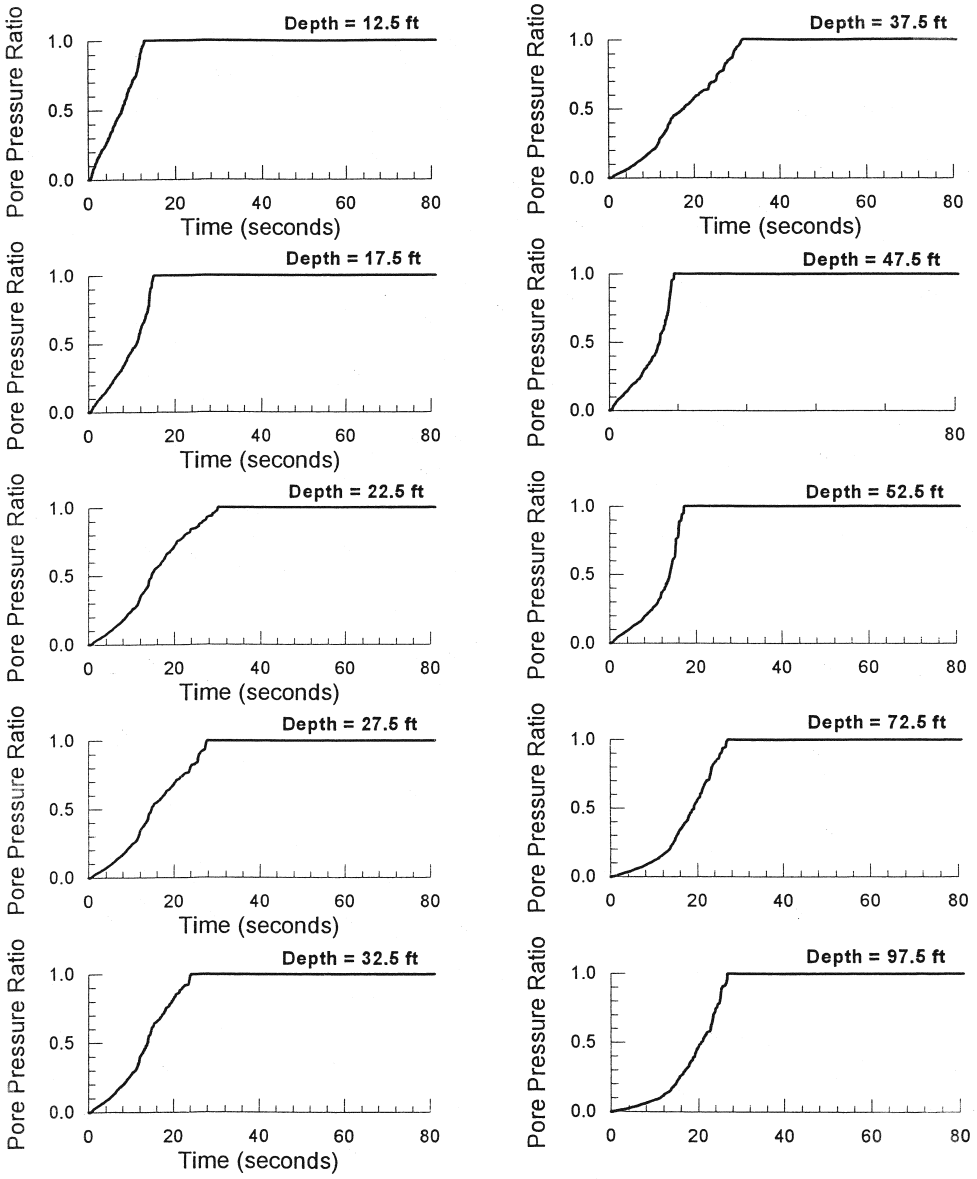

Figure 3.28 Time Histories of Pore Pressure Generation at Various Depths, 2,475-Year Earthquake without Fill, 1985 Chile Earthquake

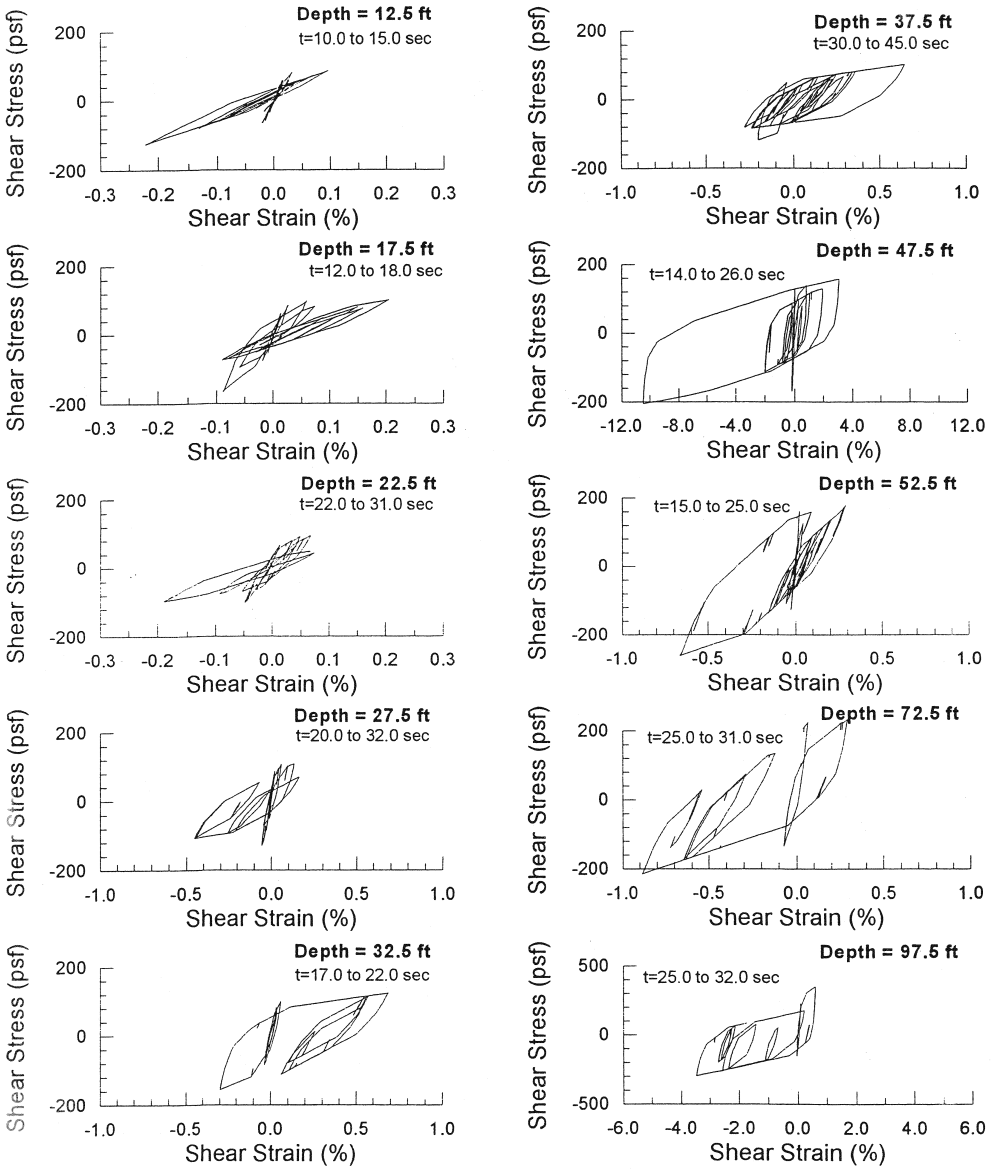

Figure 3.29 Shear Stress – Shear Strain Hysteretic Loops at Various Depths, 2,475-Year Earthquake without Fill, 1985 Chile Earthquake

3.5.2.2 With Embankment Fill

The site response for the 475- and 2,475-year earthquakes is summarized in a similar manner to the no fill case above, in Figures 3.30 through 3.37. As in the simplified method, the effect of the fill is to suppress the rate of pore water pressure build up in the DESRA-MUSC analyses (or increase the factor of safety in the case of the simplified method). However, the overall response is similar for both the 475- and 2,475-year cases, as for the no fill case.

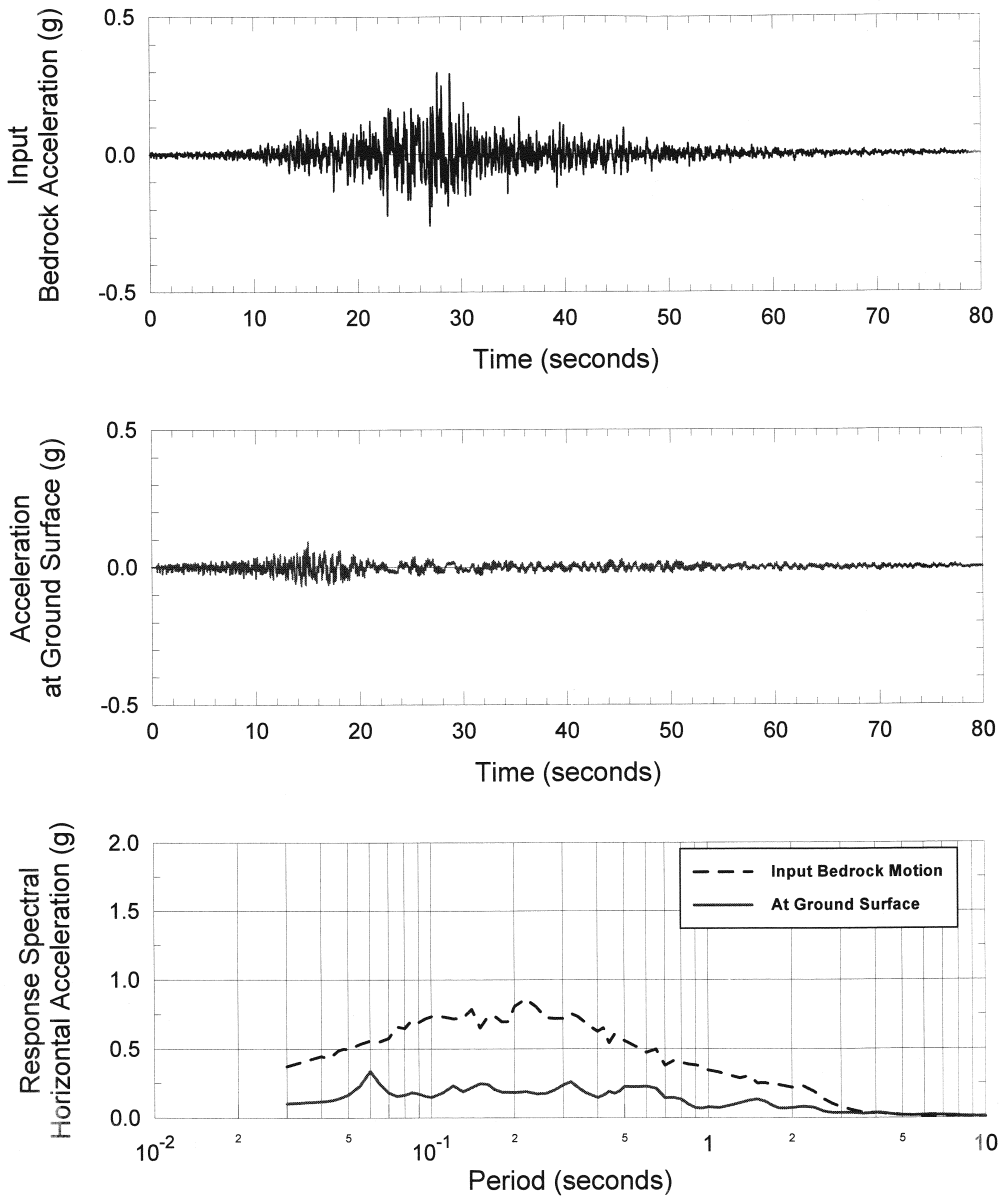

Figure 3.30 Input and Output Acceleration Histories and Response Spectra, 475-Year Earthquake with Fill, 1985 Chile Earthquake

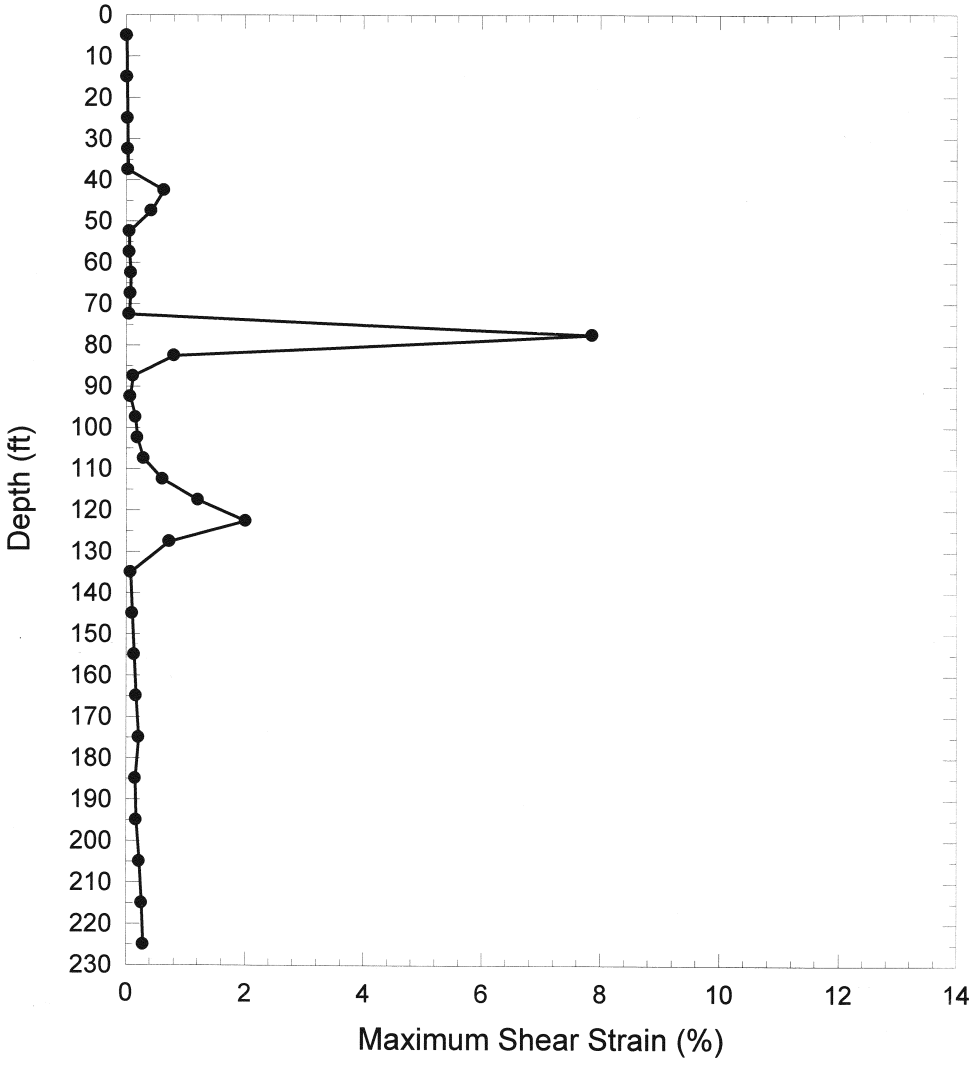

Figure 3.31 Maximum Shear Strains Induced as a Function of Depth, 475-Year Earthquake with Fill, 1985 Chile Earthquake

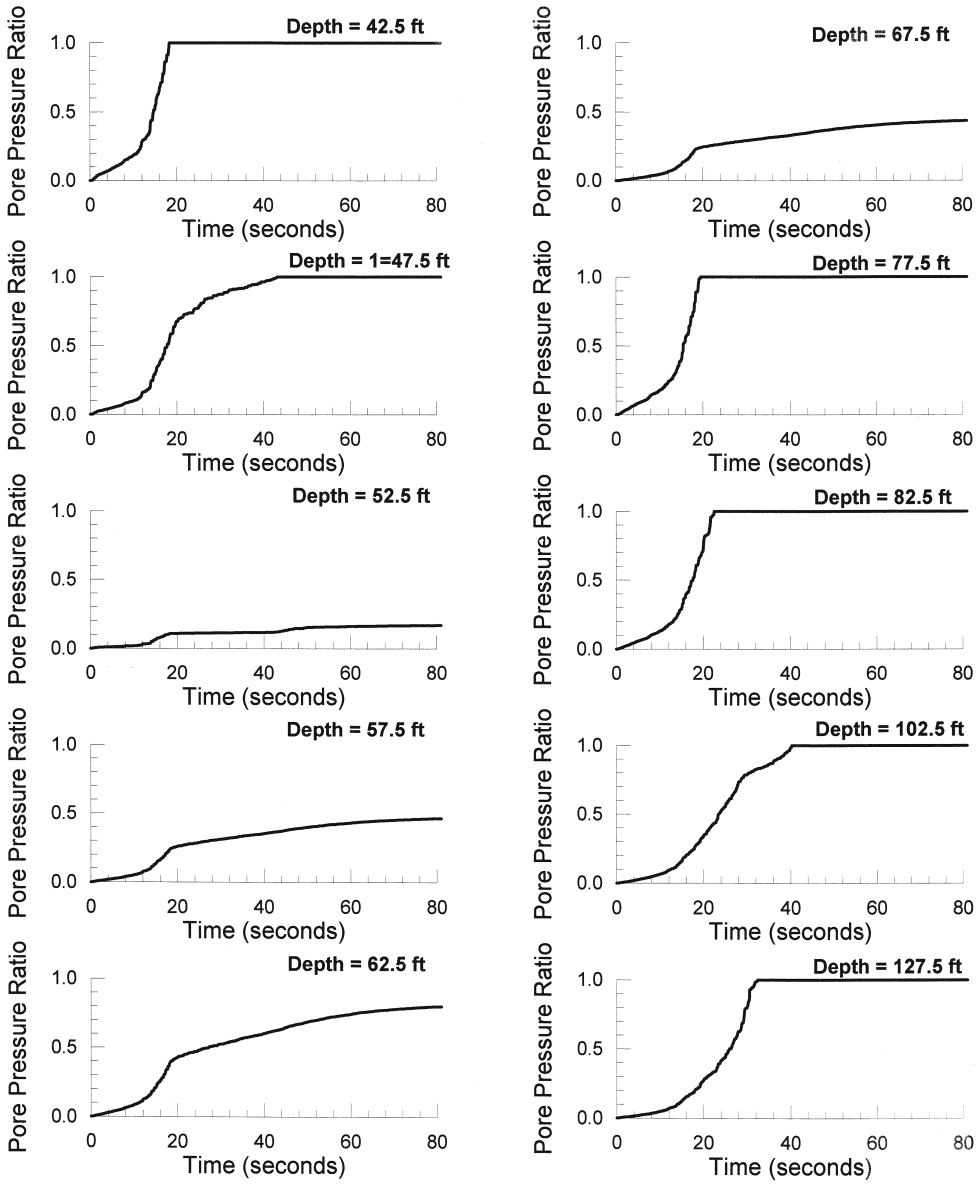

Figure 3.32 Time Histories of Pore Pressure Generation at Various Depths, 475-Year Earthquake with Fill, 1985 Chile Earthquake

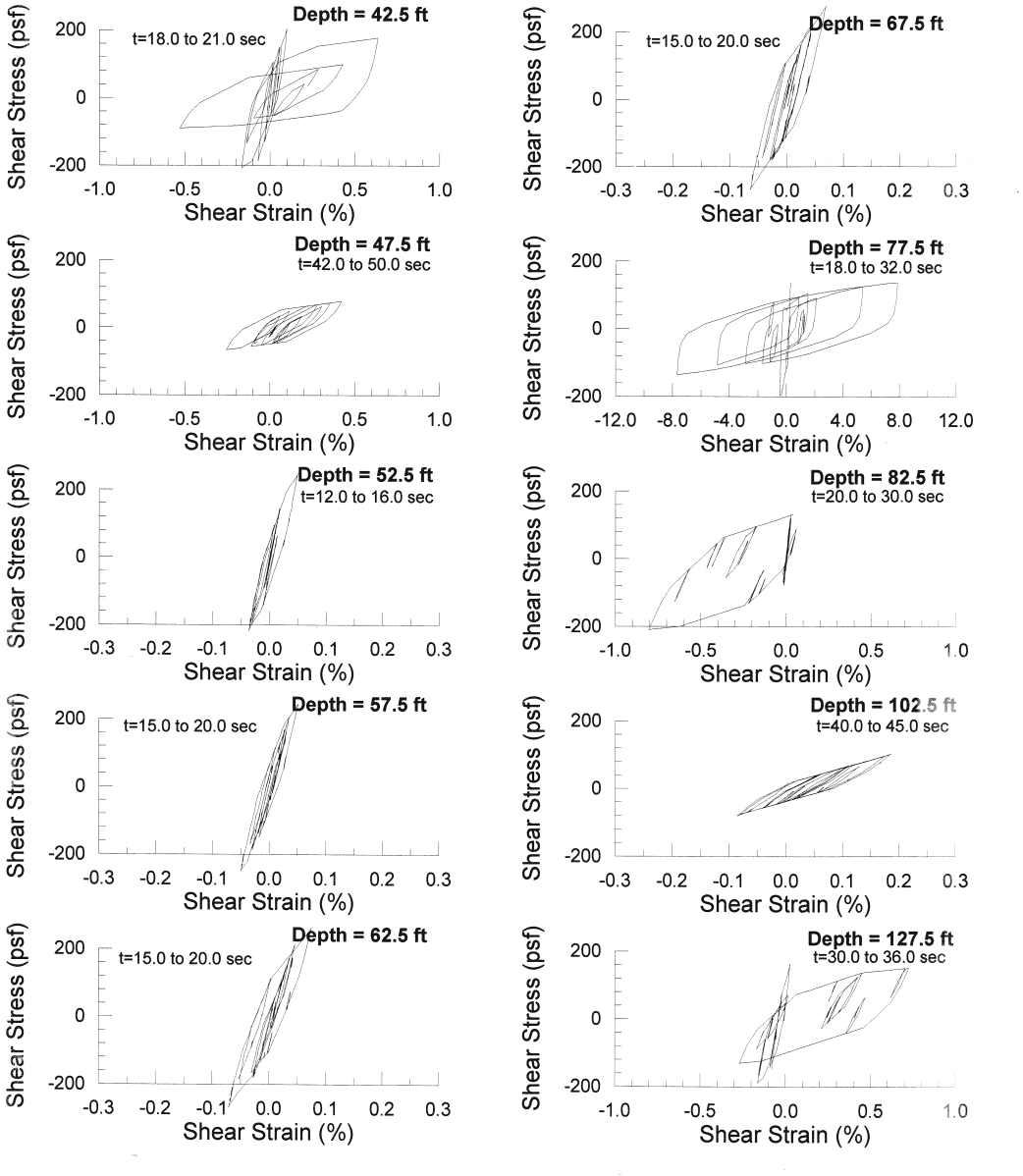

Figure 3.33 Shear Stress – Shear Strain Hysteretic Loops at Various Depths, 475-Year Earthquake with Fill, 1985 Chile Earthquake

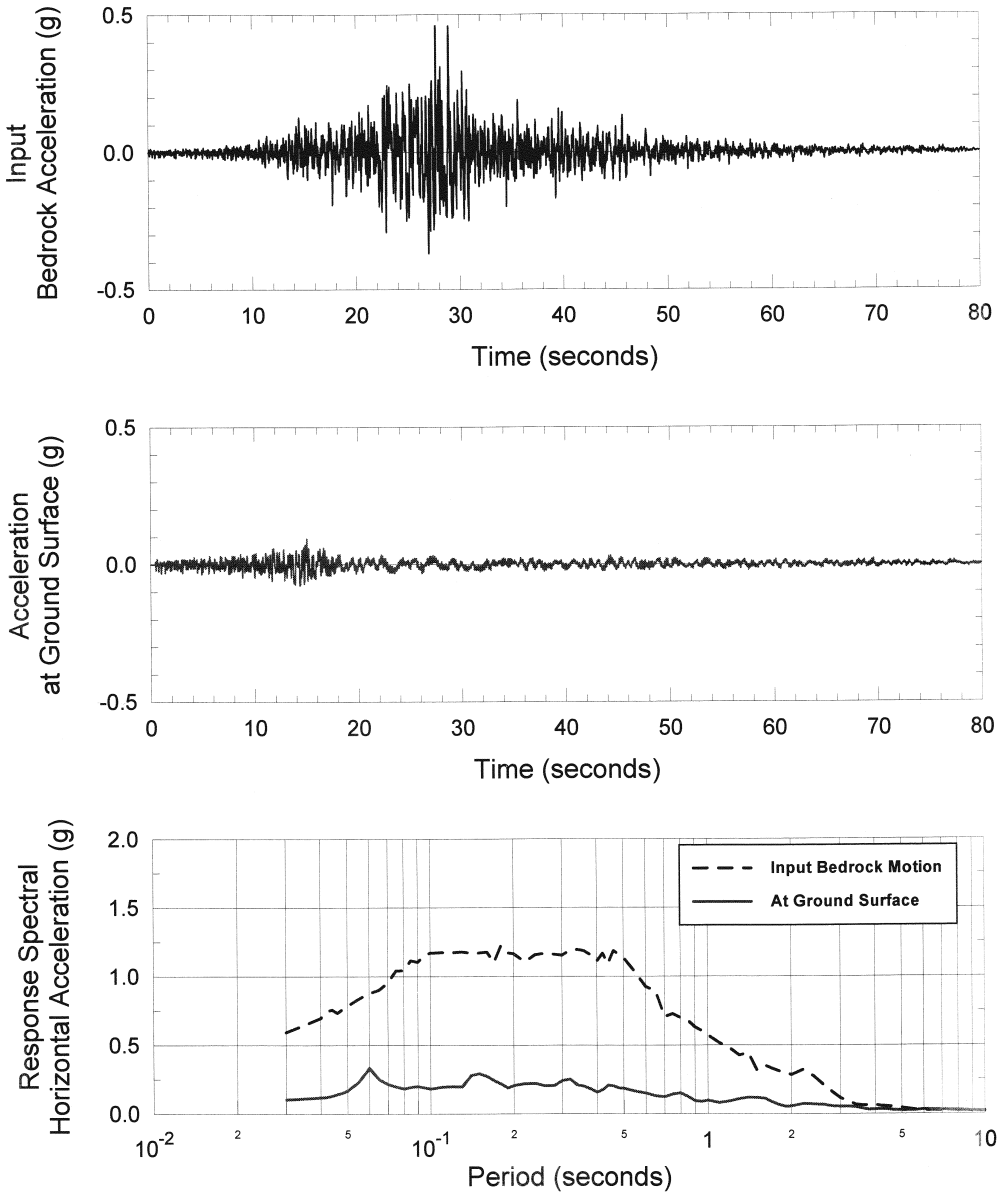

Figure 3.34 Input and Output Acceleration Histories and Response Spectra, 2,475-Year Earthquake with Fill, 1985 Chile Earthquake

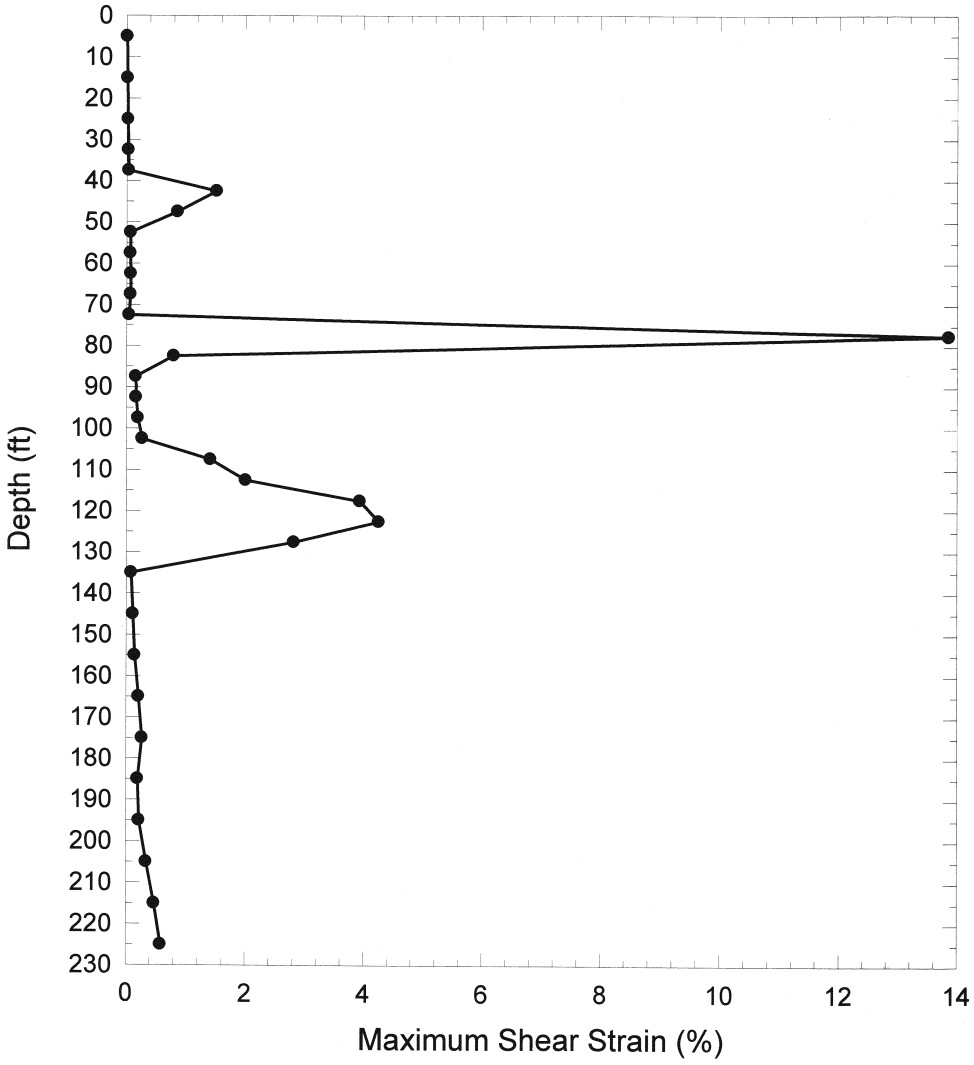

Figure 3.35 Maximum Shear Strains Induced as a Function of Depth, 2,475-Year Earthquake with Fill, 1985 Chile Earthquake

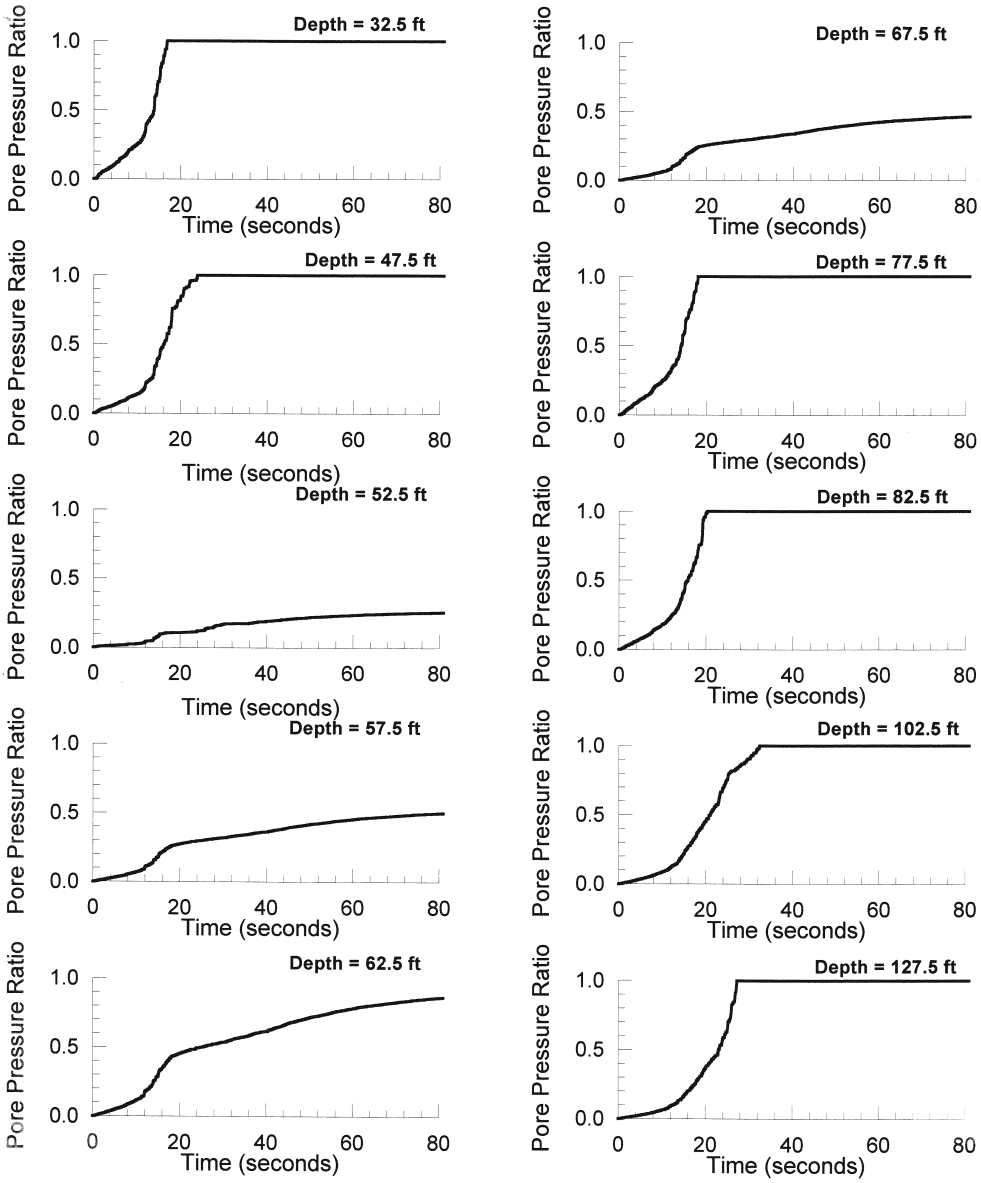

Figure 3.36 Time Histories of Pore Pressure Generation at Various Depths, 2,475-Year Earthquake with Fill, 1985 Chile Earthquake

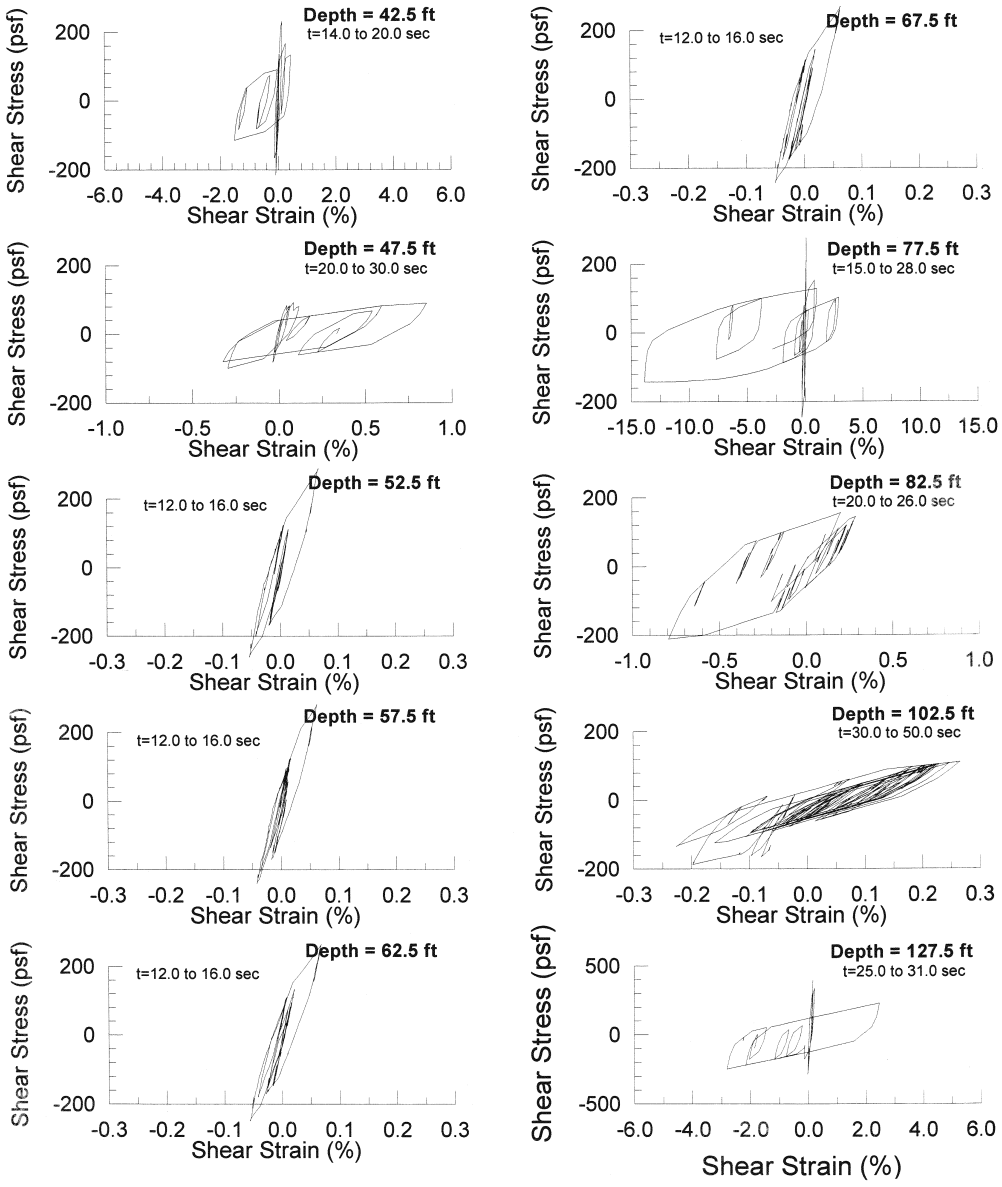

Figure 3.37 Shear Stress – Shear Strain Hysteretic Loops at Various Depths, 2,475-Year Earthquake with Fill, 1985 Chile Earthquake

Liquefaction was first triggered in the 45- to 50-foot layer, which became the focal point for shear distortion as in the no fill case. Liquefaction also occurred at about the same time for layers between 10 and 20 feet. However, liquefaction was suppressed in layers between 20 and 40 feet. The strong focal point for shear strains for the 45- to 50-foot layers, again suggests that this layer would be the primary seat of lateral spread distortion. Similar trends to those described above were also seen for the time histories based on the Olympia and Desert Hot Spring earthquakes, although as for the no fill case, liquefaction did not occur at depths greater than 55 feet for the 475-year Desert Hot Springs event.

The above results are again generally consistent with the factor of safety calculations using the simplified method, but with the notable differences that for the 475-year Olympia and Chile events, liquefaction occurred at depths between 70 and 100 feet, whereas factors of safety would have been greater than one based on the simplified method. This reflects the "bottom up" wave propagation used in DESRA-MUSC, versus the "top down" inertial loading from the simplified method.

3.5.2.3 Lateral Spread Implications

As part of Step 3 of the procedure in Section 2.5.2.1, an estimate of the amount of movement is required. For the Newmark sliding block analogy, displacements are calculated for a range of yield accelerations, which are those accelerations that will just make a soil wedge start to move. This is somewhat analogous to a coefficient of friction.

A key conclusion from these analyses was the strong likelihood that lateral spread deformations would be controlled by a failure zone in the 45- to 50-foot layer. Displacement time histories for a rigid block sliding on this layer (assuming a Newmark sliding block analogy) were generated for a range of yield accelerations, using input acceleration time histories generated at the base of the 50- to 55-foot layer. The analyses were performed using the DISPMNT computer program (Houston et. al., 1987). "Upslope" deformations were suppressed assuming a strong one directional driving force from the embankment. At time zero, drained strengths for the liquefied layer were assumed. Strengths were degraded as a function of pore water pressure increase and reduced to the assumed residual strength of 300 psf when liquefaction was triggered. As would be expected, most of the computed displacements occurred subsequent to triggering.

Results showing displacement time history plots for the 2,475-year event based on the Chile earthquake as a function of yield acceleration are shown in Figure 3.38. The input acceleration time histories used at a depth of 55 feet, are shown in Figure 3.39. Note the similarities in acceleration time histories at 55 feet for the 475- and 2,475-year events.

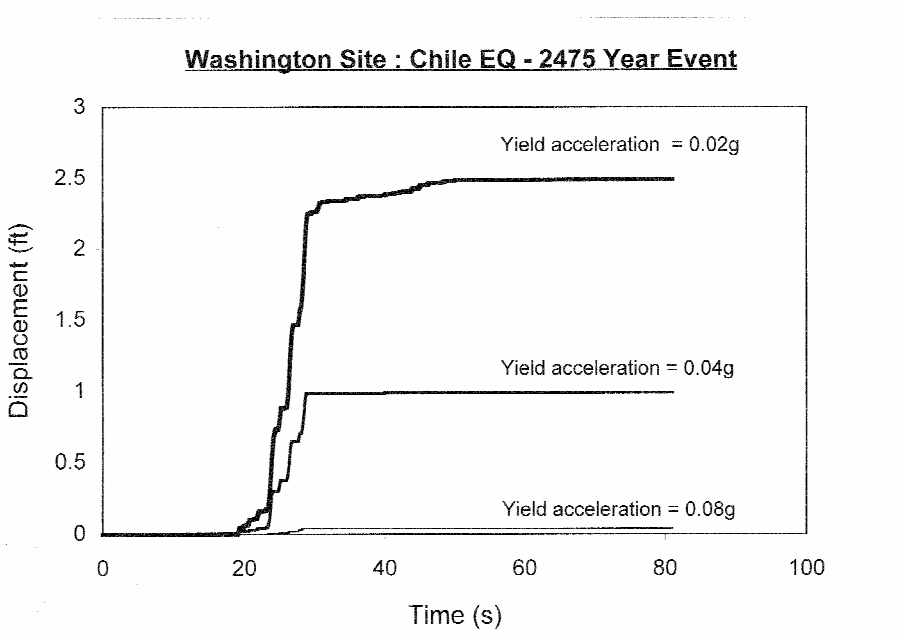

Figure 3.38 Displacement vs. Time for 2,475-Year Earthquake

Total accumulated displacements as a function of yield acceleration are shown in Figure 3.40, for the three earthquake records. These plots became a basis for discussion on remediation analyses, as described in Section 3.5.3.4, below. Similar analyses for potential failure surfaces in the depth zone of 10 to 20 feet, gave a maximum displacement of only 0.06 feet. The time histories based on the Chile earthquake, represented at a depth of 20 feet for these analyses, are also shown in Figure 3.39.

3.5.3 Lateral Ground Displacement Assessment

From the results of these liquefaction studies, two liquefiable zones were identified for stability and displacement evaluations. One extends from a depth of 10 feet to 20 feet below the ground surface. The other extends from 45 to 55 feet below the ground surface. The residual strength of these two liquefied zones was selected as 300 psf based on the SPT blow counts in each layer. Soils between 20 and 40 feet and 55 and 100 feet below the ground surface were assumed to have partial build-up in pore water pressure, resulting in a some reduction in the friction angle of the non-liquefied sand layers, as shown in the DESRA-MUSC analyses. For these conditions, the response of the end slope for the approach fill on each side of the channel was estimated by conducting pseudo-static stability evaluations followed by simplified deformation analyses using chart-based Newmark analyses. These correspond to Steps 2 and 3 of the design procedure of Section 2.5.2.1.

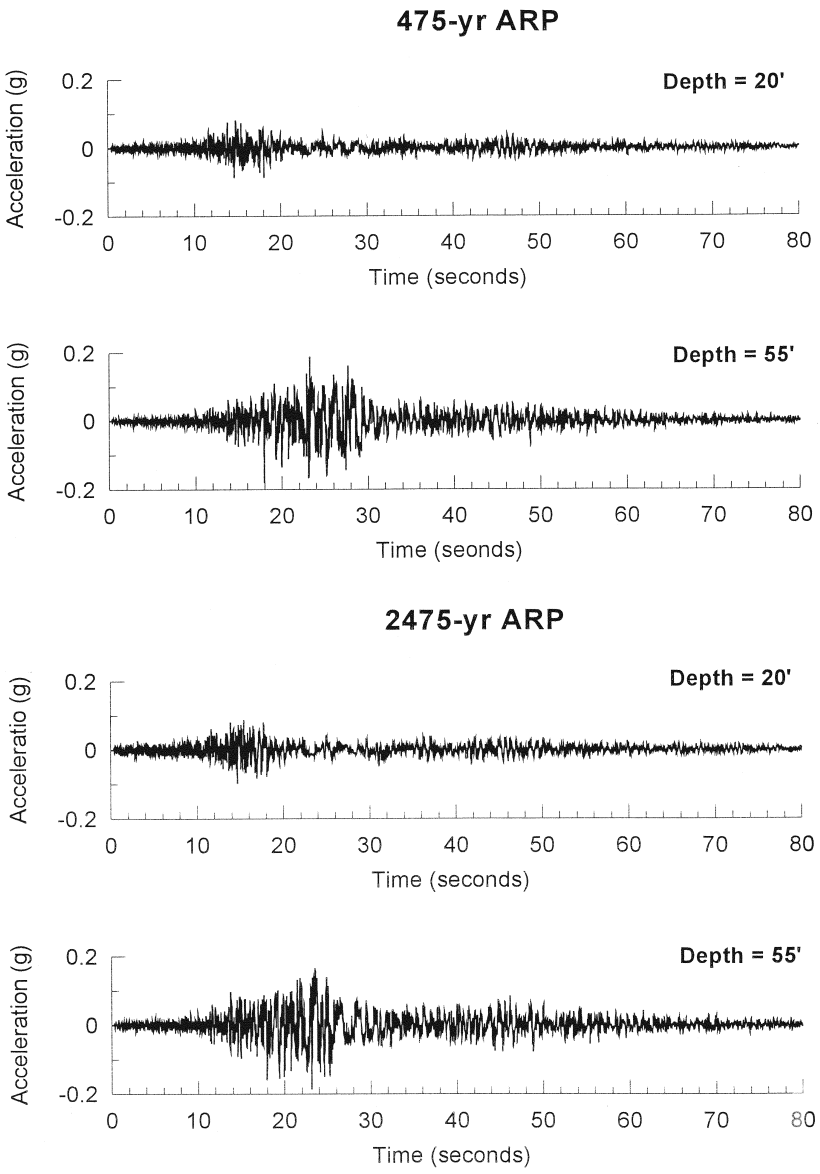

Figure 3.39 Acceleration Histories at Bottoms of Liquefiable Layers for 475- and 2,475-Year Events with Fill

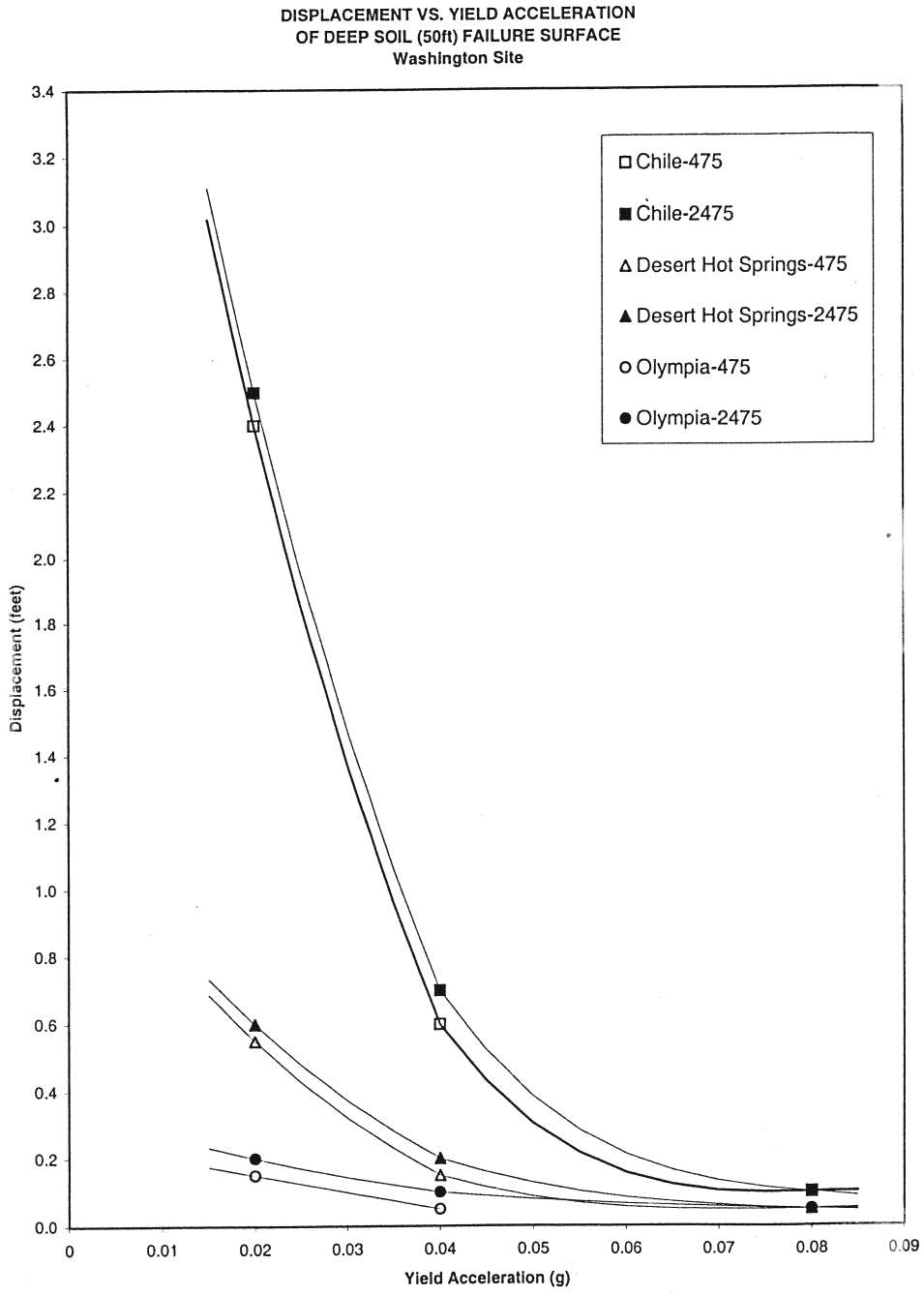

Figure 3.40 Displacement vs. Yield Acceleration for the Deep Sliding Surface of the Western U.S. Site

3.5.3.1 Initial Stability Analyses

Once liquefaction has been determined to occur, a stability analysis is performed to assess the potential for soil movement as indicated in Step 2 of the design procedure.

The computer program PCSTABL was used during these analyses. Most analyses were conducted using a simplified Janbu failure method of analysis with a wedge failure surface. This geometry was believed to be most representative of what would likely develop during a seismic event. Checks were also performed for a circular failure surface and using the modified Bishop and Spencer methods of analysis. Both pre-liquefaction and post-liquefaction strengths were used during these analyses.

Results of the pre-liquefaction studies indicate that the static FOS for the end slopes on each side of the channel were 1.5 or more, confirming acceptable static conditions. Yield accelerations (accelerations that produce FOS's of 1 on postulated failure surfaces in the pre-liquefaction state) were typically greater than 0.15, suggesting that some deformation would occur within the end slopes, even without liquefaction.

The FOS values dropped significantly when residual strengths were assigned to the two liquefied layers, as summarized in the table below. For these analyses, the geometry of the failure surfaces was constrained to force failure through the upper or lower liquefied zone. Figure 3.41 and Figure 3.42 show typical failure surfaces. Results given in the following table are for post-liquefaction conditions; i.e., no seismic coefficient for the right-hand approach fill. Supporting information for these results is presented in Appendix B.

Case	Abutment	Factor of Safety	Comment
Upper Wedge	Right	0.71	Modified Janbu
Lower Wedge	Right	0.79	Modified Janbu
Upper Circle	Right	0.81	Modified Bishop
Lower Circle	Right	0.86	Modified Bishop

Similar liquefaction stability analyses for the left approach fill gave FOS values of slightly less than 1.0 for the shallow layer and greater than 1.3 for the deeper layer. This better condition results because of the different geometry on the west side relative to the east. Because of the higher FOS values, displacements would be less, resulting in fewer requirements for mitigation. Since stability of the west abutment was found to be the less critical of the two, it was dropped from further consideration for this study of liquefaction potential. In an actual design, both abutments would have to be evaluated to determine whether one or both required special mitigation to handle potential liquefaction effects.

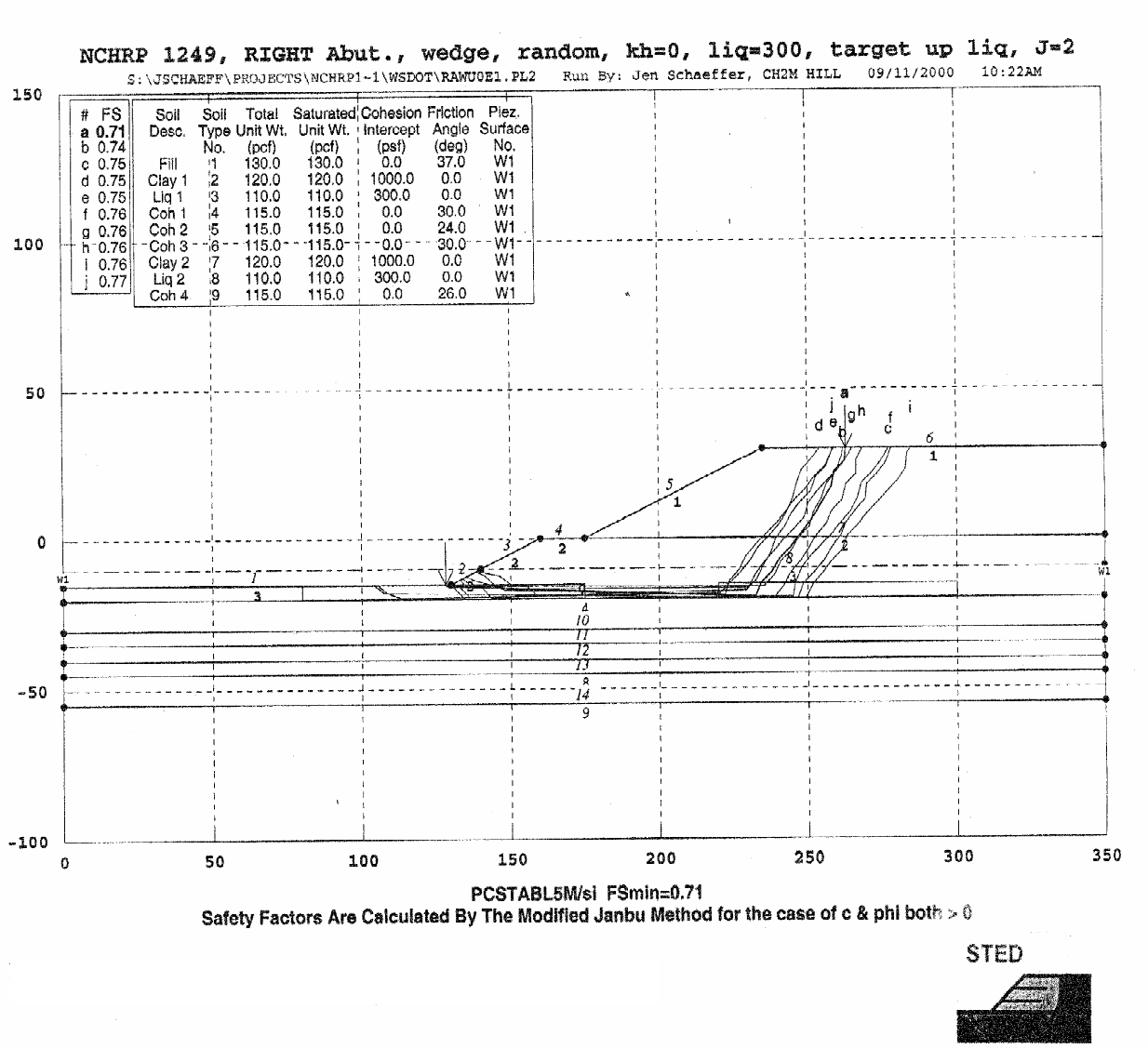

Figure 3.41 Typical Sliding Mechanism for Shallow Flow Failure for the Western U.S. Site

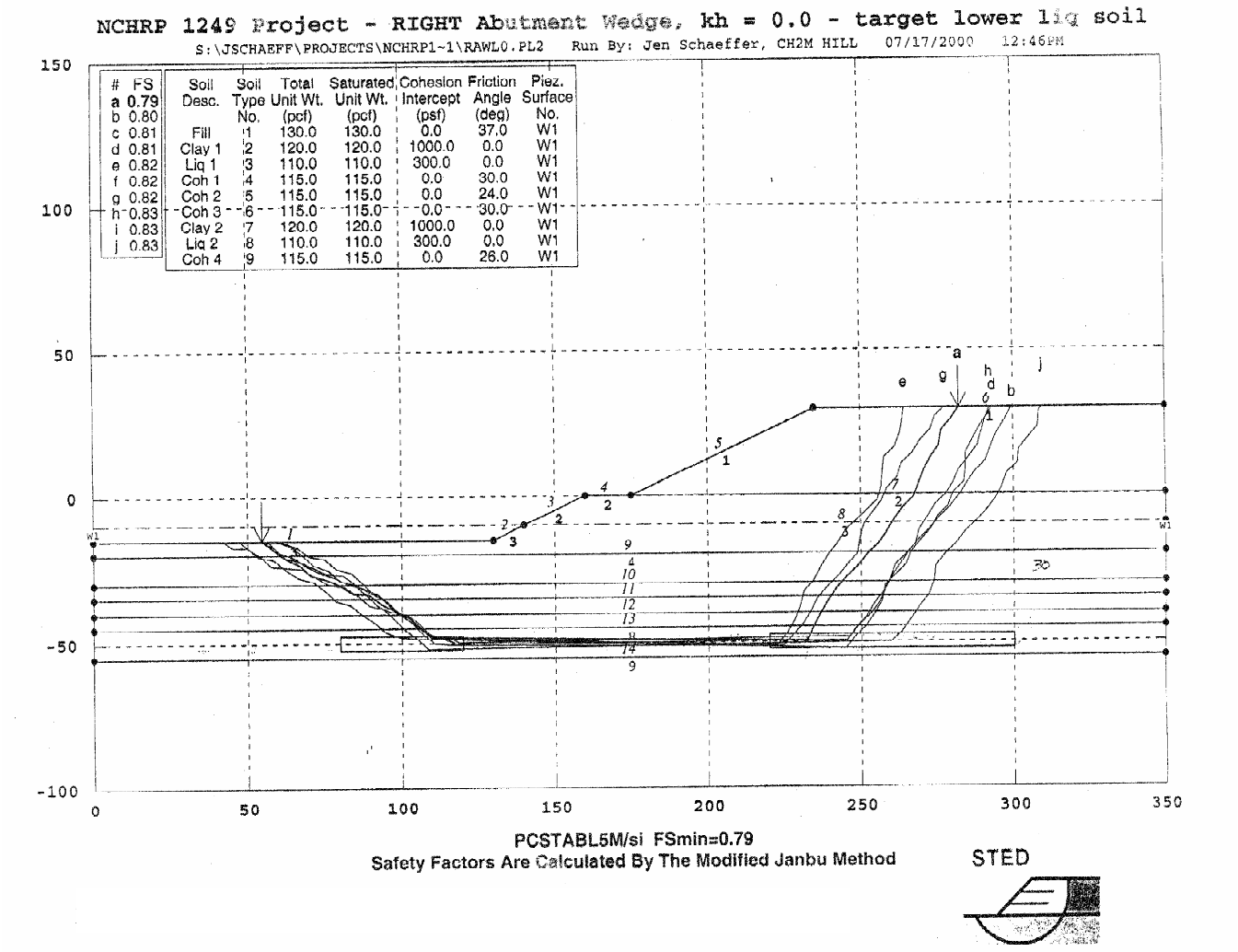

Figure 3.42 Typical Sliding Mechanism for Intermediate-Depth Flow Failure for the Western U.S. Site

Results of the stability analyses for the right-hand abutment indicate that for liquefied conditions and no inertial force in the fill (i.e., after the earthquake), factors of safety range from 0.7 to 0.9 for different assumptions of failure surface location and method of analysis. FOS values less than 1.0 indicate that lateral flow failure of the material is expected during any event that causes liquefaction in the two layers, whether it is associated with the 475-year or 2,475-year return period. The potential for instability is similar for failure surfaces through the upper and lower layers of liquefied soil, suggesting that any mitigation procedure would have to consider displacements through each layer. In other words, it would not be sufficient to improve only the upper 20 feet of soil where the FOS was lower, as a liquefaction-related failure could also occur at deeper depths.

Given the predicted occurrence of a liquefaction-induced flow failure, it would be desirable to quantify the amount of displacement expected during this flow, which corresponds to Step 3 of the design procedure. Unfortunately, this is quite difficult when flow failures are predicted to occur. The simplified chart methods or the Newmark time history analysis, described previously, cannot be used to compute displacements for flow failures. However, flow displacements could be expected to be large, and such large displacements would indicate mitigation might be needed. More detailed analyses considering both structural pinning effects and ground modifications for mitigation of displacements are discussed in the following section of this report.

3.5.3.2 Stability Analyses with Mitigation Measures

Since it has been determined that significant soil movements will occur, Step 7 of the design procedure requires an evaluation of measures that will reduce the amount of movement.

Two procedures were evaluated for mitigating the potential for lateral flow or spreading, structural pinning and ground improvement. For these analyses the additional resistance provided by the improved ground or by the structural pinning of the soil was incorporated into the stability analyses described above. If the FOS for the revised analysis was greater than 1.0, the yield acceleration for the mitigated condition was determined, which then allowed displacements to be estimated. If the FOS was still less than 1, then flow would still occur and additional mitigation measures would be required.

For the structural pinning evaluation, shear forces were calculated to be 90 kips per pile for sliding on either the upper or lower failure surfaces. Procedures for determining the amount of pinning force are given in Section 3.6.2. The abutment has 12 piles which extend through the sliding zone, resulting in 1,080 kips of additional shear reaction to sliding. Pier 5 of the bridge has 16 piles that produce 1,440 kips of pinning force. The abutment and the columns for Pier 5 are expected to develop reaction forces from passive pressure and column plastic shear. These forces were calculated to be 400 kips and 420 kips, respectively. This reaction occurs over the 48-foot abutment and pile cap widths, resulting in a total resistance of 31 and 70 kips per foot of width (or 1480 kips and 3340 kips, total) for displacement along the upper and lower liquefied zones, respectively.

This reaction force was introduced into the slope stability analysis using two methods:

1. A thin vertical slice the width of the pile group was placed at the location of the pile. This slice was assigned a strength that gives the same total pile resistance per unit width.
2. The resistance per unit width was converted into an equivalent shear strength along the shear plane in the liquefied zone and this equivalent strength was added to the residual strength of 300 psf. For these analyses, the upper failure plane was determined to be 104 feet in length giving an added component to the liquefied strength of 300 psf. The resulting strength assigned to the liquefied layer was 600 psf (i.e., 300 psf + 300 psf = 600). For the lower zone, the surface is 132 feet in length, resulting in an average pinning resistance of 530 psf and a total resistance of 830 psf.

Both procedures gave generally similar results.

The FOS for the lower surface is greater than 1.0 for the post-liquefaction case, indicating that a post-earthquake flow failure would not occur. However, under the slope inertial loading, displacement of the slope could develop, and this can be assessed using the Newmark sliding block analysis once the yield acceleration is determined. The upper surface has a FOS of 1.0, indicating that a flow failure is on the verge of occurring.

The yield acceleration for the lower surface was determined by varying the seismic coefficient within the slope stability analysis until the factor of safety was 1.0. This analysis resulted in the upper surface yield acceleration given below. For the upper surface, it was assumed that the yield acceleration was zero, since the FOS was 1.0 without any additional inertial force. Appendix B provides supporting information for these values.

Case	Yield Acceleration (g)
Upper Surface	0
Lower Surface	0.02

For the ground improvement case, different widths of improved ground were used below the abutment. The improved ground extended through each of the liquefied zones. Soil in the improved ground was assigned a friction angle of 45 degrees. This increase in strength was assumed to be characteristic of stone columns or a similar improvement procedure. As with the structural pinning case, two procedures were used to represent the improved zone. One was to model it explicitly; the second involved "smearing" the reaction from the improved strength zone across the failure surface by increasing the strength of the soil in the liquefied zone to give the same reaction. The resulting FOS was greater than 1.0 for all cases, indicating that flow would not occur. This allowed yield accelerations to be computed as a function of the width of the improved zone, in order to estimate the displacements that may occur. These values are summarized below.

Width (feet)	Yield Acceleration (g)
30	0.12
50	0.33
70	0.65

3.5.3.3 Displacement Estimates from Simplified Methods

Once lateral flow has been prevented, the amount of displacement that occurs from inertial loading on the failure wedge is estimated. This corresponds to Steps 3 and 11 of the design procedure.

Displacements were estimated for the yield accelerations given above using simplified methods. For these estimates, methods recommended by Franklin and Chang (1977), Hynes and Franklin (1984), Wong and Whitman (1982), and Martin and Qiu (1994) were used. All three methods approach the problem similarly. However, the Hynes and Franklin, as well as the Wong and Whitman and Martin and Qiu methods, eliminate some of the conservatism that is implicit to the Franklin and Chang method. For the Franklin and Chang method, it is necessary to define both the peak acceleration and velocity. The ratio of velocity to acceleration was assumed to be 30 for this study based on typical observations from recording of more distant events. For near-source events (epicentral distances less than about 15km) this ratio can be as high as 60. In the case of the Hynes and Franklin method, displacements can be obtained for the mean, mean + 1σ, and upper bound displacements. The mean displacements are used for this study. The Martin and Qui study was based on the Hynes and Franklin database, but included the peak ground acceleration as an additional variable in the data regression analyses. Mean values were also used in their regressions. Each of these simplified methods relates displacement to the ratio of yield acceleration to the peak ground acceleration (k_{max}). For these evaluations, k_{max} was 0.24g and 0.42g for the 475- and 2,475-year earthquakes, respectively. The resulting displacements for the cases cited above are summarized below.

It is the recommendation of the new provisions that a designer use the Martin and Qiu results. The Franklin and Chang and Wong and Whitman results provide possible upper and lower bound ranges on the displacements, but they are not believed to be as credible as the Hynes and Franklin and Martin and Qiu results.

Case	Displacements (inches)							
	475-Year Event				2,475-Year Event			
	F-C	H-F	W-W	M-Q	H-F	H-F	W-W	M-Q
Pile Pinning/Lower	>36	16	10	28	>36	31	23	42
Stone Columns – 30 ft	<1	<4	<1	5	13	<4	3	8
Stone Columns – 50 ft	<1	<4	<1	<1	<1	<4	<1	<1
Stone Columns – 70 ft	<1	<4	<1	<1	<1	<4	<1	<1

The approximate displacement from the Martin and Qiu method for the 475-year event is 28 inches. For the 2,475-year event the displacement is 42 inches.

3.5.3.4 Displacement Estimates Using Site Response Analysis Results

This section corresponds to Steps 3 and 11 of the design procedure, as they apply to site-specific analysis of potential displacements using the nonlinear effective stress method.

Similar estimates to the simplified methods described above may be made using the displacement versus yield acceleration curves shown in Figure 3.40. As the curves are essentially identical for the 475- and 2,475-year events, the displacement estimates shown in the table below are for both events and for the lower yield surface (45- to 55-foot depth).

Case	Displacements (inches)		
	Chile	Olympia	Desert Hot Springs
Pile Pinning	29	7	3
Stone Columns (> 30 foot width)	< 1	< 1	< 1

These estimates are generally consistent with the estimates from the simplified methods, although the site-specific results indicate that the event representative of the large mega-thrust subduction zone earthquake (Chile) will produce the largest displacements. The displacements from a moderate magnitude subduction zone intraslab earthquake (Olympia) and a moderate magnitude local shallow crustal earthquake (Desert Hot Springs) produce much more modest displacements that could be accommodated by the foundations.

3.6 Structural Analysis and Design

The design of bridge structures for liquefaction effects generally has two components. The first is that the bridge must perform adequately with just the liquefaction-induced soil changes alone. This means that the mechanical properties of the soil that may liquefy are changed to reflect their post-liquefaction values (i.e., properties such as stiffness are reduced). Design for these cases is in reality a design for structural vibration effects, and these are the effects that the code-based procedures typically cover for design. The second component of the design is the consideration of liquefaction-induced ground movements. These can take several forms: lateral spreading, lateral flow and ground settlement. Lateral spreading is a lateral movement that is induced by the ground shaking and may develop in an incremental fashion as shaking occurs. Flow, on the other hand, is movement that occurs due to the combined effects of sustained pore water pressure and gravity. Flow may even happen or continue after ground shaking has stopped.

To summarize, two design components are considered, one for vibration and one for spreading or flow. The potential interaction or combination of these effects must be addressed in the design, and at the present, there is not sufficient understanding of the phenomena to warrant performing a combined analysis. Therefore, the recommended methodology is to simply consider the two effects independently, i.e., de-coupled. The reasoning behind this was that it is not likely that the peak vibration response and the peak spreading or flow effect will occur simultaneously. In fact, for most earthquakes, the peak vibration response is likely to occur somewhat in advance of the maximum ground movement loading. Furthermore, the de-coupling of response allows the

flexibility to use separate and different performance criteria for design to accommodate the two phenomena. In some areas where extended shaking could result in the two phenomena occurring concurrently, it may be desirable to use more rigorous coupled effective stress computer models to evaluate this.

3.6.1 Vibration Design

Vibration design was done for both the AASHTO I-A provisions and for the recommended NCHRP 12-49 provisions. For the recommended LRFD provisions, both the 2,475-year and 100-year events were considered. Since the primary objective of the study was to compare the existing and recommended provisions, the designs were more of a preliminary nature, which was felt to be sufficient to highlight the major differences.

In this study, the same bridge was evaluated for each of the two specification requirements. Comparisons were then based on the amounts of reinforcing, for example, and in the case where sizes should be altered, recommendations are given. To this end, the designs represent preliminary designs that highlight the differences between the two specifications.

3.6.1.1 Modeling

The bridge was modeled using SAP2000 for both designs, and a multimode analysis was done for each. The design procedure from the recommended LRFD Specification is SDAP E, which permits a larger force reduction factor to be used, and it requires a pushover analysis as a check.

The soil effects on the piles were modeled using LPILE to develop spring stiffnesses at the pile heads. Additionally, the passive resistance offered by the sides of the pile caps and seals were included in the estimates of spring constants. Group effects were considered in the development of the pile springs. The composite springs derived from the combined resistances of all springs attached to a given pile cap were developed as input for the dynamic model of the structure.

The overhanging stub abutment provides longitudinal soil restraint against the end diaphragm, and this soil restraint was modeled as outlined in Chapter 11 of the recommended LRFD Specification. The bridge earthquake resisting system would be categorized as ‘Permissible with Owner Approval’ due to the use of the full passive longitudinal soil resistance per Chapter 11 of the recommended LRFD Specification.

For both earthquake designs, effective concrete properties were used to develop the column stiffnesses. In other elements, the gross moments of inertia were used. The piles were considered as combined steel and reinforced concrete elements. A small reduction, 1/16-inch, in wall thickness was taken to account for section loss to corrosion.

The response spectra as given in Section 3.4.1 were used as input for the modal analyses.

3.6.1.2 Results

Vibration design is the normal process of designing the structure for the spectral input as outlined by the LRFD Specification. The design includes both the unreduced and reduced soil properties and input ground motions to consider both the non-liquefied and liquefied responses. However, the point in time during ground shaking that the reduced soil stiffnesses are applicable is not known unless a full nonlinear time history analysis of the site is conducted. Therefore, the conservative approach that is typically taken is to design the structure for both the non-liquefied and the liquefied conditions. This approach then provides bounds on the actual expected behavior of the structure, and therefore the approach is conservative.

For both the existing AASHTO I-A and the recommended LRFD designs, the soil profiles used to develop the foundation springs are given in Figures 3.43 and 3.44. The required soil properties to develop the springs are also given in the figures.

For the existing AASHTO provisions, only one input spectrum is required. For the recommended LRFD provisions, spectra for both the 100- and 2,475-year events must be used. The input spectra that are used have been discussed in Section 3.4. The recommended specification does not require that a liquefaction assessment be done for the 100-year earthquake. Therefore, only the nonliquefied condition is used for that design.

The results of the elastic analyses of the SAP2000 models are given in Table 3.3 through Table 3.7. These list the elastic displacements, shear forces (including passive backfill forces), moments in the substructure, maximum moment in the superstructure, and structure fundamental vibration periods. The results are tabulated for both the non-liquefied and liquefied conditions for the 2,475-year event and for the nonliquefied condition for the 100-year event. Additionally, the nonliquefied and liquefied results are given for the 475-year event. Thus, each table contains five entries for loading.

For the 2,475-year liquefied case, the input spectrum was two-thirds of the input spectrum for the nonliquefied case. This reflects the maximum reduction allowed by the recommended LRFD provisions when site-specific analyses indicate that the input motion likely will be less than that predicted by the basic code spectrum. For this reason, the displacements and the forces induced in the liquefied case are generally smaller than those from the non-liquefied case.

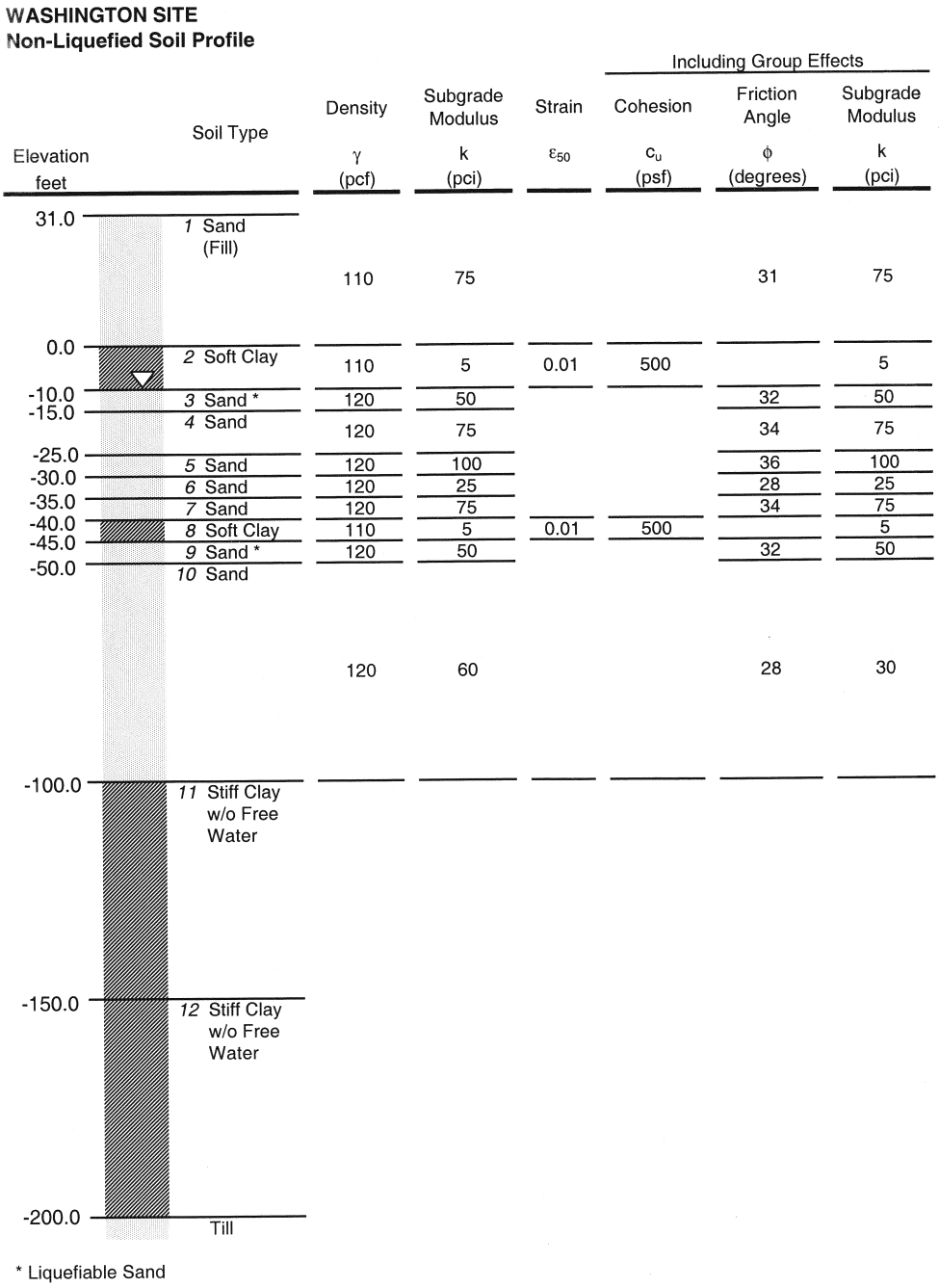

Figure 3.43 Non-Liquefied Soil Profile and Engineering Properties for the Western U.S. Site

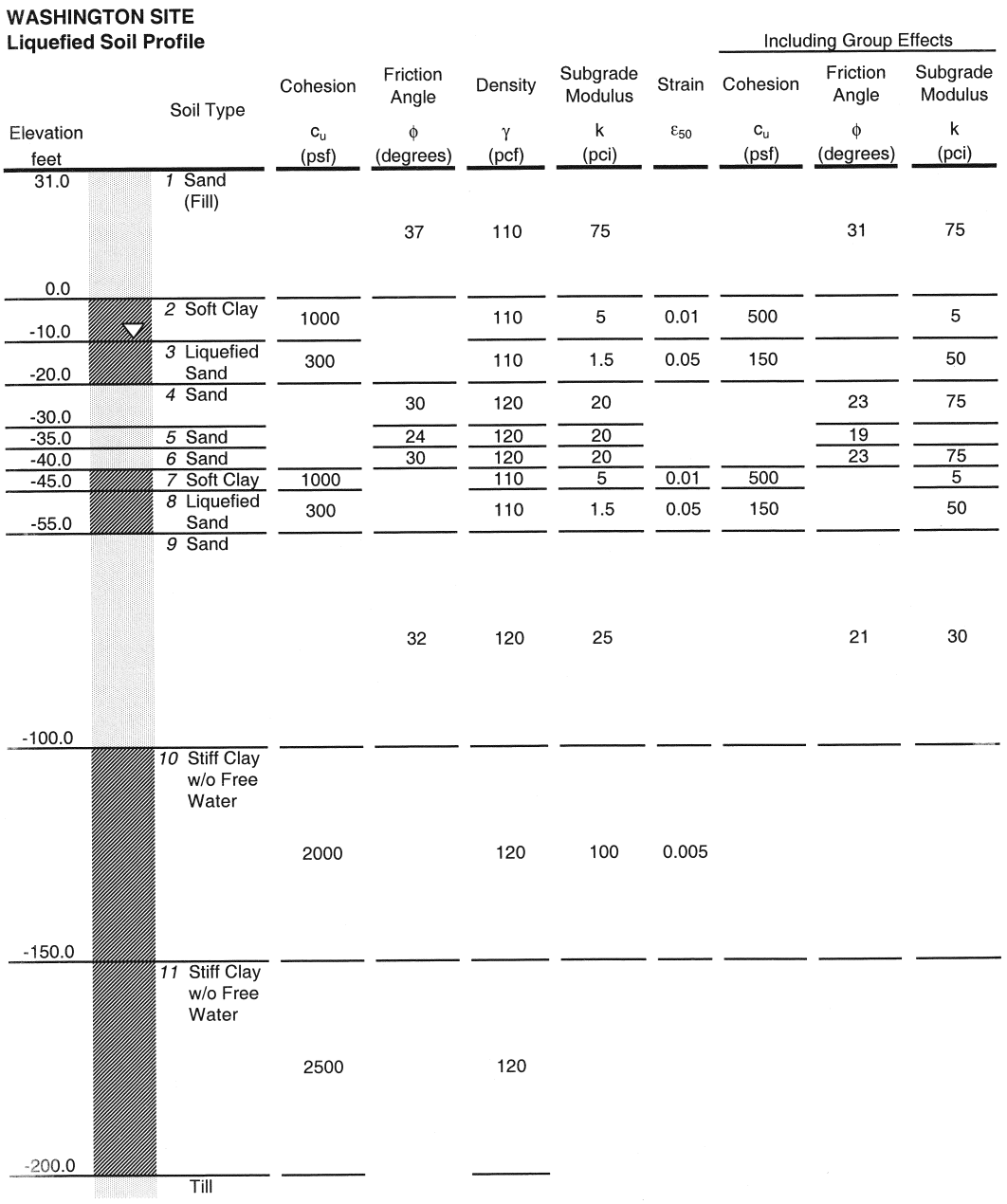

Figure 3.44 Liquefied Soil Profile and Engineering Properties for the Western U.S. Site

Table 3.3 Washington Bridge – Elastic Structural Displacements

		EQT		EQL		EQT		EQL		EQT		EQL	
		D_T	D_L	D_T	D_L	D_T	D_L	D_T	D_L	D_T	D_L	D_T	D_L
		ft	ft	ft	ft	ft	ft	ft	ft	ft	ft	ft	ft
	Joints	**2500-yr Non-Liquefied**				**2500-yr Liquefied**				**100-yr Non-Liquefied**			
Pier 1 Abutment	611	0.00	0	0	1.11	0.00	0	0	0.72	0.00	0	0	0.27
Pier 6 Abutment	661	0.01	0	0	1.16	0.00	0	0	0.72	0.00	0	0	0.27
Pier 1 at CG Super	711	0.01	0	0	1.09	0.00	0	0	0.71	0.00	0	0	0.27
Pier 2 at CG Super	721	0.43	0	0	1.11	0.30	0	0	0.71	0.14	0	0	0.27
Pier 3 at CG Super	731	1.17	0	0	1.11	0.79	0	0	0.72	0.34	0	0	0.27
Pier 4 at CG Super	741	1.72	0	0	1.11	1.15	0	0	0.72	0.50	0	0	0.27
Pier 5 at CG Super	751	1.01	0	0	1.12	0.84	0	0	0.72	0.36	0	0	0.27
Pier 6 at CG Super	761	0.01	0	0	1.12	0.00	0	0	0.72	0.00	0	0	0.27
	Joints	**500-yr Non-Liquefied**				**500-yr Liquefied**							
Pier 1 Abutment	611	0.00	0	0	0.51	0.00	0	0	0.51				
Pier 6 Abutment	661	0.00	0	0	0.52	0.00	0	0	0.51				
Pier 1 at CG Super	711	0.00	0	0	0.51	0.00	0	0	0.51				
Pier 2 at CG Super	721	0.23	0	0	0.51	0.24	0	0	0.51				
Pier 3 at CG Super	731	0.62	0	0	0.52	0.63	0	0	0.51				
Pier 4 at CG Super	741	0.92	0	0	0.52	0.93	0	0	0.51				
Pier 5 at CG Super	751	0.67	0	0	0.52	0.67	0	0	0.51				
Pier 6 at CG Super	761	0.00	0	0	0.52	0.00	0	0	0.51				

Table 3.4 Washington Bridge – Elastic Structural Shear Forces

		EQT		EQL		EQT		EQL		EQT		EQL	
		V_T	V_L	V_T	V_L	V_T	V_L	V_T	V_L	V_T	V_L	V_T	V_L
		kips	kips	kips	kips	kips	kips	kips	kips	kips	kips	kips	kips
	Joints	**2500-yr Non-Liquefied**				**2500-yr Liquefied**				**100-yr Non-Liquefied**			
Pier 1 Abutment	611/711	414	0	0	416	277	0	0	393	205	0	0	398
Pier 2 Columns (Bot.)	420,422	513	84	0	1329	341	57	0	860	170	25	0	318
Pier 3 Columns (Bot.)	430,432	415	40	0	400	280	27	0	258	119	12	0	96
Pier 4 Columns (Bot.)	440,442	448	12	0	293	299	8	0	189	129	4	0	70
Pier 5 Columns (Bot.)	450,452	446	40	0	401	298	27	0	258	129	12	0	96
Pier 6 Abutment	661/761	473	0	0	419	317	0	0	395	215	0	0	401

	Joints	**500-yr Non-Liquefied**				**500-yr Liquefied**			
Pier 1 Abutment	611/711	261	0	0	385	231	0	0	406
Pier 2 Columns (Bot.)	420,422	272	45	0	615	271	45	0	610
Pier 3 Columns (Bot.)	430,432	221	22	0	185	223	22	0	183
Pier 4 Columns (Bot.)	440,442	240	6	0	136	241	6	0	134
Pier 5 Columns (Bot.)	450,452	239	22	0	186	239	22	0	183
Pier 6 Abutment	661/754	284	0	0	387	259	0	0	408

Table 3.5 Washington Bridge – Elastic Structural Moments

	Joints	2500-yr Non-Liquefied				2500-yr Liquefied				100-yr Non-Liquefied			
		EQT		EQL		EQT		EQL		EQT		EQL	
		M_T ft-kips	M_L ft-kips	M_T ft-kips	M_L ft-kips	M_T ft-kips	M_L ft-kips	M_T ft-kips	M_L ft-kips	M_T ft-kips	M_L ft-kips	M_T ft-kips	M_L ft-kips
Pier 1 Abutment	611	1815	0	0	0	1214	0	0	0	822	0	0	0
Pier 2 Columns (Bot.)	420,422	7733	1265	0	19909	5137	854	0	12887	2566	370	0	4773
Pier 3 Columns (Bot.)	430,432	9368	911	0	8999	6314	607	0	5795	2691	281	0	2159
Pier 4 Columns (Bot.)	440,442	11235	301	0	7318	7509	206	0	4710	3236	102	0	1756
Pier 5 Columns (Bot.)	450,452	10077	906	0	9024	6729	606	0	5810	2923	265	0	2163
Pier 6 Abutment	661	2897	0	0	0	1938	0	0	0	1003	0	0	0

	Joints	500-yr Non-Liquefied				500-yr Liquefied			
		EQT		EQL		EQT		EQL	
		M_T ft-kips	M_L ft-kips	M_T ft-kips	M_L ft-kips	M_T ft-kips	M_L ft-kips	M_T ft-kips	M_L ft-kips
Pier 1 Abutment	611	1070	0	0	0	996	0	0	0
Pier 2 Columns (Bot.)	420,422	4100	672	0	9219	4076	680	0	9145
Pier 3 Columns (Bot.)	430,432	4984	490	0	4167	5044	489	0	4114
Pier 4 Columns (Bot.)	440,442	6016	151	0	3389	6037	155	0	3344
Pier 5 Columns (Bot.)	450,452	5388	485	0	4177	5398	488	0	4123
Pier 6 Abutment	661	1603	0	0	0	1562	0	0	0

Table 3.6 Washington Bridge – Maximum Elastic Transverse Moment in Superstructure

Model	Joint	EQT M_T ft-kips
2500-yr Non-Liquefied	741	29469
2500-yr Liquefied	734	20720
100-yr Non-Liquefied	734	10226
500-yr-Non-Liquefied	741	15775
500-yr Liquefied	741	16815

Table 3.7 Washington Bridge – Structural Period

Model	T_{EQL} sec	T_{EQT} sec
2500-yr Non-Liquefied	1.38	1.62
2500-yr Liquefied	1.33	1.63
100-yr Non-Liquefied	1.15	1.62
500-yr-Non-Liquefied	1.29	1.62
500-yr Liquefied	1.27	1.63

The displacements are given in Table 3.3, and as can be seen in the table, the 2,475-year nonliquefied structural displacements are approximately twice those for the 475-year event. The liquefied displacements are roughly two-thirds of the nonliquefied values. For this structure, the pile caps are generally positioned within soil layers that do not liquefy; thus the passive resistance of the soil around the caps provides a substantial portion of the lateral resistance of the caps. For this reason, the differences in the response of the bridge to the various input spectra are roughly in proportion to the differences in the spectra themselves.

Listed in the table are displacements for both the transverse and longitudinal earthquake. It is evident that the lateral displacement shape is strongly affected by the transverse restraint of the abutments and of the shorter intermediate piers, for instance, Pier 2. The largest transverse displacement occurs near Pier 4 for all the input loadings, and the largest displacement is 1.72 feet for the 2,475-year nonliquefied case. Pier 4 is approximately 50 feet tall, so this displacement represents a drift of about 3.4 percent.

For all the longitudinal displacement cases, it is evident that the displacements are similar all along the structure. Additionally, the restraining effect of the abutment backfill has been accounted for in each run by progressively altering the abutment longitudinal springs until the appropriate soil force was obtained. In all cases, including the 475-year events, this restraint was accounted for. For the 6-foot-high backwall, the displacement at which the passive resistance of the backfill was mobilized was 0.12 feet. From Table 3.3 it is apparent that all the earthquake loadings produced displacements that fully mobilized the backfill. This includes the 100-year event.

Table 3.4 lists the elastic shear forces developed in the structure at each substructure location. Included also is the passive backfill forces as reported from the model at each abutment. The listed forces, approximately 400 kips, represents half the actual force due to the modeling using half the resistance at each end for the spectral analysis. Half of the expected force is modeled at each end because the spring in the model can take either compression or tension, yet, the soil does not carry tension. To obtain an estimate of the true expected force at either abutment, the listed value in the table should be doubled.

Tables 3.8 and 3.9 provide the progression from elastic internal forces to the design moments and ultimately design plastic shears for the tallest and the shortest columns, respectively. Pier 4 is the tallest, and Pier 2 the shortest. Both the existing provisions and the recommended provisions require a combination of directional effects. In the table, the combination methods for both sets of design procedures have been included for all earthquake events for comparison.

In this case, the bridge is comprised of multicolumn bents; so the existing provisions use a force reduction factor, R, of 5 and the recommended provisions allow an R of 6, provided a nonlinear static displacement check is done. For the 100-year design, the recommended provisions allow an R of 1.3.

For the tallest columns and the recommended provisions, the 2,475-year event required a steel content in the columns of 1.4 percent, and this was controlled by the 100-year event. The 100-year event produced a design moment that was approximately 20 percent larger than the 2,475-year event. This is due to the relative magnitudes of R and of the input spectra. For the 475-year event, a design using one percent steel resulted. For Pier 2, the results were similar.

The foundation (piling), used as a starting point for both the existing and recommended provisions, was the same. This is because one objective of the study was to evaluate a system that worked for the existing provisions when subject to the effects of the larger design earthquake.

The pier designs were checked for displacement capacity, using an approximate pushover analysis, as outlined in Table 3.10 and 3.12 for Piers 4 and 2, respectively. The assessment considered the superstructure and the pile caps as rigid restraints against rotation for simplicity. While the check is only required for the recommended provisions, the checks were performed on the designs to the existing provisions as well. As noted in the tables, all the columns met the checks (i.e., the displacement capacity exceeded the demands). The recommended provisions require the checks only on a bent-by-bent basis and only in the principal direction of the substructure.

The recommended specification also requires that the displacements be checked for P-Δ effects. In other words, the lateral shear capacity of the bents defines a maximum displacement that can occur without suffering problems from displacement amplification due to P-Δ. These checks were made in Tables 3.11 and 3.13 for Piers 4 and 2, respectively. Both piers are adequate as-designed with respect to P-Δ.

Table 3.8 Washington Bridge – Combinations of Seismic Force Effects
Pier 4 Column – Tallest Pier

			H_{col} = 50.0 ft.				
		Units	**2500-yr N**	**2500-yr L**	**100-yr N**	**500-yr N**	**500-yr L**
Basic Elastic Forces	P_{DL} (Bottom)	kips	812	812	812	812	812
	P^L (Bottom)	kips	0.9	0.6	0.6	0.6	0.7
	P^T (Bottom)	kips	1070	715	308	573	575
	M_X^L (Top or Bottom)	ft-kips	0	0	0	0	0
	M_Y^L (Top or Bottom)	ft-kips	7318	4710	1756	3389	3344
	M_X^T (Top or Bottom)	ft-kips	11235	7509	3236	6016	6037
	M_Y^T (Top or Bottom)	ft-kips	301	206	102	151	155
Div 1A Method	$P^{LC1} = P^L + 0.3P^T$	kips	322	215	93	**173**	**173**
	$P^{LC2} = 0.3P^L + P^T$	kips	1070	715	308	**573**	**575**
	$M_X^{LC1} = M_X^L + 0.3M_X^T$	ft-kips	3371	2253	971	**1805**	**1811**
	$M_X^{LC2} = 0.3M_X^L + M_X^T$	ft-kips	11235	7509	3236	**6016**	**6037**
	$M_Y^{LC1} = M_Y^L + M_Y^T$	ft-kips	7408	4772	1787	**3434**	**3391**
	$M_Y^{LC2} = 0.3M_Y^L + M_Y^T$	ft-kips	2496	1619	629	**1168**	**1158**
SRSS Circ. Col.	$M^{LC1} = \text{sqrt}\left[\left(M_X^{LC1}\right)^2 + \left(M_Y^{LC1}\right)^2\right]$	ft-kips	8139	5277	2033	**3880**	**3844**
	$M^{LC2} = \text{sqrt}\left[\left(M_X^{LC2}\right)^2 + \left(M_Y^{LC2}\right)^2\right]$	ft-kips	11509	7682	3297	**6128**	**6147**
NCHRP SRSS Method	$P = \text{sqrt}\left[\left(P^L\right)^2 + \left(P^T\right)^2\right]$	kips	**1070**	**715**	**308**	573	575
	$M_X = \text{sqrt}\left[\left(M_X^L\right)^2 + \left(M_X^T\right)^2\right]$	ft-kips	**11235**	**7509**	**3236**	6016	6037
	$M_Y = \text{sqrt}\left[\left(M_Y^L\right)^2 + \left(M_Y^T\right)^2\right]$	ft-kips	**7324**	**4715**	**1759**	3392	3348
NCHRP SRSS + 100%-40% Rule	$P_1 = P$	kips	**1070**	**715**	**308**	573	575
	$M_{X1} = 0.4M_X$	ft-kips	4494	3004	1294	2406	2415
	$M_{Y1} = 0.4M_Y$	ft-kips	2930	1886	704	1357	1339
	$M_1 = \text{sqrt}\left[\left(M_{X1}\right)^2 + \left(M_{Y1}\right)^2\right]$	ft-kips	**5365**	**3547**	**1473**	2763	2761
	$P_2 = 0.4P$	kips	**428**	**286**	**123**	229	230
	$M_{X2} = M_X$	ft-kips	11235	7509	3236	6016	6037
	$M_{Y2} = 0.4M_Y$	ft-kips	2930	1886	704	1357	1339
	$M_1 = \text{sqrt}\left[\left(M_{X2}\right)^2 + \left(M_{Y2}\right)^2\right]$	ft-kips	**11611**	**7742**	**3312**	6167	6184
	$P_3 = 0.4P$	kips	**428**	**286**	**123**	229	230
	$M_{X3} = 0.4M_X$	ft-kips	4494	3004	1294	2406	2415
	$M_{Y3} = M_Y$	ft-kips	7324	4715	1759	3392	3348
	$M_3 = \text{sqrt}\left[\left(M_{X3}\right)^2 + \left(M_{Y3}\right)^2\right]$	ft-kips	**8593**	**5590**	**2184**	4159	4128

Table 3.8 (continued) Washington Bridge – Combinatons of Seismic Force Effects Pier 4 Column – Tallest Pier

			H_{col} = 50.0 ft.				
		Units	**2500-yr N**	**2500-yr L**	**100-yr N**	**500-yr N**	**500-yr L**
NCHRP 100%-40% Rule	$P^{LC1} = P^{L} + 0.4P^{T}$	kips	**44**	**29**	**13**	24	24
	$P^{LC2} = 0.4P^{L} + P^{T}$	kips	**1070**	**715**	**308**	573	575
	$M_X^{LC1} = M_X^{L} + 0.4M_X^{T}$	ft-kips	**4494**	**3004**	**1294**	2406	2415
	$M_X^{LC2} = 0.4M_X^{L} + M_X^{T}$	ft-kips	**11235**	**7509**	**3236**	6016	6037
	$M_Y^{LC1} = M_Y^{L} + 0.4M_Y^{T}$	ft-kips	**7438**	**4792**	**1797**	3449	3406
	$M_Y^{LC2} = 0.4M_Y^{L} + M_Y^{T}$	ft-kips	**3228**	**2090**	**804**	1507	1493
SRSS Circ. Col.	$M^{LC1} = \text{sqrt}\left[\left(M_X^{LC1}\right)^2 + \left(M_Y^{LC1}\right)^2\right]$	ft-kips	**8691**	**5656**	**2214**	4206	4175
	$M^{LC2} = \text{sqrt}\left[\left(M_X^{LC2}\right)^2 + \left(M_Y^{LC2}\right)^2\right]$	ft-kips	**11690**	**7794**	**3334**	6202	6219
Determine Design Moment	$P_{min} = P_{DL} - P_{EQ}$	kips	-258	97	504	239	237
	$P_{max} = P_{DL} + P_{EQ}$	kips	1882	1527	1120	1385	1387
	$M_{EQ}\left(\text{Maximum of } M^{LC1} \text{or} M^{LC2}\right)$	ft-kips	11690	7794	3334	6128	6147
	R-Factor (2-column bent)	---	6	6	1.3	5	5
	M_{EQ} / R	**ft-kips**	**1948**	**1299**	**2565**	**1226**	**1229**
Determine Design Shear	Actual M_Y (from PCA-COL)	ft-kips	3250			2700	
	Longitudinal Reinforcement	---	$20\#10, \rho = 1.40\%$			$12\#11, \rho = 1.03\%$	
	Overstrength Factor, OS	---	1.5			1.3	
	$M_{OS} = OS * M_Y$	**ft-kips**	**4875**			**3510**	
	$V_P = 2 * M_{OS} / H$	kips	195			140	

Table 3.9 Washington Bridge – Combinations of Seismic Force Effects
Pier 2 Column – Shortest Pier

			H_{col} = 30.0 ft.				
		Units	**2500-yr N**	**2500-yr L**	**100-yr N**	**500-yr N**	**500-yr L**
Basic Elastic Forces	$P_{DL}\,(\text{Bottom})$	kips	763	763	763	763	763
	$P^{L}\,(\text{Bottom})$	kips	72	47	17	33	33
	$P^{T}\,(\text{Bottom})$	kips	795	529	259	421	420
	$M_X^{L}\,(\text{Top or Bottom})$	ft-kips	0	0	0	0	0
	$M_Y^{L}\,(\text{Top or Bottom})$	ft-kips	19909	12887	4773	9219	9145
	$M_X^{T}\,(\text{Top or Bottom})$	ft-kips	7733	5137	2566	4100	4076
	$M_Y^{T}\,(\text{Top or Bottom})$	ft-kips	1265	854	370	672	680
Div 1A Method	$P^{LC1} = P^{L} + 0.3P^{T}$	kips	311	206	95	**159**	**159**
	$P^{LC2} = 0.3P^{L} + P^{T}$	kips	817	543	264	**431**	**430**
	$M_X^{LC1} = M_X^{L} + 0.3M_X^{T}$	ft-kips	2320	1541	770	**1230**	**1223**
	$M_X^{LC2} = 0.3M_X^{L} + M_X^{T}$	ft-kips	7733	5137	2566	**4100**	**4076**
	$M_Y^{LC1} = M_Y^{L} + 0.3M_Y^{T}$	ft-kips	20289	13143	4884	**9421**	**9349**
	$M_Y^{LC2} = 0.3M_Y^{L} + M_Y^{T}$	ft-kips	7238	4720	1802	**3438**	**3424**
SRSS Circ. Col.	$M^{LC1} = \text{sqrt}\left[\left(M_X^{LC1}\right)^2 + \left(M_Y^{LC1}\right)^2\right]$	ft-kips	20421	13233	4944	**9501**	**9429**
	$M^{LC2} = \text{sqrt}\left[\left(M_X^{LC2}\right)^2 + \left(M_Y^{LC2}\right)^2\right]$	ft-kips	10592	6976	3135	**5350**	**5323**
NCHRP SRSS Method	$P = \text{sqrt}\left[\left(P^{L}\right)^2 + \left(P^{T}\right)^2\right]$	kips	**798**	**531**	**260**	422	421
	$M_X = \text{sqrt}\left[\left(M_X^{L}\right)^2 + \left(M_X^{T}\right)^2\right]$	ft-kips	**7733**	**5137**	**2566**	4100	4076
	$M_Y = \text{sqrt}\left[\left(M_Y^{L}\right)^2 + \left(M_Y^{T}\right)^2\right]$	ft-kips	**19949**	**12915**	**4787**	9243	9170
NCHRP SRSS + 100%-40% Rule	$P_1 = P$	kips	**798**	**531**	**260**	422	421
	$M_{X1} = 0.4M_X$	ft-kips	3093	2055	1026	1640	1630
	$M_{Y1} = 0.4M_Y$	ft-kips	7980	5166	1915	3697	3668
	$M_1 = \text{sqrt}\left[\left(M_{X1}\right)^2 + \left(M_{Y1}\right)^2\right]$	ft-kips	**8558**	**5560**	**2173**	4045	4014
	$P_2 = 0.4P$	kips	**319**	**212**	**104**	169	169
	$M_{X2} = M_X$	ft-kips	7733	5137	2566	4100	4076
	$M_{Y2} = 0.4M_Y$	ft-kips	7980	5166	1915	3697	3668
	$M_1 = \text{sqrt}\left[\left(M_{X2}\right)^2 + \left(M_{Y2}\right)^2\right]$	ft-kips	**11112**	**7285**	**3202**	5521	5483
	$P_3 = 0.4P$	kips	**319**	**212**	**104**	169	169
	$M_{X3} = 0.4M_X$	ft-kips	3093	2055	1026	1640	1630
	$M_{Y3} = M_Y$	ft-kips	19949	12915	4787	9243	9170
	$M_3 = \text{sqrt}\left[\left(M_{X3}\right)^2 + \left(M_{Y3}\right)^2\right]$	ft-kips	**20188**	**13078**	**4896**	9388	9314

Table 3.9 (continued) Washington Bridge – Combinations of Seismic Force Effects Pier 2 Column – Shortest Pier

			H_{col} = 30.0 ft.				
		Units	**2500-yr N**	**2500-yr L**	**100-yr N**	**500-yr N**	**500-yr L**
NCHRP 100%-40% Rule	$P^{LC1} = P^{L} + 0.4P^{T}$	kips	**104**	**68**	**27**	50	50
	$P^{LC2} = 0.4P^{L} + P^{T}$	kips	**824**	**548**	**266**	434	433
	$M_X^{LC1} = M_X^{L} + 0.4M_X^{T}$	ft-kips	**3093**	**2055**	**1026**	1640	1630
	$M_X^{LC2} = 0.4M_X^{L} + M_X^{T}$	ft-kips	**7733**	**5137**	**2566**	4100	4076
	$M_Y^{LC1} = M_Y^{L} + 0.4M_Y^{T}$	ft-kips	**20415**	**13229**	**4921**	9488	9417
	$M_Y^{LC2} = 0.4M_Y^{L} + M_Y^{T}$	ft-kips	**9229**	**6009**	**2279**	4360	4338
SRSS Circ. Col.	$M^{LC1} = \text{sqrt}\left[\left(M_X^{LC1}\right)^2 + \left(M_Y^{LC1}\right)^2\right]$	ft-kips	**20648**	**13387**	**5027**	9628	9557
	$M^{LC2} = \text{sqrt}\left[\left(M_X^{LC2}\right)^2 + \left(M_Y^{LC2}\right)^2\right]$	ft-kips	**12040**	**7905**	**3432**	5985	5952
Determine Design Moment	$P_{min} = P_{DL} - P_{EQ}$	kips	-61	215	497	329	330
	$P_{max} = P_{DL} + P_{EQ}$	kips	1587	1311	1029	1197	1196
	M_{EQ} (Maximum of M^{LC1} or M^{LC2})	ft-kips	20648	13387	5027	9501	9429
	R Factor (2-column bent)	---	6	6	1.3	5	5
	M_{EQ} / R	**ft-kips**	**3441**	**2231**	**3867**	**1900**	**1886**
Determine Design Shear	Actual M_Y (from PCA-COL)	ft-kips	4500			2900	
	Longitudinal Reinforcement	---	28#11, ρ = 2.41%			14#11, ρ = 1.21%	
	Overstrength Factor, OS	---	1.5			1.3	
	$M_{OS} = OS * M_Y$	**ft-kips**	**6750**			**3770**	
	$V_P = 2 * M_{OS} / H$	kips	450			251	

Table 3.10 Washington Bridge – Approximate Displacement Check/SDAP E Pier 4 Column

					E_c =	552000	ksf
		H_{col} =	50	ft	I_{cr} =	5.0	ft^4
	Symbol	**Units**	**2500-yr N**	**2500-yr L**	**100-yr N**	**500-yr N**	**500-yr L**
Minimum Displacement Requirements for Lateral Load Resisting Piers (See Table 3.11 for computation of R_d and Δ_m.)	**$1.5R_d\Delta_{mT}$**	**ft**	**2.58**	**1.73**	**0.74**	**1.38**	**1.40**
	$1.5R_d\Delta_{mL}$	**ft**	**1.11**	**0.72**	**0.27**	**0.52**	**0.51**
Maximum Displacement Capacity $= \Delta_p + \Delta_y$ ***Check Transverse/Longitudinal Directions***	$\Delta_{capacity}$	**ft**	**3.11** **OK/OK**	**3.11** **OK/OK**	**3.11** **OK/OK**	**3.02** **OK/OK**	**3.02** **OK/OK**
Approximate Plastic Displacement $= \Theta_{pT}\left[H - 2\left(L_p/2\right)\right]$	Δ_{pT}	ft	2.747	2.750	2.747	2.747	2.750
Approximate Plastic Displacement $= \Theta_{pL}\left[H - 2\left(L_p/2\right)\right]$	Δ_{pL}	ft	2.675	2.658	2.595	2.645	2.638
Approximate Yield Displacement $= M_Y H^2/6EI$	Δ_y	ft	0.362	0.362	0.362	0.268	0.268
Yield Moment of Column	M_y	ft-kips	2400	2400	2400	1775	1775
Plastic Rotational Capacity – Transverse	Θ_{pT}	**rad**	**0.056**	**0.056**	**0.056**	**0.056**	**0.056**
Plastic Rotational Capacity – Longitudinal *("Life Safety" Conservative Value = 0.035)*	Θ_{pL}	**rad**	**0.055**	**0.054**	**0.053**	**0.054**	**0.054**
Number of Cycles of Loading – Transverse	N_{ft}	**cycles**	**2.98**	**2.97**	**2.98**	**2.98**	**2.97**
Natural Period of Vibration of the Structure – Transverse *Check Range of N_f (2 <= N_f <= 10)*	T_{nT}	sec	1.62 OK	1.63 OK	1.62 OK	1.62 OK	1.63 OK
Number of Cycles of Loading – Longitudinal	N_{fL}	**cycles**	**3.14**	**3.18**	**3.34**	**3.22**	**3.23**
Natural Period of Vibration of the Structure – Longitudinal *Check Range of N_f (2 <= N_f <= 10)*	T_{nL}	sec	1.38 OK	1.33 OK	1.15 OK	1.29 OK	1.27 OK
Effective Plastic Hinge Length	L_p	**m**	**0.94**	**0.94**	**0.94**	**0.94**	**0.94**
Shear Span of Member = M/V	fcn(H)	m	7.622	7.622	7.622	7.622	7.622
Yield Strain of Longitudinal Reinforcement	ε_y	m/m	0.00207	0.00207	0.00207	0.00207	0.00207
Diameter of Main Long. Reinforcing Bars	d_b	m	0.036	0.036	0.036	0.036	0.036
Distance between outer layers of long. reinf on opposite faces of member	**D'**	**m**	**1.07**	**1.07**	**1.07**	**1.07**	**1.07**

Table 3.11 Washington Bridge - P-Δ Requirements
Pier 4 Column – Transverse Earthquake

H_{col} = 50 ft

	Symbol	Units	2500-yr N	2500-yr L	100-yr N	500-yr N	500-yr L
Displacement Demand from the Seismic Analysis $(\Delta_m = R_d\Delta)$	**Δ_{mT}**	**ft**	**1.72**	**1.15**	**0.50**	**0.92**	**0.93**
Upper Limit ***Check (No increase in strength req'd if Upper Limit > Δ_m)***	**0.25C (W/P)H**	**ft**	**3.69 OK**	**3.69 OK**	**3.69 OK**	**2.40 OK**	**2.40 OK**
Seismic Coefficient Based on the Lateral Strength	C		0.32	0.32	0.32	0.21	0.21
Actual Shear Strength of Column	$V_{supplied}$	kips	240	240	240	156	156
Weight of the Mass participating in the Response of the Pier	W	kips	747	747	747	747	747
Vertical Load on the Pier from Non-Seismic Loads (DL, PT, etc., Not LL)	P	kips	812	812	812	812	812
Check if W/P <= 1.0			OK	OK	OK	OK	OK
Short Period Modifier	R_d		**1.00**	**1.00**	**1.00**	**1.00**	**1.00**
Ratio of Elastic Lateral Force to Lateral Strength of Pier	R		6.0	6.0	1.3	5.0	5.0
Natural period of Vibration of the Structure (Transverse)	T	sec	1.62	1.63	1.62	1.62	1.63
$1.25T_s$	T*	sec	1.17	1.17	0.55	0.75	0.75
From Response Spectrum	T_s	sec	0.933 *T > T**	0.933 *T > T**	0.442 *T > T**	0.600 *T > T**	0.600 *T > T**
Displacement Demand from the Seismic Analysis	**Δ**	**ft**	**1.72**	**1.15**	**0.50**	**0.92**	**0.93**

(continued)

Table 3.11 (continued) Washington Bridge - P-Δ Requirements
Pier 4 Column – Longitudinal Earthquake

H_{col} = 50 ft

	Symbol	Units	2500-yr N	2500-yr L	100-yr N	500-yr N	500-yr L
Displacement Demand from the Seismic Analysis $(\Delta_m = R_d\Delta)$	Δ_{mL}	**ft**	**1.11**	**0.72**	**0.27**	**0.52**	**0.51**
Upper Limit ***Check (No increase in strength req'd if Upper Limit > Δ_m)***	**0.25C (W/P)H**	**ft**	**3.69 OK**	**3.69 OK**	**3.69 OK**	**2.40 OK**	**2.40 OK**
Seismic Coefficient Based on the Lateral Strength	C		0.32	0.32	0.32	0.21	0.21
Actual Shear Strength of Column	$V_{supplied}$	kips	240	240	240	156	156
Weight of the Mass participating in the Response of the Pier	W	kips	747	747	747	747	747
Vertical Load on the Pier from Non-Seismic Loads (DL, PT, etc., Not LL)	P	kips	812	812	812	812	812
Check if W/P <= 1.0			OK	OK	OK	OK	OK
Short Period Modifier	R_d		**1.00**	**1.00**	**1.00**	**1.00**	**1.00**
Ratio of Elastic Lateral Force to Lateral Strength of Pier	R		6.0	6.0	1.3	5.0	5.0
Natural Period of Vibration of the Structure (Transverse)	T	sec	1.38	1.33	1.15	1.29	1.27
$1.25T_S$	T*	sec	1.17	1.17	0.55	0.75	0.75
From Response Spectrum	T_s	sec	0.933	0.933	0.442	0.600	0.600
			*T > T**	*T > T**	*T > T**	*T > T**	*T > T**
Displacement Demand from the Seismic Analysis	Δ	**ft**	**1.11**	**0.72**	**0.27**	**0.52**	**0.51**

Table 3.12 Washington Bridge – Approximate Displacement Check/SDAP E Pier 2 Column

					E_c =	552000	ksf
		H_{col} =	30	ft	I_{cr} =	5.0	ft^4
	Symbol	**Units**	**2500-yr N**	**2500-yr L**	**100-yr N**	**500-yr N**	**500-yr L**
Minimum Displacement Requirements for Lateral Load Resisting Piers (See Table 3.13 for computation of R_d and Δ_m.)	**$1.5R_d\Delta_{mT}$**	**ft**	**0.65**	**0.45**	**0.22**	**0.35**	**0.36**
	$1.5R_d\Delta_{mL}$	**ft**	**1.11**	**0.71**	**0.27**	**0.51**	**0.51**
Maximum Displacement Capacity = $\Delta_p + \Delta_y$ ***Check Transverse/Longitudinal Directions***	$\Delta_{capacity}$	**ft**	**1.42 OK/OK**	**1.42 OK/OK**	**1.42 OK/OK**	**1.33 OK/OK**	**1.33 OK/OK**
Approximate Plastic Displacement = $\Theta_{pT}\left[H-2\left(L_p/2\right)\right]$	Δ_{pT}	ft	1.214	1.215	1.214	1.214	1.215
Approximate Plastic Displacement = $\Theta_{pL}\left[H-2\left(L_p/2\right)\right]$	Δ_{pL}	ft	1.182	1.175	1.147	1.169	1.166
Approximate Yield Displacement = $M_yH^2/6EI$	Δ_y	ft	0.207	0.207	0.207	0.114	0.114
Yield Moment of Column	M_y	ft-kips	3800	3800	3800	2100	2100
Plastic Rotational Capacity – Transverse	Θ_{pT}	**rad**	**0.041**	**0.041**	**0.041**	**0.041**	**0.041**
Plastic Rotational Capacity – Longitudinal	Θ_{pL}	**rad**	**0.040**	**0.040**	**0.039**	**0.040**	**0.040**
("Life Safety" Conservative Value = 0.035)							
Number of Cycles of Loading – Transverse	**N_{fT}**	**cycles**	**2.98**	**2.97**	**2.98**	**2.98**	**2.97**
Natural Period of Vibration of the Structure – Transverse	T_{nT}	sec	1.62	1.63	1.62	1.62	1.63
Check Range of $N_f\left(2<=N_f<=10\right)$			OK	OK	OK	OK	OK
Number of Cycles of Loading – Longitudinal	N_{fL}	**cycles**	**3.14**	**3.18**	**3.34**	**3.22**	**3.23**
Natural Period of Vibration of the Structure – Longitudinal	T_{nL}	sec	1.38	1.33	1.15	1.29	1.27
Check Range of $N_f\left(2<=N_f<=10\right)$			OK	OK	OK	OK	OK
Effective Plastic Hinge Length	L_p	**m**	**0.69**	**0.69**	**0.69**	**0.69**	**0.69**
Shear Span of Member = M/V	fcn(H)	m	4.573	4.573	4.573	4.573	4.573
Yield Strain of Longitudinal Reinforcement	ε_y	m/m	0.00207	0.00207	0.00207	0.00207	0.00207
Diameter of Main Long. Reinforcing Bars	d_b	m	0.036	0.036	0.036	0.036	0.036
Distance between outer layers of long. reinf. on opposite faces of member	**D'**	**m**	**1.07**	**1.07**	**1.07**	**1.07**	**1.07**

Table 3.13 Washington Bridge - P-Δ Requirements
Pier 2 Column – Transverse Earthquake

H_{col} = 30 ft

	Symbol	Units	2500-yr N	2500-yr L	100-yr N	500-yr N	500-yr L
Displacement Demand from the Seismic Analysis $(\Delta_m = R_d\Delta)$	**Δ_{mT}**	**ft**	**0.43**	**0.30**	**0.14**	**0.23**	**0.24**
Upper Limit	**0.25C (W/P)H**	**ft**	**4.77**	**4.77**	**4.77**	**2.72**	**2.72**
Check (No increase in strength req'd) if Upper Limit > Δ_m)			**OK**	**OK**	**OK**	**OK**	**OK**
Seismic Coefficient Based on the Lateral Strength	C		0.65	0.65	0.65	0.37	0.37
Actual Shear Strength of Column	$V_{supplied}$	kips	485	485	485	277	277
Weight of the Mass Participating in the Response of the Pier	W	kips	747	747	747	747	747
Vertical Load on the Pier from Non-Seismic Loads (DL, PT, etc., not LL)	P	kips	763	763	763	763	763
Check if W/P <= 1.0			OK	OK	OK	OK	OK
Short Period Modifier	R_d		**1.00**	**1.00**	**1.00**	**1.00**	**1.00**
Ratio of elastic Lateral Force to Lateral Strength of Pier	R		6.0	6.0	1.3	5.0	5.0
Natural period of Vibration of the structure (Transverse)	T	sec	1.62	1.63	1.62	1.62	1.63
$1.25T_s$	T*	sec	1.17	1.17	0.55	0.75	0.75
From Response Spectrum	T_s	sec	0.933	0.933	0.442	0.600	0.600
			T>T*	T>T*	T>T*	T>T*	T>T*
Displacement Demand from the Seismic Analysis	Δ	**ft**	**0.43**	**0.30**	**0.14**	**0.23**	**0.24**

(continued)

Table 3.13 (continued) Washington Bridge - P-Δ Requirements
Pier 2 Column –Longitudinal Earthquake

H_{col} = 30 ft

	Symbol	Units	2500-yr N	2500-yr L	100-yr N	500-yr N	500-yr L
Displacement Demand from the Seismic Analysis $(\Delta_m = R_d\Delta)$	**ΔL**	**ft**	**1.11**	**0.71**	**0.27**	**0.51**	**0.51**
Upper Limit	**0.25C (W/P)H**	**ft**	**4.77**	**4.77**	**4.77**	**2.72**	**2.72**
Check (No increase in strength req'd) if Upper Limit > Δ_m)			**OK**	**OK**	**OK**	**OK**	**OK**
Seismic Coefficient Based on the Lateral Strength	C		0.65	0.65	0.65	0.37	0.37
Actual Shear Strength of Column	$V_{supplied}$	kips	485	485	485	277	277
Weight of the Mass Participating in the Response of the Pier	W	kips	747	747	747	747	747
Vertical Load on the Pier from Non-Seismic Loads (DL, PT, etc., not LL)	P	kips	763	763	763	763	763
Check if W/P <+ 1.0			OK	OK	OK	OK	OK
Short Period Modifier	R_d		**1.00**	**1.00**	**1.00**	**1.00**	**1.00**
Ratio of elastic Lateral Force to Lateral Strength of Pier	R		6.0	6.0	1.3	5.0	5.0
Natural period of Vibration of the structure (Transverse)	T	sec	1.38	1.33	1.15	1.29	1.27
$1.25T_s$	T*	sec	1.17	1.17	0.55	0.75	0.75
From Response Spectrum	T_s	sec	0.933 T>T*	0.933 T>T*	0.442 T>T*	0.600 T>T*	0.600 T>T*
Displacement Demand from the Seismic Analysis	Δ	**ft**	**1.11**	**0.71**	**0.27**	**0.51**	**0.51**

3.6.2 Lateral Spreading Structural Design/Assessment

The material in this section generally represents Steps 4, 5, 6, 8, 9 and 12 of the Design Procedure in Section 2.5.2.1, and the material addresses the structural aspects of the procedure.

In Section 3.5.3, the tendency for the soil near Piers 5 and 6 to move during or after a major earthquake was assessed. Once it had been determined that lateral spreading would occur, the next step (Step 7) was to evaluate the beneficial pinning action of the foundation system in the analysis. This section describes the method of determining the pinning force to add to the stability analyses of Section 3.5.3, and it describes the process of determining whether flow around the foundation would occur or whether the foundation will move with the soil. This involves Steps 4 and 5 of the design procedure.

3.6.2.1 Modes of Deformation

As outlined above, there are two potential sliding surfaces during liquefaction for the Pier 5/6 end of the bridge. One is at the base of the upper liquefiable layer, and the other is at the base of the lower liquefiable layer. These potential deformation modes must be determined to evaluate the forces developed by the piles and structure resistance.

The overall foundation deformation modes may be formally assessed using models that consider both the nonlinear nature of the soil resistance and the nonlinear behavior of the piles and foundations, when subject to prescribed soil displacement profiles. In this study, the deformations and structural behavior have been approximated using assumed displaced structural configurations that are approximately compatible with the constraints provided by the soil. Examples of these configurations are given in Figure 2.9 though Figure 2.11.

In this example, the abutment foundation will move in a manner similar to that shown in Figure 2.9, because there are sliding bearings at the substructure/superstructure interface. In the figure, the frictional forces transferred through these bearings have been conservatively ignored.

Pier 5 will move similar to the mode shown in Figure 2.10. Under such a displaced shape, both the columns and the piles contribute to the lateral resistance of the foundation. The columns contribute because there is an integral connection between them and the superstructure. In the current assessment, the residual displacements have been ignored. There exists some question as to whether this should be included or not. The reductions in resistance due to P-Δ effects are likewise given in the figure, but for many of the deformations and column height combinations considered in this study, this reduction is small, and therefore it has not been included in the calculations.

3.6.2.2 Foundation Movement Assessment

As described in Step 4 through 6 of the design procedure, an assessment should be made whether the soil will flow around the foundation or it will move the foundation with it as it moves. Passive capacities of the various layered soils were extracted from the p-y curves generated by

conducting LPILE[3] analyses for the piles. These forces represent the maximum force that is exerted against the piles as the soil flows around the pile. This then is the upper bound limit state of the soil force that can be developed. Additionally, the maximum passive forces that can be developed against the pile caps and abutment stemwall were developed. These calculations are included in Appendix E. Two total forces were developed; one for the shallow-seated soil failure and one for the deep failure. The shallow failure will develop approximately 1100 kips/pile and the deep failure approximately 3500 kips/pile at the point where the soil is flowing around the foundation. By comparison, one pile with a clear distance of 30 feet between plastic hinges can develop about 90 kips of shear at the point where a full plastic mechanism has formed in the pile. The conclusion from this comparison is that there is no practical likelihood that the soil will flow around the piles. Instead, the foundations will be pushed along with the soil as it displaces toward the river channel beneath the bridge.

Intuitively, it is only reasonable to expect that flow will develop around a pile if there is no crust of non-liquefied material being carried along with the displacing soil (Step 4 of the design procedure). In the case examined here, there is significant (10's of feet) non-liquefied material above the liquefiable material, and it is that material which contributes to the high passive forces. Thus, if a reasonable crust exists, the foundations are likely to move with the soil.

The next questions to be considered are: 1) can the foundation systems endure the displacement that the soil produces (Step 6), and 2) can the foundations appreciably reduce the soil movement via pinning action (Step 7)?

3.6.2.3 Pinning Force Calculation

In Section 3.5, various pinning forces were discussed and included with the stability analyses to investigate the effectiveness of including the existing foundation pinning. The following discussion accounts the development of the force values used.

Figure 3.45 illustrates qualitatively the forces developed against the foundations and how they reacted using the bridge itself as a strut. Two soil blocks are shown, Block A on the right and B on the left. Block A represents a postulated deep-seated slide that affects both Piers 5 and 6. The shears, V_{p5} and V_{p6}, represent the pinning shear force developed by the piles of Pier 5 and 6, respectively. Shear V_{c5} is the shear contributed by the Pier 5 columns. Finally, V_{pa5} is the passive resistance provided by the backfill acting against the end diaphragm.

[3] LPILE is a computer program used to evaluate lateral response of piles subjected to loads and moments at the pile head. This program is similar to COM624.

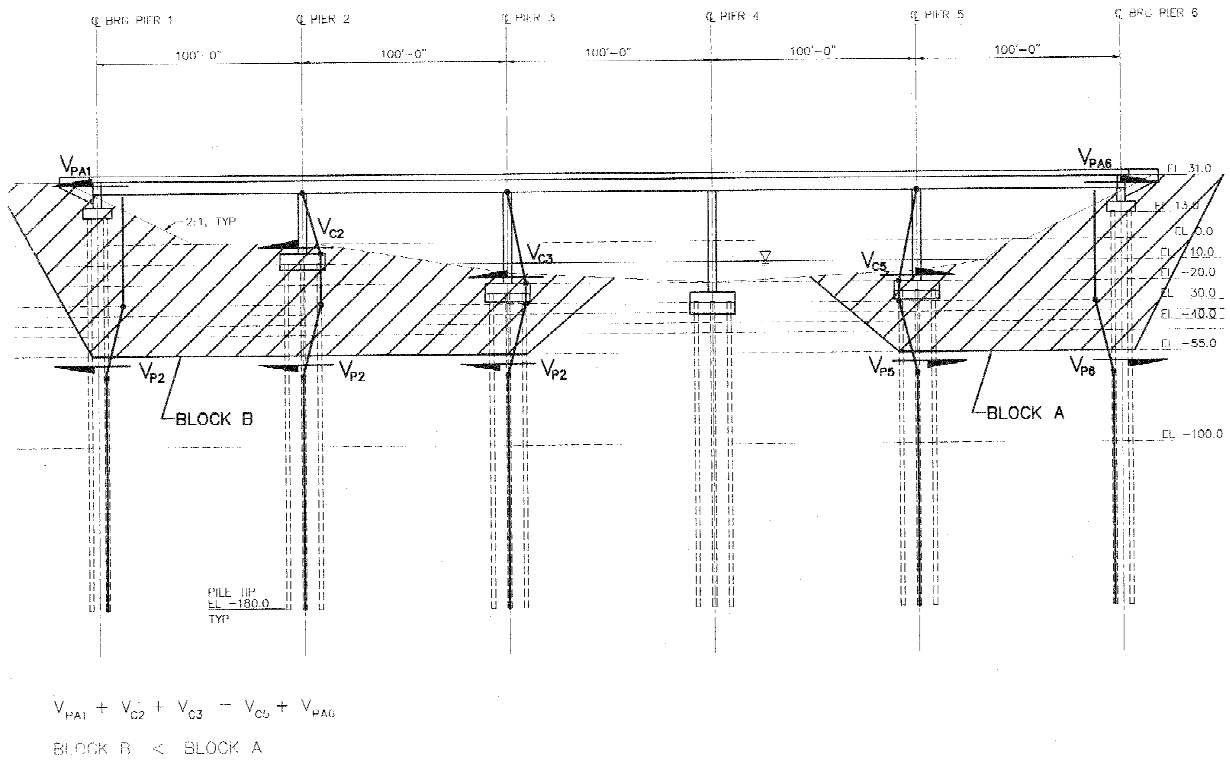

Figure 3.45 Forces Provided by Bridge and Foundation Piling for Resisting Lateral Spreading

While Block A is the most likely of the two to move, Block B is shown in this example to illustrate where and how the forces transferred into the bridge by Block A are resisted. In this case, the bridge acts as a strut. Note that if a significant skew exists, then these forces can not be resisted without some overall restraint to resist rotation of the bridge about a vertical axis.

Figure 3.46 illustrates the pinning forces acting on a soil block sliding on the lower liquefiable layer. In this case, abutment and Pier 5 piles each contribute about 90 kips, the abutment about 400 kips, and the columns at Pier 5 about 420 kips. The total abutment pile resistance is 1080 kips and corresponds to the approximate plastic mechanism shear with 30 feet clear between points of assumed fixity in the piles. This is comprised of 10 feet of liquefiable material and 5D (D = pile diameter) to fixity above and below that layer[4]. The upper portion of the soil block is assumed to move essentially as a rigid body, and therefore the piles are assumed to be restrained by the integrity of this upper block. Calculations for this pinning force are given in Appendix E.

[4] Fixity was assumed to develop 5D above the liquefied layer. In an actual design case, a lateral analysis using a computer code, such as LPILE, could be conducted to be more rigorous about the distance to fixity.

The pile resistance at Pier 5 is determined in a similar manner, and the shear that the Pier 5 piles contribute is 1440 kips. The abutment passive resistance corresponds to half of the prescribed passive capacity of the backfill and is assumed to act against the end diaphragm. The abutment fill is assumed to have slumped somewhat due to the movement of the soil block, and thus half of the nominal resistance was judged to be reasonable. The column resistance at Pier 5 is 420 kips, and this assumes that plastic hinging has occurred at the top and bottoms of the columns at this pier.

These forces (3360 kips) represent maximum values that occur only after significant plasticity develops. In the case of Pier 5, the approximate displacement limit is 22 inches, which is comprised of 4 inches to yield and 18 inches of plastic drift. The plastic drift limit is taken as 0.05 radians. The 22-inch displacement limit of Pier 5 is controlled by the piles. Because the piles of Pier 6 are the same, their limit is also 22 inches of displacement.

Because the Pier 5 columns are longer than the distance between hinges of the piles, the column displacement limits are 34 inches total and 7 inches at yield. The fact that the piles control the displacement limit in this case implies that some margin is available in the column to accommodate any residual plastic hinge rotations that remain in the column after strong shaking stops.

Figure 3.47 shows the displaced shape of the foundations for a shallow (upper layer) soil failure. In this case, the distance between plastic hinges in the piles is 30 feet, just as with the deeper failure, and thus the plastic shear per pile is 90 kips. The total contributed by the piles is 1080 kips as before. The detailed calculations for this are given in Appendix E.

In Section 3.5.3, the estimated displacements for the lower or deeper failure wedge were 28 inches for the 475-year event and 42 inches for the 2,475-year event. Neither of these is within the plastic capacity of the piles, and additional piles could be added as 'pinch' piles or ground remediation could be used[5]. It will be recalled that the yield acceleration for the upper failure was essentially zero for both the 475-year and 2,475-year events, which indicated that some remediation would be required to stabilize the fill and its toe for both design events.

[5] Pinch piles refer to piles driven at close spacing to increase the shear resistance of density of the soil mass. In the Pacific Northwest, these piles are often timber.

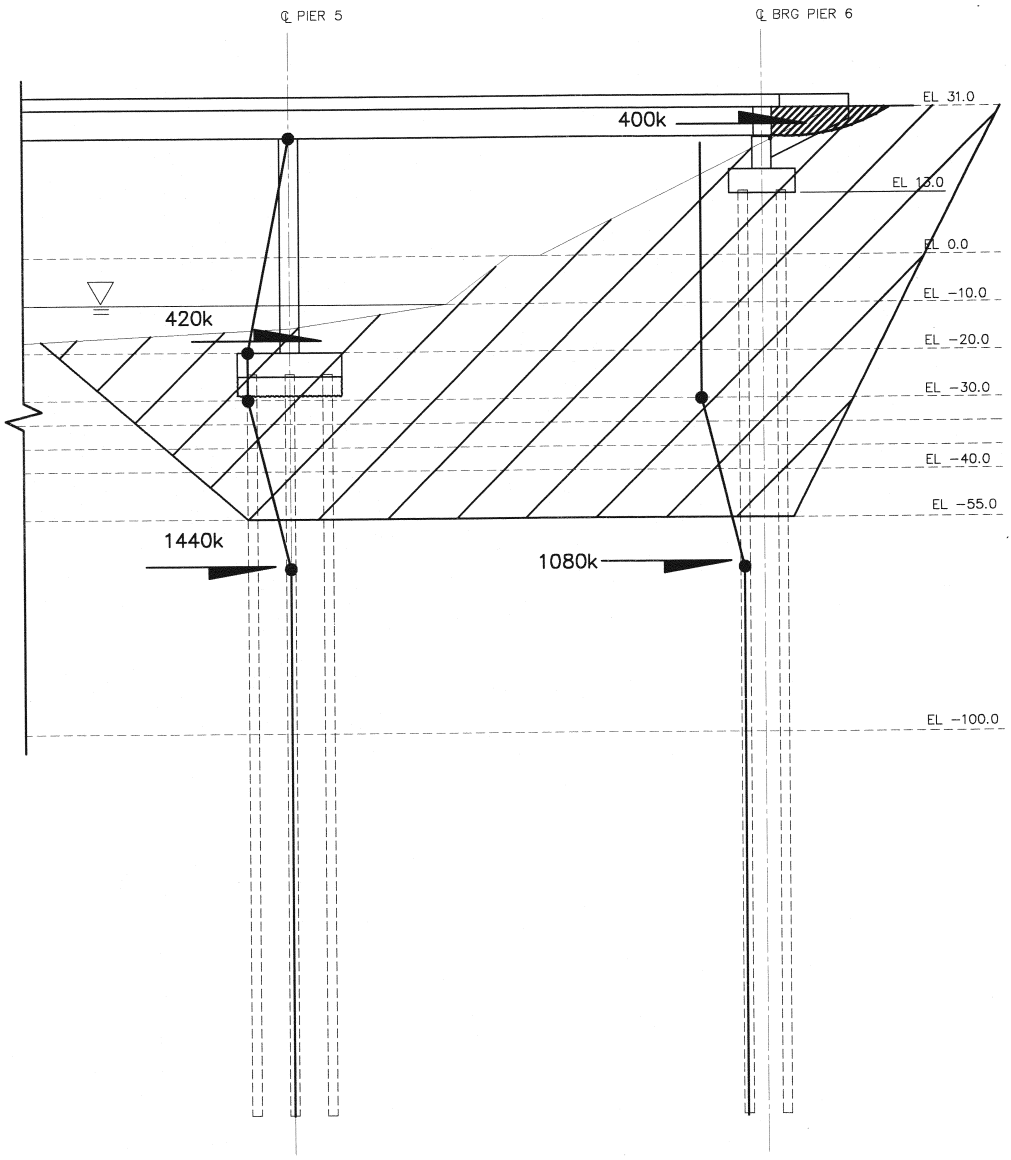

Figure 3.46 Piers 5 and 6 Resisting Lateral Spreading – Deep Wedge

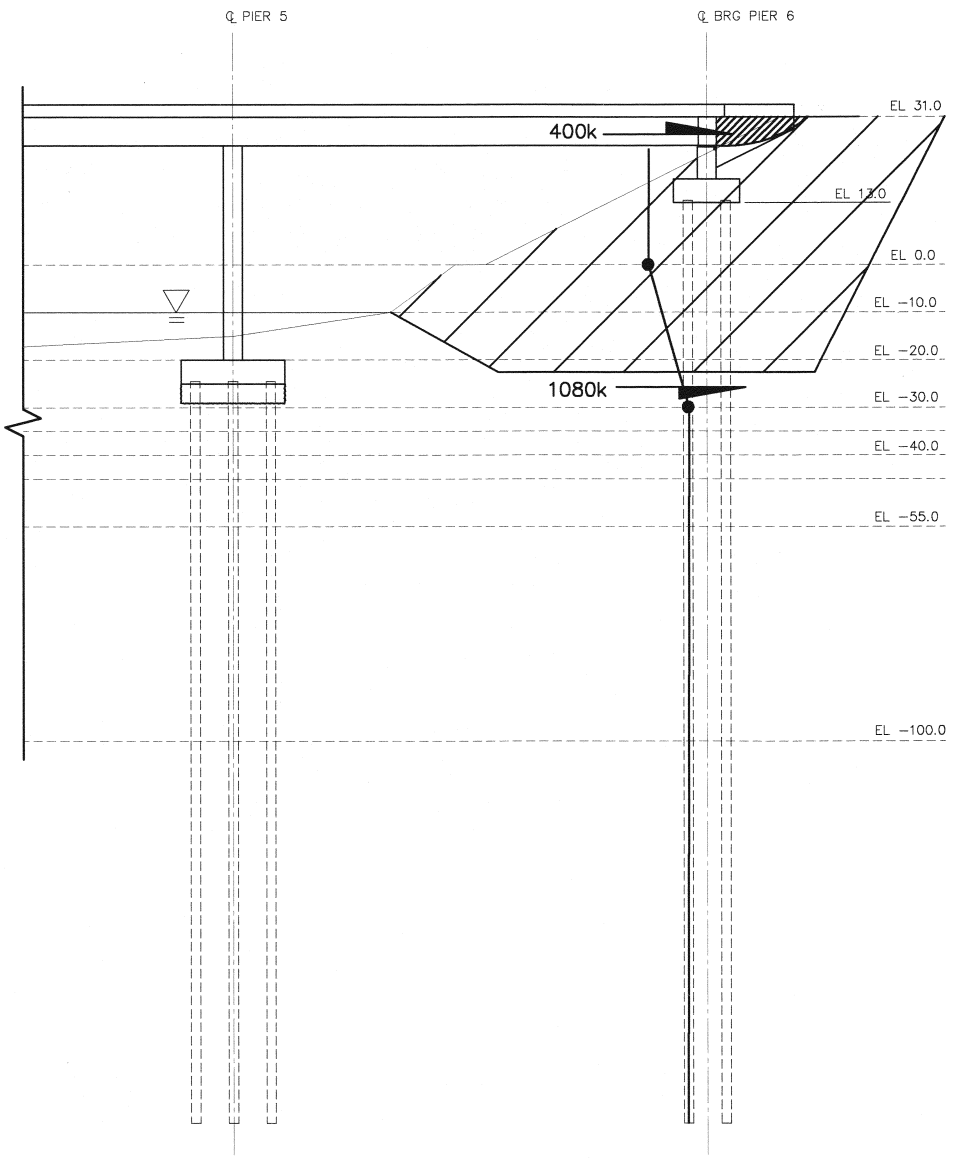

Figure 3.47 Pier 6 Resisting Lateral Spreading – Shallow Wedge

3.7 Comparison of Remediation Alternatives

The primary intent of these analyses was to determine the potential effects of increasing the seismic design criteria from its current return period of 475 years to a 2,475-year return period. Liquefaction was predicted for both return periods, and as a consequence, there is little difference in the remedial work required for the two return periods.

3.7.1 Summary of Structural and Geotechnical Options

Mitigation measures are assessed based on the desired performance requirement of the bridge. The first option is to assess the performance in its as-designed configuration. If this results in unacceptable performance, a range of mitigation measures are assessed.

For this example, some form of structural or geotechnical remediation is required at the right-hand abutment because the yield acceleration for the upper failure wedge is zero. This implies that the wedge is unstable under static conditions after the soil liquefies, which it does in both the 2,475-year event and the 475-year event[6]. Two choices for improving the conditions are to use additional piles or stone columns. Since the yield acceleration for the upper failure surface is so low, the most effective choice is likely to use stone columns. These provide the combined advantage of increasing the residual shear strength of the sliding interface, and they can reduce pore water pressure build up, thereby postponing or possibly eliminating the onset of liquefaction.

Because the lower failure wedge also has a relatively low yield acceleration, 0.02 g, it makes sense to extend the mitigation deep enough to improve the deeper soil layers, as well. This low yield acceleration results in displacements of 28 inches and 42 inches for the 475- and 2,475-year events from the simplified analyses, and displacements of approximately 29 inches for both the 475- and 2,475-year events for the site-specific Newmark analyses. The decision to improve the deeper layers implies that stone columns would extend on the order of 50 feet in depth. The stone column remediation work will provide displacements that are less than 4 inches. This will keep the piles within their elastic range and meet the highest level of operational performance objectives in the foundation system.

Although in this example the left-hand abutment was not evaluated in detail because the FOS of the initial stability analyses was greater than 1, a cost/benefit assessment would typically be made to determine if some remediation work on the left-hand abutment would be cost effective. Once a contractor is mobilized on the site, it would make some sense to provide improvement on both sides of the river. It may be that upon more in-depth investigation the stone columns could be spaced further apart or applied over a smaller width on the left-hand bank.

[6] The approach fill and ground profile condition for the bridge considered in this study are more severe than that used in the actual bridge that this example was modeled after. Thus, the implication of instability here does not imply instability in the prototype structure.

3.7.2 Comparisons of Costs

As noted above, the remedial work is required for both the 475- and 2,475-year events.

The stone column option would likely be applied over a 30-foot length (longitudinal direction of bridge), since that length produced acceptable deflections of less than 4 inches, which is within the elastic capacity of the piles. The width at a minimum would be 50 feet, and the depth also would be about 50 feet. If the columns were space roughly on 7-foot centers, then 40 stone columns would be required. At approximately $30 per lineal foot (plf), the overall cost per approach fill would be on the order of $60,000, or about $120,000 for both sides if the left-hand fill were judged to require remediation.

As a rough estimate of the cost of the overall structure, based on square-footage costs of $100 to $150 in Washington, the bridge would cost between two and three million dollars. If the higher cost were used, due to the fact that the bridge is over water and the foundation system is relatively expensive because of its depth, the cost to install stone columns on the right-hand side would run about two percent of the overall cost of the bridge. If both sides were remediated, then the costs would comprise about four percent of the bridge costs. It should be noted that this additional cost will produce a foundation performance level that meets the operational criteria for both return period events.

If pinch piles were used to augment the piles of the foundations, the pinch piles would not need to be connected to the foundation and would not need to extend as deep as the load-bearing foundation piles. The per pile cost of the foundation piles was estimated to be on the order of $10,000 to $12,000 each for 180-foot long piles. Development of the cost data is given in Appendix E. If shorter piles on the order of 80 feet long were used, their costs would be about half as much. Thus if pinch piles were used, about 10 to 12 piles per side could be installed for the same cost as the stone column remediation option. Although detailed analyses have not been performed with these pinch piles, the amount of movement anticipated would be in the range of 6 to 12 inches, rather than the 4 inches obtained with the stone columns. Therefore, the stone column option would appear the most cost effective in this situation. On a specific project, combinations of the two options would be evaluated in more depth.

It is useful to recognize that in this situation, some remediation would be required for both the 475- and 2,475-year events because of the predicted instability of the upper failure wedge. In the case of the former, the remediation is required to a depth of 50 feet because the anticipated movement of the lower failure wedge would be on the order of 28 inches for the simplified analyses and 30 inches for the site specific analysis and thus be in excess of the 22 inch limit. For the 2,475-year event, movement on the order of 42 inches is predicted by the simplified analysis, and 30 inches by the site-specific analyses. Consequently, remediation is required to a depth of 50 feet for both events. Hence, the difference in cost for this site and bridge between the two design earthquakes is minimal.

4. CENTRAL UNITED STATES SITE

4.1 General

The second bridge considered in this study is located in the New Madrid earthquake source zone in the lower southeast corner of Missouri. This general location was selected because it is one where a significant seismic hazard occurs, and there are numerous stream crossings and low-lying areas where potential for liquefaction exists. Additionally, the project team wished to include a non-western site where the effects of different source mechanisms and where the differences in shaking levels between the 475-year and 2,475-year events would be highlighted. Similar to the Western U.S. study, the analyses completed for the Missouri site are expected to be characteristic of design issues that would occur in surrounding states.

During preparation for this study, contacts were made with the bridge and geotechnical groups at Missouri Department of Transportation (MODOT) to identify a site and bridge for the study. MODOT staff expressed considerable interest in participating in the project. In the absence of face-to-face meetings with the MODOT staff, the project team prepared a description of geotechnical and bridge information that would be useful for this study. Subsequently, several telephone conference calls were held with the MODOT staff to resolve site and bridge design questions. As with the WSDOT contacts, these discussions provided very valuable insight into design methods and concerns to the project team.

4.2 Site Selection and Characterization

The site selection and characterization process for the Missouri site was much like that used in Washington. Geology and geotechnical conditions for a proposed site were reviewed by the project team, and then a simplified soil model for the site was developed.

4.2.1 General Geology for the Site

The site is located in southeastern Missouri near the New Madrid seismic zone associated with the New Madrid rift complex. It is situated along the western edge of the Mississippi River alluvial plane in Missouri. Alluvial sediments in this area are shallower than for the Western U.S. site, as they extend generally to approximately 180 feet. Dense alluvial materials are generally found at depths greater than 40 feet.

4.2.2 Site Information

The MODOT geotechnical staff identified one of their research sites for evaluation. This site is located at the St. Francis River crossing of U.S. Route 60, and is being used by MODOT as part of a lifeline study of transportation systems in Missouri. A relatively extensive exploration program has been conducted at the site. The extent of the explorations includes boreholes with

SPTs to 100 feet or more below the ground surface, CPTs to depths of 40 feet, and shear wave velocity measurements in the upper 40 feet of the soil profile. Laboratory tests have also been conducted on soils retrieved from the site to classify soils. CPT data were provided by MODOT in digital form. MODOT staff indicated that the extent of exploration work on this project was more than was typically conducted for bridge sites, but was the type of explorations that they planned for future bridges.

Following review of the information received from MODOT, a pair of explorations, Boring B-4 and CPT B-41, was selected for use in developing a simplified soil model for the liquefaction evaluations. Appendix F includes copies of this boring log and cone penetrometer sounding. Ground water was specified as being 20 feet below the ground surface, based on information obtained from the exploration program. As with the Washington site, an actual design would consider all of the explorations in the evaluation of seismic response; however, for the demonstration of the effects of the recommended changes in design ground motions, use of single sets of representative information was considered adequate.

4.2.3 Simplified Soil Model Used for Evaluation

Information provided by MODOT indicates that this site has less complexity and is somewhat shallower than the Western U.S. site. This means that the layering is less pronounced and the depth to dense material is less. Overall, the site has roughly 20 feet of clay overlying loose sand that is about 20 feet thick. This sand is underlain with denser sands where the SPT blow counts are more than 30.

A simplified soil profile was developed for the one-dimensional nonlinear effective stress liquefaction analyses. This profile is shown in Figure 4.1. Shear wave velocity (V_s), undrained shearing strength (c_u), soil friction angle (φ), and residual soil strength (S_{ur}) were interpreted from the field and laboratory data provided by MODOT. The cyclic resistance ratio (CRR) was obtained by conducting simplified liquefaction analyses using both the SPT and CPT methods to obtain CRR values. These CRR values are plotted in Figure 4.2. Average CRR values, representing clean sand values for a magnitude 7.5 event, were determined for liquefiable materials.

Figure 4.2 shows that relatively similar CRR values were obtained from the SPT and CPT. Low CRR values from the SPT below 40 feet are attributed to erratic recordings of blow counts during the SPT and not liquefiable layers. Generally, the material below 40 feet is very dense and not expected to liquefy. For this reason, the low CRR values below 40 feet were ignored when developing the simplified CRR profile.

One other significant change was made to the overall problem relative to conditions at the actual site. To vary site conditions and not have both the Washington and Missouri sites crossing a stream or river, the Missouri site was set up with a grade profile of an overcrossing. Consequently, there are approach fills on either side of the bridge. The approach fill was assumed to consist of a sandy gravel with a friction angle of 37 degrees. No modifications were made to the soil profile when making this change.

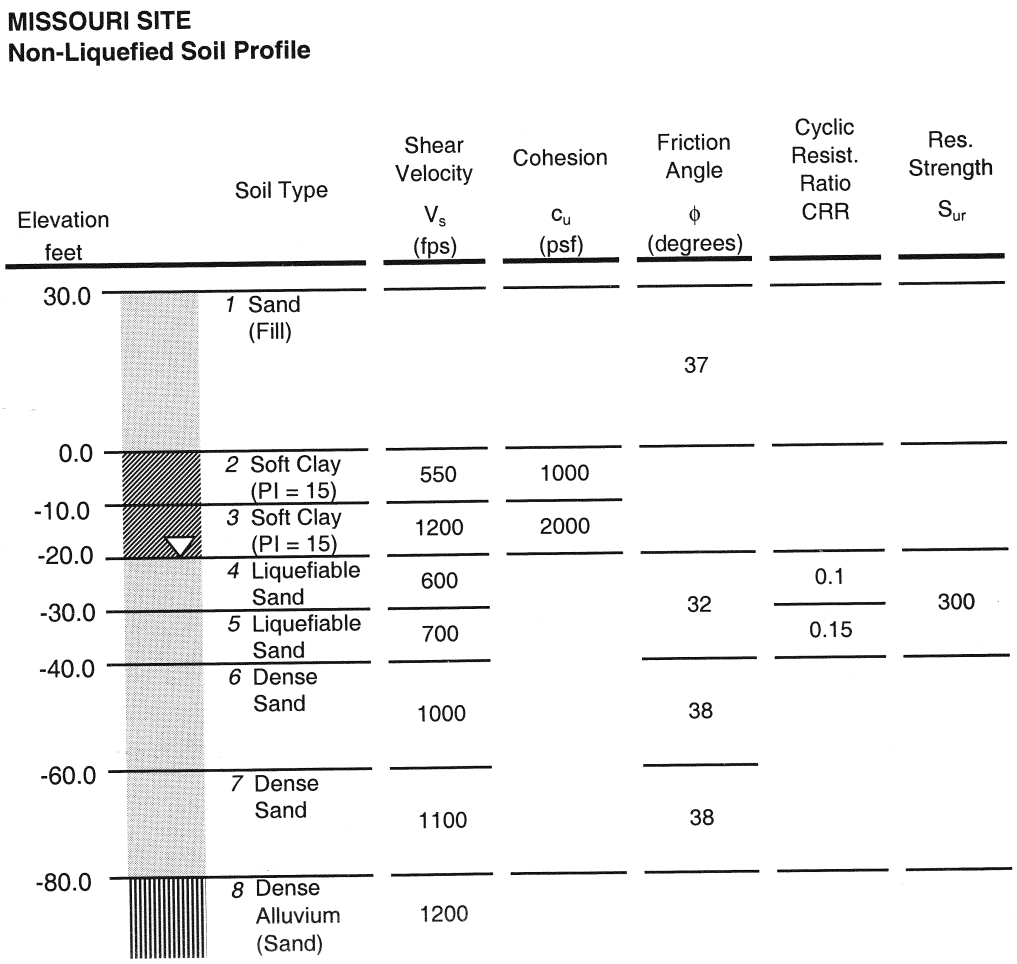

Figure 4.1 Soil Profile for the Central U.S. Site

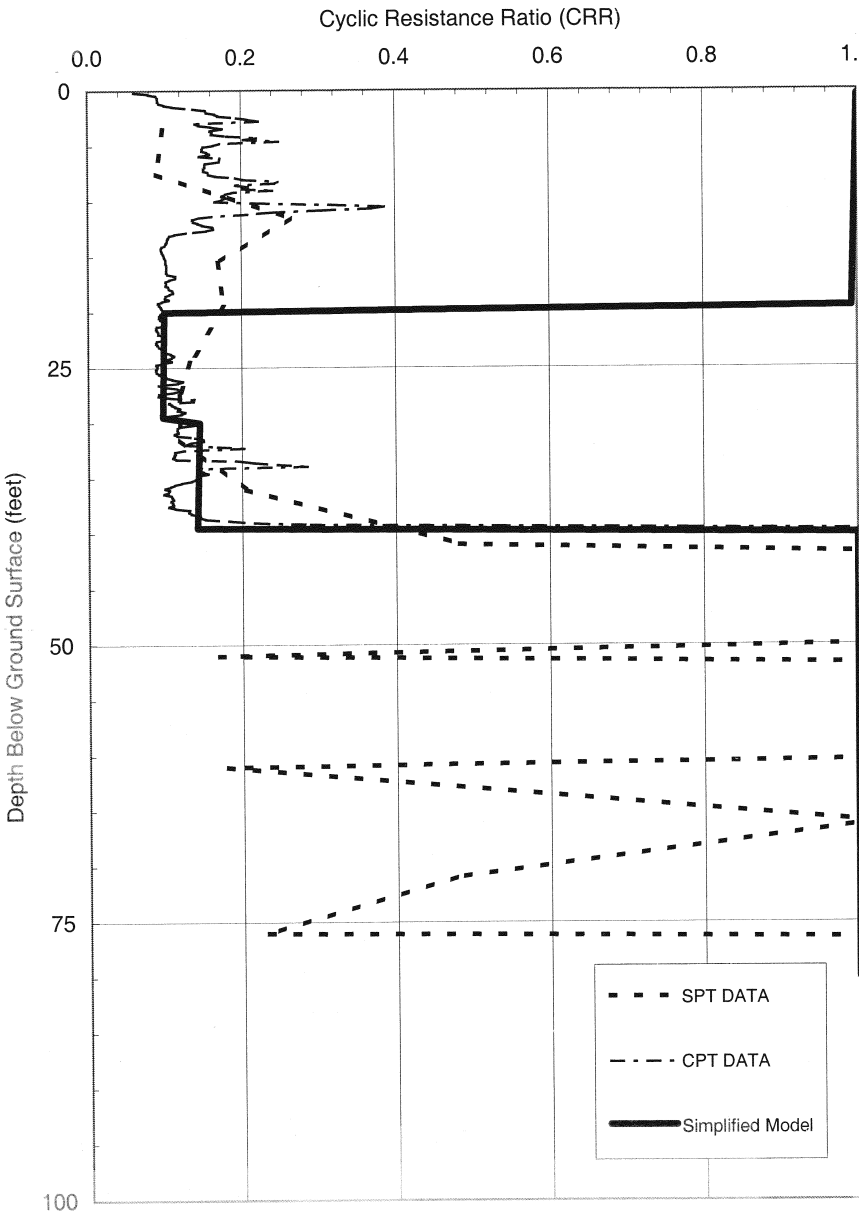

Figure 4.2 MODOT Location B-4 CRR Plot

4.3 Bridge Type

The simplified bridge used for the overcrossing is approximately 180 feet long, and comprises three roughly equal-length spans. There are no horizontal or vertical curves on the bridge, and the bridge has no skew. A general elevation of the bridge and of the ground line is given in Figure 4.3.

The bridge is a three-span structure comprised of AASHTO prestressed girders supported on three-column bents. The roadway is approximately 38 feet wide, and five 39-inch girders with a concrete deck form the superstructure. The substructure is formed of 3-foot diameter columns, which support a 40-inch dropped capbeam. The foundations of the intermediate piers are individual pile caps for each column that are supported on 14-inch steel pipe pile foundations. An elevation of one of the intermediate piers is given in Figure 4.4.

The abutments are of the integral type, where the end diaphragm is integated with the ends of the girders and deck and is directly supported by nine 14-inch-diameter pipe piles. These piles form a single line in the transverse direction to the bridge. An elevation of the abutment is shown in Figure 4.5.

The configuration of the bridge was selected, in part, due its common nature. Many states use this type of bridge or variations to it. Thus it was felt that the results for such a bridge type would be widely relevant to many other regions around the country.

4.4 Earthquake Hazard Levels

The earthquake hazards level for the project site was established in the same manner as described for the Washington site. No unique source mechanisms occurred in proximity to the site, allowing the site to be defined at its location on U.S. 60, crossing the St. Francis River.

4.4.1 Design Response Spectra

Design response spectra for the Missouri site were obtained for hazard levels defined by current AASHTO Specifications (10 percent probability of exceedance in 50 years) and the recommended revisions to the AASHTO Specifications (MCE with 3 percent probability of exceedance in 75 years; and the frequent earthquake with 50 percent probability of exceedance in 75 years).

Design spectra for the current AASHTO Specifications were constructed using a rock site peak ground acceleration of 0.17g obtained from the AASHTO map. Spectra for the MCE and for the frequent earthquake of the recommended LRFD Specifications were constructed using rock (site class B) response spectral accelerations at 0.2-second and 1.0-second periods obtained from paper maps and CD-ROMs prepared by USGS as described in Section 3.4.1 for the Washington site. These response spectral accelerations are summarized in Table 4.1. Design response spectra for the current AASHTO Specifications and the recommended LRFD Specifications were constructed using the procedures and site factors described in the respective Specifications.

Figure 4.6 presents design response spectra for current AASHTO Specifications, on site class II, and for the MCE of the recommended LRFD Specifications, on site class C. These soil types represent the assessed subsurface conditions defined at the base of the soil column, for which outcropping acceleration time histories are developed for the site response analyses to assess the liquefaction hazard at the site.

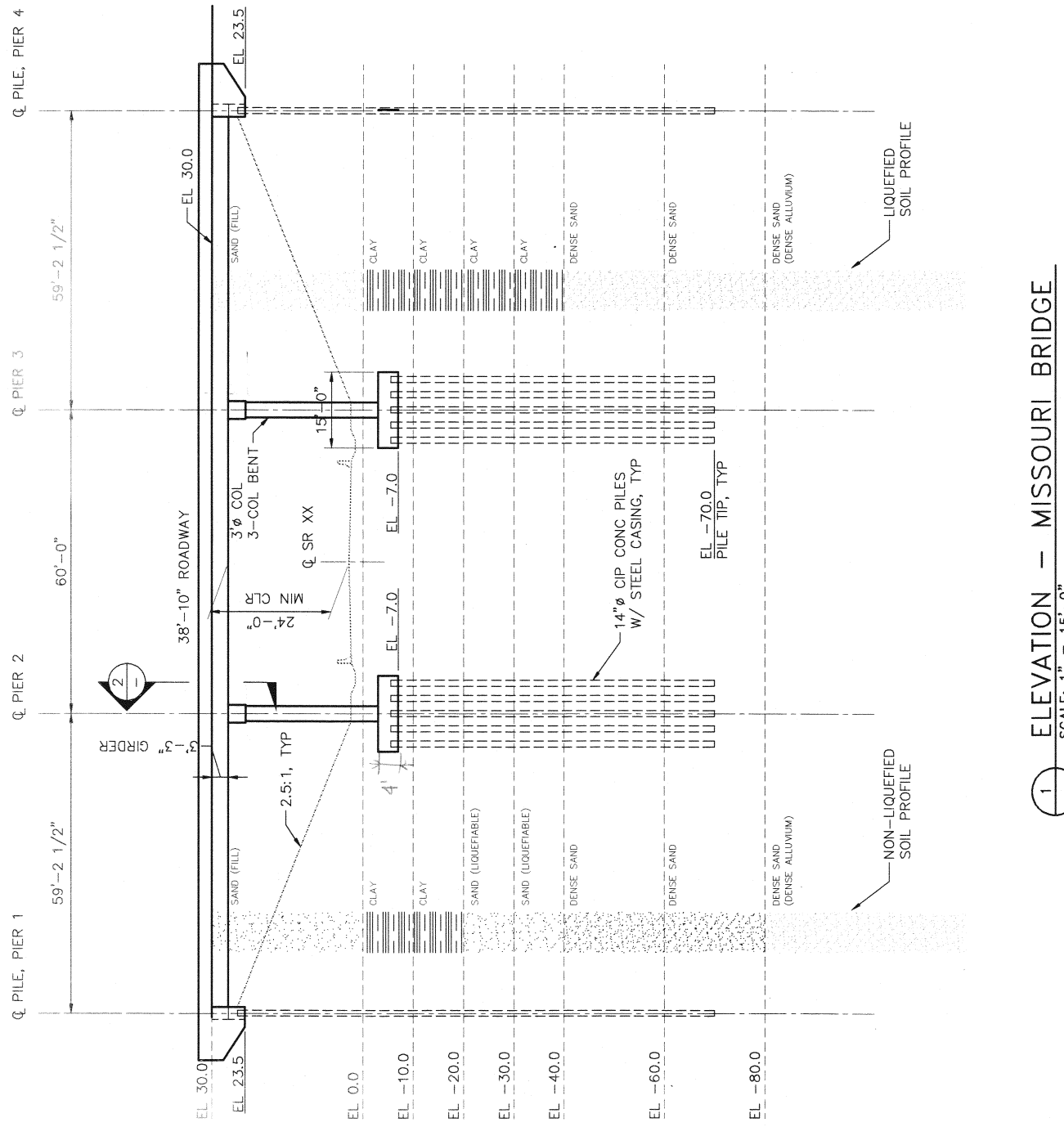

Figure 4.3 Site Profile and Structure Elevation

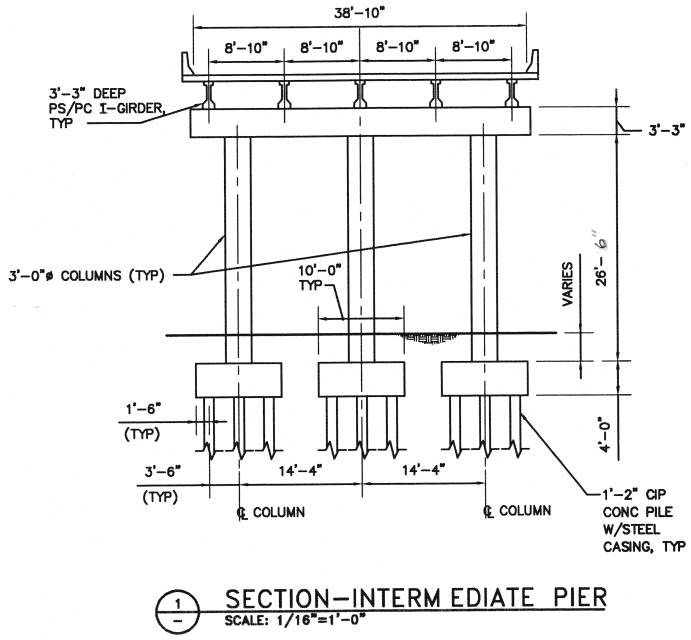

Figure 4.4 Elevation of an Intermediate Pier

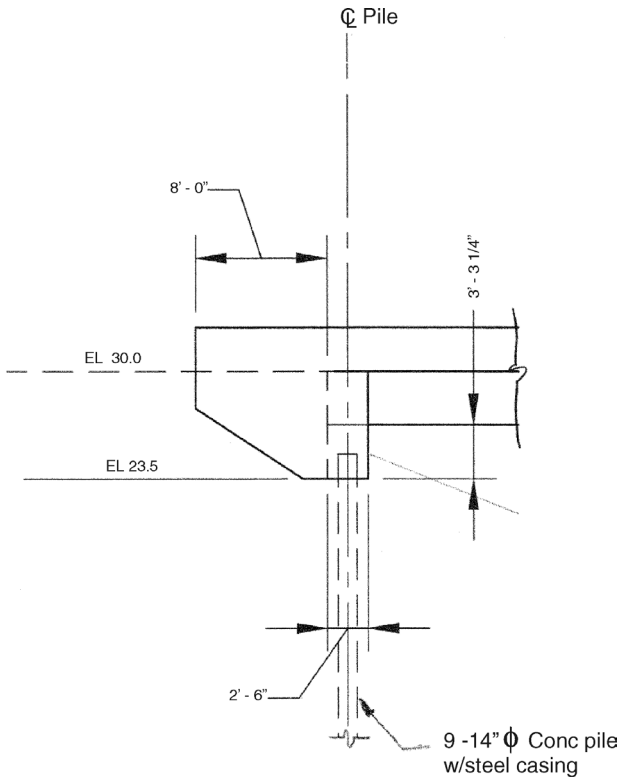

Figure 4.5 Elevation of an Integral Abutment

Table 4.1 0.2-Second and 1.0-Second Spectral Accelerations on Rock (Site Class B) for the Rare Earthquake (MCE) and the Frequent Earthquake for the Missouri Site

	Response Spectral Accelerations on Rock (Site Class B)	
Earthquake	**0.2-Second Period**	**1.0-Second Period**
MCE	1.331	0.411
Frequent	0.091	0.019

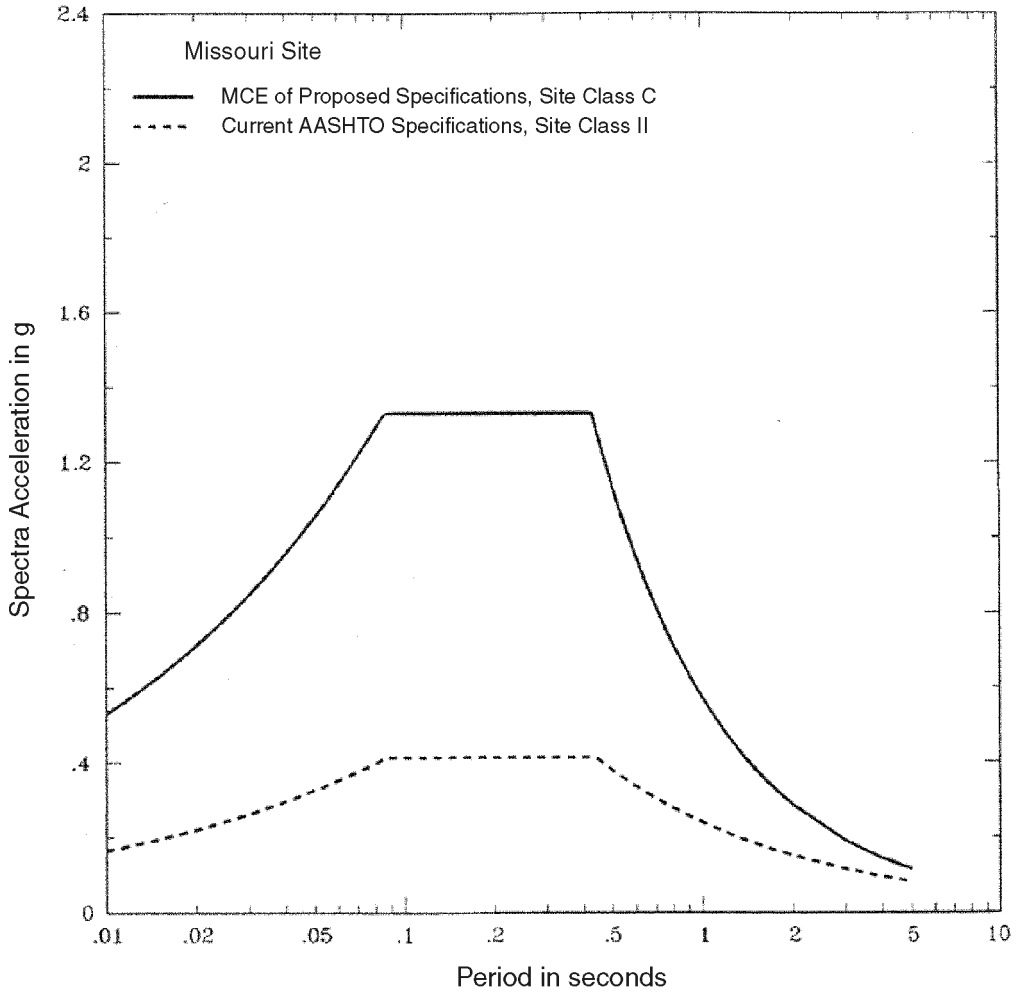

Figure 4.6 Design Response Spectra Based on Current AASHTO Specifications, Site Class II, and the MCE of Recommended LRFD Specifications, Site Class C, Missouri Site

Figure 4.7 presents the design response spectra for current AASHTO Specifications, on site class III, and for the MCE and the frequent earthquake of the recommended LRFD Specifications, on site class D. These site classifications represent the assessed soil profile below the ground surface where response spectra are defined for structural vibration design. Note in Figure 4.6 and Figure 4.7 that the short-period branch of the AASHTO spectra are assumed to drop from the acceleration plateau at a period of 0.087 seconds to the peak ground acceleration at a period of 0.01 second, the same as for the MCE spectra for the recommended LRFD Specifications. Also note that, because the long-period branch of the AASHTO spectra decline more slowly with period than those of the MCE (as $1/T^{2/3}$ in AASHTO compared to 1/T in the recommended LRFD Specifications), the AASHTO and MCE spectra come closer together as the period increases.

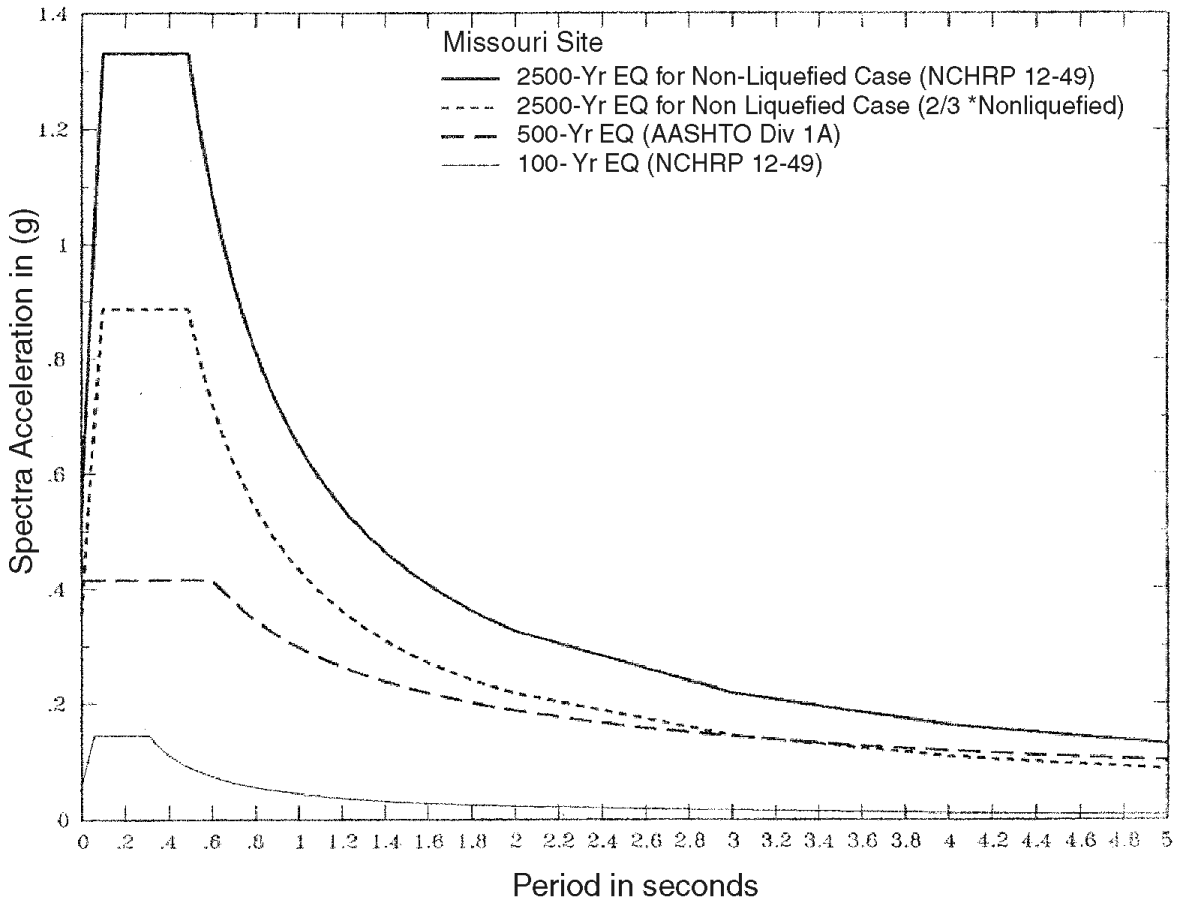

Figure 4.7 Design Response Spectra Based on Current AASHTO Specifications, Site Class III, and the MCE and the Frequent Earthquake of Recommended LRFD Specifications, Site Class E, Missouri Site

4.4.2 Acceleration Time Histories

4.4.2.1 Approach for Time History Development

Acceleration time histories consistent with current AASHTO Specifications and with MCE ground motions of recommended LRFD Specifications were developed as firm soil outcropping motions for input to the site response analyses to assess the liquefaction hazard of the site. Because strong-motion recordings of earthquakes with magnitude greater than 6 in the central and eastern United States are rare, synthetic time histories were generated and used to develop time histories for the design earthquakes. The simulation methodology used for the Missouri site is described below. These time histories were developed in accordance with the recommended LRFD Specifications and the following steps.

1. Identify earthquake magnitudes and source-to-site distances that contribute most significantly to the ground motion hazard at the site;
2. Synthesize Fourier amplitude spectra that are consistent with response spectra in Figure 4.6;
3. Select earthquake recordings according to the magnitude-distance conditions assessed in (1); and "merge" the Fourier phase spectrum of the selected recordings with the synthetic Fourier amplitude spectra developed in step (2) to generate acceleration time histories. The resulting time history has a frequency content consistent with the response spectra in Figure 4.6 and time-domain characteristics representative of the magnitude-distance conditions assessed in (1).

4.4.2.2 Deaggregation to Determine Magnitude and Distance Contributions to the Hazard

To accomplish Step 1 above, the contributions to the ground motion hazard at the Missouri site were deaggregated using the resources provided by the USGS Internet web site (*http://geohazards.cr.usgs.gov/eq/*). Hazard deaggregation was obtained for the return periods of 475 years and 2,475 years, which correspond to the probabilities of exceedance for the current AASHTO Specifications and the MCE of the recommended LRFD Specifications, respectively. Deaggregation plots for the 475- and 2,475-year return periods are shown in Figure 4.8 and Figure 4.9 for response spectral accelerations at zero-period (corresponding to peak ground acceleration). Additional results are presented in Appendix G. Figure G.1 through Figure G.4 show the 0.2-second period and 1.0-second period plots for the 475- and 2,475-year return periods, respectively.

In all of these deaggregation plots, the relative contribution to the ground motion hazard (defined as the percentage contribution to the annual frequency of exceedance, where the annual frequency of exceedance is the reciprocal of the return period) is portrayed by the relative height of the columns occupying different magnitude and distance ranges contributing to the hazard. Also indicated for each column is the distribution of contributions coming from different parts of the uncertainty band around the median predictions of the ground motion attenuation relationships used in the USGS probabilistic analyses.

The deaggregation results for the Missouri site show that, for both 475- and 2,475-year return periods and for both short periods and long periods of the response spectrum, the ground motion hazard is dominated by magnitude 8 earthquakes occurring 30 to 80 km from the site. These

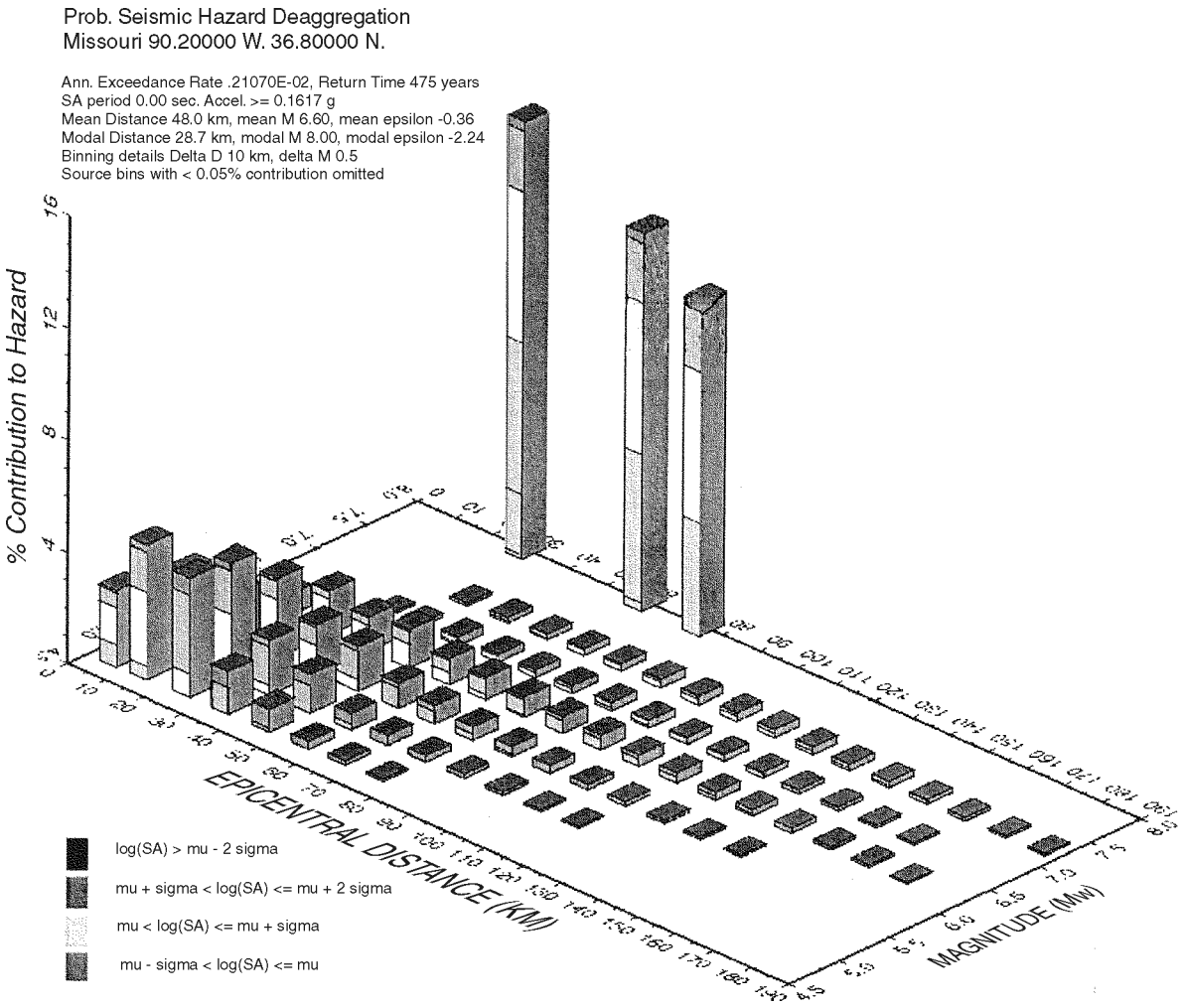

Figure 4.8 Hazard Deaggregation, 475-year Return Period, Zero-Period Spectral Acceleration, Missouri Site

earthquakes are associated with the New Madrid seismic zone. The discrete distances of 30, 60, and 75 km for contributions from the New Madrid source shown in Figure 4.8, Figure 4.9, and Figure G.1 through Figure G.4 reflect the modeling by USGS of the earthquake fault(s) as three possible locations within a relatively broad source zone, since the exact location of the fault(s) within the zone are not known.

The deaggregation results for the Missouri site differ from the results for the Washington site, where three different seismic source types and magnitude and distance ranges contributed significantly to the short period part of the response spectrum. For the Missouri site, a single, large magnitude source mechanism dominates the seismic hazard.

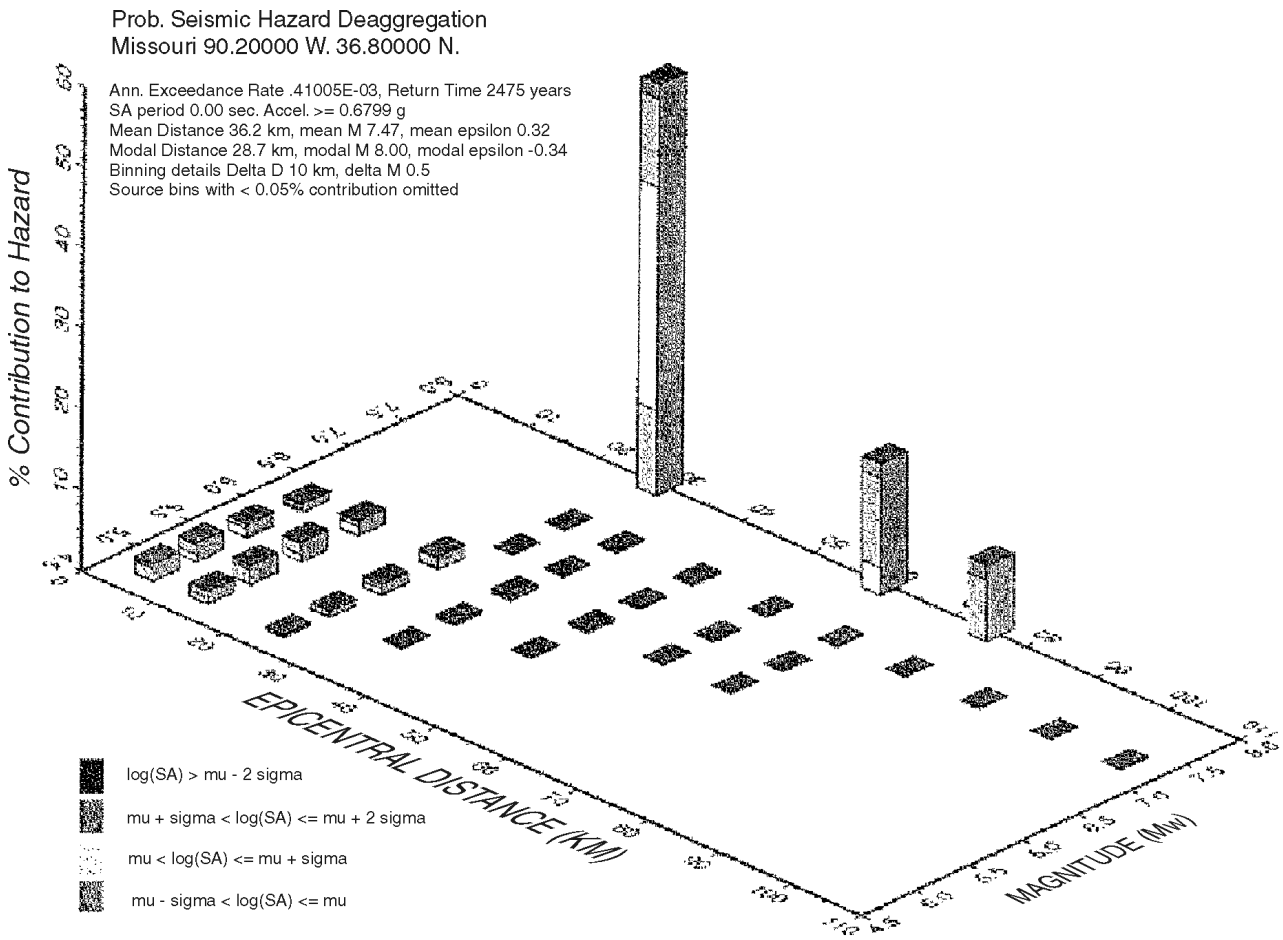

Figure 4.9 Hazard Deaggregation, 2,475-Year Return Period, Zero-Period Spectral Acceleration, Missouri Site

4.4.2.3 Synthesis of Fourier Amplitude Spectra

The Random-Vibration-Band-Limited-White-Noise (RVT-BLWN) ground motion modeling code (RASCAL) written by Silva and Lee (1987) was used to generate the Fourier amplitude spectra for ground motions from a magnitude 8 earthquake at the discrete distances of 30, 60, and 75 km. These Fourier amplitude spectra were further modified by the computer code RASCAL so that they are reasonably consistent with the response spectra shown in Figure 4.6. A similar ground-motion modeling methodology was used in the development of eastern U.S. attenuation relationships that were utilized in USGS's national hazard mapping project.

4.4.2.4 Generation of Synthetic Time Histories

Three natural recordings were selected from large-magnitude earthquakes in Mexico, Chile, and Japan to represent the time-domain characteristics of the design earthquakes for the Missouri site. The selected recordings are summarized in Table 4.2. The Fourier phase spectra of the selected time histories and the Fourier amplitude spectra developed in (1) provide the needed Fourier spectra for the generation of acceleration time histories. The intent of this simple approach is to build the recorded phasing information, which govern the time-domain characteristics such as the duration and the envelope shape, into the synthetic time histories regardless of the frequency content. Finally, the resulting acceleration time histories were further modified by the time-domain procedure of Lilhanand and Tseng (Lilhanand and Tseng, 1988; Abrahamson, 1992) to achieve closer fits to the response spectra in Figure 4.6.

Table 4.2 Time Histories Selected to Represent the Time-domain Characteristics of the Design Earthquakes for the Missouri Site

Earthquake Name	Station Name	Component	M_w	Distance (km)	PGA (g)
1985 Michoacan Earthquake	La Union	90	8	20.5	0.169
1985 Chile Earthquake	San Fernando	90	7.9	66.8	0.339
1968 Tokachi-Oki Earthquake	Hachinohe	0	8.2	117.9	0.318

Figure G.5 through Figure G.7 present the three synthetic time histories that are consistent with the design spectrum based on current AASHTO. Figure 4.10 compares the response spectra of the three time histories with the AASHTO spectrum. Similar time-history plots and comparisons to the design MCE spectrum of the recommended LRFD Specification are shown in Figure G.8 through Figure G.10 and Figure 4.11. All three time histories were matched to the entire design spectra because the magnitude 8 New Madrid seismic source contributed significantly to the frequency of exceedance at every period of vibration.

4.5 Ground Response Studies

The ground response study for the Missouri bridge site was similar to that conducted for the Washington site. First, a series of liquefaction analyses were conducted using the SPT and CPT simplified methods. Results of these analyses were then used to determine the depths at which liquefaction could occur during the 475- and 2,475-year earthquakes. These results were used as a basis for determining a simplified cyclic resistance ratio (CRR) and the residual strength of the soil for use in further liquefaction assessments. Concurrent with these simplified analyses, a series of one-dimensional nonlinear, effective stress analyses was conducted to define more explicitly the mechanisms for pore water pressure increase within the soil profile and the changes in accelerations and deformations resulting from the development of liquefaction.

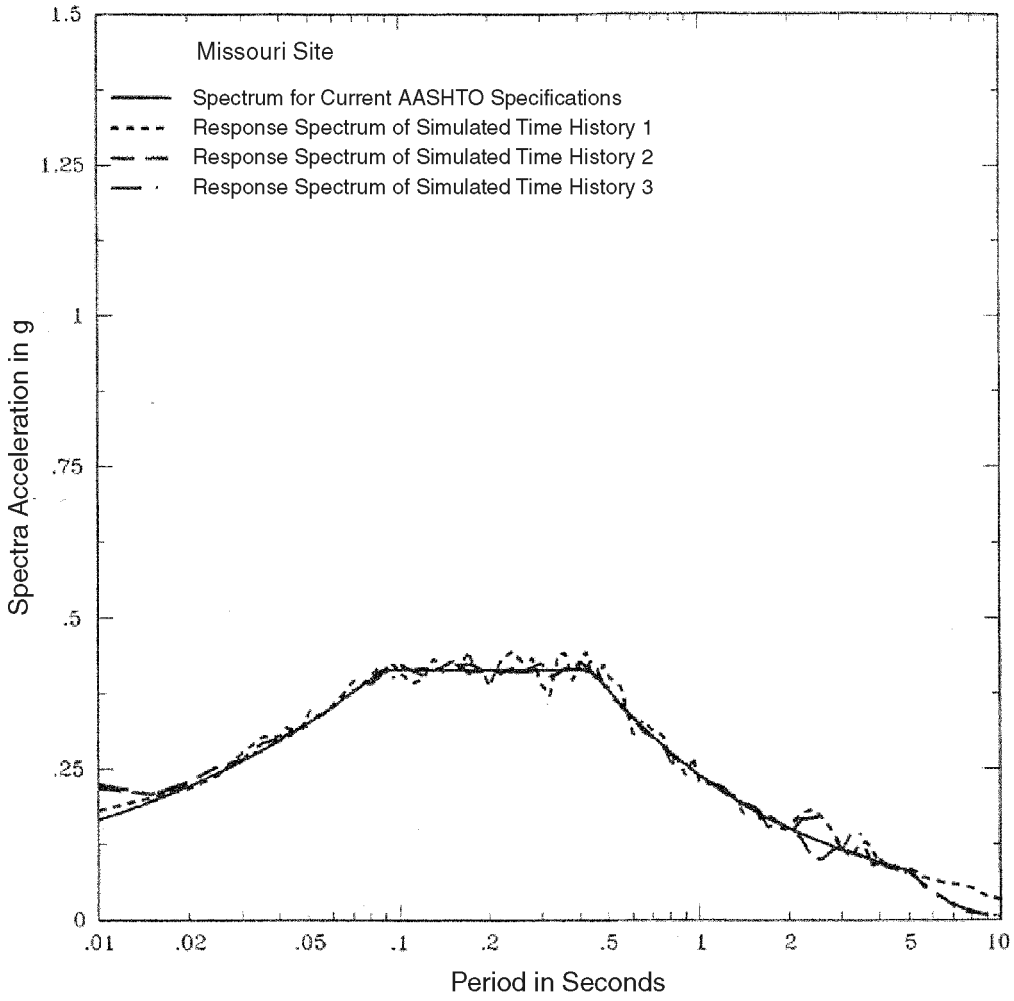

Figure 4.10 Comparison of Response Spectra of Spectrum-Matched Synthetic Time Histories with Design Response Spectrum Based on Current AASHTO Specifications, Site Class II, Missouri Site

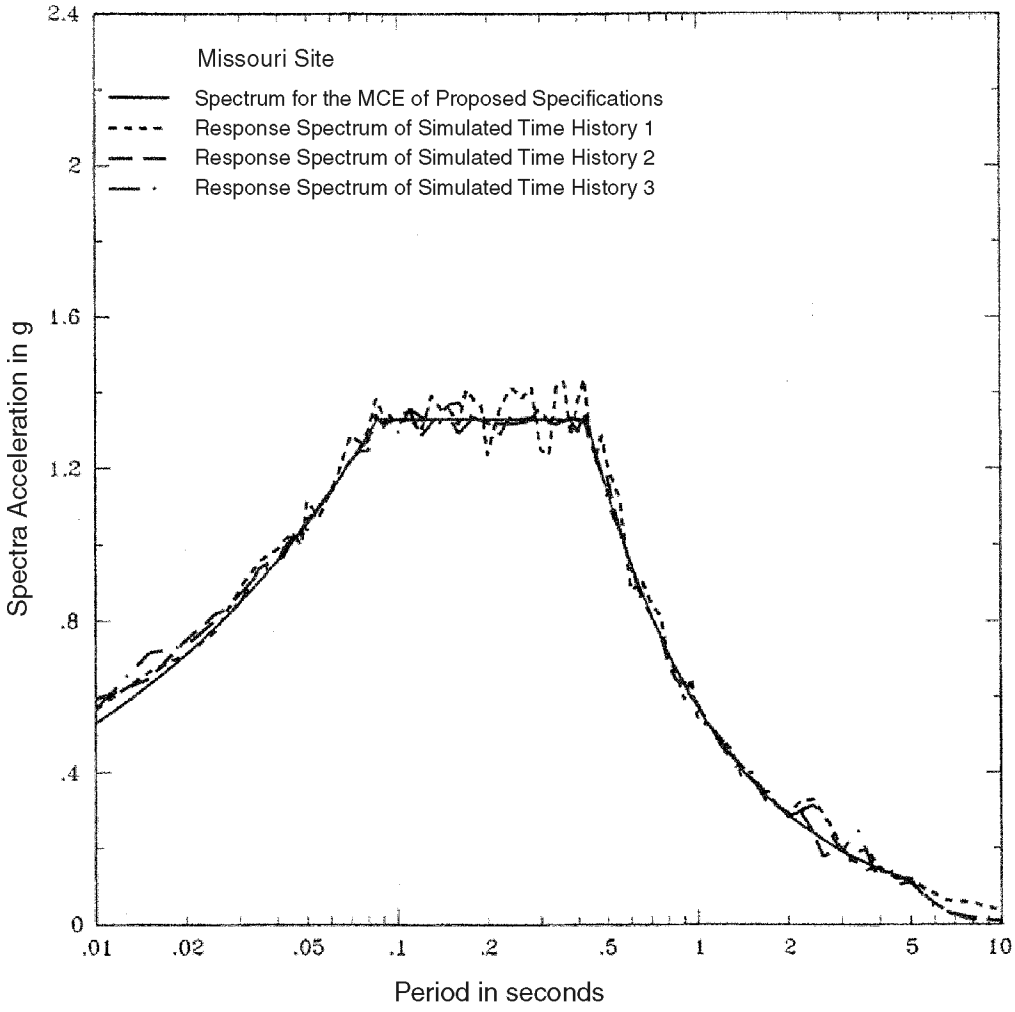

Figure 4.11 Comparison of Response Spectra of Spectrum-Matched Time Histories with MCE Design Response Spectrum of Recommended LRFD Specifications, Site Class C, Missouri Site

4.5.1 Simplified Liquefaction Analyses

The first step of the procedure outlined in Section 2.5.2.1 is to determine if liquefaction occurs.

Simplified liquefaction analyses were conducted using the procedures given in Youd and Idriss (1997). Two levels of peak ground acceleration (PGA) were used, one representing the 475-year event within the current AASHTO specifications and the other representing the recommended 2,475-year event. The PGA for the 475-year event was not adjusted for site effects, consistent with the approach recommended in the AASHTO Standard Specifications[1]. Ground motions for the 2,475-year event were adjusted to Site Class D, using the procedures given in Section 3 of the recommended LRFD provisions. The resulting PGA values for each case are summarized below.

Input Parameter	475-Year Return Period	2,475-Year Return Period
Peak ground acceleration	0.17g	0.53g
Mean magnitude	6.6	7.5

The magnitude of the design earthquake is required for the SPT and CPT simplified analyses. As discussed previously, results of deaggregation studies from the USGS database for deaggregation suggest that the mean magnitudes for the 475- and 2,475-year events are 6.6 and 7.5, respectively. The mean magnitudes reflect contributions from small to moderate magnitude earthquakes occurring closer to the site. However, the dominant event is the characteristic magnitude 8 earthquake in the New Madrid seismic zone. For the simplified liquefaction assessment, a range of magnitudes thought to be representative of practice was used in the evaluation. For time history analyses, acceleration time histories representative of the duration of the magnitude 8 New Madrid earthquake and the levels of ground motion defined by the current AASHTO spectrum and the MCE spectrum of the recommended specification were developed.

For these analyses, ground water was assumed to occur 20 feet below the ground surface for the non-fill case. Evaluations were also performed using a simplified model to evaluate the effects of the fill. For the fill model, the soil profile with the associated soil properties was the same as the free-field case. However, an additional 30 feet of embankment was added to the soil profile. As with the Washington site, this change results in a decrease in the imposed shearing stress (i.e., demand) because of the lower soil flexibility factor (R_d).

Factors of safety results from the liquefaction evaluations for the simplified soil model without fill at the three magnitudes are shown in Figure 4.12 and Figure 4.13 for the 475- and 2,475-year seismic events, respectively. These results indicate that liquefaction may or may not occur for the smaller event, depending on the assumed magnitude of the earthquake. For the magnitude based on the mean of the deaggregation for the site, liquefaction is not predicted. For the 2,475-year event, liquefaction is predicted, regardless of the assumed magnitude.

[1] Common practice is to adjust the PGA for the site factors given in Table 3.5.1 of Division 1-A. While this adjustment may be intuitively correct, these site factors are not explicitly applied to the PGA. If the site coefficient were applied at the Missouri site, the PGA would be increased by a factor of 1.5, reducing the difference in ground motions between the 475- and 2,475-year events.

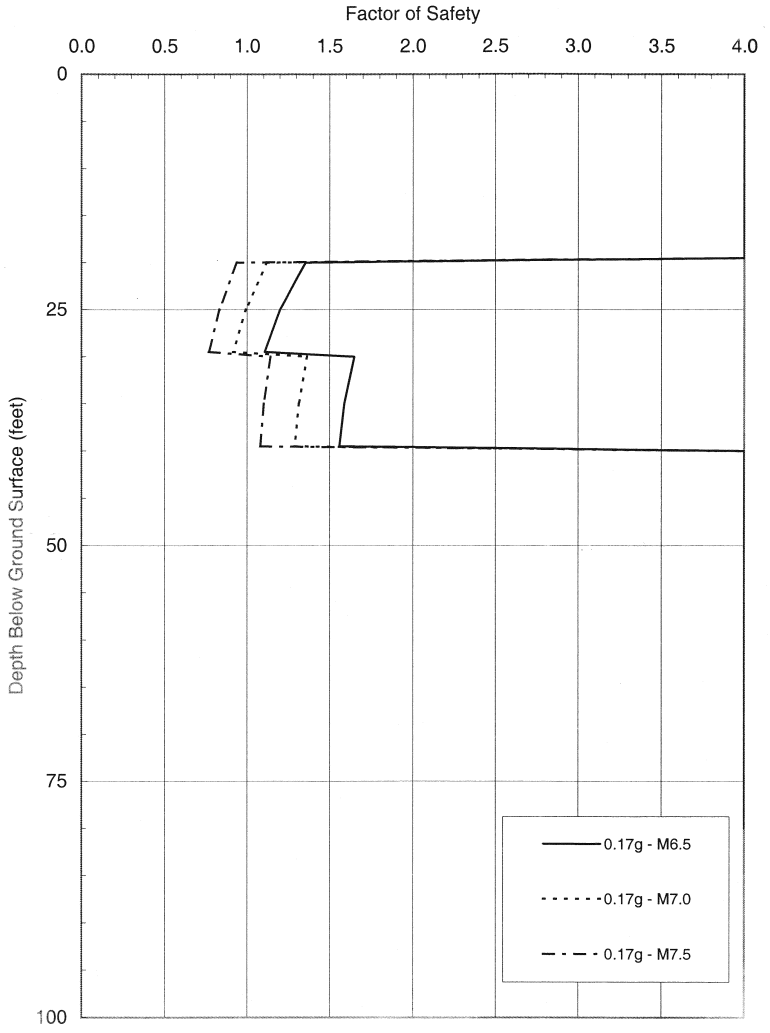

Figure 4.12 Liquefaction Potential – 475-Year Return Period

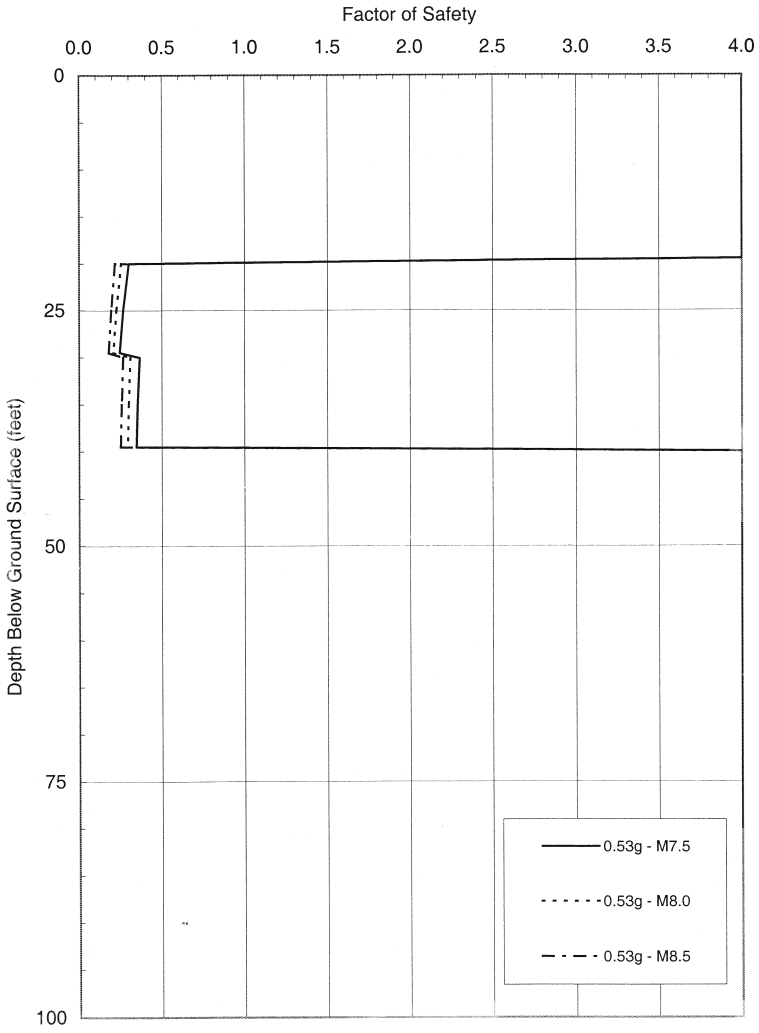

Figure 4.13 Liquefaction Potential – 2,475-Year Return Period

The results given in Figure 4.12 and Figure 4.13 are for the simplified soil model discussed in Section 4.2.3. Site-specific results of SPT and CPT liquefaction evaluations for soils borings B-4 and CPT sounding B-41 are given in Appendix F. The site-specific results are generally consistent with the simplified model, indicating that liquefaction could occur for the 475-year return period event using the CPT results but may not using SPT results. As noted in the discussion for the Washington site, factors of safety appear to be slightly lower by 0.2 to 0.3 in the liquefiable zones for the CPT results relative to the SPT results. The low factors of safety below 40 feet in the SPT analyses are thought to be erratic blow counts measured during the SPT rather than low strength layers. The liquefaction potential during the 2,475-year event is higher (i.e., lower factors of safety) for both the SPT and CPT evaluation methods, with average factors of safety being less than 0.5. An interesting observation is that the effects of magnitude are not nearly as significant for the 2,475-year return period, suggesting that the uncertainty in selecting the magnitude for the liquefaction analyses is not critical for this case.

Results of liquefaction analyses with the approach fill are shown in Figure 4.14 and Figure 4.15. As observed at the Washington site, the fill case results in somewhat lower liquefaction potential (i.e., higher FOS) due to the lower imposed shearing stress. Figure 4.16 and Figure 4.17 show a direct comparison for the most likely magnitude.

4.5.2 DESRA-MUSC Ground Response Studies

A more detailed and refined approach to assess if liquefaction occurs and to assess its affects on the ground motions expected at the site is to use a nonlinear effective stress approach. As with the Washington study, a series of ground response studies were conducted with the program DESRA-MUSC. The idealized site profile and related soil properties adopted for the response analyses are shown in Figure 4.1. Response analyses were performed for the three earthquake input motions, assuming a transmitting boundary input level at a depth of 80 feet, corresponding to the dense alluvium interface. Analyses were conducted for both the 475- and 2,475-year return events and for site profiles with and without embankment fill.

The DESRA-MUSC parameters utilized for analyses for the various soil strata (G/G_{max} curves, backbone curves and liquefaction strength curves) are documented in Appendix H together with the result of response analyses for all cases defined above. A representative set of results for the 1985 Michoacan earthquake, which has the highest energy levels of the three events used for the analyses, is described below.

4.5.2.1 Without Embankment Fill

The site response for the 475-year Michoacan earthquake is summarized in four figures:

Figure 4.18: Input and output acceleration time histories and response spectra
Figure 4.19: Maximum shear strains induced as a function of depth
Figure 4.20: Time histories of pore water pressure generation at various depths
Figure 4.21: Shear stress-shear strain hysteretic loops at various depths.

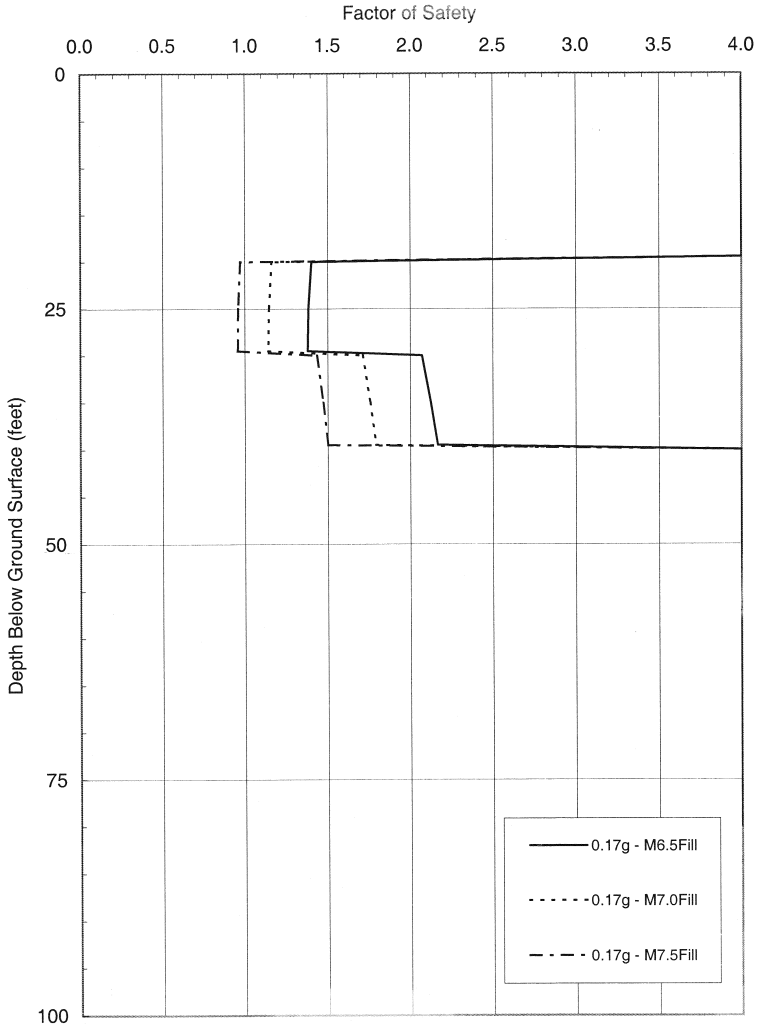

Figure 4.14 Liquefaction Potential – 475-Year Return Period with 30-Foot Fill

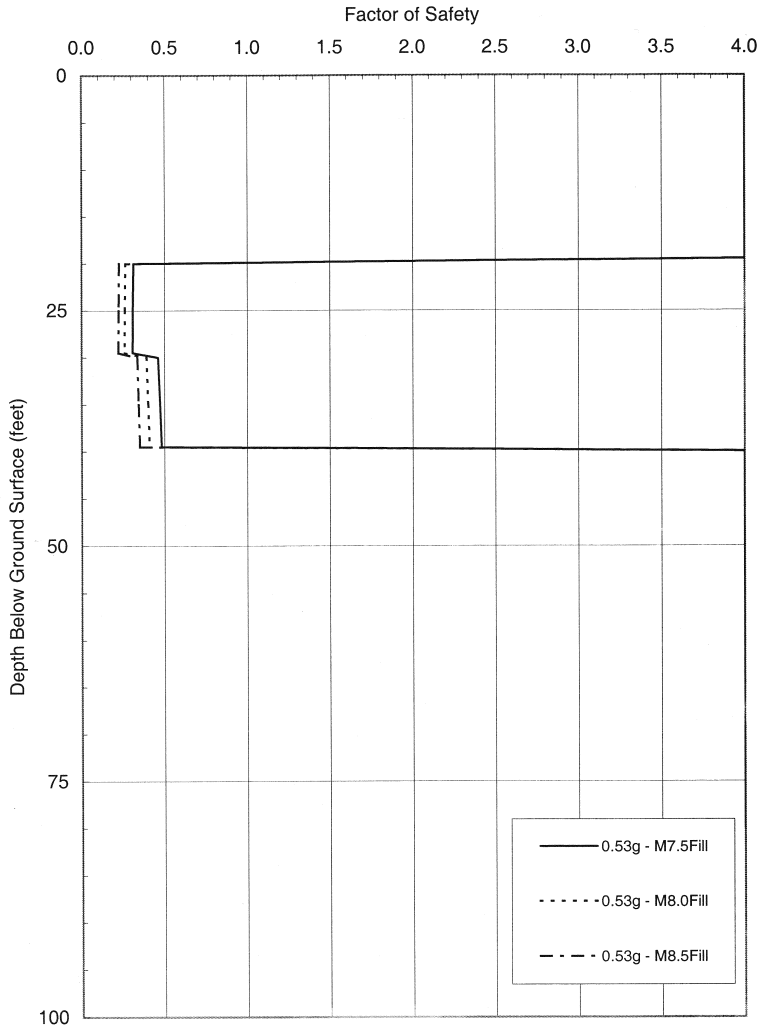

Figure 4.15 Liquefaction Potential – 2,475-Year Return Period with 30-Foot Fill

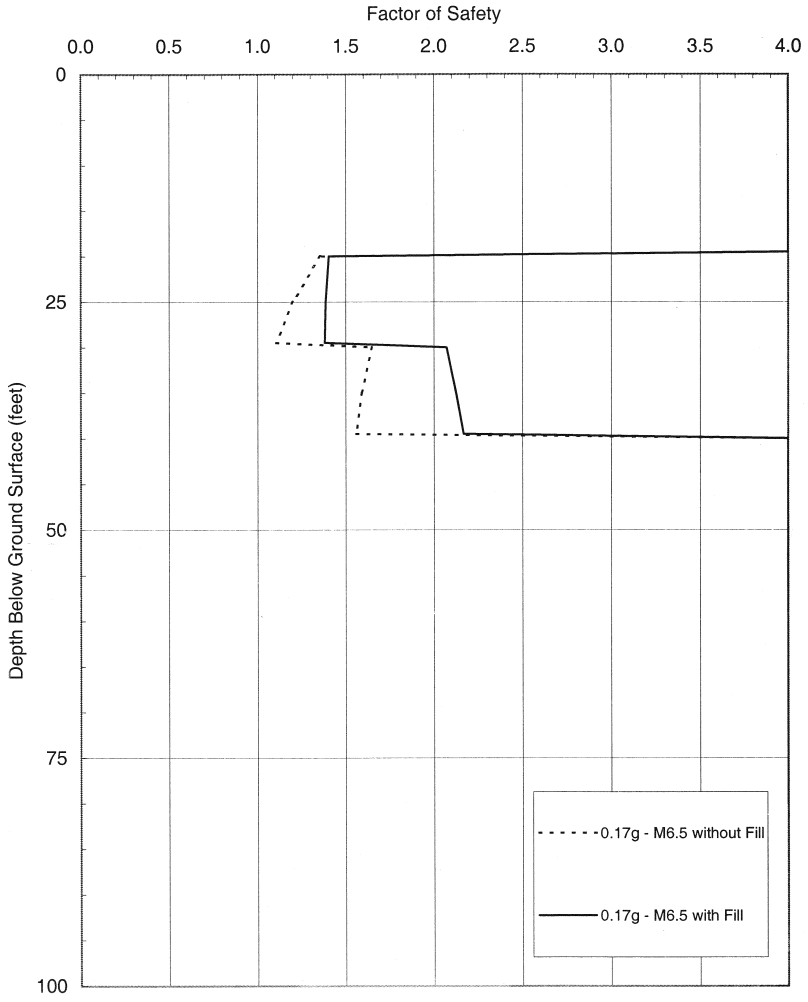

Figure 4.16 Liquefaction Potential – 475-Year Return Period without and with 30-Foot Fill

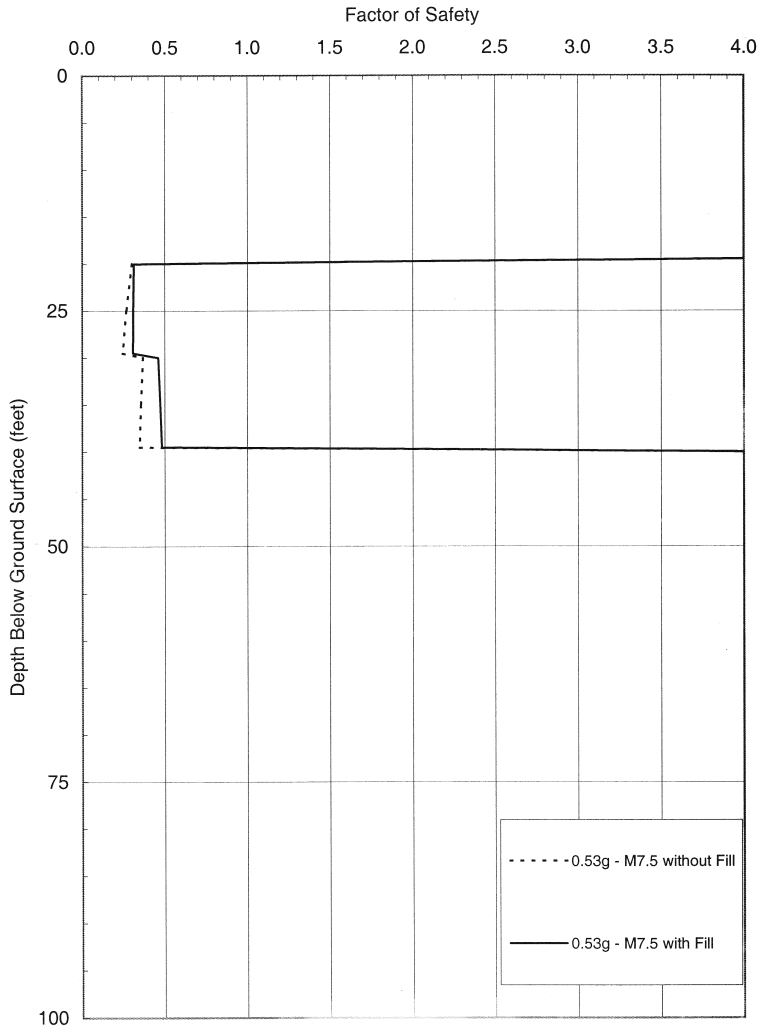

Figure 4.17 Liquefaction Potential – 2,475-Year Return Period without and with 30-Foot Fill

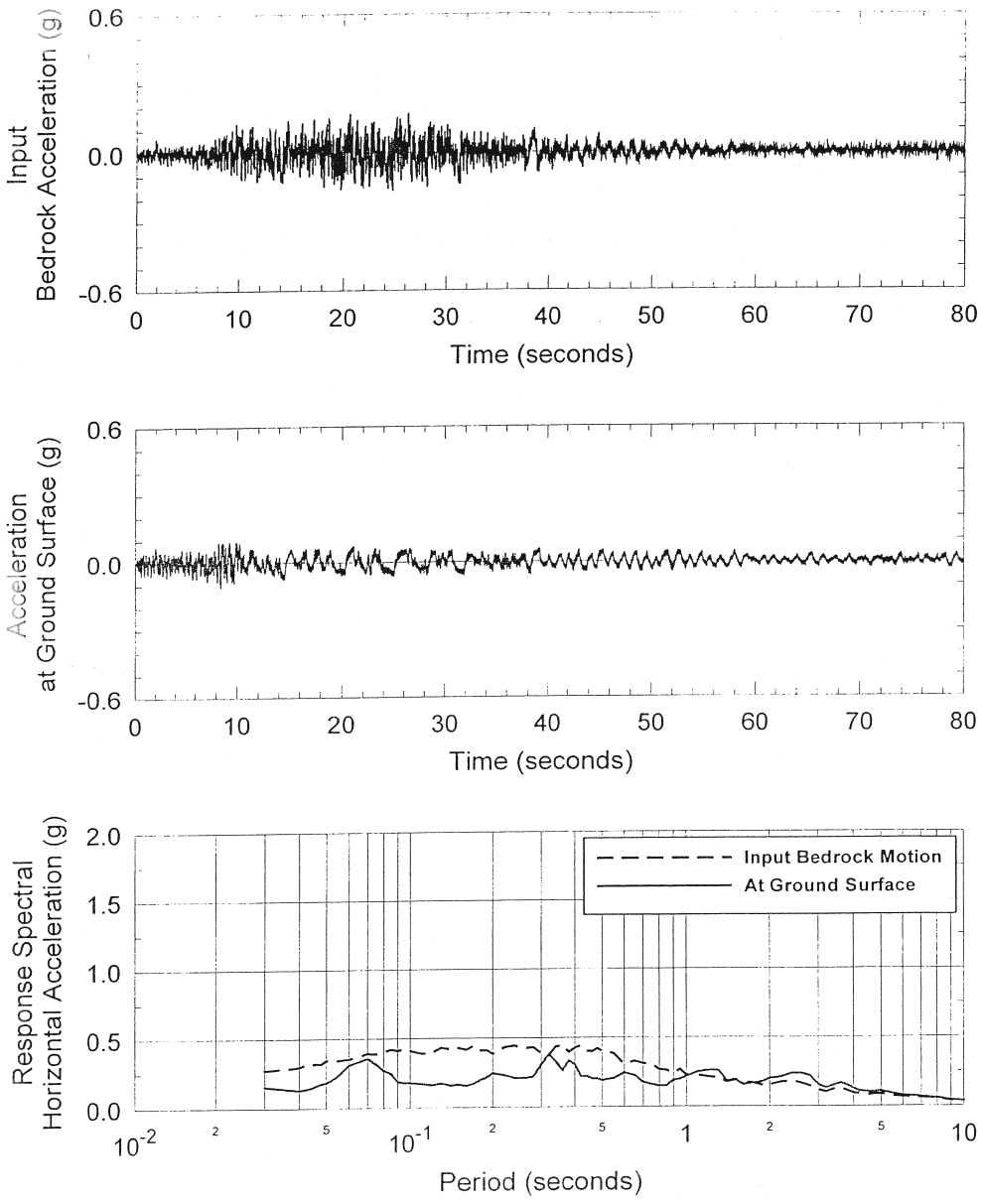

Figure 4.18 Input and Output Acceleration Time Histories and Response Spectra, 475-Year Return Period without Fill, 1985 Michoacan Earthquake

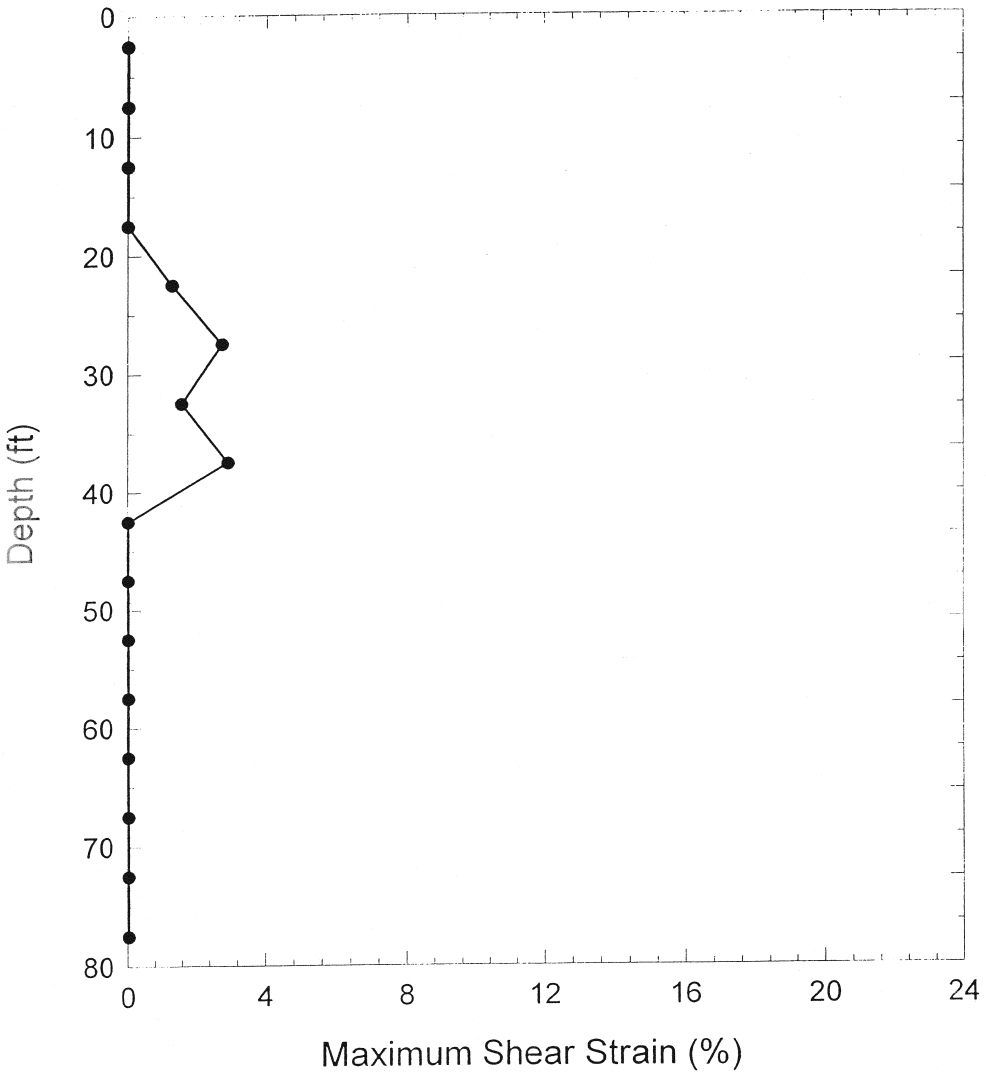

Figure 4.19 Maximum Shear Strains Induced as a Function of Depth, 475-Year Return Period without Fill, 1985 Michoacan Earthquake

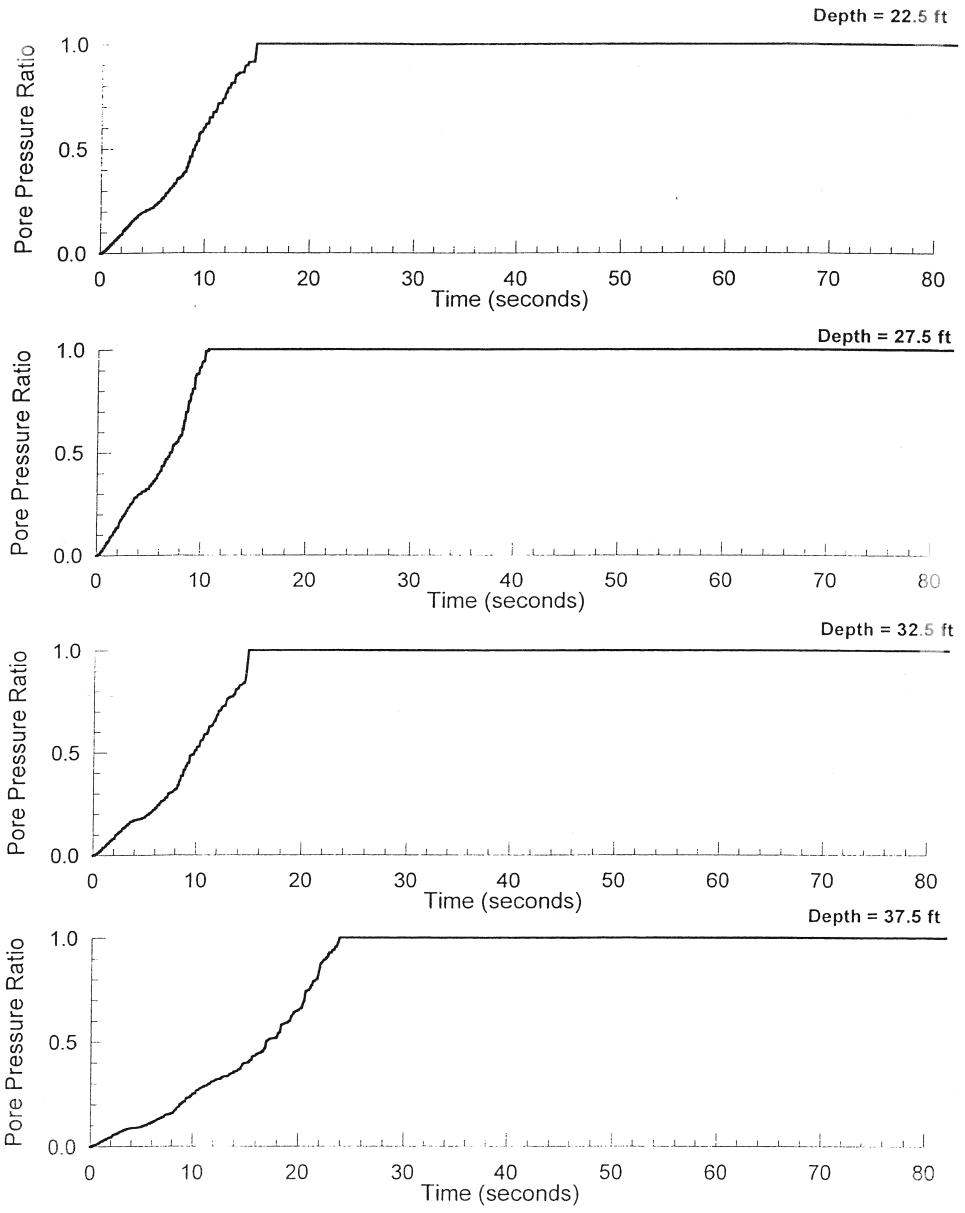

Figure 4.20 Time Histories of Pore Pressure Generation at Various Depths, 475-Year Return Period without Fill, 1985 Michoacan Earthquake

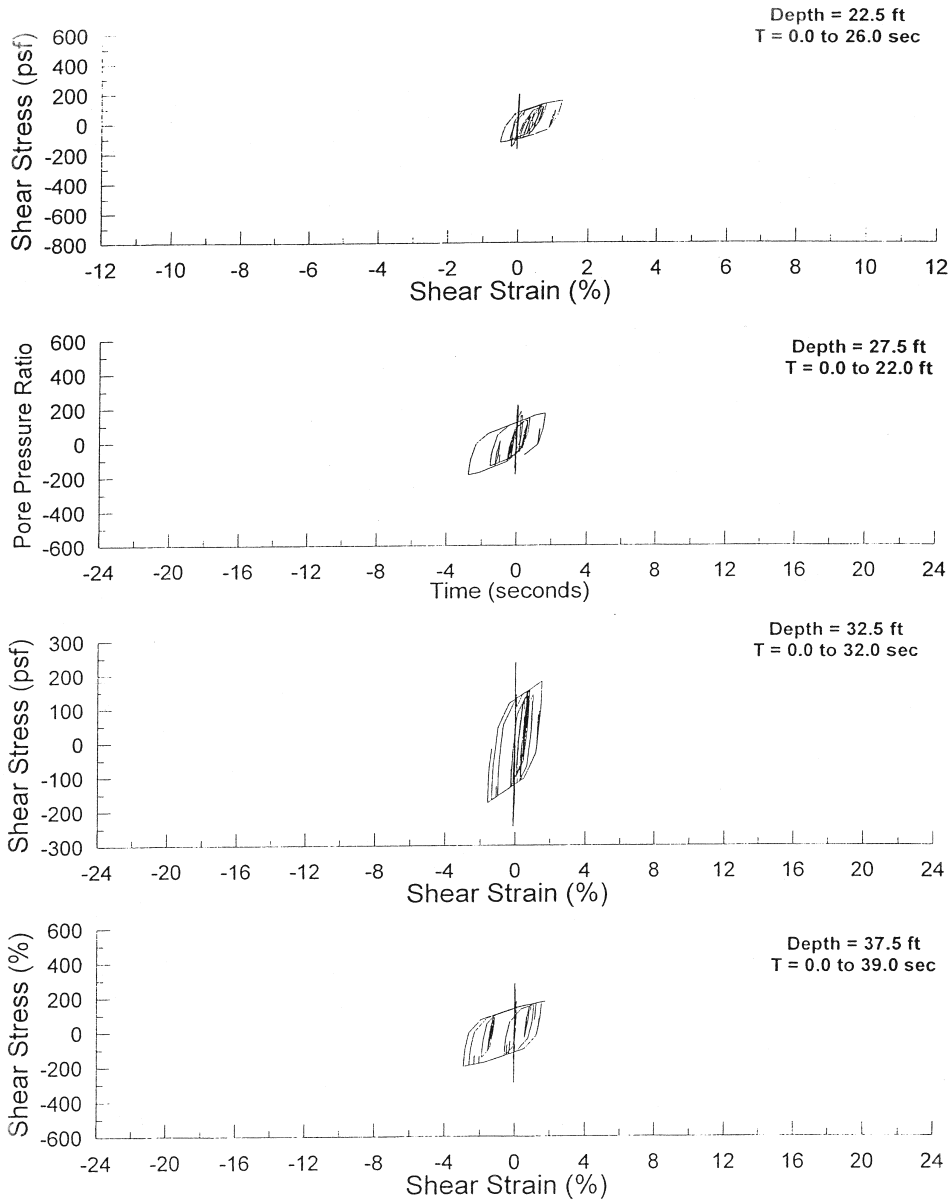

Figure 4.21 Shear Stress - Shear Strain Hysteretic Loops at Various Depths, 475-Year Return Period without Fill, 1985 Michoacan Earthquake

Figure 4.22 through Figure 4.25 summarize similar data for the 2,475-year earthquake. The following are key observations from the data plots.

1. For the 475-year earthquake, Figure 4.20 shows that liquefaction was first initiated in the more liquefiable layer between 20 and 30 feet after about 10 to 15 seconds of shaking, followed by the denser liquefiable layer between 30 and 40 feet over the time period 15 to 25 seconds. The input accelerations triggering initial liquefaction were about 0.15g, but the subsequent higher input accelerations were suppressed by the liquefaction as shown in Figure 4.18. Maximum shear strains induced in the liquefiable layers were of the order of 2 to 3 percent.
2. For the 2,475-year earthquake, a similar pattern to that described above evolved. However, the liquefaction was induced more rapidly, occurring in the 20- to 30-foot layer after 4 to 8 seconds and for the 30- to 40-foot layer after 8 to 12 seconds as shown in Figure 4.24. The input acceleration triggering liquefaction was again about 0.15g, with subsequent suppression of high accelerations as shown in Figure 4.22. Maximum shear strains focused on the deepest layer between 35 and 40 feet and were about 7 percent.

Similar trends to those described above were seen for the Chile and Tokachi-oki earthquakes, as may be seen in Appendix H.

The above results are generally consistent with the factor of safety calculations using the simplified method if a magnitude 8 event is assumed for analyses, which is representative of the Michoacan event.

4.5.2.2 With Embankment Fill

The site response for the 475- and 2,475-year earthquakes are summarized in a similar manner to the no fill case above, in Figure 4.26 through Figure 4.33. The effect of the fill is to suppress the rate of pore water pressure build up, which would correspond to the observed increase in factor of safety for the simplified method. Liquefaction is seen to again occur between the 20-40 ft liquefiable layers.

In the case of the Michoacan 2,475 year event, the focal point for maximum shear strains occurred in the 30- to 40-foot layer, suggesting that this layer could be the focal zone for lateral spread deformations. However, the results for the Chile and Tokachi-oki earthquakes, although showing similar liquefaction trends (see Appendix H), tended to suggest that lateral spread deformations would be broadly distributed over the 20- to 40-foot depth of the liquefied zone.

Results are consistent with the simplified method if a magnitude 8 event is assumed, except for the 475-year event between 30-40 feet, where the simplified method would indicate a factor of safety greater than one.

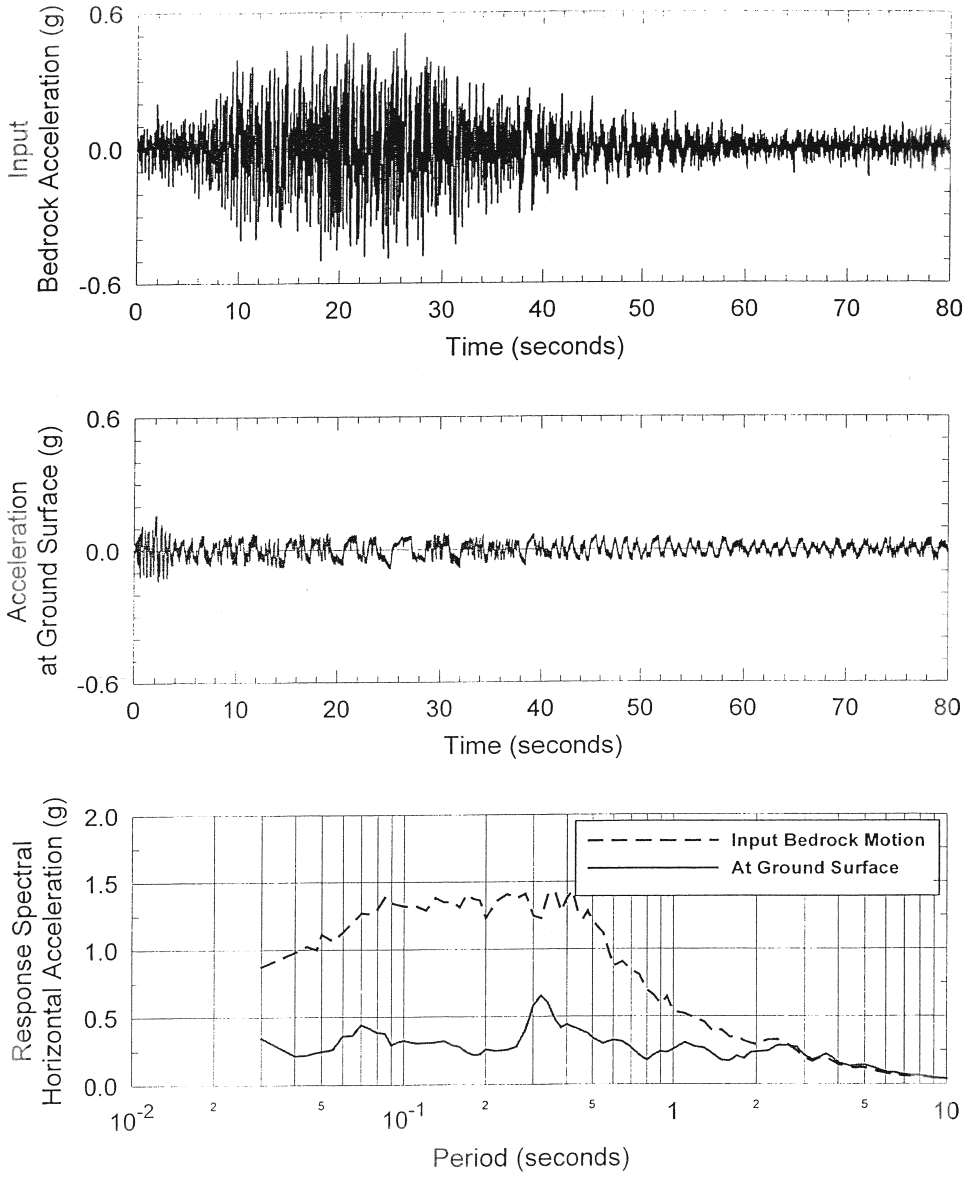

Figure 4.22 Input and Output Acceleration Time Histories and Response Spectra, 2,475-Year Return Period without Fill, 1985 Michoacan Earthquake

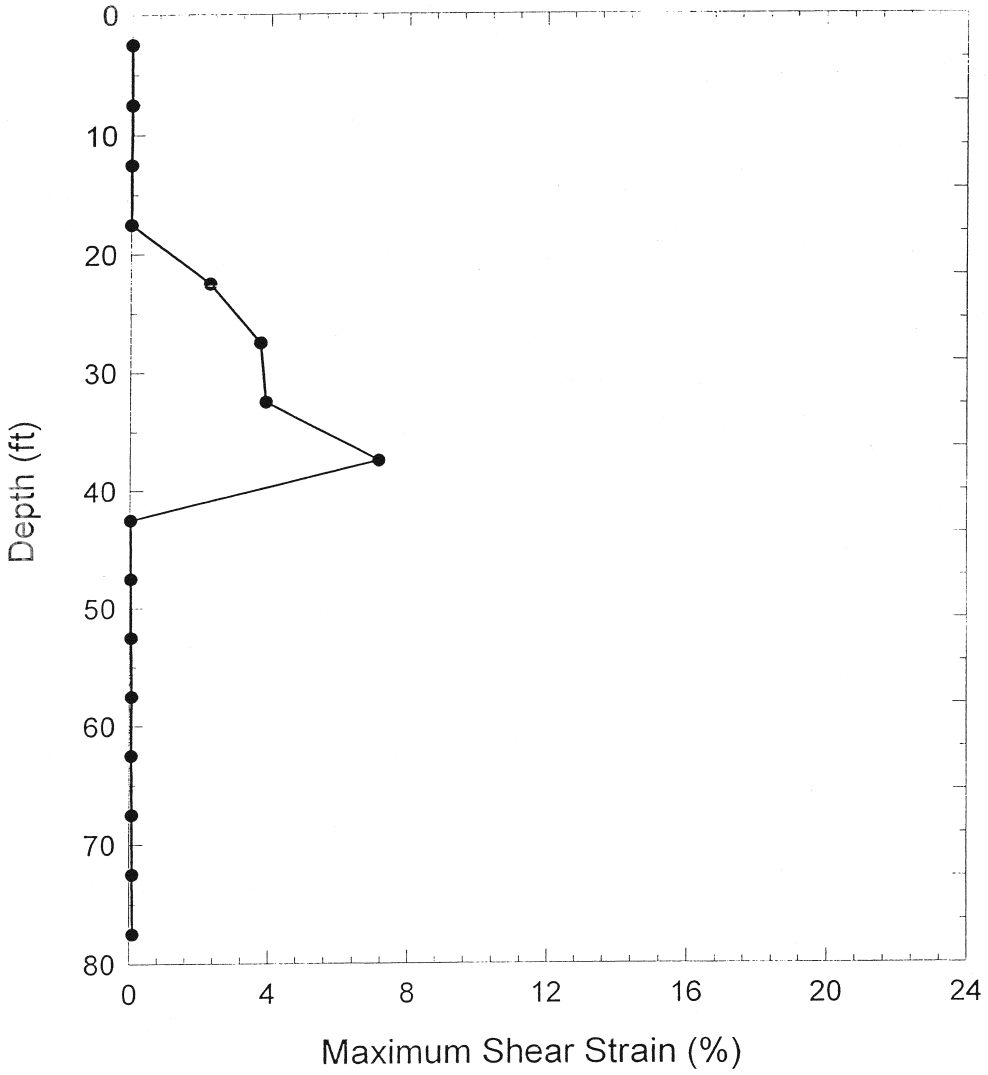

Figure 4.23 Maximum Shear Strains Induced as a Function of Depth, 2,475-Year Return Period without Fill, 1985 Michoacan Earthquake

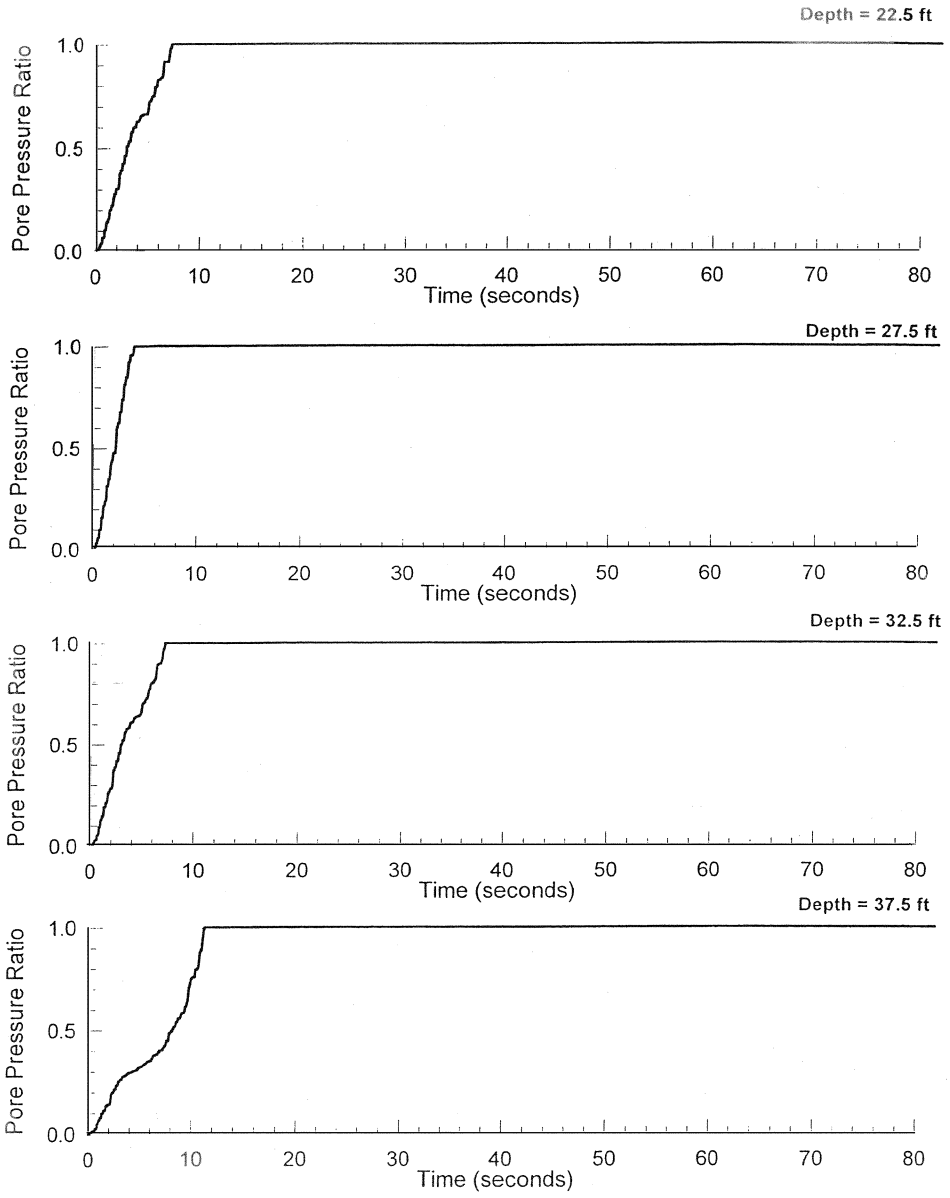

Figure 4.24 Time Histories of Pore Pressure Generation at Various Depths, 2,475-Year Return Period without Fill, 1985 Michoacan Earthquake

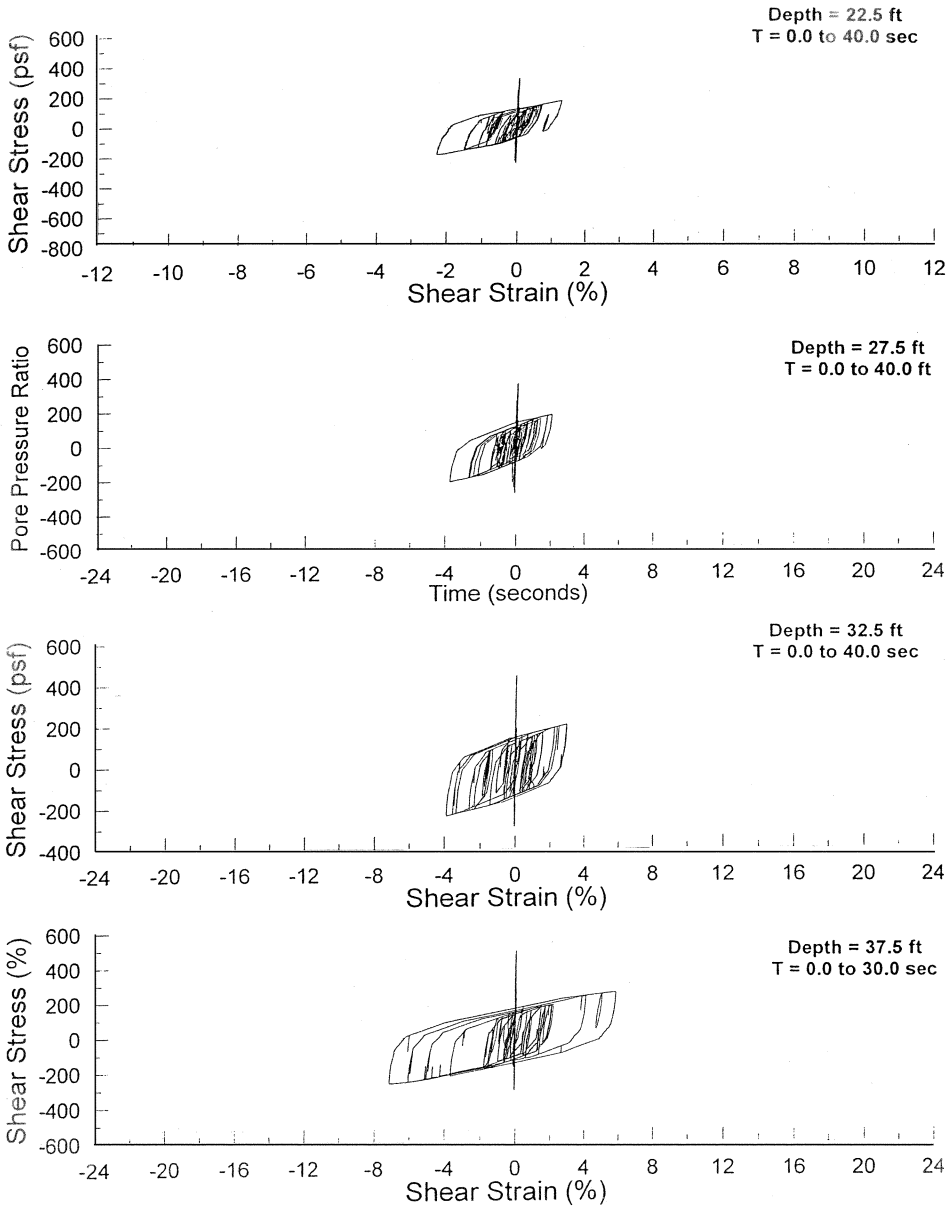

Figure 4.25 Shear Stress - Shear Strain Hysteretic Loops at Various Depths, 2,475-Year Return Period without Fill, 1985 Michoacan Earthquake

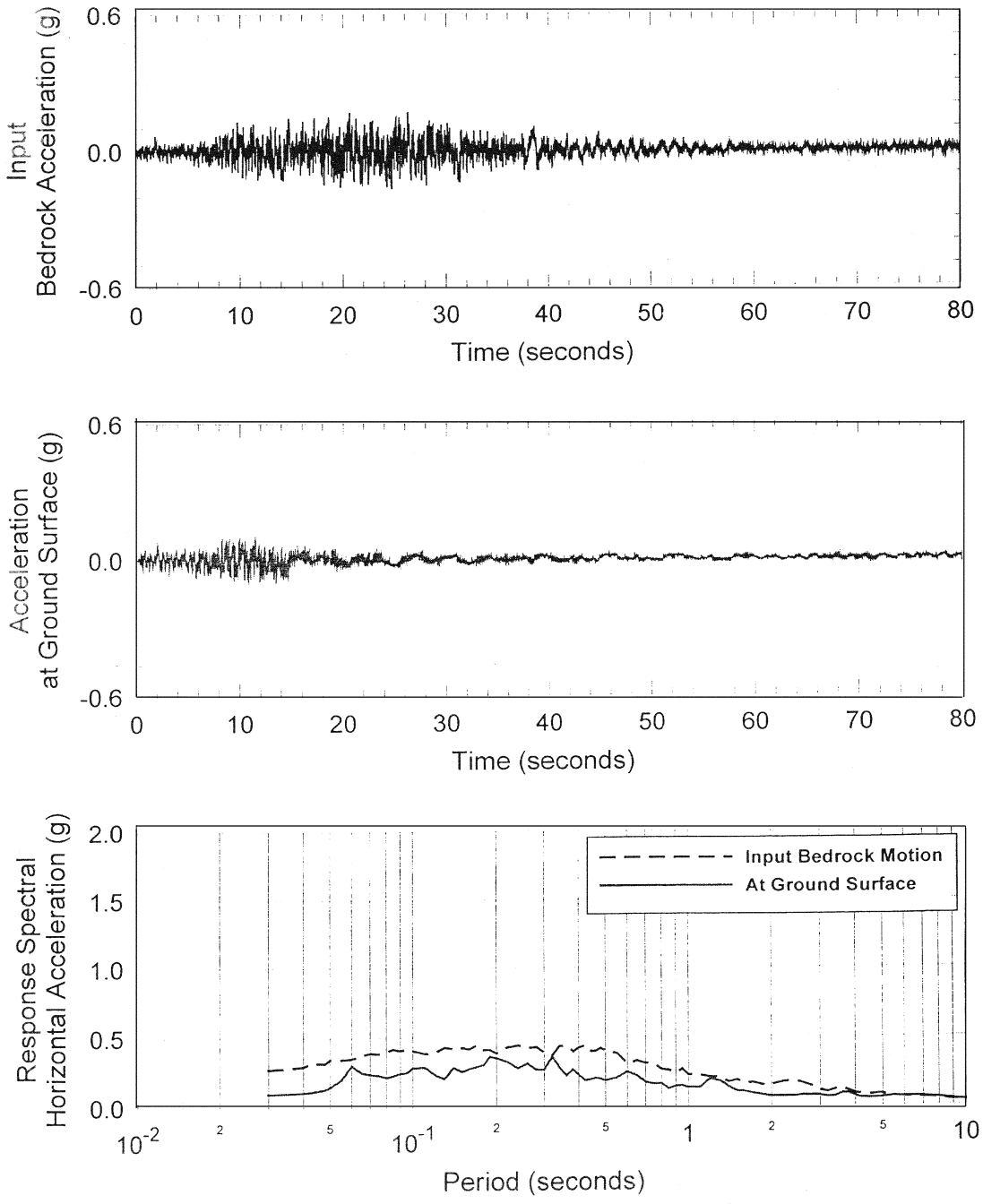

Figure 4.26 Input and Output Acceleration Time Histories and Response Spectra, 475-Year Return Period with Fill, 1985 Michoacan Earthquake

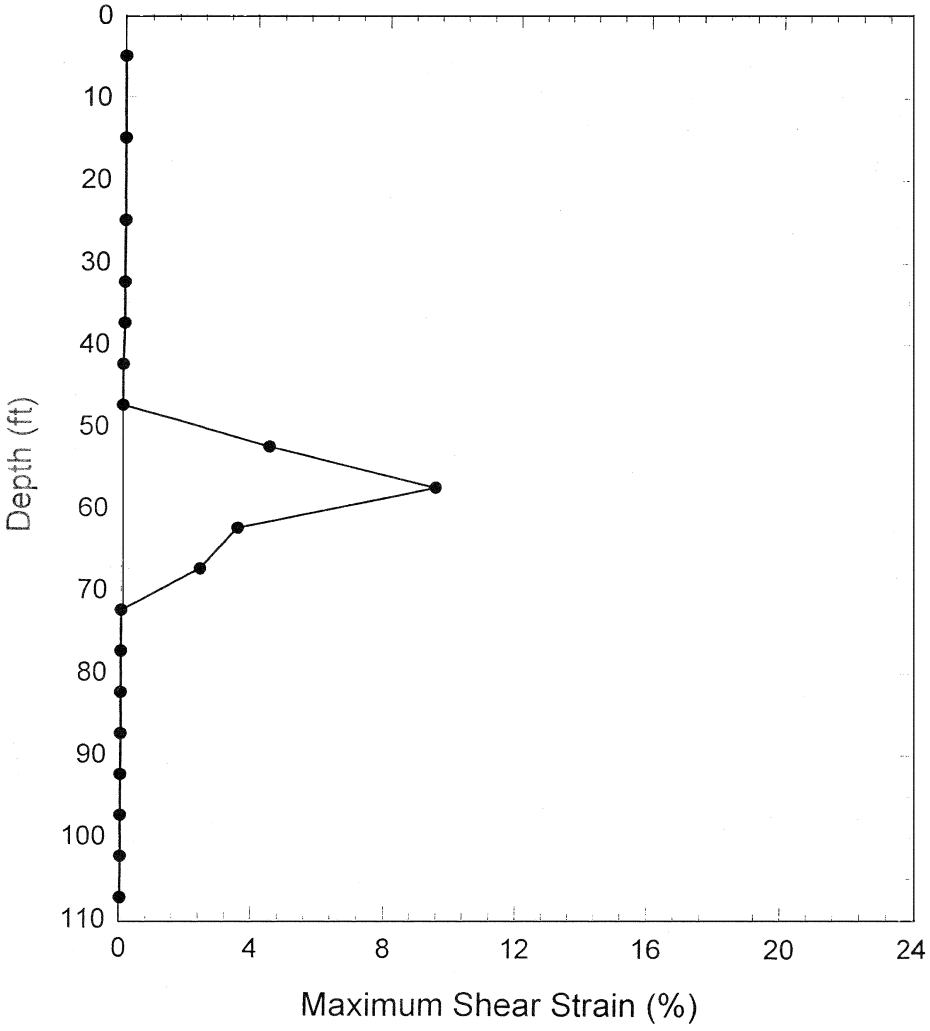

Figure 4.27 Maximum Shear Strains Induced as a Function of Depth, 475-Year Return Period with Fill, 1985 Michoacan Earthquake

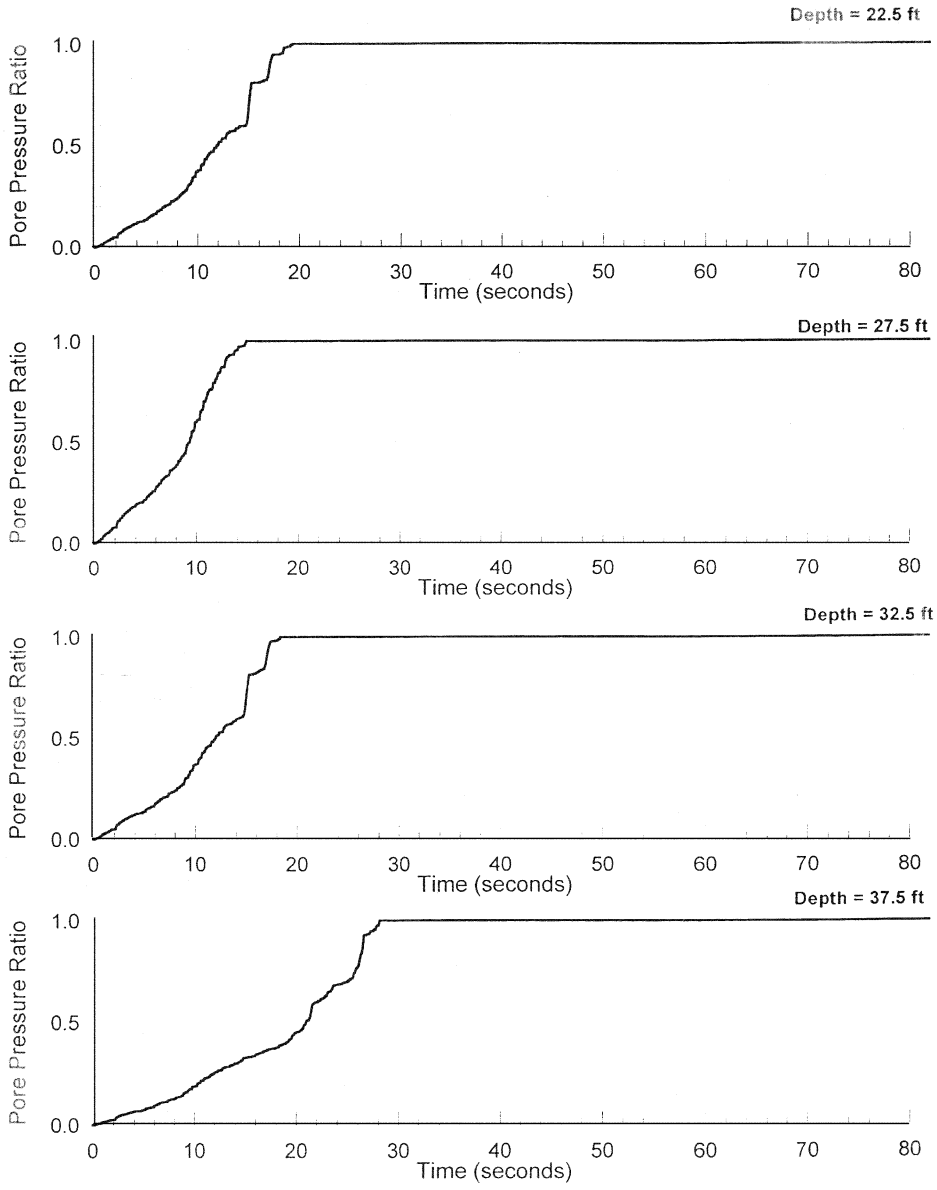

Figure 4.28 Time Histories of Pore Pressure Generation at Various Depths, 475-Year Earthquake with Fill, 1985 Michoacan Earthquake

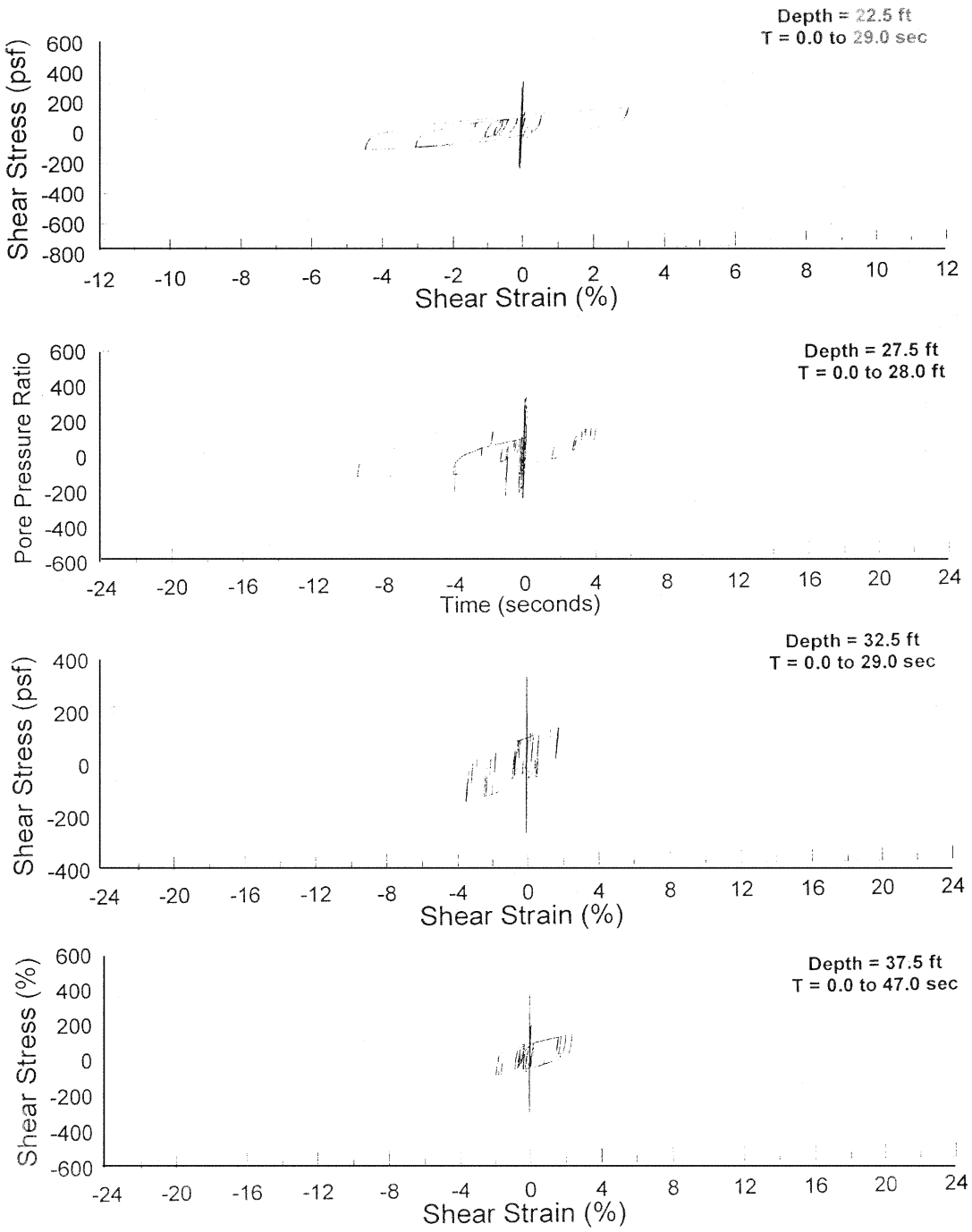

Figure 4.29 Shear Stress - Shear Strain Hysteretic Loops at Various Depths, 475-Year Earthquake with Fill, 1985 Michoacan Earthquake

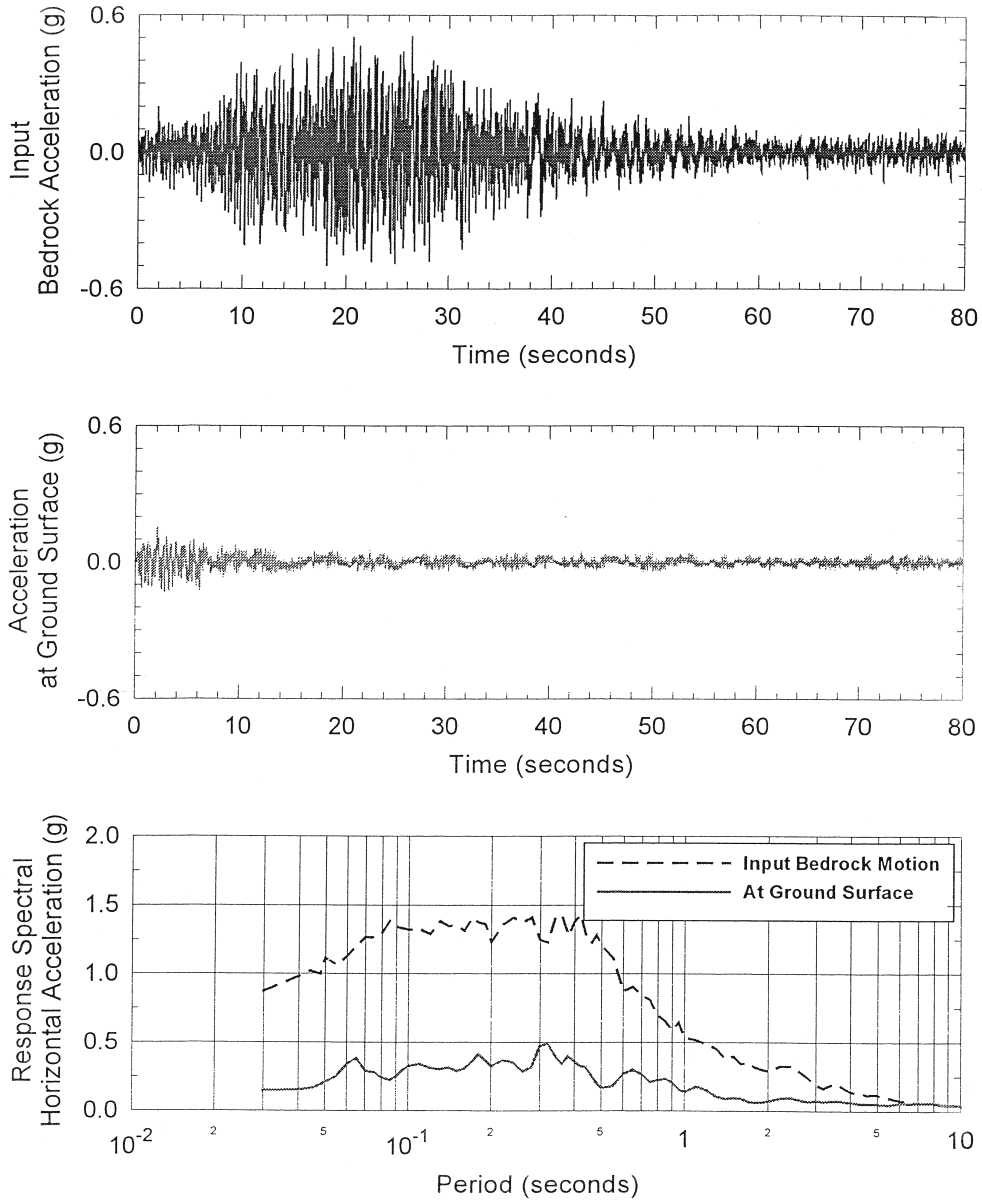

Figure 4.30 Input and Output Acceleration Time Histories and Response Spectra, 2,475-Year Earthquake with Fill, 1985 Michoacan Earthquake

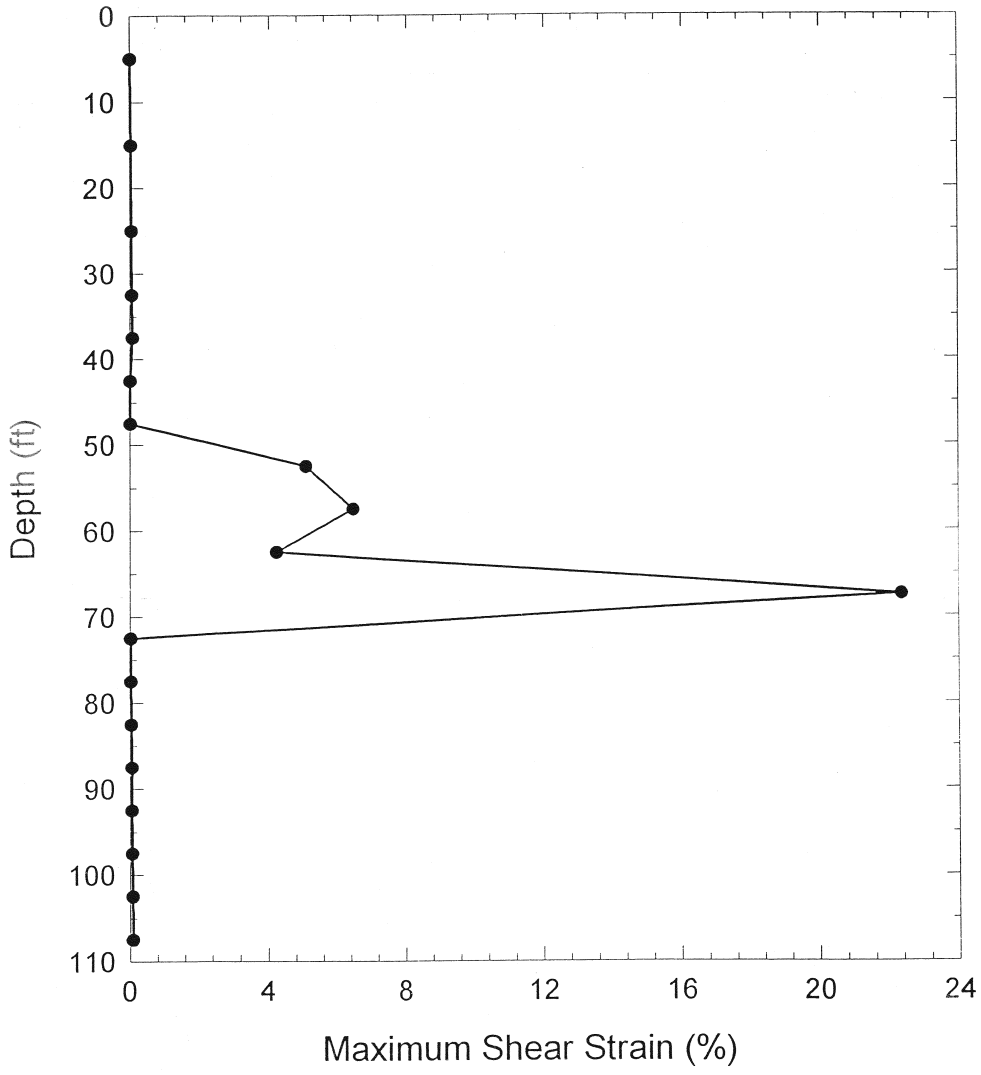

Figure 4.31 Maximum Shear Strains Induced as a Function of Depth, 2,475-Year Earthquake with Fill, 1985 Michoacan Earthquake

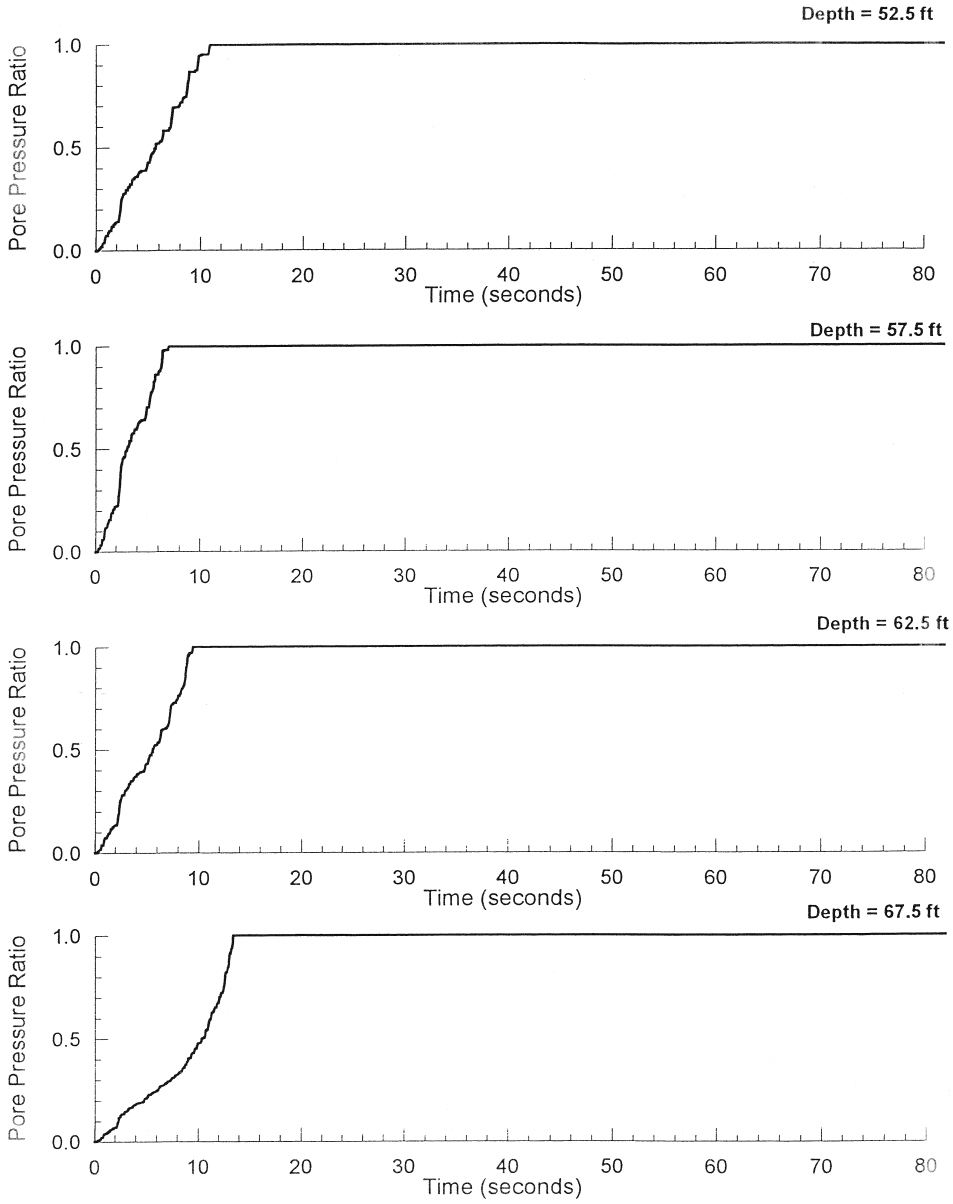

Figure 4.32 Time Histories of Pore Pressure Generation at Various Depths, 2,475-Year Earthquake with Fill, 1985 Michoacan Earthquake

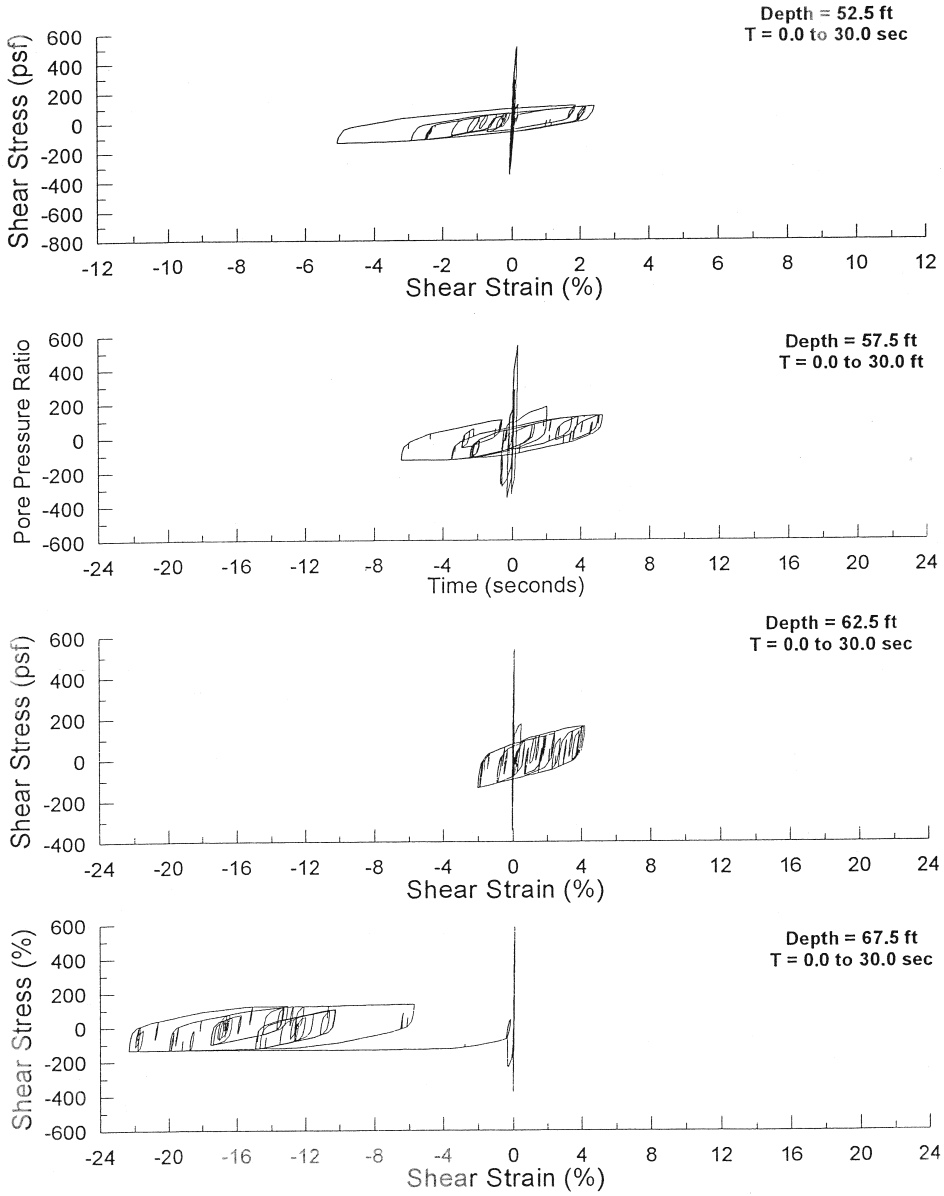

Figure 4.33 Shear Stress - Shear Strain Hysteretic Loops at Various Depths, 2,475-Year Earthquake with Fill, 1985 Michoacan Earthquake

4.5.2.3 Lateral Spread Implications

Based on the simplified liquefaction analyses and on the nonlinear effective stress modeling, it was concluded that lateral spread deformations would be distributed over the 20- to 40-foot depth. However, for analysis purposes, in order to compute likely displacement magnitudes of the overlying 20 feet of clay and embankment fill, it was assumed that ground accelerations, at the 40 feet interface depth would control the displacement, assuming a Newark sliding block analogy. As for the WSDOT site, analyses were also performed using the DISPMNT computer program in combination with the DESRA-MUSC results. "Upslope" deformations were suppressed assuming a strong one-directional driving force from the embankment. Strengths on the interface were degraded as a function of pore water pressure increases for the 35- to 40-foot layer, and reduced to the 300 psf residual strength when liquefaction was triggered.

Results showing displacement time history plots for the 2,475-year Michoacan earthquake as a function of yield acceleration are shown Figure 4.34. The input acceleration time histories used at a depth of 40 feet (70 feet with 30 feet of fill) are shown in Figure 4.35. The time histories are very similar for the no fill and fill cases. Total accumulated displacements for all earthquake events are shown in Figure 4.36, where it may be seen that the 2,475-year event generated significantly larger displacements than 475-year event, at low values of yield acceleration. These displacements were used as a basis for discussion of remediation analyses, as described in Section 4.5.3.4.

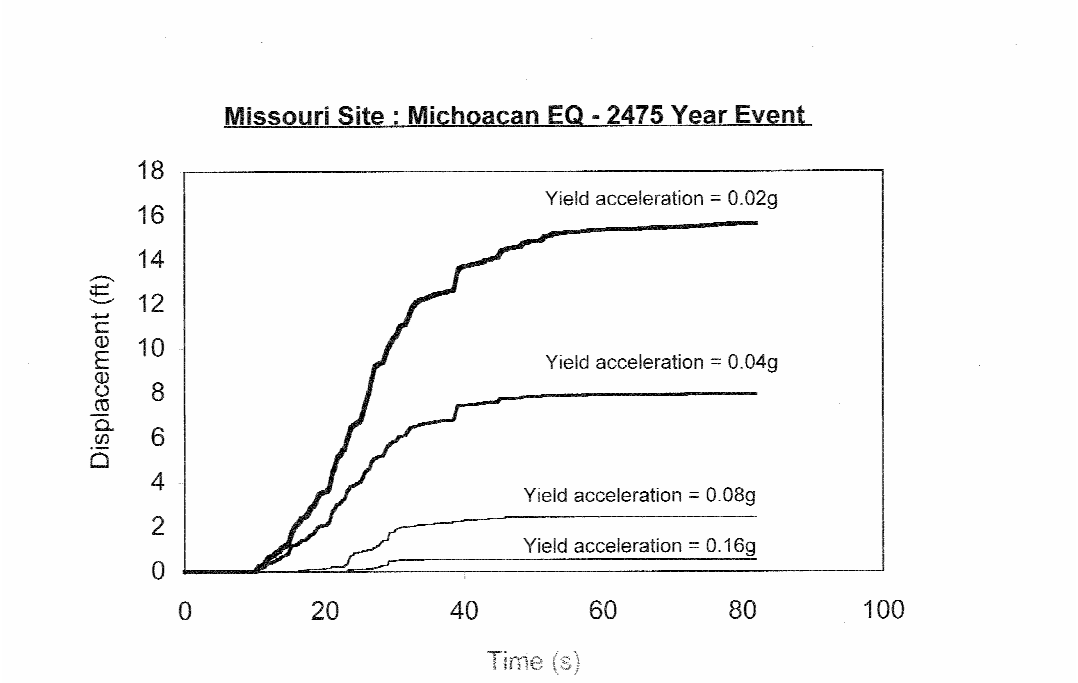

Figure 4.34 Displacement vs. Time for 2,475-Year Earthquake

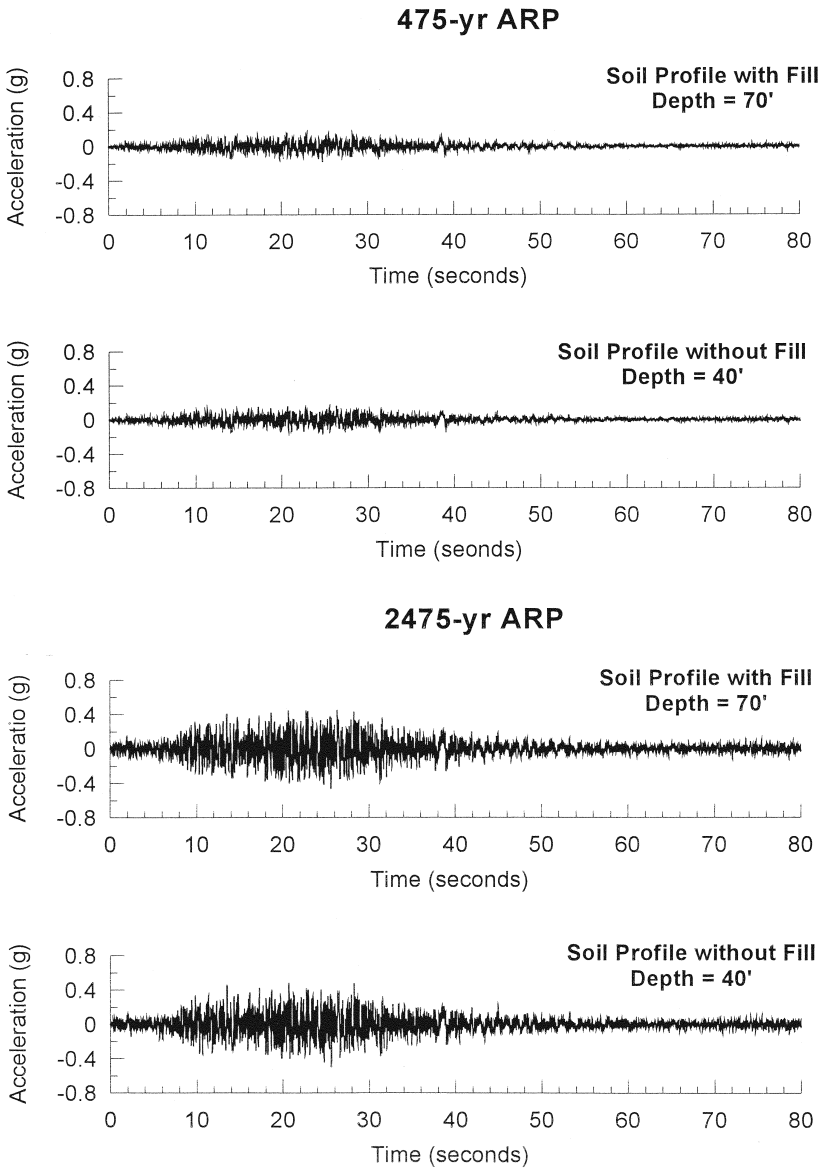

Figure 4.35 Acceleration Histories at Bottoms of Liquefiable Layers for 475- and 2,475-Year Events with Fill

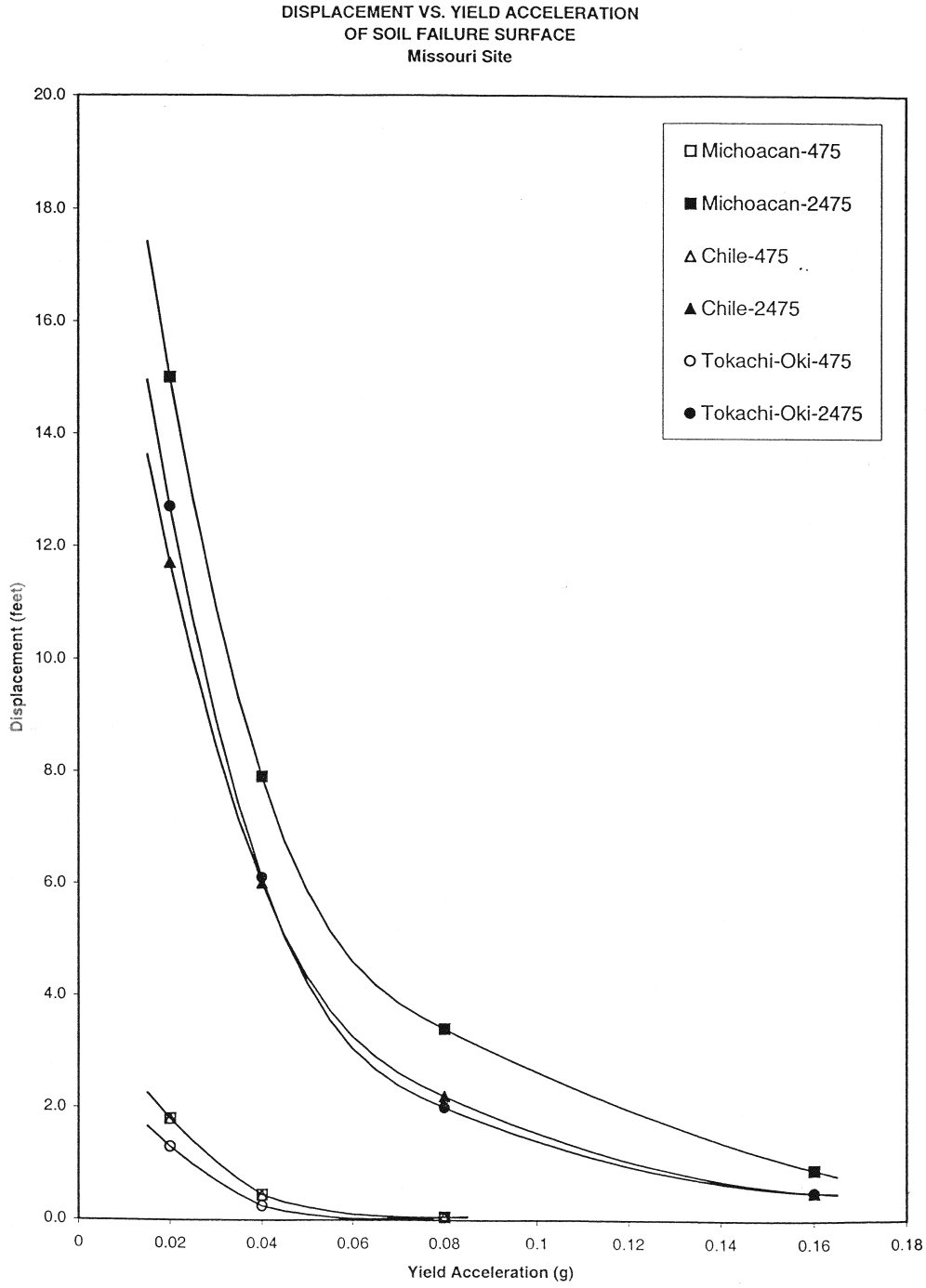

Figure 4.36 Displacement vs. Yield Acceleration of the Soil Failure Surface for the Central U.S. Site

4.5.3 Lateral Ground Displacement Assessment

From the results of these liquefaction studies, a single liquefiable zone was identified for stability and displacement evaluations. This zone extends from a depth of 20 to 40 feet below the ground surface. The residual strength of this zone was selected as 300 psf based on the SPT blow counts in the layer. No modifications were made to the layers above or below the liquefied zone for the Missouri analyses. One layer is cohesive in consistency and should not be affected by liquefaction. The sands below the liquefied zone are very dense and therefore also should not be affected by liquefaction of the overlying material. Using these conditions, the response of the end slope for the approach fill for the overcrossing was estimated by conducting pseudo-static stability followed by a deformation analyses.

4.5.3.1 Initial Stability Analyses

This section outlines Steps 2 and 3 of the design procedure in Section 2.5.2.1. Once liquefaction has been determined to occur, a stability analysis is performed to assess the potential for soil movement.

The computer program PCSTABL was used during these analyses. As with the study of the Washington site, most of the analyses were conducted using a simplified Janbu failure method of analysis with a wedge failure surface. This geometry was believed to be most representative of what would likely develop during a seismic event. Checks were also performed for a circular failure surface and using the modified Bishop and Spencer methods of analysis. Both pre-liquefaction and post-liquefaction strengths were used during these analyses. The geometry for this overcrossing is symmetric, and therefore only one side was evaluated.

Results of the pre-liquefaction studies indicate that the static FOS for the end slope is two or higher. The yield acceleration without liquefaction is approximately 0.27. The much higher static FOS for this site was the result of the deeper ground water level and the 20-foot thickness of the relatively stiff clay above the loose sand.

The first step in the liquefaction evaluation involved an analysis of the post-earthquake stability. In this analysis, stability was evaluated for the liquefied condition but without a seismic coefficient. This check was performed to determine if a flow failure would occur in the liquefied state. Results from these analyses show that the FOS dropped significantly when a residual strength was assigned to the liquefied layer; however, the FOS was greater than 1.0, indicating that a flow failure was not expected. This allowed displacements to be estimated using the simplified Newmark method described previously in Section 2.2.3.

Yield accelerations were estimated without consideration of the pinning effects of piles by re-running the stability analyses for the liquefied soil profile, with different applied seismic coefficients. The yield acceleration from these analyses is the inertial force required to produce a FOS of 1 and was determined to be approximately 0.02. Displacements were estimated using the same methods and assumptions as presented for the Washington site, except that the peak ground

acceleration and the yield acceleration were those for the Missouri site. The displacements determined for the two return periods are summarized below.

Case	Displacements (inches)							
	475-Year Event				2,475-Year Event			
	F-C	H-F	W-W	M-Q	F-C	H-F	W-W	M-Q
End Slope	>36	>10	5	5	>36	28	32	32

In these analyses, methods proposed by Franklin and Chang (1977), Hynes and Franklin (1984), Wong and Whitman (1990), and Martin and Qiu (1994) were evaluated. The provisions recommend that mitigation decisions be based on the results from the Martin and Qiu (M-Q) simplified method, which give results of 5 inches and 32 inches for the 475- and 2,475-year events, respectively.

These displacements are large enough, particularly for the 2,475-year event, that some mitigation procedures would have to be considered. These mitigation methods could involve structural pinning or ground improvement as described in the next section.

4.5.3.2 Stability Analyses with Mitigation Measures

This section outlines Step 7 of the procedure described in Section 2.5.2.1.

Two procedures were evaluated for reducing the amount of displacement being predicted, structural pinning and ground improvement. For these analyses, the additional resistance provided by the improved ground or by the structural pinning of the soil was incorporated into the stability analyses as described previously.

For the structural pinning evaluation, shear forces were calculated for two cases. In the first case, the shear failure occurred at the toe of the end slope in front of Pier 3 (Figure 4.37). This gave an increase in resistance of 16 kip/foot for the 43-foot width of the abutment. Both pile pinning and abutment passive resistance are included in this reaction. This reaction occurs over the 35-foot abutment width, resulting in a resistance of 33 to 44 kips/foot of width. This reaction force was introduced into the slope stability analysis using the smearing method described for the Washington study. For this method, the resistance per unit width was converted into equivalent shear strength along the shear plane in the liquefied zone and the equivalent strength was added to the residual strength of 300 psf. For these analyses, the failure plane was determined to be 90 feet in length, providing an added component to the liquefied strength of 180 psf. The resulting strength assigned to the liquefied layer was 480 psf (i.e., 180 psf + 300 psf = 480 psf).

For the second case, the shear failure was allowed to extend to the opposite embankment, as shown in Figure 4.38. The pinning force for this case was 32 kip/foot, resulting in an additional 355 psf of smeared resistance. The resulting assigned strength for the layer was 655 psf (i.e., 355 psf + 300 psf = 655 psf).

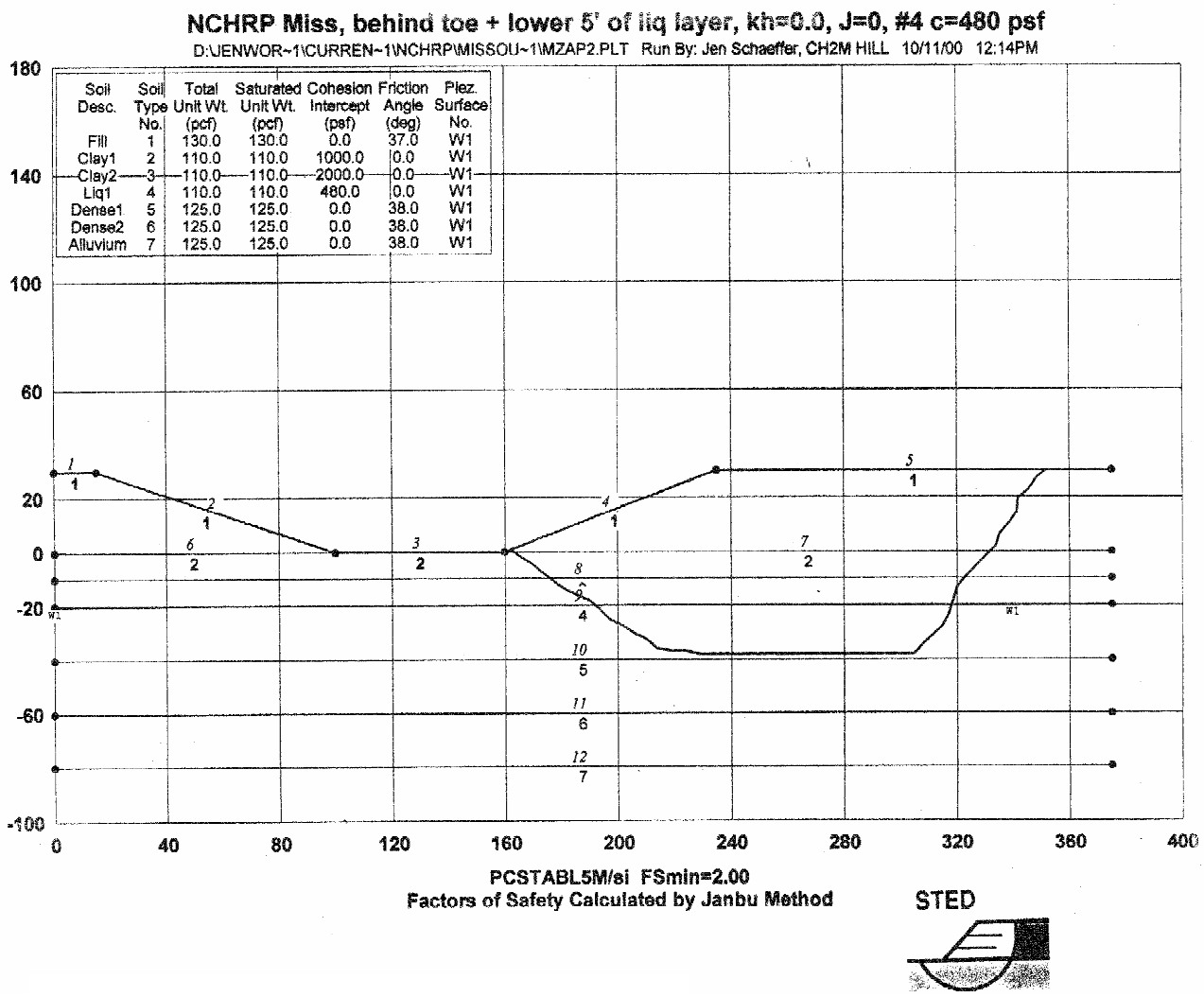

Figure 4.37 Geometry of Toe Failure Wedge for Central U.S. Site

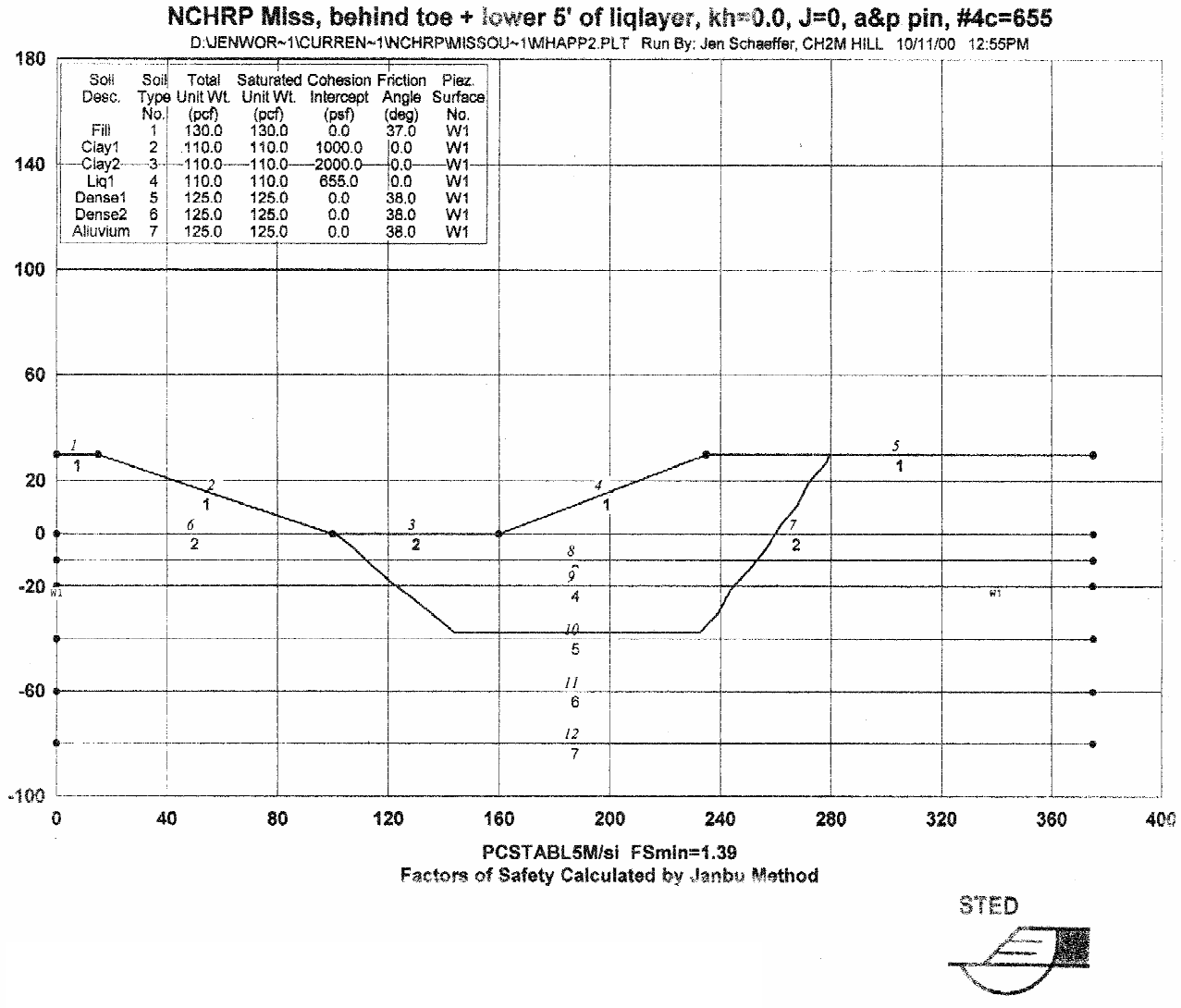

Figure 4.38 Geometry of Deep Failure Wedge for Central U.S. Site

Yield accelerations for both cases were determined by varying the seismic coefficient within the slope stability analysis until the factor of safety was 1.0. This analysis gave the following yield accelerations for the two cases.

Case	Yield Acceleration (g)
Toe Wedge	0.12
Deep Wedge	0.10

For the ground improvement case, different widths of improved ground were used below the abutment. The improved ground extended through each of the liquefied zones. Soil in the improved ground was assigned a friction angle of 45 degrees. This increase in strength was assumed to be characteristic of stone columns or a similar improvement procedure. As with the ground improvement studies for the Washington site, two procedures were used to represent the improved zone. One was to model it explicitly[2]; the second involved "smearing" the reaction from the improved strength zone across the failure surface by increasing the strength of the soil in the liquefied zone to give the same reaction. The resulting FOS was greater than 1.0 for all cases. This allowed yield accelerations to be computed as a function of the width of the improved zone. These values are summarized below.

Width (feet)	Yield Acceleration (g)
10	0.18
30	0.33
50	0.53

4.5.3.3 Displacement Estimates from Simplified Methods

Once it has been established that lateral flow will not occur (i.e., FOS greater than 1 in the stability analysis), then the amount of displacement that occurs from inertial loading on the failure wedge is estimated. This corresponds to Steps 3 and 11 of the procedure outlined in Section 2.5.2.1.

Displacements were estimated for each of the yield accelerations given above. In these analyses, methods recommended by Franklin and Chang (1977), Hynes and Franklin (1984), Wong and Whitman (1990), and Martin and Qiu (1994) were used. The same assumptions as made for the Washington site were used during these analyses. The resulting displacements for the cases cited above are summarized below.

[2] The "explicit" case involves modeling the geometry of the correct width of improved ground in the computer. While fundamentally more correct, it is also time consuming to change the geometry of the problem for each width. The smearing technique involved a simple change in strength of the soil layer, which could be accomplished very quickly.

Case	Displacements (inches)							
	475-Year Event				2,475-Year Event			
	F-C	H-F	W-W	M-Q	F-C	H-F	W-W	M-Q
Toe Wedge	<1	<4	<1	<1	>36	<4	5	3
Deep Wedge	<1	<4	<1	<1	>36	5	8	5
Stone Columns – 10 ft	<1	<4	<1	<1	8	<4	2	1
Stone Columns – 30 ft	<1	<4	<1	<1	<1	<4	<1	1
Stone Columns – 50 ft	<1	<4	<1	<1	<1	<4	<1	<1

The estimates for the recommended Martin and Qui method indicate that for the 475-year event, the displacements will be approximately less than one inch for the toe and deep wedge, respectively. For the 2,475-year event, the toe wedge case gives three inches and the deep wedge five inches. Virtually any pinning or ground improvement method will limit displacements to less than about one inch for the 475-year event and less than about 0.5 feet for the 2,475-year event (disregarding the F-C displacements, which are based on a limited database and also reflect an upper bound).

4.5.3.4 Displacement Estimates Using Site Response Analysis

Steps 3 and 11 of the procedure require that displacements be estimated for the inertial loading condition.

Similar displacement estimates to the simplified methods described above, may be made using the displacement versus yield acceleration curves shown in Figure 4.36. The free field displacements without mitigation corresponding to a yield acceleration of 0.02 are summarized below:

Case	Displacement (inches)					
	475-year event			2,475-year event		
	M	C	T-O	M	C	T-O
End Slope	21	21	16	180	150	140

M = Michoacan earthquake
C = Chile earthquake
T-O = Tokachi – Oki earthquake

For the pile pinning and ground remediation yield accelerations described in Section 4.5.3.3 above, the displacement estimates are summarized below:

Case	Displacement (inches)					
	475-year event			2,475-year event		
	M	C	T-0	M	C	T-0
Toe wedge	<1	<1	<1	24	12	12
Deep wedge	<1	<1	<1	30	18	18
SC – 10 ft	<1	<1	<1	6	4	4
SC – 30 ft	<1	<1	<1	<1	<1	<1
SC – 50 ft	<1	<1	<1	<1	<1	<1

SC = stone column

For the 2,475-year earthquake event, the displacements tabulated above are in general less than the Franklin and Chang estimates but higher than the Hynes and Franklin, Wong & Whitman, and Martin and Qiu estimates.

4.6 Structural Analysis and Design

As with the western bridge, the Central U.S. bridge was first designed for the effects of vibration alone. Both non-liquefied and liquefied soil conditions were considered for the designs. Also, designs for both the AASHTO I-A and NCHRP 12-49 provisions were done.

4.6.1 Vibration Design

The same approach as for the Western U.S. site was used for the Central U.S. site and bridge. For vibration design, both the non-liquefied and liquefied conditions were considered. Both specifications were used to develop the designs and for the recommended LRFD provisions, both the 2,475-year and 100-year events were considered.

In this study, the same bridge was evaluated for each of the two specification requirements. Comparisons were then based on the amounts of reinforcing, for example, and in the case where sizes should be altered, recommendations are given. To this end, the designs represent preliminary designs that highlight the differences between the two specifications.

The bridge was modeled using SAP2000 for both designs, and a multimode analysis was done for each. The design procedure from the recommended LRFD Specification is SDAP E, which permits a larger force reduction factor to be used, but it requires a pushover analysis as a check.

The soil effects on the piles were modeled using LPILE to develop spring stiffnesses at the pile heads. Additionally, the passive resistance offered by the sides of the pile caps and seals were included in the estimates of spring constants. Group effects were considered in the development of the pile springs. The composite springs derived from the combined resistances of all springs attached to a given pile cap were developed as input for the dynamic model of the structure.

4.6.1.1 Modeling

The vibration design of the Missouri bridge follows the same approach as conducted for the Washington bridge. Similarly, the input spectra for the 2,475-year, 100-year, and 475-year return periods and foundation springs for both non-liquefied and liquefied conditions are developed. The approach is discussed in Section 3.6.1.1. The response spectra as given in Section 4.4.1 were used as input for the modal analyses.

The integral abutment provides longitudinal soil restraint against the backwall, and this soil restraint was modeled as outlined in Chapter 11 of the recommended LRFD Specification. As with the Washington bridge, the bridge earthquake resisting system would be categorized as 'Permissible with Owner Approval' due to the use of the full passive longitudinal soil resistance per Chapter 11 of the recommended LRFD Specification.

For earthquake designs of both the existing and recommended provisions, effective concrete properties were used to develop the column stiffnesses. In other elements, the gross moments of inertia were used. The piles were considered as combined steel and reinforced concrete elements. A small reduction, 1/16-inch, in wall thickness was taken to account for section loss to corrosion.

4.6.1.2 Results

For both the existing AASHTO I-A and the recommended LRFD designs, the soil profiles used to develop the foundation springs are given in Figure 4.39 and Figure 4.40. The required soil properties to develop the springs are also given in the figures.

The results of the elastic analyses of the SAP2000 models are given in Table 4.3 through Table 4.7. These list the elastic displacements, shear forces (including passive backfill forces), moments in the substructure, maximum moment in the superstructure, and structure fundamental vibration periods. The results are tabulated for both the non-liquefied and liquefied conditions for the 2,475-year event and for the non-liquefied condition for the 100-year event. Additionally, the non-liquefied and liquefied results are given for the 475-year event. Thus, each table contains five entries for loading.

As with the Washington bridge for the 2,475-year liquefied case, the input spectrum was two-thirds of the input spectrum for the non-liquefied case. This reflects the maximum reduction allowed by the recommended LRFD provisions when site-specific analyses indicate that the input motion likely will be less than that predicted by the basic code spectrum. For this reason, the displacements and the forces induced in the liquefied case are generally smaller than those from the non-liquefied case.

The displacements are given in Table 4.3, and as can be seen in the table, the 2,475-year non-liquefied structural displacements are approximately two to three times those for the 475-year event. For this structure, the pile caps are positioned within soil layers that do not liquefy. The difference between the foundation springs developed for the non-liquefied and liquefied soil profiles is practically negligible; thus, the foundation springs used in the various vibration

MISSOURI SITE
Non-Liquefied Soil Profile

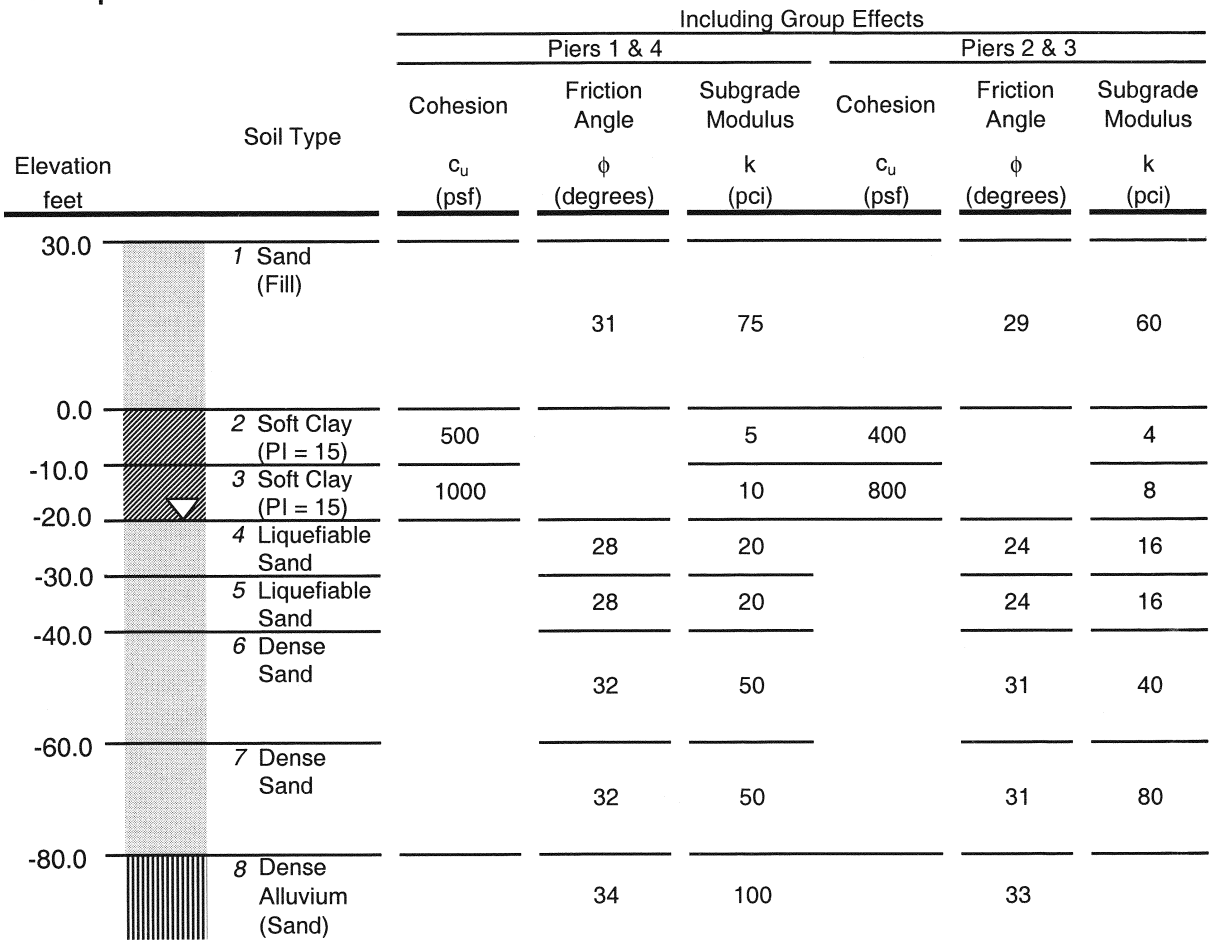

Figure 4.39 Non-Liquefied Soil Profile and Engineering Properties for the Central U.S. Site

MISSOURI SITE
Liquefied Soil Profile

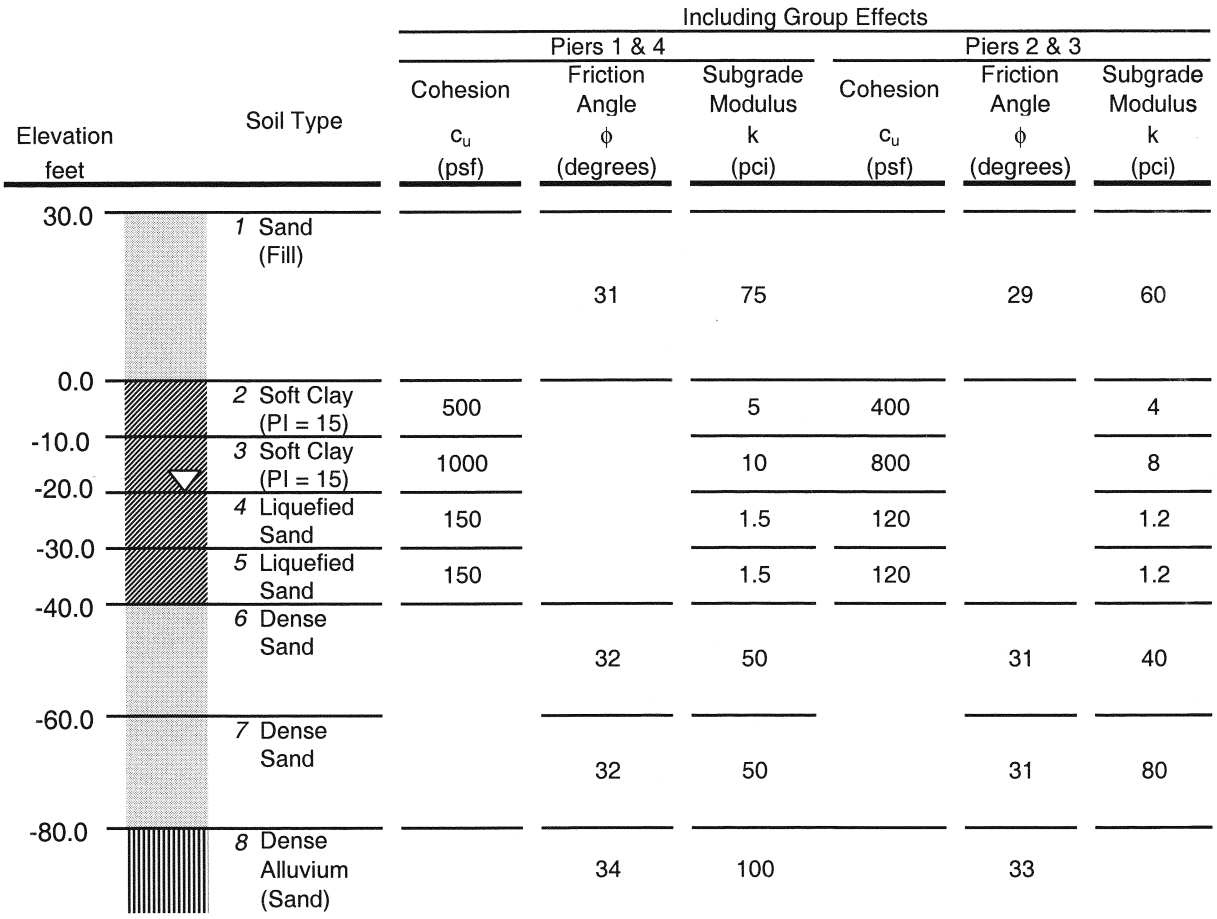

Figure 4.40 Liquefied Soil Profile and Engineering Properties for the Central U.S. Site

Table 4.3 Missouri Bridge – Elastic Structural Displacements

		EQT		EQL		EQT		EQL		EQT		EQL	
		D_T	D_L	D_T	D_L	D_T	D_L	D_T	D_L	D_T	D_L	D_T	D_L
		ft	ft	ft	ft	ft	ft	ft	ft	ft	ft	ft	ft
	Joints	**2500-yr Non-Liquefied**				**2500-yr Liquefied**				**100-yr Non-Liquefied**			
Pier 1 Abutment	611	0.124	0	0	0.190	0.083	0	0	0.105	0.011	0	0	0.014
Pier 4 Abutment	641	0.124	0	0	0.190	0.083	0	0	0.105	0.011	0	0	0.014
Pier 1 at CG Super	711	0.124	0	0	0.190	0.083	0	0	0.105	0.011	0	0	0.014
Pier 2 at CG Super	721	0.344	0	0	0.192	0.229	0	0	0.106	0.027	0	0	0.014
Pier 3 at CG Super	731	0.344	0	0	0.192	0.229	0	0	0.106	0.027	0	0	0.014
Pier 4 at CG Super	741	0.124	0	0	0.190	0.083	0	0	0.105	0.011	0	0	0.014
	Joints	**500-yr Non-Liquefied**				**500-yr Liquefied**							
Pier 1 Abutment	611	0.046	0	0	0.044	0.046	0	0	0.044				
Pier 4 Abutment	641	0.046	0	0	0.044	0.046	0	0	0.044				
Pier 1 at CG Super	711	0.046	0	0	0.044	0.046	0	0	0.044				
Pier 2 at CG Super	721	0.136	0	0	0.045	0.136	0	0	0.045				
Pier 3 at CG Super	731	0.136	0	0	0.045	0.136	0	0	0.045				
Pier 4 at CG Super	741	0.046	0	0	0.044	0.046	0	0	0.044				

Table 4.4 Missouri Bridge – Elastic Structural Shear Forces

		EQT		EQL		EQT		EQL	
		V_T	V_L	V_T	V_L	V_T	V_L	V_T	V_L
		kips	kips	kips	kips	kips	kips	kips	kips
	Joints	**2500-yr Non-Liquefied**				**2500-yr Liquefied**			
Pier 1 Abutment (Bot.)	611	372	0	0	571	248	0	0	314
Pier 2 Columns (Top)	420, 421, 422	169	27	0	90	113	18	0	49
Pier 3 Columns (Top)	430, 431, 432	169	27	0	90	113	18	0	49
Pier 4 Abutment (Bot.)	641	372	0	0	571	248	0	0	314
Passive soil Force	711 + 741				1026				890
	Joints	**500-yr Non-Liquefied**				**500-yr Liquefied**			
Pier 1 Abutment (Bot.)	611	137	0	0	133	137	0	0	133
Pier 2 Columns (Top)	420, 421, 422	67	10	0	21	67	10	0	21
Pier 3 Columns (Top)	430, 431, 432	67	10	0	21	67	10	0	21
Pier 4 Abutment (Bot.)	641	137	0	0	133	137	0	0	133
Passive Soil Force	711 + 741				373				373
	Joints	**100-yr Non-Liquefied**							
Pier 1 Abutment (Bot.)	611	32	0	0	42				
Pier 2 Columns (Top)	420, 421, 422	13	2	0	7				
Pier 3 Columns (Top)	430, 431, 432	13	2	0	7				
Pier 4 Abutment (Bot.)	641	32	0	0	42				
Passive Soil Force	711 + 741				119				

Table 4.5 Missouri Bridge – Elastic Structural Moments

		EQT		EQL		EQT		EQL	
		M_T	M_L	M_T	M_L	M_T	M_L	M_T	M_L
		ft-kips	ft-kips	ft-kips	ft-kips	ft-kips	ft-kips	ft-kips	ft-kips
	Joints	**2500-yr Non-Liquefied**				**2500-yr Liquefied**			
Pier 1 Abutment (Bot.)	611	1274	0	0	0	849	0	0	0
Pier 2 Columns (Top)	420, 421, 422	2193	357	9	1194	1461	238	0	652
Pier 3 Columns (Top)	430, 431, 432	2193	357	0	1194	1461	238	0	652
Pier 4 Abutment (Bot.)	641	1274	0	0	0	849	0	0	0
	Joints	**500-yr Non-Liquefied**				**500-yr Liquefied**			
Pier 1 Abutment (Bot.)	611	470	0	0	0	470	0	0	0
Pier 2 Columns (Top)	420, 421, 422	867	135	0	275	867	135	0	275
Pier 3 Columns (Top)	430, 431, 432	867	135	0	275	867	135	0	275
Pier 4 Abutment (Bot.)	641	470	0	0	0	470	0	0	0
	Joints	**100-yr Non-Liquefied**							
Pier 1 Abutment (Bot.)	611	108	0	0	0				
Pier 2 Columns (Top)	420, 421, 422	170	29	0	88				
Pier 3 Columns (Top)	430, 431, 432	170	29	0	88				
Pier 4 Abutment (Bot.)	641	108	0	0	0				

Table 4.6 Missouri Bridge – Maximum Elastic Transverse Moment in Superstructure

Model	Joint	EQT M_T ft-kips
2500-yr Non-Liquefied	711	6942
2500-yr Liquefied	711	4626
100-yr Non-Liquefied	711	537
500-yr Non-Liquefied	711	2746
500-yr Liquefied	711	2746

Table 4.7 Missouri Bridge – Structural Period

Model	T_{EQL} Sec	T_{EQT} Sec
2500-yr Non-Liquefied	0.41	0.62
2500-yr Liquefied	0.37	0.62
100-yr Non-Liquefied	0.37	0.62
500-yr Non-Liquefied	0.37	0.62
500-yr Liquefied	0.37	0.62

models were exactly the same. Also, the passive resistance of the soil around the caps provides a substantial portion of the lateral resistance of the caps. For these reasons, the differences in the response of the bridge to the various input spectra are in proportion to the differences in the spectra themselves and are not related to the foundation springs.

Listed in the table are displacements for both the transverse and longitudinal earthquake. It is evident that the lateral displacement shape is strongly affected by the transverse restraint of the integral abutments. As the structure and soil profiles are symmetrical, the largest transverse displacement occurs near the intermediate piers for all the input loadings, and the largest displacement is 0.34 feet for the 2,475-year non-liquefied case. Piers 2 and 3 are approximately 26 feet tall, so this displacement represents a drift of about 1.3 percent.

For all the longitudinal displacement cases, it is evident that the displacements are similar all along the structure. Additionally, the restraining effect of the abutment backfill has been accounted for in each run. Except for the non-liquefied 2,475-year case, the abutment backfill did not yield. For the non-liquefied 2,475-year event, the backfill yielded; so the abutment longitudinal spring was progressively altered until the appropriate passive soil force was obtained. For the 6-foot high portion of the backwall below the approach slab, the displacement at which the passive resistance of the backfill was mobilized was 0.12 feet.

Table 4.4 lists the elastic shear forces developed in the structure at each substructure location. Included also is the passive backfill forces as reported from the model at each abutment. The

listed forces represent the full actual force, which is the total from both abutments since the modeling uses half the resistance at each end for the spectral analysis. The passive soil force, approximately 1,040 kips, is obtained for the non-liquefied 2,475-year case only. The other models stay in the elastic range.

Tables 4.8 and 4.9 provide the progression from elastic internal forces to the design moments and ultimately design plastic shears for the intermediate piers and elastic forces to the abutments, respectively. Both the existing provisions and the recommended provisions require a combination of directional effects. In the tables, the combination methods for both sets of design procedures have been included for all earthquake events for comparison.

In this case, the bridge comprises multicolumn bents; therefore, the existing provisions use a force reduction factor, R, of 5 and the recommended provisions allow an R of 6, provided a nonlinear static displacement check is done. For the 100-year design, the recommended provisions allow an R of 1.3.

For the intermediate pier columns, both the 2,475-year and 475-year events required a steel content in the columns of 1.0 percent. The 2,475-year event produced a design moment that was approximately 2.5 times than the 100-year event. This is due to the relative magnitudes of the input spectra.

The foundation (piling) for both the existing and recommended provisions were the same at the intermediate piers, because a system that worked for the existing provisions was the starting point for the design and an assessment of that system in the larger event was one objective. The same foundations were also assumed at the abutments; however, the 2,475-year event requires the piles have a reinforced concrete core. The steel content required for the 2,475-year event is 3.2 percent at the point of maximum moment. The number of piles could be increased to reduce the amount of reinforcement required by the recommended provisions.

The intermediate pier design was checked for displacement capacity, using an approximate pushover analysis, as outlined in Table 4.10. The assessment considered the superstructure and the pile caps as rigid restraints against rotation for simplicity. While the check is only required for the recommended provisions, the checks were performed on the designs to the existing provisions, as well. As noted in the table, the columns met the checks (i.e., the displacement capacity exceeded the demands). The recommended provisions require the checks only on a bent-by-bent basis and only in the principal directions of the substructure.

The recommended specification also requires that the displacements be checked for P-Δ effects. In other words, the lateral shear capacity of the bents defines a maximum displacement that can occur without suffering problems from displacement amplification due to P-Δ. These checks were made in Table 4.11. Both piers are adequate as designed with respect to P-Δ.

Table 4.8 Missouri Bridge – Combinations of Seismic Force Effects Piers 2 & 3 Columns

		H_{col} = 26.0 ft					
		Units	**2500-yr N**	**2500-yr L**	**100-yr N**	**500-yr N**	**500-yr L**
Basic Elastic Forces	P_{DL} (Bottom)	kips	231	231	231	231	231
	P^L (Bottom)	kips	14	7	1	3	3
	P^T (Bottom)	kips	337	225	26	133	133
	M_X^L (Top or Bottom)	ft-kips	0	0	0	0	0
	M_Y^L (Top or Bottom)	ft-kips	1194	652	88	275	275
	M_X^T (Top or Bottom)	ft-kips	2193	1461	29	135	135
	M_Y^T (Top or Bottom)	ft-kips	357	238	170	867	867
Div 1A Method	$P^{LC1} = P^L + 0.3P^T$	kips	115	75	9	**43**	**43**
	$P^{LC2} = 0.3P^L + P^T$	kips	341	227	26	**134**	**134**
	$M_X^{LC1} = M_X^L + 0.3M_X^T$	ft-kips	658	438	9	**41**	**41**
	$M_X^{LC2} = 0.3M_X^L + M_X^T$	ft-kips	2193	1461	29	**135**	**135**
	$M_Y^{LC1} = M_Y^L + 0.3M_Y^T$	ft-kips	1301	723	139	**535**	**535**
	$M_Y^{LC2} = 0.3M_Y^L + M_Y^T$	ft-kips	715	434	196	**950**	**950**
SRSS Circ. Col.	$M^{LC1} = \text{sqrt}\left[\left(M_X^{LC1}\right)^2 + \left(M_Y^{LC1}\right)^2\right]$	ft-kips	1458	846	139	**537**	**537**
	$M^{LC2} = \text{sqrt}\left[\left(M_X^{LC2}\right)^2 + \left(M_Y^{LC2}\right)^2\right]$	ft-kips	2307	1524	199	**959**	**959**
NCHRP SRSS Method	$P = \text{sqrt}\left[\left(P^L\right)^2 + \left(P^T\right)^2\right]$	kips	**337**	**225**	**26**	133	133
	$M_X = \text{sqrt}\left[\left(M_X^L\right)^2 + \left(M_X^T\right)^2\right]$	ft-kips	**2193**	**1461**	**29**	135	135
	$M_Y = \text{sqrt}\left[\left(M_Y^L\right)^2 + \left(M_Y^T\right)^2\right]$	ft-kips	**1246**	**694**	**191**	910	910
NCHRP SRSS + 100%-40% Rule	$P_1 = P$	kips	**337**	**225**	**26**	133	133
	$M_{X1} = 0.4M_X$	ft-kips	877	584	12	54	54
	$M_{Y1} = 0.4M_Y$	ft-kips	498	278	77	364	364
	$M_1 = \text{sqrt}\left[\left(M_{X1}\right)^2 + \left(M_{Y1}\right)^2\right]$	ft-kips	**1009**	**647**	**77**	368	368
	$P_2 = 0.4P$	kips	**135**	**90**	**10**	53	53
	$M_{X2} = M_X$	ft-kips	2193	1461	29	135	135
	$M_{Y2} = 0.4M_Y$	ft-kips	498	278	77	364	364
	$M_1 = \text{sqrt}\left[\left(M_{X2}\right)^2 + \left(M_{Y2}\right)^2\right]$	ft-kips	**2249**	**1487**	**82**	388	388
	$P_3 = 0.4P$	kips	**135**	**90**	**10**	53	53
	$M_{X3} = 0.4M_X$	ft-kips	877	584	12	54	54
	$M_{Y3} = M_Y$	ft-kips	1246	694	191	910	910
	$M_3 = \text{sqrt}\left[\left(M_{X3}\right)^2 + \left(M_{Y3}\right)^2\right]$	ft-kips	**1524**	**907**	**192**	911	911

(continued)

Table 4.8 (continued) Missouri Bridge – Combinations of Seismic Force Effects Piers 2 & 3 Columns

		H_{col} = 26.0 ft.					
		Units	**2500-yr N**	**2500-yr L**	**100-yr N**	**500-yr N**	**500-yr L**
NCHRP 100%-40% Rule	$P^{LC1} = P^{L} + 0.4P^{T}$	kips	**27**	**16**	**2**	8	8
	$P^{LC2} = 0.4P^{L} + P^{T}$	kips	**343**	**228**	**26**	134	134
	$M_X^{LC1} = M_X^{L} + M_X^{T}$	ft-kips	**877**	**584**	**12**	54	54
	$M_X^{LC2} = 0.4M_X^{L} + M_X^{T}$	ft-kips	**2193**	**1461**	**29**	135	135
	$M_Y^{LC1} = M_Y^{L} + 0.4M_Y^{T}$	ft-kips	**1337**	**747**	**156**	622	622
	$M_Y^{LC2} = 0.4M_Y^{L} + M_Y^{T}$	ft-kips	**835**	**499**	**205**	977	977
SRSS Circ. Col	$M^{LC1} = \text{sqrt}\left[\left(M_X^{LC1}\right)^2 + \left(M_Y^{LC1}\right)^2\right]$	ft-kips	**1599**	**949**	**156**	624	624
	$M^{LC2} = \text{sqrt}\left[\left(M_X^{LC2}\right)^2 + \left(M_Y^{LC2}\right)^2\right]$	ft-kips	**2346**	**1544**	**207**	986	986
Determine Plastic Moment	$P_{min} = P_{DL} - P_{EQ}$	kips	-112	3	205	97	97
	$P_{max} = P_{DL} + P_{EQ}$	kips	574	459	257	365	365
	M_{EQ} (Maximum of M^{LC1} or M^{LC2})	ft-kips	2346	1544	207	959	959
	R Factor (2-column Bent)	---	6	6	1.3	5	5
	M_{EQ}/R	**ft-kips**	**391**	**257**	**159**	**192**	**192**
Determine Plastic Shear	Actual M_Y (from PCA-COL)	ft-kips	950			950	
	Longitudinal Reinforcement	---	$13\#8, \rho = 1.01\%$			$13\#8, \rho = 1.01\%$	
	Overstrength Factor, OS	---	1.5			1.3	
	M_{OS}=OS*M_Y	**ft-kips**	**1425**			**1235**	
	$V_P = 2 * M_{OS} / H$	kips	110			95	

Table 4.9 Missouri Bridge – Combinations of Seismic Force Effects Piers 1 & 4 – Abutments

		Units	2500-yr N	2500-yr L	100-yr N	500-yr N	500-yr L
Basic Elastic Forces	P_{DL} (Bottom)	kips	207	207	207	207	207
	P^L (Bottom)	kips	66	36	5	15	15
	P^T (Bottom)	kips	0	0	0	0	0
	M_X^L (Top or Bottom)	ft-kips	0	0	0	0	0
	M_Y^L (Top or Bottom)	ft-kips	0	0	0	0	0
	M_X^T (Top or Bottom)	ft-kips	1274	849	108	470	470
	M_Y^T (Top or Bottom)	ft-kips	0	0	0	0	0
Div 1A Method	$P^{LC1} = P^L + 0.3P^T$	kips	66	36	5	**15**	**15**
	$P^{LC2} = 0.3P^L + P^T$	kips	20	11	2	**5**	**5**
	$M_X^{LC1} = M_X^L + 0.3M_X^T$	ft-kips	382	255	32	**141**	**141**
	$M_X^{LC2} = 0.3M_X^L + M_X^T$	ft-kips	1274	849	108	**470**	**470**
	$M_Y^{LC1} = M_Y^L + 0.3M_Y^T$	ft-kips	0	0	0	**0**	**0**
	$M_Y^{LC2} = 0.3M_Y^L + M_Y^T$	ft-kips	0	0	0	**0**	**0**
SRSS Circ. Col.	$M^{LC1} = \text{sqrt}\left[\left(M_X^{LC1}\right)^2 + \left(M_Y^{LC1}\right)^2\right]$	ft-kips	382	255	32	**141**	**141**
	$M^{LC2} = \text{sqrt}\left[\left(M_X^{LC2}\right)^2 + \left(M_Y^{LC2}\right)^2\right]$	ft-kips	1274	849	108	**470**	**470**
NCHRP SRSS Method	$P = \text{sqrt}\left[\left(P^L\right)^2 + \left(P^T\right)^2\right]$	kips	**66**	**36**	**5**	150	15
	$M_X = \text{sqrt}\left[\left(M_X^L\right)^2 + \left(M_X^T\right)^2\right]$	ft-kips	**1274**	**849**	**108**	470	470
	$M_Y = \text{sqrt}\left[\left(M_Y^L\right)^2 + \left(M_Y^T\right)^2\right]$	ft-kips	**0**	**0**	**0**	0	0
NCHRP SRSS + 100% - 40% Rule	$P_1 = P$	kips	**66**	**36**	**5**	15	15
	$M_{X1} = 0.4M_X$	ft-kips	510	340	43	188	188
	$M_{Y1} = 0.4M_Y$	ft-kips	0	0	0	0	0
	$M_1 = \text{sqrt}\left[\left(M_{X1}\right)^2 + \left(M_{Y1}\right)^2\right]$	ft-kips	**510**	**340**	**43**	188	188
	$P_2 = 0.4P$	kips	**26**	**14**	**2**	6	6
	$M_{X2} = M_X$	ft-kips	1274	849	108	470	470
	$M_{Y2} = 0.4M_Y$	ft-kips	0	0	0	0	0
	$M_1 = \text{sqrt}\left[\left(M_{X2}\right)^2 + \left(M_{Y2}\right)^2\right]$	ft-kips	**1274**	**849**	**108**	470	470
	$P_3 = 0.4P$	kips	**26**	**14**	**2**	6	6
	$M_{X3} = 0.4M_X$	ft-kips	510	340	43	188	188
	$M_{Y3} = M_Y$	ft-kips	0	0	0	0	0
	$M_3 = \text{sqrt}\left[\left(M_{X3}\right)^2 + \left(M_{Y3}\right)^2\right]$	ft-kips	**510**	**340**	**43**	188	188

(continued)

Table 4.9 (continued) Missouri Bridge – Combinations of Seismic Force Effects Piers 1 & 4 – Abutments

		Units	2500-yr N	2500-yr L	100-yr N	500-yr N	500-yr L
NCHRP 100%-40% Rule	$P^{LC1} = P^{L} + 0.4P^{T}$	kips	**66**	**36**	**5**	15	15
	$P^{LC2} = 0.4P^{L} + P^{T}$	kips	**26**	**14**	**2**	6	6
	$M_X^{LC1} = M_X^{L} + M_X^{T}$	ft-kips	**510**	**340**	**43**	188	188
	$M_X^{LC2} = 0.4M_X^{L} + M_X^{T}$	ft-kips	**1274**	**849**	**108**	470	470
	$M_Y^{LC1} = M_Y^{L} + 0.4M_Y^{T}$	ft-kips	**0**	**0**	**0**	0	0
	$M_Y^{LC2} = 0.4M_Y^{L} + M_Y^{T}$	ft-kips	**0**	**0**	**0**	0	0
SRSS Circ. Col	$M^{LC1} = \text{sqrt}\left[\left(M_C^{LC1}\right)^2 + \left(M_Y^{LC1}\right)^2\right]$	ft-kips	**510**	**340**	**43**	188	188
	$M^{LC2} = \text{sqrt}\left[\left(M_X^{LC2}\right)^2 + \left(M_Y^{LC2}\right)^2\right]$	ft-kips	**1274**	**849**	**108**	470	470
Determine Design Moment	$P_{min} = P_{DL} - P_{EQ}$	kips	141	171	202	192	192
	$P_{max} = P_{DL} + P_{EQ}$	kips	273	243	212	222	222
	M_{EQ} (Maximum of M^{LC1} or M^{LC2})	ft-kips	1274	849	108	470	470
	R Factor	---	1	1	1	1	1
	M_{EQ}/R	**ft-kips**	**1274**	**849**	**108**	**470**	**470**

(continued)

Table 4.9 (continued) Missouri Bridge – Combinations of Seismic Force Effects Piers 1 & 4 – Abutments

		Units	2500-yr N	2500-yr L	100-yr N	500-yr N	500-yr L
Basic Elastic Forces	V_X^L (Top or Bottom)	kips	571	314	32	137	137
	V_Y^L (Top or Bottom)	kips	0	0	0	0	0
	V_X^T (Top or Bottom)	kips	0	0	0	0	0
	V_Y^T (Top or Bottom)	kips	372	248	42	133	133
Div 1A Method	$V_X^{LC1} = V_X^L + 0.3V_X^T$	kips	571	314	32	**137**	**137**
	$V_X^{LC2} = 0.3V_X^L + V_X^T$	kips	171	94	10	**41**	**41**
	$V_Y^{LC1} = V_Y^L + 0.3V_Y^T$	kips	112	74	13	**40**	**40**
	$V_Y^{LC2} = 0.3V_Y^L + V_Y^T$	kips	372	248	42	**133**	**133**
SRSS Circ. Col.	$V^{LC1} = \text{sqrt}\left[\left(V_X^{LC1}\right)^2 + \left(V_Y^{LC1}\right)^2\right]$	kips	582	323	34	**143**	**143**
	$V^{LC2} = \text{sqrt}\left[\left(V_X^{LC2}\right)^2 + \left(V_Y^{LC2}\right)^2\right]$	kips	410	265	43	**139**	**139**
NCHRP SRSS	$V_X = \text{sqrt}\left[\left(V_X^L\right)^2 + \left(V_X^T\right)^2\right]$	kips	**571**	**314**	**32**	137	137
	$V_Y = \text{sqrt}\left[\left(V_Y^L\right)^2 + \left(V_Y^T\right)^2\right]$	kips	**372**	**248**	**42**	133	133
NCHRP SRSS + 100%-40% Rule	$V_{X1} = 0.4V_X$	kips	228	126	13	55	55
	$V_{Y1} = 0.4V_Y$	kips	149	99	17	53	53
	$V_1 = \text{sqrt}\left[\left(V_{X1}\right)^2 + \left(V_{Y1}\right)^2\right]$	kips	**273**	**160**	**21**	76	76
	$V_{X2} = V_X$	kips	571	314	32	137	137
	$V_{Y2} = 0.4V_Y$	kips	149	99	17	53	53
	$V_1 = \text{sqrt}\left[\left(V_{X2}\right)^2 + \left(V_{Y2}\right)^2\right]$	kips	**590**	**329**	**36**	147	147
	$V_{X3} = 0.4V_X$	kips	228	126	13	55	55
	$V_{Y3} = V_Y$	kips	372	248	42	133	133
	$V_3 = \text{sqrt}\left[\left(V_{X3}\right)^2 + \left(V_{Y3}\right)^2\right]$	kips	**437**	**278**	**44**	144	144
NCHRP 100%-40% Rule	$V_X^{LC1} = V_X^L + 0.4V_X^T$	kips	**571**	**314**	**32**	137	137
	$V_X^{LC2} = 0.4V_X^L + V + I10_X^T$	kips	**228**	**126**	**13**	55	55
	$V_Y^{LC1} = V_Y^L + 0.4V_Y^T$	kips	**149**	**99**	**17**	53	53
	$V_Y^{LC2} = 0.4V_Y^L + V_Y^T$	kips	**372**	**248**	**42**	133	133
SRSS Circ. Col.	$V^{LC1} = \text{sqrt}\left[\left(V_X^{LC1}\right)^2 + \left(V_Y^{LC1}\right)^2\right]$	kips	**590**	**329**	**36**	147	147
	$V^{LC2} = \text{sqrt}\left[\left(V_X^{LC2}\right)^2 + \left(V_Y^{LC2}\right)^2\right]$	kips	**437**	**278**	**44**	144	144

Table 4.10 Missouri Bridge – Approximate Displacement Check/SDAP E
Piers 2 & 3 Columns

					E_c =	552000	ksf
		H_{col} =	26	ft	I_{cr} =	1.6	ft^4
	Symbol	Units	**2500-yr N**	**2500-yr L**	**100-yr N**	**500-yr N**	**500-yr L**
Minimum Displacement Requirements for Lateral Load Resisting Piers (See Table 4.11 for computation of R_d and Δ_m.)	$1.5R_d\Delta_{mT}$	**ft**	**0.52**	**0.34**	**0.04**	**0.20**	**0.20**
	$1.5R_d\Delta_{mL}$	**ft**	**0.24**	**0.15**	**0.01**	**0.05**	**0.05**
Maximum Displacement Capacity $= \Delta_p + \Delta_y$ ***Check Transverse/Longitudinal Directions***	$\Delta_{capacity}$	**ft**	**1.26** **OK/OK**	**1.26** **OK/OK**	**1.26** **OK/OK**	**1.26** **OK/OK**	**1.26** **OK/OK**
Approximate Plastic Displacement $= \Theta_{pT}\left[H - 2\left(L_p/2\right)\right]$	Δ_{pT}	ft	1.165	1.165	1.165	1.165	1.165
Approximate Plastic Displacement $= \Theta_{pL}\left[H - 2\left(L_p/2\right)\right]$	Δ_{pL}	ft	1.087	1.069	1.069	1.069	1.069
Approximate Yield Displacement $= M_Y H^2/6EI$	Δ_y	ft	0.093	0.093	0.093	0.093	0.093
Yield Moment of Column	M_y	ft-kips	730	730	730	730	730
Plastic Rotational Capacity – Transverse	Θ_{pT}	**rad**	**0.046**	**0.046**	**0.046**	**0.046**	**0.046**
Plastic Rotational Capacity – Longitudinal *("Life Safety" Conservative Value = 0.035)*	Θ_{pL}	**rad**	**0.043**	**0.042**	**0.042**	**0.042**	**0.042**
Number of Cycles of Loading – Transverse	N_{ft}	**cycles**	**4.10**	**4.10**	**4.10**	**4.10**	**4.10**
Natural Period of Vibration of the Structure – Transverse *Check Range of N_f (2 <= N_f <= 10)*	T_{nT}	sec	0.62 OK	0.62 OK	0.62 OK	0.62 OK	0.62 OK
Number of Cycles of Loading – Longitudinal	N_{fL}	**cycles**	**4.71**	**4.88**	**4.88**	**4.88**	**4.88**
Natural Period of Vibration of the Structure – Longitudinal *Check Range of N_f (2 <= N_f <= 10)*	T_{nL}	sec	0.41 OK	0.37 OK	0.37 OK	0.37 OK	0.37 OK
Effective Plastic Hinge Length	L_p	**m**	**0.64**	**0.64**	**0.64**	**0.64**	**0.64**
Shear Span of Member = M/V	fcn(H)	m	3.963	3.963	3.963	3.963	3.963
Yield Strain of Longitudinal Reinforcement	ε_y	m/m	0.00207	0.00207	0.00207	0.00207	0.00207
Diameter of Main Long. Reinforcing Bars	d_b	m	0.036	0.036	0.036	0.036	0.036
Distance between outer layers of long. Reinf on opposite faces of member	D'	**m**	**0.76**	**0.76**	**0.76**	**0.76**	**0.76**

Table 4.11 Missouri Bridge – P-Δ Requirements
Pier 2 & 3 Columns – Transverse Earthquake

	H_{col} =	**26**	**ft**				
	Symbol	**Units**	**2500-yr N**	**2500-yr L**	**100-yr N**	**500-yr N**	**500-yr L**
Displacement Demand from the Seismic Analysis $(\Delta_m = R_d\Delta)$	Δ_{mT}	**ft**	**0.34**	**0.23**	**0.03**	**0.14**	**0.14**
Upper Limit ***Check (No increase in strength req'd if Upper Limit > Δ_m)***	**0.25C(W/P)H**	**ft**	**3.38** **OK**	**3.38** **OK**	**3.38** **OK**	**2.93** **OK**	**2.93** **OK**
Seismic Coefficient Based on the Lateral Strength	C		0.72	0.72	0.72	0.63	0.63
Actual Shear Strength of Column	$V_{supplied}$	kips	120	120	120	104	104
Weight of the Mass participating in the Response of the Pier	W	kips	166	166	166	166	166
Vertical Load on the Pier from Non-Seismic Loads (DL, PT, etc., not LL)	P	kips	231	231	231	231	231
Check if W/P <= 1.0			OK	OK	OK	OK	OK
Short Period Modifier	R_d		**1.00**	**1.00**	**1.00**	**1.00**	**1.00**
Ratio of Elastic Lateral Force to Lateral Strength of Pier	R		6.0	6.0	1.3	5.0	5.0
Natural period of Vibration of the Structure (Transverse)	T	sec	0.62	0.62	0.62	0.62	0.62
$1.25T_s$	T*	sec	0.54	0.54	0.38	0.47	0.47
From Response Spectrum	T_s	sec	0.432 T>T*	0.432 T>T*	0.305 T>T*	0.375 T>T*	0.375 T>T*
Displacement Demand from the Seismic Analysis	**Δ**	**ft**	**0.34**	**0.23**	**0.03**	**0.14**	**0.14**

(continued)

Table 4.11 Missouri Bridge – P-Δ Requirements
Pier 2 & 3 Columns – Longitudinal Earthquake

	H_{col} =	**26**	**ft**				
	Symbol	**Units**	**2500-yr N**	**2500-yr L**	**100-yr N**	**500-yr N**	**500-yr L**
Displacement Demand from the Seismic Analysis $(\Delta_m = R_d\Delta)$	Δ_{mL}	**ft**	**0.24**	**0.15**	**0.01**	**0.05**	**0.05**
Upper Limit ***Check (No increase in strength req'd if Upper Limit >*** Δ_m	**0.25C(W/P)H**	**ft**	**3.38 OK**	**3.38 OK**	**3.38 OK**	**2.93 OK**	**2.93 OK**
Seismic Coefficient Based on the Lateral Strength	C		0.72	0.72	0.72	0.63	0.63
Actual Shear Strength of Column	$V_{supplied}$	kips	120	120	120	104	104
Weight of the Mass participating in the Response of the Pier	W	kips	166	166	166	166	166
Vertical Load on the Pier from Non-Seismic Loads (DL, PT, etc., not LL)	P	kips	231	231	231	231	231
Check if W/P <= 1.0			OK	OK	OK	OK	OK
Short Period Modifier	R_d		**1.26**	**1.38**	**1.01**	**1.21**	**1.21**
Ratio of Elastic Lateral Force to Lateral Strength of Pier	R		6.0	6.0	1.3	5.0	5.0
Natural Period of Vibration of the Structure (Transverse)	T	sec	0.41	0.37	0.37	0.37	0.37
$1.25T_s$	T*	sec	0.54	0.54	0.38	0.47	0.47
From Response Spectrum	T_s	sec	0.432	0.432	0.305	0.375	0.375
			OK	OK	OK	OK	OK
Displacement Demand from the Seismic Analysis	Δ	**ft**	**0.19**	**0.11**	**0.01**	**0.05**	**0.05**

4.6.2 Lateral Spreading Structural Design/Assessment

The material in this section generally represents Steps 4, 5, 6, 8, 9 and 12 of the design procedure in Section 2.5.2.1, and the material addresses the structural aspects of the procedure.

In Section 4.5.3, the tendency for the soil near Piers 3 and 4 to move toward the center span of the bridge during a major earthquake was assessed. The beneficial pinning action of the piles in the foundation systems was also included in the assessment. This section describes the method of determining the pinning force used in the stability analyses.

4.6.2.1 Modes of Deformation

In the western U.S. bridge spreading assessment, a comparison was made between the passive forces acting on the piles when soil flows around the piles and the plastic shear force the piles can produce. The flow forces greatly exceeded the plastic resistance forces that the piles could produce, and subsequently the inference was made that the foundations will move with the soil rather than the soil flowing around them. The large passive forces primarily stemmed from non-liquefied material above the liquefied layers.

For the Central U.S. bridge, a significant amount of non-liquefied material likewise exists above the liquefied material. There is 20 feet of clay near the original ground surface and the approach fills, both of which will not liquefy. For this reason, the passive forces corresponding to flow were not directly calculated because it is obvious that the foundations will move with the soil wedge should lateral spreading movement occur.

The soil wedges that are likely to develop have been described in Section 4.5.3 above. The assumed deformed shapes of the foundations for the two stability conditions investigated are similar to those shown in Figure 2.10 and Figure 2.11. The first figure describes the plastic deformation of the intermediate pier under the action of soil spreading movements, and the second figure describes the plastic deformed shape of the abutment piles.

In this bridge, the abutments are integral-type abutments where the piles are integrally connected to the superstructure. Thus, there is no ability for the founding piles to move independently of the superstructure. Therefore, if spreading develops adjacent to the abutment, the superstructure can act as a strut to resist movement at the top of the abutment piles. This is a different behavior than that of the western U.S. bridge. Due to the restraint, the abutment piles are more effective at developing pinning resistance than if a seat-type abutment was used.

Pier 3 will move similar to that shown in Figure 2.10. Under such a displaced shape, the three columns and the piles contribute to the lateral resistance of the foundation. The columns contribute because they are semi-integral with the superstructure. In the current assessment, residual displacements from the vibration movement of the structure have been ignored. The reductions in resistance due to P-Δ effects have been shown in the figure, but have been omitted from the calculations here because the displacements and axial forces are not large enough to produce a significant reduction in available resistance.

4.6.2.2 Pinning Force Calculations

As with the western bridge, the soil movements will induce forces in the superstructure, if either the toe wedge or the deep soil wedge failure develops. The toe wedge only involves the abutment for pinning force, whereas the deep wedge involves both Pier 3 and the abutment. Additionally, the same potential failure modes exist for the left-hand end of the bridge, but since the bridge is symmetric, the results for one end apply to the other.

Figure 4.41 illustrates the pinning forces acting on the soil block comprising the toe wedge. In this case, the nine piles contribute 105 kips at the bottom of the slide and 53 kips at the top. The top force is smaller than the bottom because the top is assumed to be a pinned condition. These pile forces are developed in calculations in Appendix I. The location of the central plastic hinge is taken at mid-height of the soil column. The abutment backwall also contributes lateral force that resists the movement of the toe wedge, and that resistance is 520 kips, which is half that typically available. The reduction is taken to recognize the potential for slumping of the backfill due to movement of the toe wedge of soil.

These forces represent maximum values that only occur after significant plasticity develops. In the case of the piles, about 7 to 8 inches of lateral movement occurs at the center plastic hinge shown in the figure before full yield is attained. Subsequent to yielding, the maximum deflection that can be tolerated with 0.05 radians of plastic drift is 18 inches. This is the maximum total structural deflection allowed for the toe wedge movement.

Figure 4.42 shows the displaced shape when the deep wedge of soil moves. This involves the abutment piles and Pier 3. For the abutment, the same resistances and allowable deformations apply as with the toe wedge failure addressed above. For Pier 3, the piles can develop 531 kips of resistance, based on plastic hinges forming 5D above and below the liquefiable layers. This results in about 32 feet of length between plastic hinges in the piles. Additionally, the columns contribute 166 kips to the resistance. The bent was assumed to be connected to the superstructure with a pin connection. This is a reasonable bound for the common details used to connect girder superstructures, provided a full-depth diaphragm is used. The connection typically then behaves as a ‘piano hinge.’

The allowable displacements for the deeper wedge failure are approximately 2 feet, which represents total displacement. Pier 3 develops yield at about 6 inches and can then tolerate roughly 18 inches of plastic deformation. However, because both the abutment piles and Pier 3 move as a unit, the 18 inch total displacement is allowed at the abutment controls. Therefore, 18 inches is the allowable displacement.

In Section 4.5.3, the estimated deformations for the 475-year event are less than one inch for both the deep and toe wedge failures. For the 2,475-year event, the pinning effect of the substructure produces displacements of 3 and 5 inches for the toe and deep wedge failures, respectively. This is less than the yield displacements for the piles, and is thus acceptable. Recall that without the pinning effect, the displacements were 5 inches and 32 inches, respectively, for the 475- and 2,475-year events. This illustrates the potential beneficial effect of considering pinning.

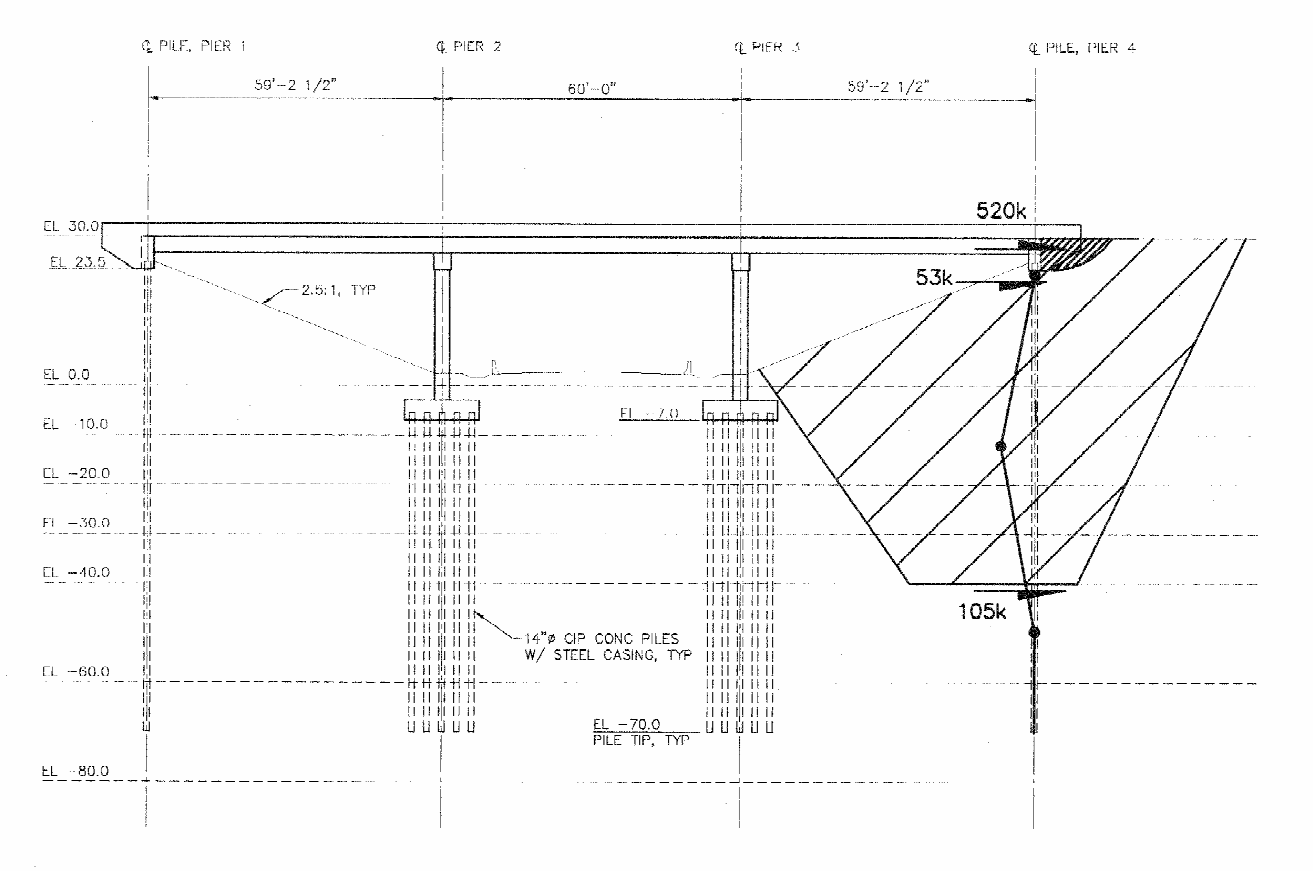

Figure 4.41 Pier 4 Structural Forces Resisting Lateral Spreading

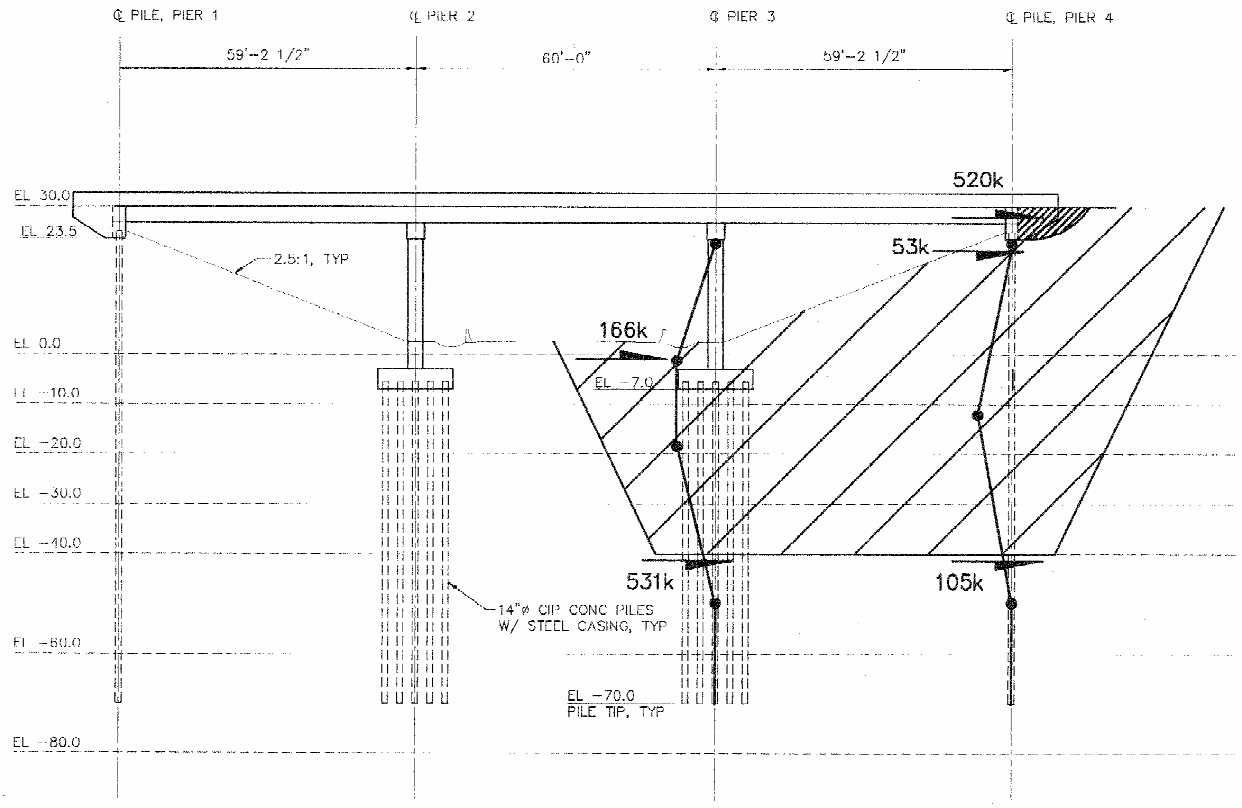

Figure 4.42 Piers 3 and 4 Structural Forces Resisting Lateral Spreading

The site-specific predictions of ground motion are given in Figure 4.36, and at a yield acceleration of about 0.1g, which applies for the pinning options, the average displacement of the three time histories is about 20 inches. In this case, the site-specific data produces displacements (due mainly to the Michoacan earthquake record) that exceed the simplified methods' predictions, but are close to the plastic capacity of the piles.

The conclusion is that if one wished to be conservative and use the results of the site-specific analysis and not risk displacements close to the capacity of the piles, then some remediation would be desirable to protect the substructure. However, if one used the simplified methods for estimating displacements, then the structure, as designed, could withstand the 2,475-year event and the liquefaction that it induces. This range in predicted displacements illustrates the uncertainty associated with the prediction of ground movements.

4.7 Comparisons of Remediation Alternatives

As with the study of the Western U.S. bridge, the intent of the Central U.S. study was to assess the potential consequences of changing the AASHTO seismic design provisions. This comparison met the objectives by having little if any liquefaction under the 475-year event and large amounts of liquefaction and associated ground movements during the 2,475-year event. It is clear that the structure, as designed, is capable of resisting the lateral spreading associated with the liquefaction without the need for any additional expenditure of funds.

4.7.1 Summary of Structural and Geotechnical Alternatives

Because the estimated performance under the 2,475-year event produces spreading displacements that may exceed the elastic capacity of the piles, it was worthwhile to investigate mitigation measures that would produce higher levels of performance, so that the piles can remain within their elastic capacity.

As outlined in Section 4.5.3, stone columns could also be used to limit the displacement of the toe and deep soil wedges. In that section, 10-, 30- and 50-foot wide buttresses of stone columns were considered. The calculated displacements were all less than about four inches for the 2,475-year event when the stone columns were employed, and this provides the operational performance level for the foundations. This displacement ensures that the piles remain within their yield displacement.

It is evident that mitigation, if it is deemed necessary to meet higher performance levels, is only required for the 2,475-year event. All the displacements for the 475-year event, when pinning is considered, are acceptable.

If additional piles are considered for limiting the overall soil displacements, then the objective would likely be to install enough to reduce the estimated displacements down to values that would be tolerable for the substructure. This would likely require a large number of piles since the existing restraint at the superstructure level currently provides over 50 percent of the pinning

resistance. Thus, the inference is that if the deformations need to be limited beyond that which the foundation pinning alone can produce, then stone columns appear to be the rational choice.

4.7.2 Comparisons of Costs

There are no additional costs necessary in order to meet the life-safety performance requirements of the 2,475-year event. In this example, spreading displacements on the order of less than five inches would be estimated, and these can be accommodated in the piles. If the site-specific data were used and a higher level of performance is desired, such that the piles remain within their elastic limits and spreading displacements are desired to be less than six inches, then some remediation work is necessary for the 2,475-year event.

The stone column option would likely only need to be applied over a 10-foot length (longitudinal direction of bridge), since that length produced acceptable deflections of four inches or less in the Newmark analysis and less than six inches in the site-specific analysis. The width at a minimum would be 50 feet, and the depth also would be about 40 feet. If the columns were spaced roughly on 7-foot centers (the width would grow to 14 feet), then about 20 stone columns would be required. At approximately $30 plf, the overall cost per side would be on the order of $24,000 or about $50,000 for both sides.

As a rough estimate of the cost of the overall structure, based on square-footage costs of $80 to $100, the bridge would cost between about $600,000 and $800,000. Thus, the cost to install stone columns would run about 6 to 8 percent of the overall cost of the bridge. This expenditure would ensure a high level of performance of the structure because foundation movements would be less than the yield level of the piles.

If pinch piles were used to augment the piles of the foundations, the piles would not need to be connected to the foundation, and they would not need to extend as deep as the load-bearing foundation piles. The per pile costs for the foundation piles were estimated to be on the order of $2,500 each for 70-foot long piles. Development of the cost data is given in Appendix I. If shorter piles on the order of 40-feet long were used, their costs would be roughly $1,500 each. Thus if pinch piles were used, about 15 piles per side could be installed for the same cost as the stone column remediation option. It is not likely that this number of piles would be as effective in limiting soil movement as the stone columns, although they would produce an acceptable level of performance. Therefore, the stone column option would appear the most cost effective in this situation.

5. SUMMARY AND CONCLUSIONS

5.1 Recommended Procedures

These recommendations apply when liquefaction at a site has been determined to be likely as a result of the 2,475-year earthquake. The specific criteria are given in Section 3.10.5 of the recommended LRFD provisions.

There are two phenomena that must be considered in design of a bridge on a liquefiable site. The first is the traditional vibration design based effectively on the response spectra for the site. This corresponds to the design cases dealt with in the current AASHTO Division I-A. The second phenomenon is lateral forces induced by flow sliding or lateral spreading if these potential consequences of liquefaction are predicted to occur. Flow sliding describes the condition where a soil mass is statically unstable after liquefaction-induced weakening of the soil occurs. Such an unstable condition can lead to quite large deformations. Lateral spreading describes deformations that progressively occur during ground shaking due to the combined static plus transient inertial forces exceeding the resistance of the liquefied soil. Deformations due to lateral spreading typically are smaller than those due to flow sliding.

For the MCE event, when the recommended performance objective is life-safety, inelastic deformation is allowed in the foundation for the lateral spreading or flow spreading case. Mitigation measures are able to achieve higher levels of performance, so that piles remain within their elastic capacity when desired. The vibration cases are designed, as they always are, for inelastic response above ground and at inspectable locations. It is believed that allowing some inelastic action in the presence of large spreading movements during the MCE is necessary. Because spreading-induced deformations are ‘displacement-controlled’, instability of the system is unlikely even though some damage may exist in the foundations. The implication of this decision is that a bridge and its foundations may need to be replaced after a MCE event, but it avoids a significant expenditure of funds to prevent the displacement from occurring.

The design for vibration and lateral spreading is split into two independent activities, as coupling of the vibration load case and the spreading load case is not usually warranted. The vibration design is considered separately from the spreading design, because it is unlikely that the maximum vibration effect and the maximum lateral spreading forces occur simultaneously. Furthermore, the maximum demands on the foundation elements often occur in different locations for vibration and spreading. The de-coupled approach is considered reasonable with respect to the current state of the art.

The approach recommended is to determine the likely ground movements that may occur at the site, including the effects of altered site configurations such as fills and the beneficial effects of the pinning of piles. This prediction of lateral spreading can be made using either currently accepted simplified methods or site-specific analyses, as outlined in this report. As noted in the two cases studied, there can be significant variation in the predicted displacements using the different methods, and this indicates that a designer must be aware that there can be a significant

range in anticipated movements. Refined accuracy is not warranted. The beneficial resistance of the substructure should be included in the assessment of movements. The substructure is then assessed for the predicted movements, and if it can not tolerate the predicted displacements, then ground or structural remediation should be used.

It is important to recognize that the two case histories considered in this report are based on conditions whereby lateral spreading is parallel to the superstructure, which typically is one of the strong directions of the bridge. If the spreading effect is skewed with respect to the superstructure, then the skew must be accounted for in determining the likely plastic mechanism that will control.

5.2 Conclusions

The conclusions from this study of the effects of liquefaction when the design earthquake return period is increased from the existing AASHTO I-A 475-year return period to 2,475-years are summarized as follows.

- For both the Western and Central U.S. examples, there were minimal or no additional costs required to address the recommended liquefaction requirements when a bridge was designed for the current 475-year earthquake and was then subjected to the 2,475-year earthquake recommended in the LRFD provisions for the life-safety level of performance, despite significant increases in the PGA for the 2,475-year event.

- For the Western U.S. example, liquefaction occurred for the 475-year event, and it was necessary to provide stone column mitigation measures in the upper 30 feet or so. This would also most likely be necessary at both abutments (only one was studied in-depth in this effort). The cost for the stone columns at both abutments was estimated to be about 2.5 percent of the bridge cost. For the 2,475-year event, similar measures were required with the depth of the stone columns extended to 50 feet. The estimated cost of this remediation is of the order of 4 percent of the bridge cost.

- For the Central U.S. example, liquefaction did not occur for the 475-year event; however, the bridge was capable of meeting the liquefaction requirements for the new LRFD provisions for the 2,475-year event, with liquefaction occurring at a depth of 20 to 40 feet, through pinning action of the piles. By allowing some inelastic deformations in the piles, no ground improvement was required.

- For the Central and Western U.S. sites, the higher operational level of performance can be achieved in the foundation system (i.e., piles remain in their elastic capacity) for the 2,475-year event by improving the ground using stone columns. This improvement can be achieved for less than 5 percent additional cost in the case of the Western U.S. site and less than 10 percent additional cost in the case of the Central U.S. site.

This study demonstrates the beneficial effects of considering the resistance that the substructure of the bridge offers to lateral movement of soil, 'pinning.' These effects can be significant and should be considered in predictions of lateral soil movements.

The study also shows the benefit of allowing inelastic behavior in the foundation under the action of lateral ground movement. For many cases, relatively large displacements of the ground may be accommodated by the structure without collapse.

There has been considerable advancement in the state of the art in assessing impacts of liquefaction since the AASHTO Division I-A provisions were developed. These have been included in the recommended LRFD provisions and used in the two case studies. They are relatively easy to use, and they permit a much better understanding of the effects of liquefaction and lateral spreading. A summary of the new enhancements is as follows:

- A better ability to estimate the displacements that may occur as a result of lateral spreading. Currently, this is not always done in liquefaction studies.

- The ability to incorporate the beneficial effects of "pinning' of the piles and ground movement in resisting lateral flow movements.

- The new information available from USGS on the deaggregation of the ground shaking hazard into the contributions of different seismic sources, earthquake magnitude, and distances for a particular site.

- The ability to perform nonlinear stress analysis time-history studies using realistic acceleration histories of ground motion to better understand the sequence of events that occur during liquefaction and the modification in ground motions that occur as a result.

The implications of the new LRFD recommendations in going to a 2,475-year return period event is that there is a greater area that now requires more detailed seismic design, including a liquefaction assessment. The specific details of when liquefaction should be considered are covered in Section 3.10.5 of the provisions, but in general, liquefaction is considered for bridges classified as SDR 3 or greater for a site that has a mean magnitude earthquake from deaggregation greater than 6.4. If the mean magnitude is less than 6.0, then liquefaction is not required to be considered. Between a mean magnitude of 6.0 and 6.4, liquefaction may or may not be required to be considered depending on the combinations of soil type and acceleration levels. Although liquefaction must be assessed in certain designs, the Central U.S. example has demonstrated that a bridge may meet the recommended performance requirements of the new provisions without any additional expenditure of funds. It is difficult to draw wider implications from this study without additional study.

5.3 Limitations and Further Study

It should be recognized that that approach recommended here for large, infrequent earthquakes is a departure from the traditional approach of preventing damage in the foundation. For ground

movements on the order of those expected, it is felt that often either remediation is necessary or allowance of some inelastic action in foundation is necessary. It is recognized that only two specific examples were considered in this study, and that with time, refinement will be possible as more structures are studied and designed. It is also recognized that the prediction of earthquake-induced ground movement is approximate at best, and much remains to be learned by the profession on how to produce more accurate predictions. Of all the issues, the greatest uncertainty lies in the methods of predicting ground displacements as seen in the variations of the simplified methods and the more precise nonlinear analyses. However, it is felt that the recommended approach is a reasonable beginning to rationally designing for such earthquake-induced hazards. The broader implications of these results deserve additional effort that was not part of this scope of work.

6. REFERENCES AND ACRONYMS

AASHTO, 1996, *Standard Specifications for Highway Bridges*, 16th Edition, American Association of State Highway and Transportation Officials, Washington, DC.

AASHTO, 1998a, *LRFD Bridge Design Specifications*, 2nd Edition, American Association of State Highway and Transportation Officials, Washington, DC.

AASHTO, 1998b, *LRFD Bridge Construction Specifications*, American Association of State Highway and Transportation Officials, Washington, DC.

AASHTO, 1999, *Guide Specifications for Seismic Isolation Design*, 2nd Edition, American Association of State Highway and Transportation Officials, Washington, DC.

Abrahamson, N.A., 1992, "Non-stationary spectral matching program," *Seismological Research Letters*, Vol. 63, No. 1, p. 30.

Andrus, R.D. and Chung, R.M., 1995, *Ground Improvement Techniques for Liquefaction Remediation Near Existing Lifelines*, National Institute of Standards and Technology, Report NISTIR 5714, Gaithersburg, MD, 74 p.

ASCE, 1997, *Ground Improvement, Ground Reinforcement, Ground Treatment, Developments 1987-1997,* Committee on Soil Improvement and Geosynthetics of the Geo-Institute, Geotechnical Special Publication, No. 69, ASCE, New York, 616 p.

Applied Technology Council, 1981, *Seismic Design Guidelines for Highway Bridges*, ATC-6 Report, Redwood City, California, 210 pp.

ATC/MCEER, 2003, *Recommended LRFD Guidelines for the Seismic Design of Highway Bridges, Part I: Specifications and Part II: Commentary and Appendices*, MCEER/ATC 49 Report, ATC/MCEER Joint Venture, a partnership of the Applied Technology Council and the Multidisciplinary Center for Earthquake Engineering Research, Redwood City, California, 164 p. and 294 p., respectively.

Baez, J.I., 1995, *A Design Model for the Reduction of Soil Liquefaction by Vibro-Stone Columns*, Ph.D. Thesis, University of Southern California.

Baez, J.I. and Martin, G.R., 1995, "Permeability and Shear Wave Velocity of Vibro-Replacement Stone Columns," *Soil Improvement for Earthquake Hazard Mitigation,* Geotechnical Special Publication, No. 49, ASCE, pp. 66-81.

Berrill, J.B., Christensen, SA., Keenan, R J., Okada, W. and Pettinga, J.R., 1997, "Lateral-spreading Loads on a Piled Bridge Foundation," *Seismic Behavior of Ground and Geotechnical Structures, Proc., Special Technical Session on Earthquake Geotechnical Engineering, 14th ICSMFE,* A. A. Balkema, Rotterdam, pp. 173-183.

Boulanger, R.W. and Hayden, R.F., 1995, "Aspects of Compaction Grouting of Liquefiable Soils," *Journal of Geotechnical Engineering*, Vol. 1121, No. 12, pp. 844-855.

Cooke, H.G. and Mitchell, J.K., 1999, *Guide to Remedial Measures for Liquefaction Mitigation at Existing Highway Bridge Sites*, Technical Report MCEER-99-0015, Multidisciplinary Center for Earthquake Engineering Research, University at Buffalo, Buffalo, NY, 176 p.

Egan, J. A., Hayden, R. F., Scheibel, L. L., Otus, M. and Servanti, G.M., 1992, "Seismic Repair at Seventh Street Marine Terminal." *Proc. of Grouting, Soil Improvement and Geosynthetics, ASCE Conference,* New Orleans, R. H. Borden, R.D. Holtz, and I. Juran (eds), Geotechnical Special Publication, No. 30, Vol. 2, pp. 867-878.

Frankel, A.D., and Leyendecker, E.V., 2000, *Uniform Hazard Response Spectra and Seismic Hazard Curves for the United States*, CD-ROM, U.S. Geological Survey National Seismic Hazard Mapping Project, March.

Franklin, A.G. and Chang, F.K., 1977, *Earthquake Resistance of Earth and Rock-Fill Dams; Permanent Displacements of Earth Embankments by Newmark Sliding Block Analysis*, Miscellaneous Paper S-71-17, Report 5, U.S. Army Waterways Experiment Station, CE, Vicksburg, MS.

Hayden, R.F., and Baez, J.I., 1994, "State of Practice for Liquefaction Mitigation in North America." *Proc. of Int. Workshop on Remedial Treatment of Liquefiable Soils*, Tsukuba Science City, Japan, July 4-6.

Houston, S.L., Houston, W.N. and Padilla, J.M., 1987, "Microcomputer-Aided Evaluation of Earthquake-Induced Permanent Slope Displacements," *Microcomputers in Civil Engineering*, Vol. 2, pp. 207-222.

Hynes, M.E. and Franklin, A.G., 1984, *Rationalizing the Seismic Coefficient Method*, Miscellaneous Paper GL-84-13, U.S. Army Waterways Experiment Station, Vicksburg, MS, July, 21 p.

Idriss, I.M., and Sun, J.I., 1992, *User's Manual for SHAKE91*, Center for Geotechnical Modeling, Department of Civil and Environmental Engineering, University of California, Davis, California, 13 p. (plus Appendices).

Ishihara, K. and Cubrinovski, M., 1998, "Problems Associated with Liquefaction and Lateral Spreading During Earthquake," *Geotechnical Earthquake Engineering and Soil Dynamic III, ASCE*, Geotechnical Special Publication, No. 75, Vol. 1, pp. 301-312.

ITASCA, 1998, *FLAC, Fast Lagrangian Analysis of Continua, Version 3.40 User's Guide*, Itasca Consulting Group, Inc., Minneapolis, Minnesota.

Jackura, K.A. and Abghari, A., 1994, "Mitigation of Liquefaction Hazards at Three California Bridge Sites," *Proc., 5th U.S.-Japan Workshop on Earthquake Resistant Design of Lifeline Facilities and Countermeasures Against Soil Liquefaction*, Technical Report NCEER-94-0026, National Center for Earthquake Engineering Research, University at Buffalo, Buffalo, NY, pp. 495-513.

Kramer, S.L., 1996, *Geotechnical Earthquake Engineering*, Prentice Hall, New Jersey.

Leyendecker, E.V., Frankel, A.D. and Rukstales, K.S., 2000, "Seismic Design Parameters for use with the 2000 International Building Code, 2000 International Residential Code, *1997 NEHRP Seismic Design Provisions, and 1997 NEHRP Rehabilitation Guidelines,* CD-ROM, U.S. Geological Survey in cooperation with the Federal Emergency Management Agency and the Building Seismic Safety Council.

Lilihanand, K., and Tseng, W.S., 1988, "Development and Application of Realistic Earthquake Time-histories Compatible with Multiple-damping Design Spectra," *Proceedings of the 9th World Conference of Earthquake Engineering*, Tokyo-Kyoto, Japan Association for Earthquake Disaster Prevention.

Luehring, R., Dewey, B., Mejia, L., Stevens, M. and Baez, J., 1998, "Liquefaction Mitigation of Silty Dam Foundation Using Vibro-Stone Columns and Drainage Wicks – A Test Section Case History at Salmon Lake Dam," *Proceedings of the 1998 Annual Conference Association of State Dam Safety Officials*, Las Vegas, Nevada.

Mace, N., 1999, *An Investigation of Compaction Grouting for Liquefaction Mitigation*, Ph.D. Thesis, Department of Civil Engineering, University of Southern California.

Makdisi, F.I. and Seed, H.B., 1978, "Simplified Procedure for Estimating Dam and Embankment Earthquake-Induced Deformations," *Journal of Geotechnical Engineering*, ASCE, Vol. 104, No. 7, pp. 849-867.

Martin, G.R., 1998, *Development of Liquefaction Mitigation Methodologies: Ground Densification Methods*, Final Task Report for Project 112-D-4.3, Multidisciplinary Center for Earthquake Engineering Research, University at Buffalo, Buffalo, NY.

Martin, G.R. and Qiu, P., 1994, *Effects of Liquefaction on Vulnerability Assessment*, Year One Research Tasks – Technical Research Papers, FHWA Contract No. DTFH61-92-C00106, National Center for Earthquake Engineering Research, University at Buffalo, Buffalo, NY.

Meyersohn, W.D., O'Rourke, T.D., and Miura, F., 1992, Lateral Spread Effects on Reinforced Concrete Pile Foundations, *Fifth U.S.-Japan Workshop on Earthquake Disaster Prevention for Lifeline Systems*, Tsukuba, Japan.

Mitchell, J.K., Baxter, C.D.P. and Munson, T.C., 1995, "Performance of Improved Ground During Earthquakes," *Soil Improvement for Liquefaction Hazard Mitigation*, Geotechnical Special Publication, No. 49, ASCE, pp. 1-36.

Mitchell, J.K., Cooke, H.G. and Schaeffer, J.A., 1998, "Design Considerations in Ground Improvement for Seismic Risk Mitigation," *Proceedings*, *Geotechnical Earthquake Engineering and Soil Dynamics III,* Vol. I, Geotechnical Special Publication, No. 75, ASCE, Reston, VA, pp. 580-613.

Newmark, N.M., 1965, "Effects of Earthquakes on Dams and Embankments," *Geotechnique*, Vol. 15, No. 2, pp. 139-160.

Olson, S.M. and Stark, T.M., 2002, "Liquefied Strength Ratio from Liquefaction Flow Failure Case Histories," *Canadian Geotechnical Journal*, Vol. 39, pp. 629-647.

O'Rourke, T.D., Meyersohn, W.D., Shiba, Y. and Chaudhuri, D., 1994,"Evaluation of Pile Response to Liquefaction-Induced Lateral Spread," *Proceedings*, *5th U.S.-Japan Workshop on Earthquake Resistant Design of Lifeline Facilities and Countermeasures Against Soil Liquefaction*, Technical Report NCEER-94-0026, National Center for Earthquake Engineering Research, University at Buffalo, Buffalo, NY, pp. 457-478.

Qiu, P., 1998, *Earthquake Induced Nonlinear Ground Deformation Analyses*, Ph.D. Thesis, Department of Civil Engineering, University of Southern California.

Reese, L.C., Wang, S.T., Arrellaga, J.S. and Hendrix, J., 1998, *LPILE Plus*, ENSOFT, Inc., Austin, TX.

Riemer, M.F., Lok, T.M. and Mitchell, J.K., 1996,"Evaluating Effectiveness of Liquefaction Remediation Measures for Bridges," *Proceedings*, *6th U.S.-Japan Workshop on Earthquake Resistant Design of Lifeline Facilities and Countermeasures Against Soil Liquefaction*, Technical Report NCEER-96-0006, National Center for Earthquake Engineering Research, University at Buffalo, Buffalo, NY.

Salgado, R., Boulanger, R.W. and Mitchell, J.V., 1997, "Lateral Stress Effects on CPT Liquefaction Resistance Correlations," *Journal of Geotechnical and Geoenvironmental Engineering*, ASCE, August.

Seed, R.B. and Harder, L.F., Jr., 1990, "SPT-Based Analysis of Cyclic Pore Pressure Generation and Undrained Residual Strength," *Proceedings, H. Bolton Seed Memorial Symposium*, BiTech Publishers, Ltd., pp. 351-376.

Seed, H.B. and Idriss, I.M., 1971, "Simplified Procedure for Evaluating Soil Liquefaction Potential, *Journal of the Soil Mechanics and Foundations Division*, American Society of Civil Engineers, Vol. 97, No. SM9, September, pp. 1249-1273.

Silva, W. and Lee, K., 1987, *State-of-the-art for Assessing Earthquake Hazards in the United States: Report 24, WES RASCAL Code for Synthesizing Earthquake Ground Motions*, U.S. Army Engineer Waterways Experiment Station, Vicksburg, Mississippi, Miscellaneous Paper 5-73-1.

Soydemir, C., Zoli, T., LaPlante, K., Kraemer, S., Davidson, W. and McCabe, R., 1997, "Seismic Design of Central Artery Bridges Across Charles River in Boston: Geotechnical/Substructure Aspects," *NCEER Post Liquefaction Ground Deformation Workshop*, University of Southern California, August (original source unknown).

Stark, T.D. and Olson, S.M., 1995, "Liquefaction Resistance using CPT and Field Case Histories," *Journal of Geotechnical Engineering*, Vol. 121, No. 12, pp. 856-869.

Wang, S.T. and Reese, L.C., 1998, "Designing Pile Foundations in Liquefied Soils," *Geotechnical Earthquake Engineering and Soil Dynamics III*, ASCE Geotechnical Special Publication, No. 75, Vol. 2, pp. 1331-1343.

Wilson, D.W., Boulanger, R.W. and Kutter, B.L., 1999, "Lateral Resistance of Piles in Liquefying Sand," *Analysis, Design, Construction, and Testing of Deep Foundation, Proc., Offshore Technology Research Center '99 Conference*, Geotechnical Special Publication, No. 88, ASCE, Reston, VA, pp. 165-179.

Wong, C.P. and Whitman, R.V., 1982, *Seismic Analysis and Improved Seismic Design Procedure for Gravity Retaining Walls*, Research Report 82-83, Department of Civil Engineering, Massachusetts Institute of Technology, Cambridge, MA.

Youd, T.L. and Idriss, I.M., 1997, *Proceedings of the NCEER Workshop on Evaluation of Liquefaction Resistance of Soils*, Technical Report NCEER-97-0022, National Center for Earthquake Engineering Research, University at Buffalo, Buffalo, NY, December, 276 p.

Acronyms

AASHTO	American Association of State Highway Transportation Officials
ASCE	American Society of Civil Engineers
ATC	Applied Technology Council
BSSC	Building Seismic Safety Council
CDMG	California Division of Mines & Geology
CD-ROM	compact disk, read-only memory
CUS	central United States
CPT	Core Penetrometer Test
CRR	cyclic resistance ratio
CSR	cyclic stress ratio

EERI	Earthquake Engineering Research Institute
FHWA	Federal Highway Administration
FOS	factor of safety
g	acceleration of gravity
IBC	International Building Code
ICC	International Code Council
LRFD	Load and Resistance Factor Design
M	magnitude
MCE	Maximum Considered Earthquake
MCEER	Multidisciplinary Center for Earthquake Engineering Research (MCEER supersedes NCEER)
MODOT	Missouri Department of Transportation
N	number of blows
NCEER	National Center for Earthquake Engineering Research (superseded by MCEER)
NCHRP	National Cooperative Highway Research Program
NEHRP	National Earthquake Hazard Reduction Program
NSF	National Science Foundation
PGA	peak ground acceleration
PLF	per linear foot
RVT-BLWN	Random-Vibration-Band-Limited-White-Noise
SDAP	Seismic Design and Analysis Procedure
SDR	Seismic Detailing Requirement
SPT	Standard Penetration Test
SRSS	square root of the sum of the squares
UBC	Uniform Building Code
USCS	Unified Soil Classification System
USGS	U.S. Geological Survey
WSDOT	Washington State Department of Transportation
WUS	western United States

7. PROJECT PARTICIPANTS

PROJECT MANAGEMENT

Ian Friedland (Principal Investigator)
Federal Highway Administration
Office of Bridge Technology, HIBT-30
400 Seventh Street, SW
Washington, DC 20590

Ronald Mayes (Project Manager)
Simpson Gumpertz & Heger, Inc.
The Landmark at One Market Street, Suite 600
San Francisco, California 94105

NCHRP MANAGEMENT

David B. Beal (Project Officer)
Transportation Research Board
National Research Council
2101 Constitution Ave. N.W., Room 300
Washington, DC 20418

PROJECT ENGINEERING PANEL

Ian Buckle (Co-Chair)
University of Reno
Civil Engineering Department
Mail Stop 258
Reno, Nevada 89557

Christopher Rojahn (Co-Chair)
Applied Technology Council
201 Redwood Shores Parkway, Suite 240
Redwood City, California 94065

Serafim Arzoumanidis
Steinman Boynton Gronquist Birdsall
110 William Street
New York, New York 10038

Mark Capron
Sverdrup Civil, Inc.
13723 Riverport Drive
Maryland Heights, MO 63043

Ignatius Po Lam
Earth Mechanics Inc.
17660 Newhope Street, Suite E
Fountain Valley, California 92708

Paul Liles
State Bridge Engineer
Georgia Department of Transportation
No. 2 Capitol Square, S.W.
Atlanta, GA 30334

Brian H. Maroney
California Dept. of Transportation
P. O. Box 942874
Davis, California 94274

Joseph Nicoletti
Consulting Structural Engineer
1185 Chula Vista Drive
Belmont, California 94002

Charles Roeder (ATC Board Representative)
University of Washington, Dept. of CE
233B More Hall, FX-10
Seattle, WA 98195

Freider Seible
University of California
Structural Systems, MC 0085
La Jolla, California 92093-0085

Theodore Zoli
HNTB Corporation
330 Passaic Avenue
Fairfield, NJ 07004

CONSULTANTS

Donald Anderson
CH2M Hill
777 108th Avenue NE
Bellevue, WA 98004

Michel Bruneau
SUNY at Buffalo
Department of Civil Engineering
114 Red Jacket Quadrangle
Buffalo, NY 14260

Gregory Fenves
University of California
Civil Engineering Department
729 Davis Hall, #1710
Berkeley, California 94720-1710

John Kulicki
Modjeski & Masters
4909 Louise Drive
Mechanicsburg, PA 17055

John B. Mander
University of Canterbury
Department of Civil Engineering
Private Bag 4800
Christchurch 8020 New Zealand

Lee Marsh
Berger/Abam Engineers, Inc.
33301 Ninth Avenue South
Federal Way, WA 98003

Geoffrey Martin
University of Southern California
Civil Engineering Department
Los Angeles, California 90089

Andrzej Nowak
2340 G.G. Brown Laboratory
2351 Hayward
University of Michigan
Ann Arbor, MI 48109-2125

Richard V. Nutt
Consulting Structural Engineer
9048 Hazel Oak Court
Orangevale, California 95662

Maurice Power
Geomatrix Consultants, Inc.
2101 Webster Street, 12th Floor
Oakland, California 94612

Andrei Reinhorn
SUNY at Buffalo
Civil Structural & Environmental Engineering
Department
231 Ketter Hall
Buffalo, NY 14260